INTEGRATED ELECTRIC ALTERNATORS/ACTIVE FILTERS

A Dissertation

by

MEHDI TOWLIAT ABOLHASSANI

Submitted to the Office of Graduate Studies of
Texas A&M University
in partial fulfillment of the requirements for the degree of

DOCTOR OF PHILOSOPHY

May 2004

Major Subject: Electrical Engineering

INTEGRATED ELECTRIC ALTERNATORS/ACTIVE FILTERS

A Dissertation

by

MEHDI TOWLIAT ABOLHASSANI

Submitted to Texas A&M University
in partial fulfillment of the requirements
for the degree of

DOCTOR OF PHILOSOPHY

Approved as to style and content by:

Prasad Enjeti (Co-Chair of Committee)	Hamid Toliyat (Co-Chair of Committee)
Jo Howze (Member)	Reza Langari (Member)
Chanan Singh (Head of Department)	

May 2004

Major Subject: Electrical Engineering

ABSTRACT

Integrated Electric Alternators/Active Filters.

(May 2004)

Mehdi Towliat Abolhassani, B.S., Tehran University;

M.S., Iran University of Science and Technology

Co-Chairs of Advisory Committee: Dr. Prasad Enjeti
Dr. Hamid Toliyat

In response to energy crisis and power quality concerns, three different methodologies to integrate the concept of active filtering into the alternators are proposed. Wind energy, due to its free availability and its clean and renewable character, ranks as the most promising renewable energy resource that could play a key role in solving the worldwide energy crisis. An Integrated Doubly-fed Electric Alternator/Active filter (IDEA) for wind energy conversion systems is proposed. The proposed IDEA is capable of simultaneous capturing maximum power of wind energy and improving power quality, which are achieved by canceling the most significant and troublesome harmonics of the utility grid and power factor correction and reactive power compensation in the grid. The back-to-back current regulated power converters are employed to excite the rotor of IDEA. The control strategy of rotor-side power converter is based on position sensoreless field oriented control method with higher power density. Analysis and experimental results are presented to demonstrate the effectiveness of the proposed IDEA.

In next step, an integrated synchronous machine/active filter is discussed. The proposed technology is essentially a rotating synchronous machine with suitable modification to its field excitation circuit to allow dc and ac excitations. It is shown that by controlling the ac excitation, the 5^{th} and 7^{th} harmonics currents of the utility are compensated. The proposed method is cost effective because it can be applied to existing standby generators in commercial and industrial plants with minimal modification to the excitation circuits.

To boost the gain of harmonic compensatory, an advanced electric machine is proposed. An Asymmetric Airgap Concentrated Winding Synchronous Machine (AACWSM) with ac and dc excitation was designed and employed. It is shown that the AACWSM with its unique design, in addition to power generation capability, could be used to compensate the most dominant current harmonics of the utility. The proposed AACWSM can compensate for the 5^{th} and 7^{th} harmonics currents in the grid by controlling the ac field excitation. In addition, the 11^{th} and 13^{th} harmonics currents are also significantly reduced. This system can be used at medium and low voltages for generation or motoring mode of operation.

TABLE OF CONTENTS

Page

Page

LIST OF FIGURES

Page

Page

Page

Page

Page

Page

Page

Page

LIST OF TABLES

Page

CHAPTER I

INTRODUCTION

A recent issue of extreme concern is the electric power quality. With the increased use of nonlinear loads in industry, computers for office automation and other sensitive electronic circuitry, Electric Power Quality has become an important issue. Solid state control of ac power using semiconductor switches is widely employed to feed controlled electric power to electrical loads, such as adjustable speed drives (ASD's), computer power supplies and etc. It is well known that these kind of nonlinear loads demand non-sinusoidal currents from the utility and contribute to numerous power system problems. The current drawn from the ac lines are rich in harmonics with the order of $6k\pm1$, that is 5, 7, 11, 13, etc, that results in lower power factor and possible overheating. They also cause disturbance to other consumers and interference in nearby communication networks. In three-phase systems, they could also cause unbalance and draw excessive neutral currents. With the widespread use of harmonic-producing equipment, the control of harmonic currents to maintain a high level of power quality is becoming important. In response to the power quality of typical power distribution systems in terms of harmonic current distortion and power factor, IEEE 519 [1] and IEC EN 61000-3 [2] standards specify regulations governing harmonic compliance.

This dissertation follows the style of *IEEE Transactions on Power Delivery*.

Current practice to address this issue is to install passive harmonic filters [3-4]. However, passive 5^{th} and 7^{th} harmonic filters are known to cause resonance and cannot adapt to changing load conditions and have the drawback of fixed compensation and large size. The increased severity of harmonic pollution in power networks has attracted the attention of power electronics and power system engineers to develop dynamic and adjustable solution to the power quality problems. Such equipment, generally known as active filters (AFs) are also called active power line conditioners (APLCs) and active power filter (APFs).

In this dissertation, several methodologies to integrate the concept of active filtering into the alternators for alternative energy applications are proposed. Wind, a green and renewable and nonpolitical energy will be a viable alternative energy resource. Since the mid eighties the worldwide installed wind turbine power has increased dramatically and several international forecasts expect the growth to continue. Much of the growth in wind-produced energy is due to the development of more efficient turbines, making wind power competitive with other energy sources and more than just a green power fad.

I.1. RESEARCH OBJECTIVE AND APPROACHES

I.1.1. PROBLEM STATEMENT

In recent years, the issue of power quality is in the forefront as never before, as power suppliers, electrical engineers and technicians are all challenged to meet the needs of today's sensitive electronic technologies and other specialized uses of power. The

scope of power quality problems, which must be solved, range from those found in the largest of power plants to the smallest electronic devices, and from the vastness of the world's power distribution networks to the immediacy of devices sharing a wall.

Power quality issues cause companies to lose billions of dollars every year to work stoppages, diagnosis, and service damaged equipment. These disruptions can also affect hard-earned reputations. Therefore, clean power is essential to remaining profitable and competitive. The injection of harmonic currents into an electrical distribution system, which is based on a non-mitigating 'conventional design', will normally produce several unacceptable outcomes; such as lower power factor, overheating, high neutral currents and electromagnetic interference (EMI). With the increased use of nonlinear loads in industry, computers for office automation and other sensitive electronic circuitry, Electric Power Quality has become an important issue. How big a problem is Power Quality for US industries on an annual basis? Although the exact cost of power quality cannot be known with certainty, in [5] the cost of power quality has been estimated $26.5 billion in year 1987. These order-of-magnitude estimates indicate that it is easily high enough to matter, especially in the high—value-added industries. Example scenarios of the economics of poor power quality include: interruptions to semiconductor batch processing, momentary outage at automobile manufacturing plants and an outage of just five cycles (83 ms) to a glass plant. Although the exact cost of Power Quality cannot be known with certainty, these order of magnitude estimates indicate that it is easily high enough to matter. In particular, for high value added

modern industries that are essential to maintain US competitive advantage, preventive measures to improve power quality can be shown to be very cost-effective [5-6].

In other hand, the contemporary era of rapid industrialization and technological development has raised a global energy crisis, which is one of the major concerning issues. The so-called energy crisis of 1973 served to highlight the finite nature of fossil fuels and the way they were being consumed at an increasing rate; developed countries like US with limited indigenous fuel became vulnerable to external events that affected sharply the price and availability of fuel imports. The increase rate of depletion of fossil energy resources in one hand and growing energy demand on the other hand has initiated considerable research activity worldwide to explore means for tapping of renewable energy resources.

Wind energy due to its freely available, clean and renewable character ranks as the most promising renewable energy resource that could play a key role in solving the worldwide energy crisis. The yearly installed power is showing an annual growth of 40% during the last 5 years [7]. The next technological breakthrough in the development of wind power generation will be penetration into area with lower energy costs and poorer wind regimes. In the recent years, researchers and scientists have focused on the economical utilization of wind energy on a large scale. Improvement in design of turbines and increasing the use of power electronics converters for VAR compensation and/or frequency conversion has given a boost to this industry.

I.1.2. RESEARCH OBJECTIVE

This dissertation will address the total viable solutions to the power quality concerns and energy crises. The objective of this research is to develop several new integrated technologies to resolve energy concerns as well as improving power quality issues. This research focuses on new combined alternators/active filters that are capable of generating active power while simultaneously improving the power quality of the grid by means of the cancellation of the most troublesome harmonics current of the grid and reactive power compensation. It is wise and cost-effective to notice on improving power quality at the point of generation while electromechanical active filtering is possible dynamically. In this Ph.D. dissertation, three new approaches on integration of power generators and power conditioner are proposed. Wind power, a viable solution for energy challenge is specially considered as renewable energy generation. Improving power density of wind alternators with integrated active filter is one of the main objectives of this research.

I.1.3. RESEARCH APPROACHES

In response to power quality concerns and future of energy concerns, three novel, simple and low cost integrated alternators/active filters for different applications are proposed. The proposed technologies are capable of simultaneous generation of active power plus improving power quality by canceling the most significant and troublesome harmonics of the utility lines. Power factor correction and reactive power control are the other two major characteristics of the proposed system. Wind power as renewable and

low cost energy is considered as a viable alternative energy. In following, the proposed solutions to address the power quality concerns and energy crises are explained.

I.1.3.1. An integrated doubly-fed electric alternator/active filter (IDEA) for variable speed wind energy conversion system

In response to recent energy concerns and power quality issues, a viable, simple and low cost sensoreless integrated doubly-fed electric alternator/active filter (IDEA) for variable wind energy conversion system (WECS) is proposed. The proposed technology is capable of simultaneous generation of optimized green power and improving power quality, which are achieved by canceling the most significant and troublesome harmonics of the utility lines. Power factor correction and reactive power control are the other two significant features of the proposed technology. A sensoreless field oriented method to control the IDEA with higher power density is also part of this development. This method can be applied to medium and large wind turbine system. This technology is detailed in Chapter II.

I.1.3.2. Integrated synchronous machine/active filter

Another proposed solution is an integrated synchronous machine/active filter. The proposed electromechanical harmonic filter is essentially a rotating synchronous machine with suitable modification to its field excitation circuit. It is shown that by injecting 2^{nd}, 4^{th} and 6^{th} harmonics currents into the field winding, 5^{th} and 7^{th} harmonic currents are generated in the stator winding. By proper control of the field excitation, the

proposed electromechanical harmonic filter can compensate for the 5^{th} and 7^{th} harmonic currents in the electric power distribution system. The proposed method is cost effective since it can be applied to existing standby generators in commercial and industrial plants with minimal modification to their excitation circuits. This topology will be explained in Chapter III.

I.1.3.3. Harmonic compensation using advanced electric machines

This topology proposes an Asymmetric Air gap Concentrated Winding Synchronous Machine (AACWSM) with ac and dc excitation of the field winding. It is shown that the AACWSM with its unique design, in addition to power generation capability can be used to compensate the most dominant current harmonics of the utility. The back-EMF voltage of this advanced machine behaves as non-sinusoidal voltage source owing to its asymmetric airgap geometry and ac field excitation. With the proper ac field excitation, the proposed electromechanical harmonic filter can compensate for the 5^{th} and 7^{th} harmonic currents in the electric power distribution system. In addition, 11^{th} and 13^{th} harmonics magnitudes are also significantly reduced. This system can be adopted to be used in medium and low voltages in generation or motoring mode of operations.

I.2. LITERATURE STUDY

I.2.1. SOLID STATE ACTIVE FILTERS

The active filtering AF technology is now mature for providing compensation for harmonics, reactive power, and/or neutral current in ac grids. It has evolved in the past quarter of century of development with varying configurations, control strategies and solid-state devices. AFs are also used to eliminate voltage harmonics, to regulate terminal voltage, to suppress voltage flicker, and to improve voltage balance in three-phase systems. This wide range of application is achieved individually or in combination, depending upon the requirements and control strategy and configuration, which have to be selected approximately.

Following the widespread use of solid-state control of ac power, the power quality issues became significant. There are a large number of publications covering the power quality survey, measurements, analysis, cause, and effects of harmonics and reactive power in the electric networks [8-14]. Active filters [15-23] are basically categorized into three types, namely, two-wire (single phase), three-wire, and four-wire three-phase configurations to meet the requirements of the three types of nonlinear loads on supply systems. Single-phase loads, such as domestic lights and ovens, TVs, computer power supplies, air conditioners, laser printers, and copy machines behave as nonlinear loads and cause power quality problems. Several configurations and control strategies to meet the needs of single-phase nonlinear loads have been reported. Configurations, such as the active series filter, active shunt filter, and combination of shunt and series filters

have been developed and commercialized also for uninterruptible power supply (UPS). Both concepts based on a current source inverter (CSI) with inductive energy storage and a voltage-source inverter (VSI) with capacitive energy storage are used to develop single-phase AFs.

However, three-phase loads such as adjustable speed derives ASD with solid-state control consume major amounts of ac power. Lately, many ASD systems incorporate AFs in their front-end design. A substantial number of publications have reported on three-phase three wire AFs starting in 1976. Active shunt, active series, and combinations of both, named as active power quality conditioners, as well as passive filters combined with active shunt and active series AF's are some typical configurations used. Many control strategies such as instantaneous reactive power theory initially developed by Akagi *et al.* [15].

Power circuit configuration plays an important role in the selection of the applications, as some circuits are suitable only for certain aspect of control and power ranges. Figure 1-1 presents the electrical scheme of a shunt active filter for a three-phase system, which is able to compensate for both current harmonics and power factor. Furthermore, it allows load balancing and eliminates current in neutral wire. The power stage is basically, the voltage source inverter with only a single capacitor in the dc side (the active filter does not require any internal power supply), controlled in a way that acts like a current source inverter. Figure 1-2 shows the scheme of the series active filter for a three-phase power system. It is the dual of the shunt active filter, and is able to compensate for distortion in the power line voltages and also compensation voltage

harmonics. The filter consists of a voltage source inverter behaving as a voltage controlled source and requires 3 single-phase transformers to interface with the power system.

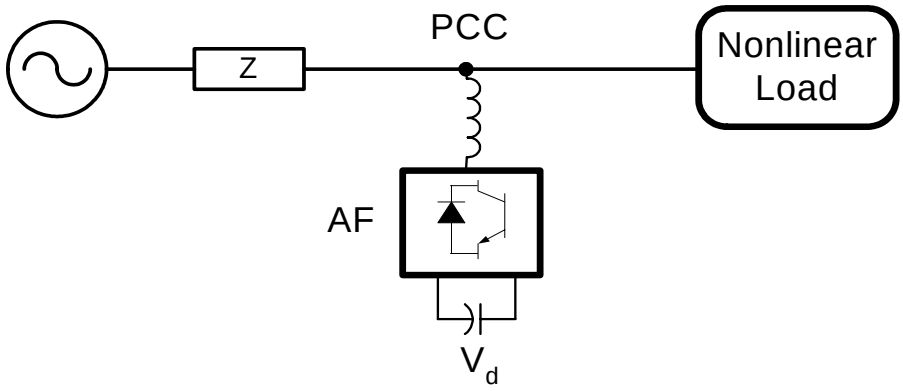

Figure 1-1: Parallel active filter

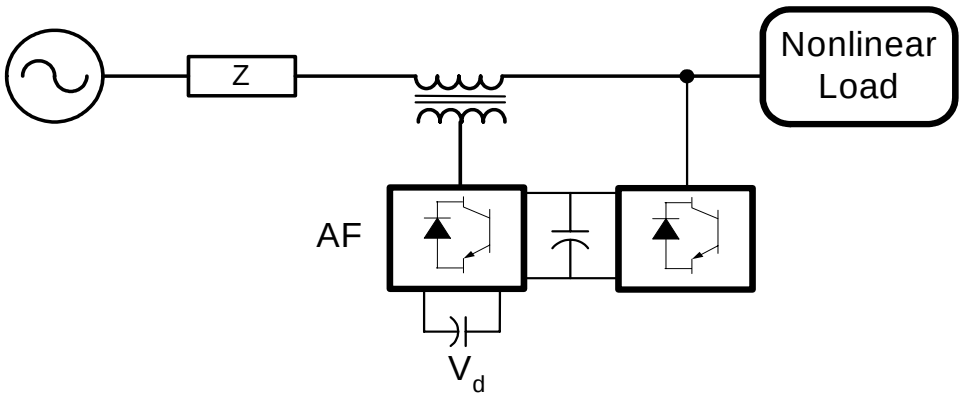

Figure 1-2: Combination of parallel and series active filter

The series active filter does not compensate for load current harmonics but it acts as high impedance to the current harmonics coming to the power source side. Series active filters are less common industrially than their rivals, parallel active filters. This is because of the main drawback of series circuits, namely that they have to handle high load currents, which increase their current rating considerably compared with parallel filters, especially in the secondary side of coupling transformer (increasing the IR^2 losses and the physical size of the filter). The main advantage of series filters over parallel ones is that they are ideal for eliminating voltage waveform harmonics and for balancing three-phase voltages. This, in fact, means that this category of filter is used to improve the quality of the system voltage for the benefit of the load. It provides the load with a pure voltage sinusoidal waveform that is important for voltage sensitive devices.

To gain the advantages of both series and parallel inverter type configurations, a combination of series and parallel inverter- type configurations, a combination of both type of filter shown in Fig.1-3, can be employed to achieve the demanding power system requirements. The demand for combined filters is limited because of their control complexity and higher cost. The control complexity is due to the dependency of the switching pattern of both parallel and series circuits. Configuration of active filter in series with parallel passive filters is shown in Fig. 1-4. This approach is fairly important, especially for medium and high voltage applications where the passive filter reduces the voltage stress applied to the switches in the active filter.

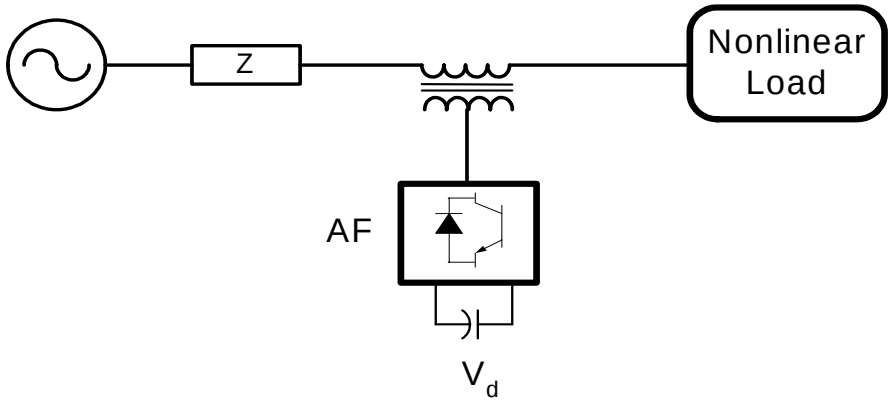

Figure 1-3: Series active filter

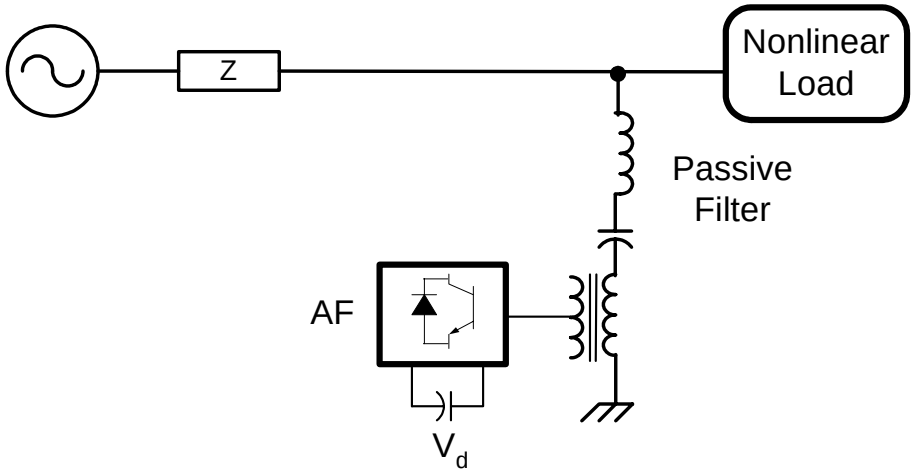

Figure 1-4: Active filter in series with parallel passive filter combination

I.2.2. HARMONIC COMPENSATION USING ELECTRICAL MACHINERY

The subject of harmonic compensation with electrical machinery has not been paid attention sufficiently. However, in [24-25] harmonic compensation method using synchronous machine have been proposed. In these methods, an auxiliary field winding in q-axis is also needed. Field excitation includes dc and ac excitation. Compensation of the 5^{th} and 7^{th} harmonics currents are performed by controlling the 6^{th} harmonics in d-axis and q-axis field windings. However, this method can not be supported by conventional synchronous machines due to requiring a filed winding in q-axis. The authors are holding a US patent on this compensatory method [26].

CHAPTER II

AN INTEGRATED DOUBLY FED ELECTRIC ALTERNATOR/ ACTIVE FILTER (IDEA) FOR WIND ENERGY CONVERSION SYSTEMS

II.1. INTRODUCTION

The contemporary era of rapid industrialization and technological development has raised a global energy crisis, which is one of the major concerning issues. The increase rate of depletion of fossil energy resources in one hand and growing energy demand on the other hand has initiated considerable research activity worldwide to explore means for tapping of renewable energy resources.

Wind energy due to its freely available, clean and renewable character ranks as the most promising renewable energy resource that could play a key role in solving the world wide energy crisis. Since the mid eighties, the worldwide installed wind turbine power has increased dramatically and several international forecasts expect the growth to continue. Much of the growth in wind-produced energy is due to the development of more efficient turbines, making wind power competitive with other energy sources—and more than just a green power fad.

In recent years, researchers and scientists have focused on the economical utilization of wind energy on a large scale. Improvement in design of turbines and

increasing the use of power electronics converters for VAR compensation and/or frequency conversion has given a boost to this industry.

In the area of wind and other power generation systems, where the input resource power varies considerably, variable-speed generation (VSG) is more attractive than fixed speed systems. In these systems, a maximum power point tracker adjusts a system quantity (such as the rotational speed in the case of wind turbines) to maximize turbine power output. Using singly-fed systems, such as induction, synchronous or reluctance drives, the maximum power point tracking sets the operating point of the electrical machine, and thus the losses of the electrical generator associated with that operating point. As the power flow path is fixed (turbine to generator to converter to grid) at a given speed and magnetic flux level of the generator, losses and, thus, conversion efficiency are fixed.

In doubly-fed induction generators, however, at a fixed operating point (power and speed), power flow can be regulated between the two winding systems on the machine. This feature can be utilized to minimize losses associated with the given operating point or achieve other desired performance enhancements. This capability is directly related to the fact that a doubly-fed system requires one degree of freedom (frequency) to establish the maximum turbine power point, leaving one degree of freedom (current magnitude) for other control laws, such as efficiency maximization and better iron utilization. Doubly fed induction machine can be fed and controlled from either or both the stator and the rotor. Of the different possible combinations, rotor side control is advantageous since the power converter only needs to handle the slip power. Thus, if machine is

operated within a limited slip range, then the power converter rating can be brought down remarkably.

On the other hands, the issue of power quality is in the forefront as never before, as power suppliers, electrical engineers and technicians are all challenged to meet the needs of today's sensitive electronic technologies and other specialized uses of power. The scope of power quality problems, which must be solved, range from those found in the largest of power plants to the smallest electronic devices, and from the vastness of the world's power distribution networks to the immediacy of devices sharing a wall. With the increased use of nonlinear loads in industry, computers for office automation and other sensitive electronic circuitry, Electric Power Quality has become an important issue. In response to the power quality of typical power distribution systems in terms of harmonic current distortion and power factor, IEEE 519 [1] and IEC EN 61000-3 [2] standards specify regulations governing harmonic compliance.

In response to these concerns, an Integrated Doubly-fed Electric Alternator/Active filter (IDEA) for wind energy conversion systems is proposed. The proposed technology is capable of simultaneous generation of optimized green power plus improving power quality by canceling the most significant and troublesome harmonics of the utility lines. Power factor correction and reactive power control are the other two major characteristics of the proposed system. A current regulated voltage source power converter based on field oriented control method will dynamically excite the rotor circuitry of IDEA. While work on a similar problem has progressed sporadically, a clear vector control algorithm that can be used with non-sinusoidally wound rotor induction

generator has yet to appear. One of the chief stumbling blocks to such work has specifically been the lack of a suitable mathematical model for non-sinusoidally wound induction generators. The development of such a model and the appropriate vector control algorithm is a major contribution of the work contained in this dissertation.

II.2. SIGNIFICANCE OF THE PROPOSED WORK

II.2.1. FUTURE ENERGY CHALLENGES, WIND ENERGY A VIABLE RESOURCE

The so-called energy crisis of 1973 served to highlight the finite nature of fossil fuels and the way they were being consumed at an increasing rate. Developed countries like US with limited indigenous fuel became vulnerable to external events that affected sharply the price and availability of fuel imports. At the same time, nuclear generation, which had been regarded as a middle-term remedy, became subject to major uncertainties regarding environmental acceptance on an increasing scale. There is a growing awareness that, ultimately, all the essentials of life must flow from replaceable or recyclable processes, many involving technologies, which need substantial lead times before their introduction.

Wind, being widely available and perhaps the most predictable (on annual basis) of natural energy sources, arguably has strong claims for exploitation in many global situations that appear favorable. The next technological breakthrough in the development of wind power generation will be penetration into area with lower energy costs and poorer wind regimes. The task of a wind turbine is to convert the energy stored in the

wind into mechanical energy, which can be used directly or further converted into electrical energy. In this dissertation, the focus is on the electrical energy conversion point of view.

II.2.2. ADJUSTABLE SPEED WIND ENERGY CONVERSION SYSTEMS

Modern high-power wind turbines are capable of adjustable speed operation. Key advantages of using adjustable speed generators (ASGs) compared to fixed speed generators (FSGs) in wind energy conversion systems are:

Cost effective and simple pitch control; controlling speed of the generator (frequency) allows the pitch control time constants to become longer and to reduce pitch control complexity and peak power requirements. At lower wind speed, the pitch angle is usually fixed. Pitch angle control is performed only to limit maximum output power at high wind speed.

- Reduction of mechanical stresses; gusts of wind can be absorbed.
- Dynamic compensation of torque and power pulsation caused by backpressure of the tower. This backpressure causes noticeable torque pulsation at a rate equal to the turbine rotor speed times the number of rotor wings.
- Improved power quality; torque pulsation can be reduced due to the elasticity of the wind turbine system. This eliminates electrical power variations, i.e. fewer flickers.
- Improved system efficiency; turbine speed is adjusted as a function of wind speed to maximize output power. Operation at the maximum power point can be

realized over a wide power range. As a result, up to 10% energy efficiency improvement is possible.

- Decoupled control of the active and reactive powers, which becomes more and more important with increased use of wind turbines in the utility grids.
- Acoustic noise reduction because low speed operation is possible at low power conditions.

In addition, most ASG based wind turbines can offer island operation capability. Island operation is difficult to realize with the so-called Danish concept.

II.2.3. DOUBLY-FED INDUCTION GENERATOR SYSTEMS

Recent developments seek to avoid most disadvantages of direct-in-line converter based ASGs. Figure 2-1 shows an alternative ASG concept, which consists of a doubly-fed induction generator (DFIG) with a 4-quadrant ac-to-ac converter connected to the rotor windings. Compared to direct-in-line systems, this DFIG offers the following advantages:

- Reduced inverter cost because inverter rating is typically 25% of the total system power, while the speed range of the ASG is ± 33% around the synchronous speed.
- No need for bulky inverter filters and EMI filters.
- Improved system efficiency.

- VAR control can be implemented at lower cost because the DFIG system (4-quadrant converter and induction machine) basically operates similar to a synchronous generator.

The converter has to provide only excitation energy for fundamental power and harmonic power for canceling the unwanted utility harmonics (proposed in this dissertation). In addition, compared to SCR based Kramer drives, the DFIG with 4-quadrant converter in the rotor circuit enables decoupled control of active and reactive power of the generator. A number of other important features are available which not only promise efficiency enhancement but also contribute greatly towards improved reliability. These features are rapid speed response to wind transients, damping of torsional modes, performance enhancement during electrical transients, and efficient system start-up and shutdown.

Current and proposed generators include systems based mainly on dc machine, synchronous and ac induction machines technologies as well as reluctance machines.

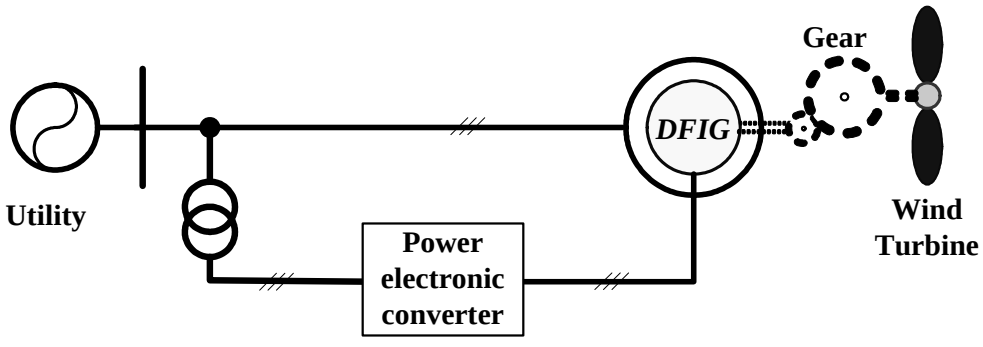

Figure 2-1: Wind energy conversion system using doubly-fed induction machine

While extracting more energy from the wind, most proposed variable-speed systems suffer a cost disadvantage due to the required variable speed generator drive. This cost penalty may eventually render the additional energy capture meaningless. Thus, reducing the cost of the power electronic hardware is essential for variable-speed generating systems to achieve viable and competitive $/kWh ratios. It is strongly believed that the proposed IDEA system in this dissertation will have a significant cost advantage to the existing systems.

II.2.4. APPLICATION OF POWER ELECTRONICS IN WIND TURBINE

Due to fast development of power electronics offering both higher capability and lower price/kW, the applicability of power electronics in wind turbines will further increase. The application of power electronic converters in wind turbines is getting more and more attention by the wind turbine manufacturers due to increasing controllability and power quality demands imposed by the utility companies. At the same time, the size and weight are steadily decreasing. The back-to-back four-quadrant PWM-VSI converter is widely used in wind turbines today. Recently in the literatures, the following four converter topologies have been investigated for applications in wind turbines:

- Tandem converter,
- Matrix converter,
- Multilevel converter,
- Resonant converter.

From the analysis it turned out that the matrix and multilevel converters were the most serious competitors to the back-to-back converter. Meanwhile, new power semiconductor devices can change this picture.

II.2.5. POWER QUALITY ISSUES

Power quality issues cause companies to lose billions of dollars every year to work stoppages, diagnosis, and service damaged equipment. These disruptions can also affect hard-earned reputations. Therefore, clean power is essential to remaining profitable and competitive. The injection of harmonic currents into an electrical distribution system, which is based on a non-mitigating 'conventional design', will normally produce several unacceptable outcomes; such as lower power factor, overheating, high neutral currents and electromagnetic interference (EMI). With the increased use of nonlinear loads in industry, computers for office automation and other sensitive electronic circuitry, Electric Power Quality has become an important issue. Example scenarios of the economics of poor power quality include: interruptions to semiconductor batch processing, momentary outage at automobile manufacturing plants and an outage of just five cycles (83 ms) to a glass plant. Although the exact cost of Power Quality cannot be known with certainty, these order of magnitude estimates indicate that it is easily high enough to matter. In particular high value added modern industries, which are essential to maintain US competitive advantage, preventive measures to improve power quality can be shown to be very cost-effective. In response to the power quality concerns of typical power distribution systems in terms of harmonic current distortion and power

factor, IEEE 519 and IEC EN 61000-3 standards specify regulations governing harmonic compliance [1-2]. Passive filter has been a viable approach because of low cost and high efficiency. However, the performance of the passive scheme has a limitation since the addition of the passive filter interfaces with the system impedance and cause resonance with other network. Numerous active solutions, which are becoming a more effective means to meet the harmonic standards by overcoming the drawback of the passive filter, have been proposed [16-26].

II.3. WIND ENERGY CONCEPTS, CONFIGURATIONS

Worldwide, wind energy exceeds 31,000 MW of installed capacity, generating enough to power the equivalent of 7.5 million average American households. Wind power installations grew by 33% in 2002 in Europe—the global leader in wind energy—alone. The European Wind Energy Association estimates that the global wind power market could be worth $25 billion a year by 2010. Wind is a clean, competitive energy source that can help power the 21st century.

The scope of this section is to describe the state of art of wind turbines seen from an electrical point of view, using two approaches. The first approach describes the state of art from technical point of view, while the second approach applies a market-based point of view. This section will investigate different old and new concepts for wind energy conversion systems. Before going through the conventional wind energy conversion system schemes, it is necessary to review nature of wind energy and express the mathematical model of wind turbine.

II.3.1. MATHEMATICAL MODEL OF WIND TURBINE

A wind energy conversion system is basically comprised of three main concepts, the aerodynamic component and the electrical component. The turbine forms a major constituent of the aerodynamic system. The energy that could be captured from wind by a specific turbine depends on its design particulars and operating conditions. In this section all aspects related to the power conversion from kinetic wind energy to rotational energy that are of relevance for the stability model are explained.

The kinetic energy E_k of a mass of air m having the speed v_w is given by:

$$E_k = \frac{m}{2} \cdot v_w^2 \tag{2-1}$$

The power associated to this moving air mass is the derivative of the kinetic energy with respect to time can be expressed as follows:

$$P_o = \frac{\partial E_k}{\partial t} = \frac{1}{2} \cdot \frac{\partial m}{\partial t} \cdot v_w^2 = \frac{1}{2} \cdot q \cdot v_w^2 \tag{2-2}$$

where q represents the mass flow given by the expression:

$$q = \rho \cdot v_w \cdot A \tag{2-3}$$

where:

ρ : Air density;

A: Cross section of the air mass flow.

Only a fraction of the total kinetic power can be extracted by a wind turbine and converted into rotational power at the shaft. This fraction of power (P_{WIND}) depends on

the wind speed, rotor speed and blade position (for pitch and active stall control turbines) and on the turbine design. The aerodynamic efficiency *Cp* is defined as follows:

$$C_p = \frac{P_{wind}}{P_o} \tag{2-4}$$

For a specific turbine design, the values of $Cp(\beta,\lambda)$ are usually presented as a function of the pitch angle (β) and the tip speed ratio (λ). The tip speed ratio is given by:

$$\lambda = \frac{\omega_{tur} \cdot R}{v_w} \tag{2-5}$$

where:

R: Radius of the turbine blades;

ω_{tur} : Turbine angular speed.

The aerodynamic efficiency $Cp(\beta,\lambda)$ is usually defined as a form of a two-dimensional lookup characteristic (for different values of β and λ) by actual measurement. A two dimensional, cubic spline-interpolation method is used for calculating points between measured values. The high accuracy of the interpolation method avoids the need of entering a large number of points. Alternatively, analytical approaches for approximating the aerodynamic efficiency $Cp(\beta,\lambda)$ characteristic could be used but since these data are usually available in tabular formats.

Finally, the mechanical power extracted from the wind is calculated using:

$$P_{mech} = \frac{\rho}{2} \cdot \pi \cdot R^2 \cdot C_p(\lambda,\beta) \cdot v_w^3 \tag{2-6}$$

The aerodynamic efficiency $Cp(\beta,\lambda)$ characteristic can be calculated using special software for aerodynamic designs that is usually based on blade-iteration techniques or it

can be obtained from actual measurements. The shaft torque developed by a wind turbine having can be expressed by:

$$T_{mech} = \frac{\rho}{2} \cdot \pi \cdot R^3 \cdot C_t(\lambda, \beta) \cdot v_w^2 \tag{2-7}$$

where:

$$C_t = \frac{C_p}{\lambda} \tag{2-8}$$

Using above equations, a family of characteristics representing output power and developed torque as a function of turbine speed for a number of wind speeds can be deduced from C_p versus λ characteristics. Typical power-speed and torque- speed characteristics are given in Fig. 2-2.

From (2-6), it can be interpreted that the power developed can be maximized at any wind speed if the power coefficient (C_p) is constrained to remain at its maximum value. This can be achieved by maintaining the tip-speed ratio at its optimum value (λ_{opt}) as can be observed from Fig. 2-2 (a).

Usually the rated speed of the turbine corresponds to the maximum values of Cp for a given wind speed. If the shaft speed held constant the efficiency of conversion will decrease at wind speeds other than this value.

However, if the shaft speed is allowed to follow the variations in wind speed such that the tip speed ratio is maintained at its optimum value (λ_{opt}), the turbine could be made to develop maximum power at any wind speed.

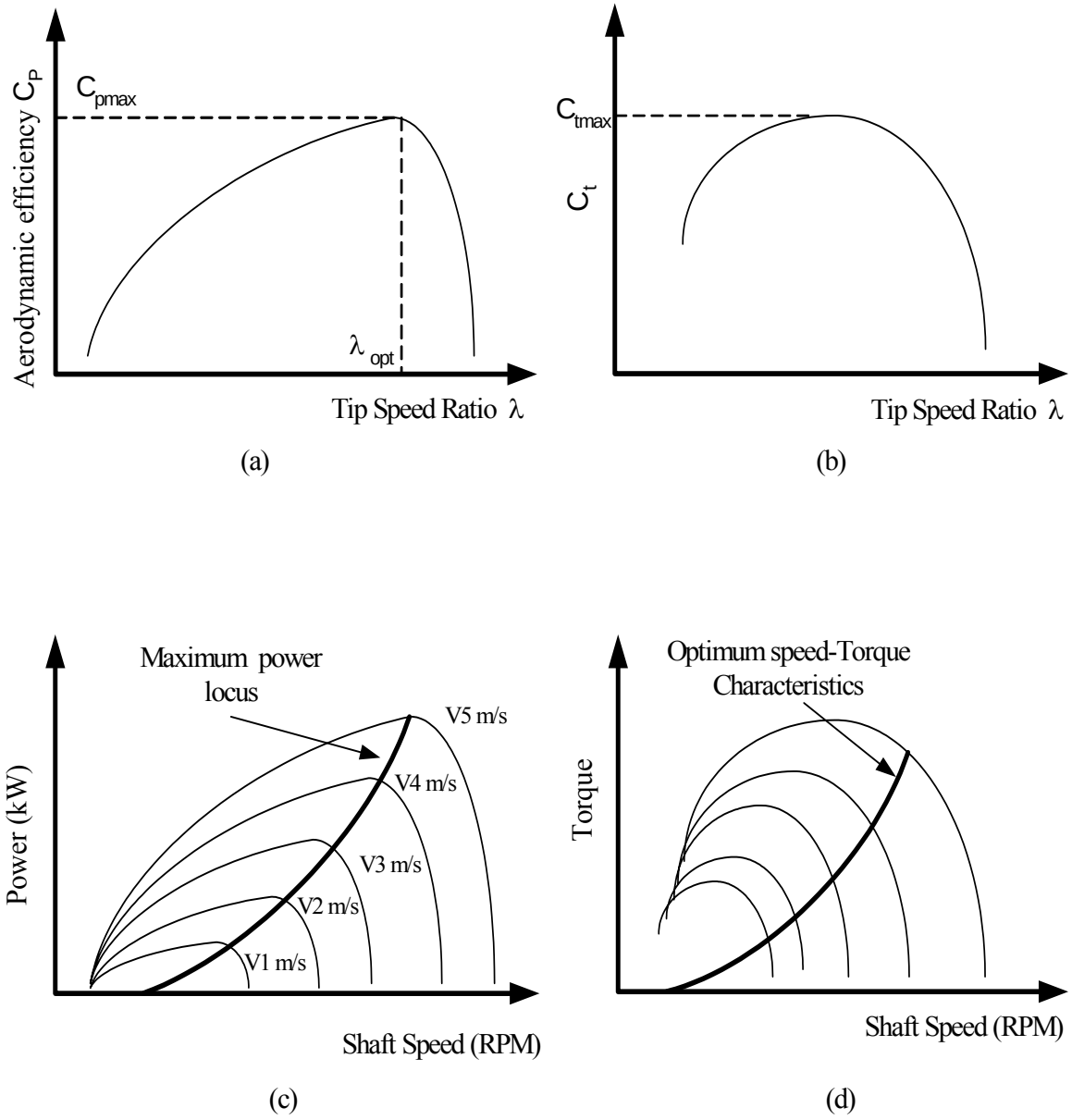

Figure 2-2: Typical characteristics of a horizontal axis wind turbine. (a) Power coefficient versus tip speed ratio, (b)Torque coefficient versus tip speed ratio, (c) Output power versus shaft speed at different wind speeds and (d) Developed torque versus shaft speed at different wind speeds

The locus of turbine shaft speed for maximum output for varying wind speeds is given by the maximum power points at Fig. 2-2 (c) labeled with " Maximum power locus".

The torque corresponding to maximum power for a given wind speed is obtained by substituting $C_{t\text{-}opt}$ in (2-7). $C_{t\text{-}opt}$ can be obtained by:

$$C_{t-opt} = \frac{C_{p\max}}{\lambda_{opt}} \tag{2-9}$$

The locus of torque corresponding to maximum power is also shown in Fig. 2-2 (d). It is important to note that maximum torque points do not lie on this locus.

II.3.2. THE CONVENTIONAL WIND ENERGY CONVERSION TOPOLOGIES

Due to the highly fluctuating nature of the wind, the turbine rotor spins at varying speeds following the speed of the wind resulting in a variable frequency output power. A constant frequency output can be made either by constraining the generator shaft speed to remain constant irrespective of the wind speed or the variable frequency output can be converted into constant frequency using power electronic converters. Accordingly the conventional wind energy conversion systems are broadly classified into two main categories:

- The constant speed constant frequency systems (CSCF)
- The variable speed constant frequency systems (VSCF)

II.3.2.1. The constant speed constant frequency system

Until recently, the non-availability of cost-effective power electronic converters made the CSCF systems virtually obligatory in grid-connected applications. The constant speed of generator shaft is achieved by means of mechanical control, electrical control or both. The blade pitch angle control in one of the mechanical control approaches, where the blade pitch is varied with wind speed to maintain a constant level of power derived from wind. The yaw control, coning, etc. is some of the other alternative mechanical control approach to maintain constant shaft speed.

Power speed characteristics of CSCF system has been shown in Fig. 2-3. Constant speed control is also possible by means of coupling the turbine to a generator capable of converting maximum shaft power into electrical energy. By regulating the load on the generator through control of its excitation the generator shaft speed is held constant [27].

A cage induction generator connected to an infinite bus, the so-called Danish concept, can also be considered as a CSCF system. Because the machine can operate only over a narrow speed range corresponding to 1-5% negative slip which is a relatively negligible variation as compared to the wind speed fluctuation [28].

Because wind power varies with cube of wind speed, violent fluctuation in input to the machine during gust periods may lead to loss of synchronism in case of synchronous generators. With induction generators, the operating point may fall into the unstable region if the input exceeds that corresponding to the pull out torque. Therefore, in CSCF systems mechanical controls are usually supplemented to damp out the transient input surges.

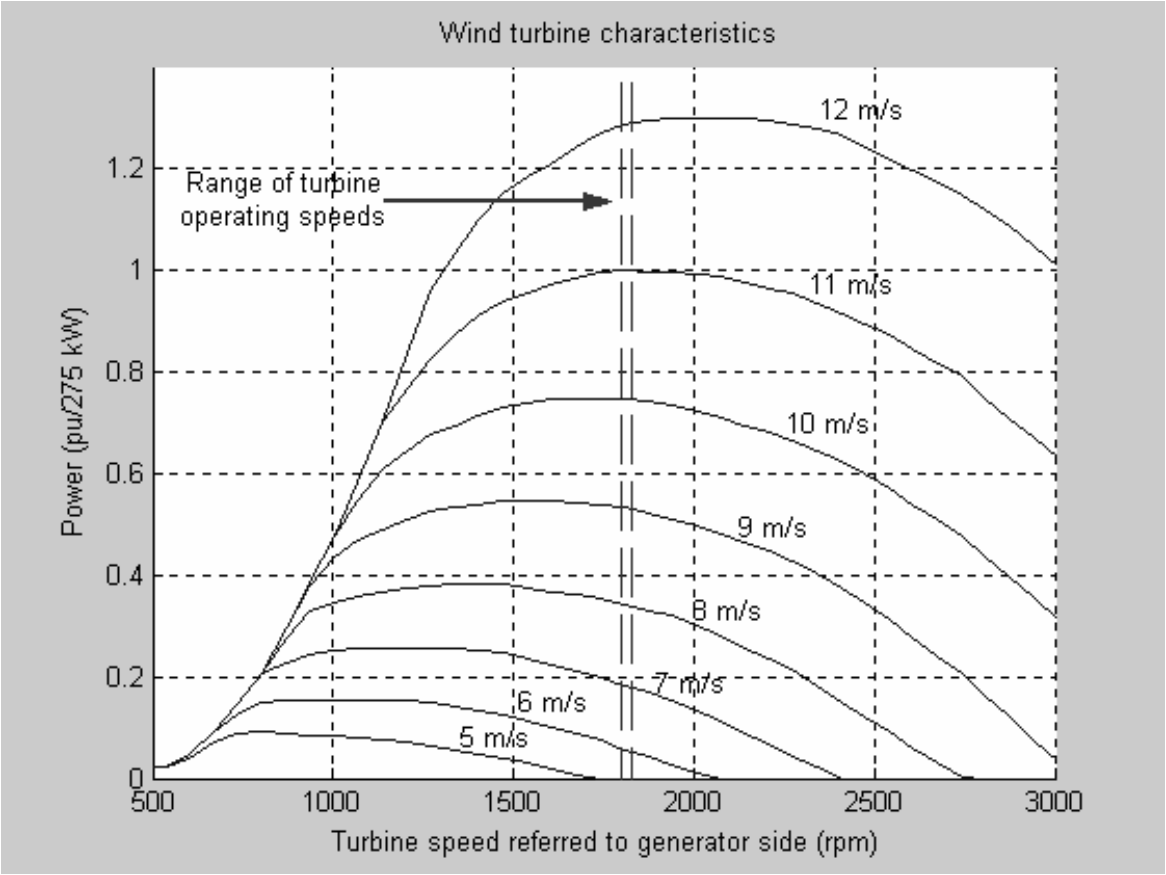

Figure 2-3: Power speed characteristics of CSCF system

II.3.2.2. The variable speed constant frequency (VSCF) wind energy conversion systems

As primarily discussed, one of the most significant criteria in designing a wind energy conversion system is to maximize the captured energy from wind power. The captured power by turbine and hence its conversion efficiency varies with tip-speed to wind speed ratio. In order to maximize the captured energy from fluctuating wind it is necessary to ensure operation of the system at maximum turbine efficiency throughout by maintaining the optimal value of tip-speed ratio λ_{opt} .

This is the fundamental idea behind the variable speed wind energy systems, which, the turbine speed is allowed to vary with wind speed along the maximum power locus. A wind energy conversion system operated under this condition is called variable speed constant frequency systems (VSCF). Hence, from efficiency conversion point of view, the variable speed constant frequency systems are more desirable than constant frequency constant speed systems where the maximization of power conversion efficiency is just possible at certain wind speed. However the implementation of VSCF systems are more complicated than CSCF systems.

To realize a VSCF system, it is obvious that some sort of maximum power point tracking mechanism must be provided that ensures operation of the system along the maximum power locus. At steady state the generator should develop a torque to counter balance the turbine torque. Therefore, the actual speed of turbine rotation is determined by the point of intersection of the generator and turbine speed-torque characteristics.

Consequently, the generator speed-torque characteristic needs to be matched with the new turbine characteristics at the point of maximum power with varying the wind speed. In VSCF system the point of intersection of the generator power and turbine power must necessarily lie on the optimum torque-speed characteristics. This is accomplished in several ways depending on the type of machine and control strategy. In Fig. 2-4 power speed characteristic of wind energy conversion system using a doubly fed induction generator is shown. As it is observed, the power locus beyond synchronous speed increases slightly. This phenomenon will be discussed later on.

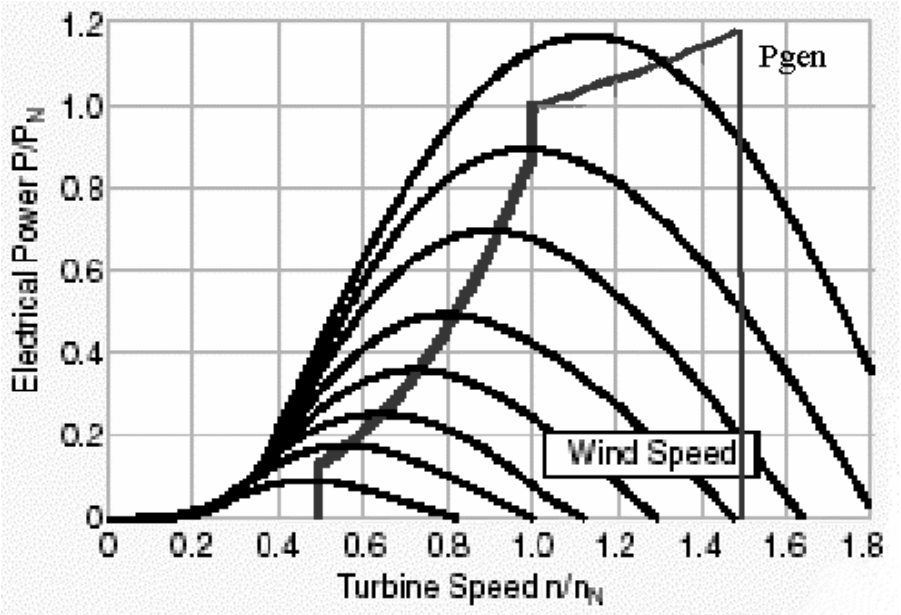

Figure 2-4: Operating region of WECS with doubly–fed induction machine

Figure 2-5 presents a road map on how to convert mechanical energy into electrical energy applying the optional control concept of variable speed, i.e. conversion of a mechanical torque input at variable speed to an electrical power output at fixed frequency. These concepts have been illustrated in Fig.2-6.

II.3.2.3. Comparison of wind turbine generating systems

In this section, the three main wind energy conversion systems; constant speed constant frequency, variable speed variable frequency (VSCF) using doubly fed induction generator and direct drive system VSCF using permanent magnet machines are compared. Each of these wind energy conversion systems has some unique advantages and drawbacks. The advantage of a constant speed system is that it is relatively simple and cheap. Therefore, the list price of constant speed turbines tends to be lower than that of variable speed turbines. However, constant speed turbines must be more mechanically robust than variable speed turbines. Since the rotor speed cannot be varied, fluctuations in wind speed translate directly into drive train torque fluctuations, causing higher structural loads than with variable speed operation. This partly cancels the cost reduction achieved by using a relatively cheap generating system. Further, more noise can be a problem. Because the noise level is related to the blade tip speed and hence to the rotational speed of the rotor, which of course cannot be changed in constant speed turbines. This problem is, however, alleviated by using a generator whose number of pole pairs can be changed, allowing the turbine to run at lower rotational speed when wind speed is low.

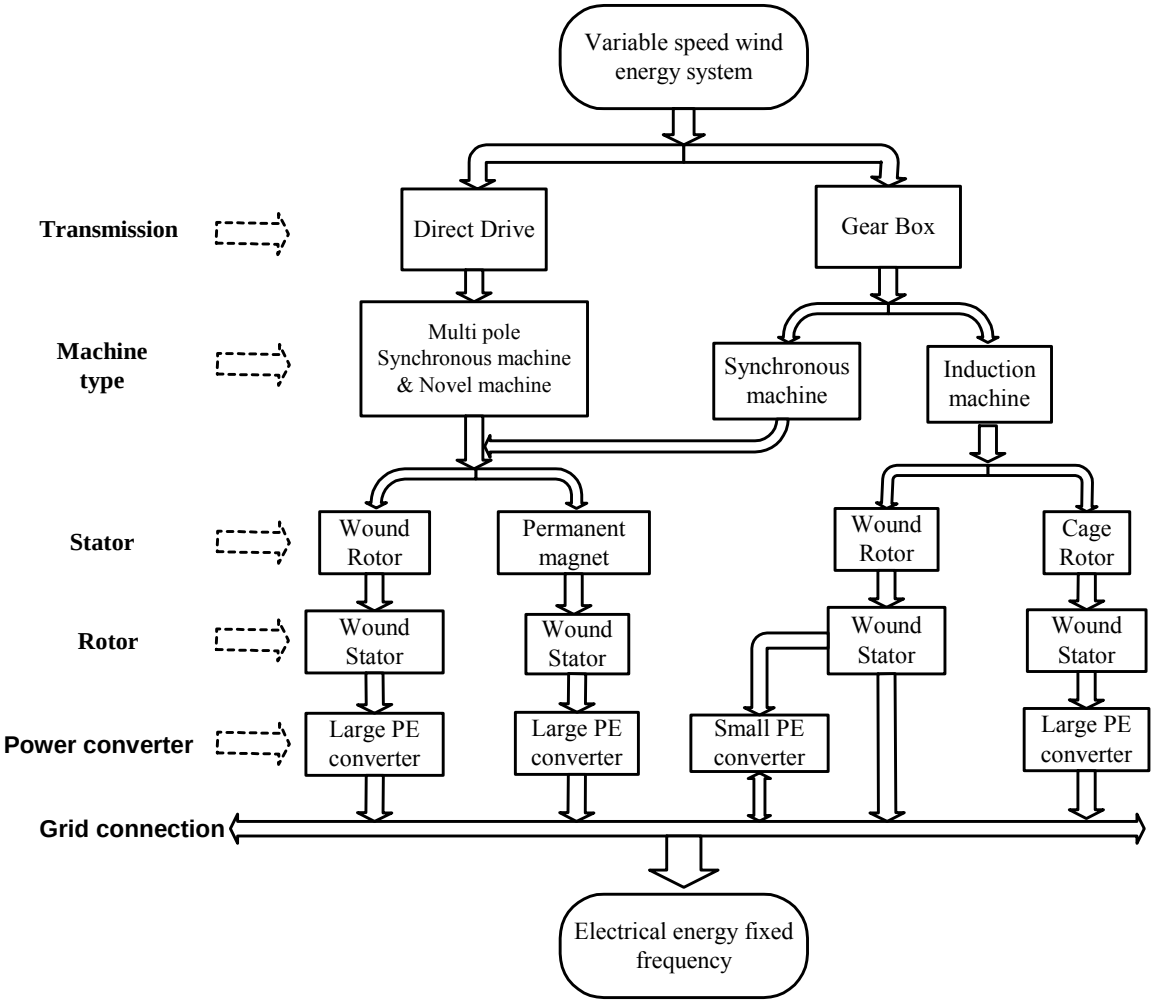

Figure 2-5: Conversion process of mechanical energy to electrical energy in variable speed wind energy conversion systems

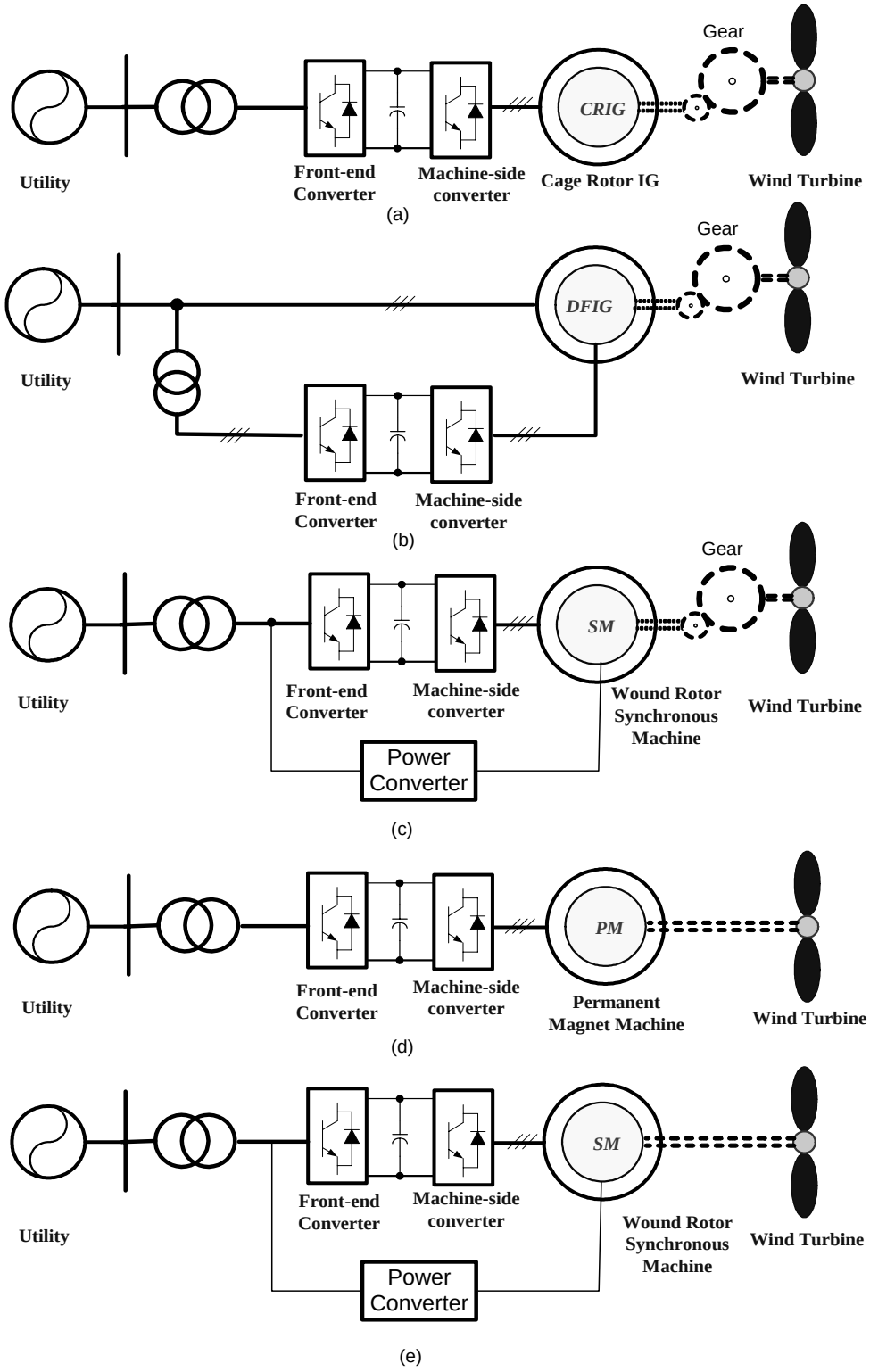

Figure 2-6: Concepts and wind turbine configuration in VSCF systems

From efficiency conversion point of view, the variable speed constant frequency systems are more desirable than constant frequency constant speed systems where the maximization of power conversion efficiency is just possible at certain wind speed. However, in variable speed conversion system turbine speed is allowed to vary with changes in wind speed to reach the maximum turbine efficiency at different wind speed. [29,30]. There is also less mechanical stress, because the rotor acts as a flywheel (storing energy temporarily as a buffer), reducing the drive train torque variations. Noise problems are reduced as well, because the turbine runs at low speed when there is little wind.

The main drawback of variable speed generating systems is complexity and cost of power electronics converters. However, using a variable speed conversion system can also give major savings in other subsystems of the turbine, such as lighter foundations in offshore applications, limiting the overall cost. Furthermore, the price of power electronic components is dropping steadily.

When comparing the two variable speed designs, it can be concluded that the advantages of the concept based on the doubly fed induction generator are that a more or less standard generator and a smaller and hence cheaper power electronics converter can be used. However, in doubly fed induction generator brushes are used for rotor excitation circuitry. This cause maintenance-intensive and potentially unreliable gearbox for doubly fed induction generator compared to direct drives systems.

Table 2-1: Advantage and drawbacks of wind energy conversion systems

	CSCF	VSCF	
		Doubly Fed	Direct Drive
Strength	Simple and robust; Less expensive; Electrically efficient; Standard generator.	Less mechanical stress; Less noisy; Aerodynamically Efficient; Standard generator; Small PE; Decouple control of active and reactive power; Torque pulsation reduction.	Less mechanical stress; Less noisy; Aerodynamically Efficient; No gearbox; Decouple control of active and reactive power; Torque pulsation reduction.
Weakness	Aerodynamically less efficient; Gearbox included; Noisy.	Electrically less efficient; Gearbox included; Expensive; Needs maintenance.	Electrically less efficient; Large converter; Expensive; Heavy and large Generator; Complex generator.

Electrical generators in direct drive systems comparing to the other systems are large, heavy and complex. Also power electronic converters in these systems are large which all of the generated power has to pass through. Instead, power electronic converters in doubly fed induction generator just regulate the slip power that is much smaller than actual power. In doubly fed generator the size of power converters can be reduced to 1/3. The advantages and drawbacks of the different generating systems are summarized in Table 2-1.

II.3.3. MARKET ASPECTS

Renewable energy has an increasing role to play in future worldwide energy supply. Another way of describing the state of the art technologies applied to wind turbines is to survey the supply rates of the manufacturers. The top 10 list of suppliers in 1999 according to (BTM Consults Aps, 2000) is presented in Table 2.2 and the two largest wind turbines employed concepts of each manufacturer are shown in Table 2.3. The particular configurations are illustrated in Fig.2-7. All the configurations presented in the table are 3-bladed and upwind wind turbines with tubular tower.

Table 2-2: The top 10 suppliers in 1999

Top 10 Suppliers		Sold MW 1999	Share in %	Accu. MW 1999	Share in %
1	NEG Micon	761	18.9	3034	21.0
2	Vestas	652	16.2	2530	17.5
3	Gamesa	494	12.3	853	5.9
4	Enercon	488	12.1	1553	10.7
5	Enron	360	8.9	1153	8.0
6	Bonus	338	8.4	1197	8.3
7	Nordex	306	7.6	638	4.4
8	Made	218	5.4	450	3.1
9	Ecotecnia	59	1.5	136	0.9
10	Dewind	58	1.4	86	0.6
	other	298	7.4	2839	19.6
	Total	4032	100	14469	100

Table 2-3: Applied concepts of top 10 suppliers in 1999

Top 10 Suppliers	Turbine Model	Config. Fig.2-5	Power control feature	Comments
NEG Micon	NM 2000/72	a	Active Stall	Two speed
	NM 1500/64	a	Stall	Two speed
Vestas	V80-2 MW	b	Pitch and variable speed	Range:905-1915 rpm
	V66-1.65	b	Pitch and optiSlip	Range:1500-1650 rpm
Gamesa	G52-850 kW	b	Pitch and variable speed	Range:900-1650 rpm
	G47-660 kW	b	Pitch and variable speed	Range:1200-1625 rpm
Enercon	E66-1.8 MW	e	Pitch and variable speed	Gearless,Range:10-22 rpm
	E58-1 MW	e	Pitch and variable speed	Gearless,Range:10-24 rpm
Enron Wind	1.5s-1.5 MW	b	Pitch and variable speed	Range:989-1798 rpm
	900s-900 kW	b	Pitch and variable speed	Range:1000-2000 rpm
Bonus	2 MW	a	Active Stall	Two speed
	1.3 MW	a	Active Stall	Two speed
Nordex	N80/2500 kW	b	Pitch and variable speed	Range:700 rpm to 1303 rpm
	N60/1300	a	Stall	Two speeds
Made	No information available			
Ecotenia	No information available			
Dewind	D4- 600kW	b	Pitch and variable speed	Range:905-1915 rpm
	D6-1.25 MW	b	Pitch and variable speed	Range:905-1915 rpm

The manufacturers applying configuration “c” and “d” are all using IGBT-based converters. Thus, the present state-of-art of large wind turbines includes:

- Active stall with a two-speed induction generator,
- Pitch control combined with variable speed. The variable speed concept is mainly realized using configuration “c”, i.e. the doubly fed induction generator with a rotor connected IGBT-based frequency converter,
- Only one of the top 10 manufacturers is building a gearless (variable speed) wind turbine.

The most significant reason for the popularity of the doubly fed induction generator concept is the relatively small size of power converter – approximately 10-25 % of nominal turbine power – which is a cost effective solution in order to obtain variable speed. Meanwhile, one drawback is the inevitable application of slip-rings. However, they have been significantly improved over the past several years.

II.4. DESCRIPTION OF THE PROPOSED METHOD

An Integrated Doubly-fed Electric Alternator/Active filter (IDEA) for variable speed wind energy conversion systems is proposed. The IDEA, a viable solution towards energy crisis and power quality issue, is capable of capturing the maximum energy from fluctuating wind, controlling the reactive power and compensating for the harmonics currents of the utility. Proper dynamically excitation of the rotor circuitry of the wound rotor induction machine is made by a current regulated voltage source power converter. The proposed control strategy of this power converter is based on the stator flux field

oriented control and both fundamental and harmonics currents are controlled. This new system is proposed to capture both the maximum power of wind energy, and also improve the power quality of utility grid. It is well known that nonlinear loads draw non-sinusoidal currents from the utility and contribute to numerous power system problems. The currents drawn from the ac lines are rich in harmonics with the order of $6k \pm 1$ that is 5, 7, 11, 13, etc. These harmonics currents result in lower power factor, overheating and electromagnetic interference (EMI).

The block diagram of the proposed alternator/active filter is shown in Fig. 2-7. The IDEA is a grid connected variable speed wind energy conversion system. It is assumed that the total harmonics currents demanded by nonlinear loads connected to the utility are either estimated or sampled through the current sensors that contain the 5^{th}, 7^{th}, 11^{th}, 13^{th}, etc. This total harmonics current makes the command harmonics current for the rotor side power converter. The command power P* is also generated in regard to the wind speed and wind turbine characteristics. The reactive power command Q* is also set in regard to the utility reactive power demand. Having these input commands and applying the control strategy to current regulated voltage source inverter, the rotor side power converter provides the proper rotor excitation. The IDEA is controlled to generate the optimized active power, and compensate reactive power and cancel harmonics currents of the grid independently. Output current of the IDEA will be a combination of the fundamental and harmonics currents. The generated harmonics will compensate for the harmonic currents needed by the non-linear load. The fundamental current controls the active and reactive powers. So, the utility current will be a pure sine wave.

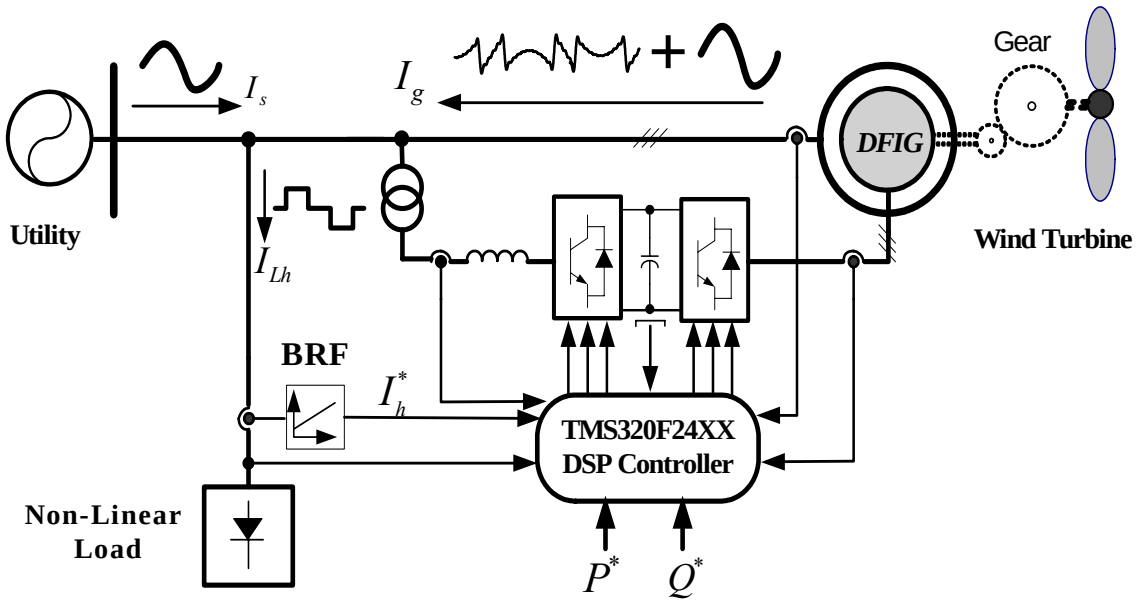

Figure 2-7: Block diagram of the proposed IDEA for wind power conversion system

Decoupled control of the active and reactive powers and harmonic compensation are met. As it is shown in this block diagram, the nonlinear load current is sampled through the current sensors, and then using a band rejection filter the fundamental current is removed. This makes the command harmonics current, I_h^*. A stator flux field oriented control is developed to control the DFIG. Decoupled control of the active and reactive powers and harmonic compensation are met and suitable current is generated to supply the rotor circuit. In this system, while rotor side power converter controls the proper excitation of IDEA, the front- end power converter allows the bi-directional power flow in the rotor circuitry and operation at sub synchronous speed and super synchronous speed modes.

The advantages of the proposed approach are:

- Adjustable speed control of wind turbine in order to capture maximum wind energy, while independently control the reactive power,
- Compensation of the harmonics in the grid,
- Improving the power factor and reactive power control and totally improving power quality,
- The approach is rugged and can be adapted to low and medium voltage systems,
- The system can be controlled to simultaneously generate active green power, compensate for the reactive power and harmonics generated by the nonlinear loads in an industrial plant.

II.5. ANALYSIS OF THE PROPOSED INTEGRATED DOUBLY-FED ALTERNATOR/ ACTIVE FILTER (IDEA)

II.5.1. OPERATIONAL PRINCIPLE

The operation of whole system can be divided into two sections; front-end line side operation and electrical machine side operation as it is shown in Fig 2-8. The front-end power converter maintains the dc bus voltage at its rated value by controlling the power flow between the grid and the dc bus as well as maintaining the interface of the overall system to the grid at nearly unity power factor. Rotor side power converter excites the wound rotor induction machine to control generation of active power, reactive power compensation and harmonic cancellation of the grid.

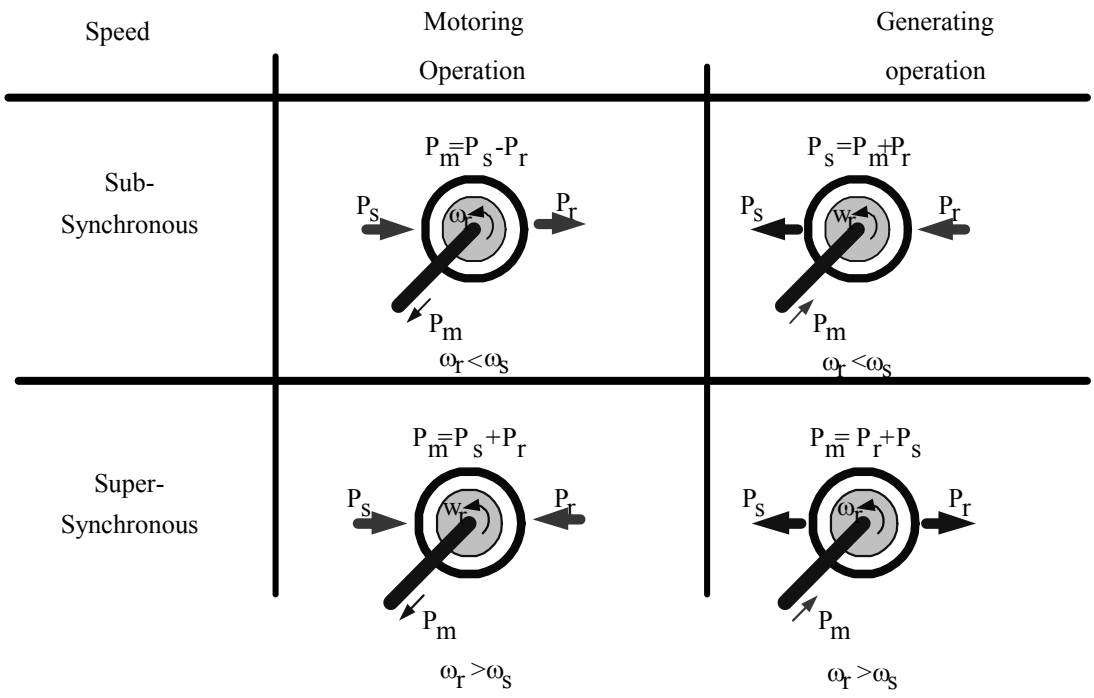

Figure 2-8:Power flow chart of DFIM modes of operation

A doubly fed induction machine (DFIM) is formed when a power converter is utilized in the rotor circuit of wound rotor induction machine. The DFIM is controlled by directing the power flow into and out of the rotor windings. As DFIM can operate as either a motor or a generator at sub-synchronous and super-synchronous speeds, there are four operational modes in which the DFIM operates. The principle of a DFIM control in these modes can be understood by the power flow diagrams given in Fig. 2-8. In these power flow charts, P_s is the stator power, P_r is the rotor power and P_m is the mechanical power. When DFIM is operating as a motor in the sub-synchronous or below synchronous speed, power is taken out of the rotor. This is the mode of operation that is known as slip power recovery. Now, if in motoring mode of operation, speed increases so that DFIM is operating at super-synchronous speed, the rotor power flow direction changes and slip power should be supplied to the rotor circuitry.

When the DFIM is operating as a generator in the sub synchronous speed, slip power and mechanical power are delivered to the rotor. If mechanical torque is increased so that DFIM operates at super synchronous speed, then both stator and rotor circuitry supply power to the grid. The wind energy conversion system arrangement using IDEA has been shown in Fig. 2-7, with employing two back-to-back power converters, is capable of bi-directional power flow allowing sub-synchronous and super synchronous mode of generating operations. During sub-synchronous generation, the rotor circuit absorbs the fraction of power generated by the stator windings (slip power), whereas under a super-synchronous operation, both stator and the rotor feed in power to the grid.

Thus, if the stator generates 1 pu at slip of s pu, then the total generated power will be (1+s) pu. The converter rating in this system depends on the range of operating speed. Assuming 50% pu slip on either side of the synchronous speed, the power converter can be downsized to half of the rated power of the generator.

The operation region of the wind energy conversion systems using IDEA is shown in Fig. 2-9. In this figure, the speed of operation is limited to the range of 0.5 pu to 1.5 pu. When the wind velocity exceeds the cut-in value, the system is allowed to accelerate until the generator shaft speed reaches 0.5 pu.

The system is connected to the grid at this moment and the rotor side control is activated. During this operation, if the generator power falls below P_{min} (corresponds to maximum power locus at V1 m/s wind velocity), the rotor speed is maintained at 0.5 pu by operating in speed control mode. Once the power exceeds P_{min}, the system goes into peak-power tracking mode up to the synchronous speed. At this point, the stator of IDEA has reached its rated power and the rotor power is negligible as slip is zero. This also corresponds to the rated torque of IDEA. From synchronous speed to 1.5 pu, the machine operates at constant rated torque with slip power recovery from rotor circuit. The total generated power follows a straight-line locus above the synchronous speed with an additional 0.5 pu power being generated from rotor circuit at speed of 1.5 pu. Therefore, operation up to a higher wind velocity can be achieved before the system goes to pitch control mode.

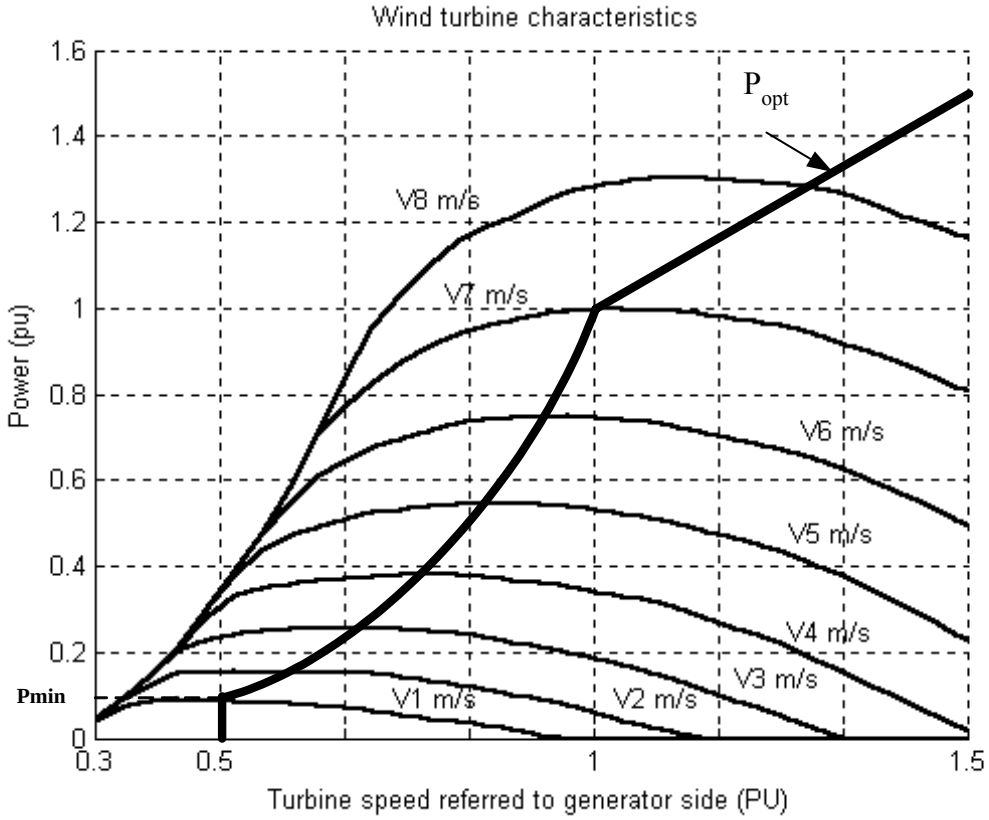

Figure 2-9: Operating region of WECS with IDEA

II.5.2. MATHEMATICAL MODEL OF GRID-CONNECTED DFIM

As it was discussed, a wound rotor induction (dubbed as doubly-fed) may deliver power both through stator and rotor windings. The main merit of Doubly Fed Induction Generator (DFIG) is its capability to deliver constant voltage and constant frequency over a wide range of speed, such as ±(20-50)% variation around synchronous speed. So the power ratting of power electronic converters and step-down transformer in rotor circuit are also decreased to (20-50)% PU of rated stator power.

It is apparent that the extensive amount of coupling between the six circuits of rotor and stator windings makes the analysis of this machine a rather formidable task. However, we are in a position to determine if there is any simplification that can be expected in these coupled equations. A very useful and compact format of the machine equations for a uniform air gap machines is obtained by using complex variable notation and employing complex space vectors. In the following, the mathematical model of DFIG with representing in complex space vectors format is developed.

The voltage equations describing the stator and rotor circuits can be written conveniently in matrix form as:

$$[V] = [R] * [i] + \frac{d}{dt}[\Lambda] \tag{2-10}$$

where :

$$[V] = [v_{as} \quad v_{bs} \quad v_{cs} \quad v_{ar} \quad v_{br} \quad v_{cr}]^T \tag{2-11}$$

$$[i] = [i_{as} \quad i_{bs} \quad i_{cs} \quad i_{ar} \quad i_{br} \quad i_{cr}]^T \tag{2-12}$$

$$[R] = diag[R_s \quad R_s \quad R_s \quad R'_r \quad R'_r \quad R'_r] \tag{2-13}$$

$$[\Lambda] = [\lambda_{as} \quad \lambda_{bs} \quad \lambda_{cs} \quad \lambda_{ar} \quad \lambda_{br} \quad \lambda_{cr}]^T = [L_{a_s b_s b_s a_r b_r c_r}(\theta_r)] * [i] \tag{2-14}$$

$$[L_{a_s b_s b_s a_r b_r c_r}(\theta_r)] =$$

$$\begin{bmatrix}
L_{ls}+L_{sm} & -\frac{1}{2}L_{sm} & -\frac{1}{2}L_{sm} & L_{sm}Cos\theta_r & L_{sm}Cos\left(\theta_r+\frac{2\pi}{3}\right) & L_{sm}Cos\left(\theta_r-\frac{2\pi}{3}\right) \\
-\frac{1}{2}L_{sm} & L_{ls}+L_{sm} & -\frac{1}{2}L_{sm} & L_{sm}Cos\left(\theta_r-\frac{2\pi}{3}\right) & L_{sm}Cos\theta_r & L_{sm}Cos\left(\theta_r+\frac{2\pi}{3}\right) \\
-\frac{1}{2}L_{sm} & -\frac{1}{2}L_{m} & L_{ls}+L_{sm} & L_{sm}Cos\left(\theta_r-\frac{2\pi}{3}\right) & L_{sm}Cos\left(\theta_r-\frac{2\pi}{3}\right) & L_{sm}Cos\theta_r \\
L_{sm}Cos\theta_r & L_{sm}Cos\left(\theta_r-\frac{2\pi}{3}\right) & L_{sm}Cos\left(\theta_r+\frac{2\pi}{3}\right) & L'_{lr}+L_{sm} & -\frac{1}{2}L_{sm} & -\frac{1}{2}L_{sm} \\
L_{sm}Cos\left(\theta_r+\frac{2\pi}{3}\right) & L_{sm}Cos\theta_r & L_{sm}Cos\left(\theta_r-\frac{2\pi}{3}\right) & -\frac{1}{2}L_{sm} & L'_{lr}+L_{sm} & -\frac{1}{2}L_{sm} \\
L_{sm}Cos\left(\theta_r-\frac{2\pi}{3}\right) & L_{sm}Cos\left(\theta_r+\frac{2\pi}{3}\right) & L_{sm}Cos\theta_r & -\frac{1}{2}L_{sm} & -\frac{1}{2}L_{sm} & L'_{lr}+L_{sm}
\end{bmatrix}$$

(2-15)

L_{ls}: Stator leakage inductance;

$L_{lr}^{'}$: Rotor leakage inductance referred to stator circuit;

L_{sm}: Self magnetizing inductance;

R_s: Stator resistance;

$R_r^{'}$: Rotor resistance referred to stator circuit;

θ_r: Rotor angular displacement;

Now consider the representation of the machine equation in complex variable form. Transformation of the voltage equation is indeed, almost trivial. Now, we define complex space vectors for real variables expressed in (2-10) with considering:

$$\underline{v}_{abcs} = \frac{2}{3}\left(v_{as} + a\, v_{bs} + a^2 v_{cs}\right)$$
$$\underline{v}'_{abcr} = \frac{2}{3}\left(v'_{ar} + a\, v'_{br} + a^2 v'_{cr}\right) \tag{2-16}$$

$$\underline{i}_{abcs} = \frac{2}{3}\left(i_{as} + a\, i_{bs} + a^2 i_{cs}\right)$$
$$\underline{i}'_{abcr} = \frac{2}{3}\left(i'_{ar} + a\, i'_{br} + a^2 i'_{cr}\right) \tag{2-17}$$

Where: $a = e^{j2\pi/3}$.

The vectors $\underline{v}_{abcs}$, $\underline{v}'_{abcr}$, $\underline{i}_{abcs}$, $\underline{i}'_{abcr}$ are complex space vectors representation of stator voltages, rotor voltages referred to the stator circuits, stator currents and rotor currents referred to the stator circuit, respectively. These vectors are located in two-dimensional complex plane where space vectors of voltage and current of the stator rotate with angular velocity of supply frequency and space vectors representing rotor voltage and rotor current spin with angular velocity of slip frequency.

If we multiply the second row of voltage matrix in (2-10) by 'a' and third row by 'a^2', and add the first three rows and multiply the entire result by 2/3, after some simplification, the stator voltage equations in complex space vector form will be obtained as:

$$\underline{v}_{abcs} = R_s \underline{i}_{abcs} + (L_{ls} + L_m) p\underline{i}_{abcs} + L_m (p\underline{i}'_{abcr}) e^{j\theta_r} + j\omega_r L_m \underline{i}'_{abcr} e^{j\theta_r} \tag{2-18}$$

where, $L_m = \frac{3}{2} L_{ms}$ is magnetizing inductance and $\omega_r = \frac{d\theta}{dt}$ represents the rotor angular velocity. In the same manner, we can find the rotor voltage equation in complex space vector form as following:

$$\underline{v}'_{abcr} = r'_r \underline{i}'_{abcr} + (L'_{lr} + L_m) p \underline{i}'_{abcr} + L_m p(\underline{i}_{abcs}) e^{-j\theta_r} - j\omega_r L_m \underline{i}_{abc} e^{-j\theta_r} \quad (2\text{-}19)$$

Note that the rotor variables are referred to stator circuit. While the complex vector approach to writing the machine equations results in a compact form, the essential sinusoidal coupling between the stator and rotor remains. This coupling can essentially be eliminated, however, if the stator and rotor equations are referred to a common frame of reference. In order to have a common frame of reference for both stator and rotor equations, one can suggest a rotating set of q-d axes rotating at an angular displacement of θ. The stator variables can be transformed to this arbitrary q-d reference frame using the following equations:

$$\begin{bmatrix} f_q \\ f_d \\ f_o \end{bmatrix} = T(\theta) \begin{bmatrix} f_a \\ f_b \\ f_c \end{bmatrix} \quad (2\text{-}20)$$

$$T(\theta) = \frac{2}{3} \begin{bmatrix} \cos\theta & \cos(\theta - \frac{2\pi}{3}) & \cos(\theta + \frac{2\pi}{3}) \\ \sin\theta & \sin(\theta - \frac{2\pi}{3}) & \sin(\theta + \frac{2\pi}{3}) \\ 1/\sqrt{2} & 1/\sqrt{2} & 1/\sqrt{2} \end{bmatrix} \quad (2\text{-}21)$$

where $T(\theta)$ is the transformation matrix and f represents currents, voltages or flux linkages. The complex variables may be decomposed in plane along two orthogonal d and q axes rotating at speed of ω to obtain the d-q park model where q axis is real axis and d- axis will be imaginary axis. We can define a general rotating axis complex vector transformation,

$$\underline{f}_{qds} = f_{qs} - j f_{ds} = \frac{2}{3} e^{-j\theta} \underline{f}_{abcs} \quad (2\text{-}22)$$

$$\underline{f}_{qdr} = f_{qr} - j\, f_{dr} = \frac{2}{3} e^{-j(\theta-\theta_r)}\, \underline{f}_{abcr} \tag{2-23}$$

Now these equations can be used to transform the machine complex vector equations to a rotating reference frame. To reduce the complexity of the voltage equations, the reference frame is attached to the stator flux and is denoted as the excitation 'e' or synchronous reference frame. The q-axis relay the real axis and is in phase with phase a–axis. Now, the reference frame is rotating with angular velocity ω_e, so synchronous angular displacement will be $\theta_e = \omega_e t$. Multiply (2-10) by $e^{-j\theta_e}$ and after some simplification yields:

$$\underline{v}_{qds} = R_s \underline{i}_{qds} + (L_{ls} + L_m) p \underline{i}_{qds} + L_m p \underline{i}'_{qdr} + j\,\omega_e \left[(L_{ls} + L_m) \underline{i}_{qds} + L_m \underline{i}'_{qdr} \right] \tag{2-24}$$

Here, we define slip angular displacement θ_s as:

$$\theta_s = \int (\omega_e - \omega_r) \cdot dt = \theta_e - \int \omega_r \cdot dt = \theta_e - \theta_r \tag{2-25}$$

where ω_r is rotor angular velocity. So we have:

$$\frac{d\theta_s}{dt} = \omega_e - \omega_r = S\,\omega_e \tag{2-26}$$

and then:

$$\theta_s = S\,\omega_e t + \delta \tag{2-27}$$

δ is the rotor voltage phase angle. In the same manner, using (2-27) and noting that θ-θr in this equation in synchronous reference frame will be denoted as $\theta_s = S\,\omega_e t + \delta$, the

rotor circuit equations in complex format and in synchronous reference frame can be represented by:

$$\underline{v}'_{qdr} = R'_r \underline{i}'_{qdr} + (L'_{lr} + L_m) p \underline{i}'_{qdr} + L_m p \underline{i}_{qds} + jS\omega_e \left[(L'_{lr} + L_m) \underline{i}'_{qdr} + L_m \underline{i}_{qds} \right] \tag{2-28}$$

Also, DFIG is connected to the grid with an infinite power bus voltage, the three-phase stator voltages will be:

$$\begin{aligned} v_{as} &= \sqrt{2} V_s \cos(\omega_e t) \\ v_{bs} &= \sqrt{2} V_s \cos(\omega_e t - \frac{2\pi}{3}) \\ v_{cs} &= \sqrt{2} V_s \cos(\omega_e t - \frac{4\pi}{3}) \end{aligned} \tag{2-29}$$

The d-q stator voltages in synchronous reference frame are:

$$v_{qs}^e = \underline{v}_{qds} = \sqrt{2} V_s \tag{2-30}$$

$$v_{qs}^e = 0 \tag{2-31}$$

At constant speed and in case of no harmonic compensation, the rotor voltage can be expressed as:

$$\begin{aligned} v_{ar} &= \sqrt{2} V_r \cos(S\omega_e t - \delta) \\ v_{br} &= \sqrt{2} V_r \cos(S\omega_e t - \frac{2\pi}{3} - \delta) \\ v_{cr} &= \sqrt{2} V_r \cos(S\omega_e t - \frac{4\pi}{3} - \delta) \end{aligned} \tag{2-32}$$

In the same manner, the rotor voltage components in two-phase synchronous reference frame are obtained as:

$$v_{qr}^{e} = \sqrt{2}\, V_r \cos\delta \tag{2-33}$$

$$v_{dr}^{e} = -\sqrt{2}\, V_r \sin\delta \tag{2-34}$$

$$\underline{v}'_{qdr} = \sqrt{2}\, V_r \angle\delta \tag{2-35}$$

As it is clear, in synchronous reference frame, the d-q stator voltage components of the DFIG are dc quantities. Under steady state and constant rotor phase angle δ and without harmonic compensation, the rotor voltages are also dc values.

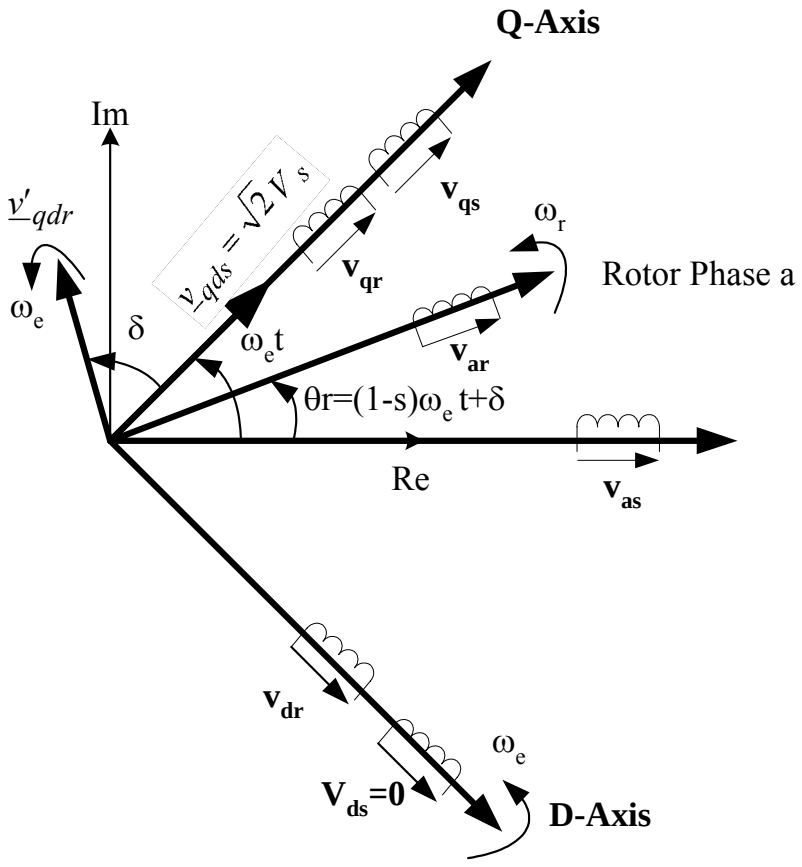

Figure 2-10: The d-q synchronous reference frame and stator and rotor complex space vector voltages

The angle of δ maybe considered as the power angle and thus the DFIG operates as synchronous machine. The rotor voltage magnitude V_r and power angle δ with respect to stator voltage in synchronous reference frame (rotor phase angle) and slip S are thus the key factors which determine the generating or motoring mode of machine operation and performance. The proper relationships between V_r, δ for various speeds (slips) represent the fundamental operating modes. The rotor and synchronous angular phase displacements and two-phase synchronous reference frame including the rotor and stator complex space vector voltages have been shown in Fig. 2-10.

II.5.3. EQUIVALENT CIRCUITS OF IDEA

Equations (2-15) and (2-19) will lead to a general complex space vector equivalent circuit. As these variables are represented in synchronous reference frame, $\underline{i}'_{qdr}$ and $\underline{i}_{qds}$ are dc values in steady state so the operator of P is equal to zero. The complex space vector equivalent circuit at steady state for fundamental voltage of IDEA is shown in Fig. 2-11.

Now we are at the point to obtain the harmonic equivalent circuit of IDEA. As it was shown in Fig. 2-7, IDEA is directly connected to the grid with a sinusoidal voltage waveform for it. Harmonic slip of n is denoted as S_n and is defined as follows:

$$S_n = \frac{\omega_n - \omega_r}{\omega_n} \tag{2-36}$$

where: $\omega_n = n\,\omega_e$.

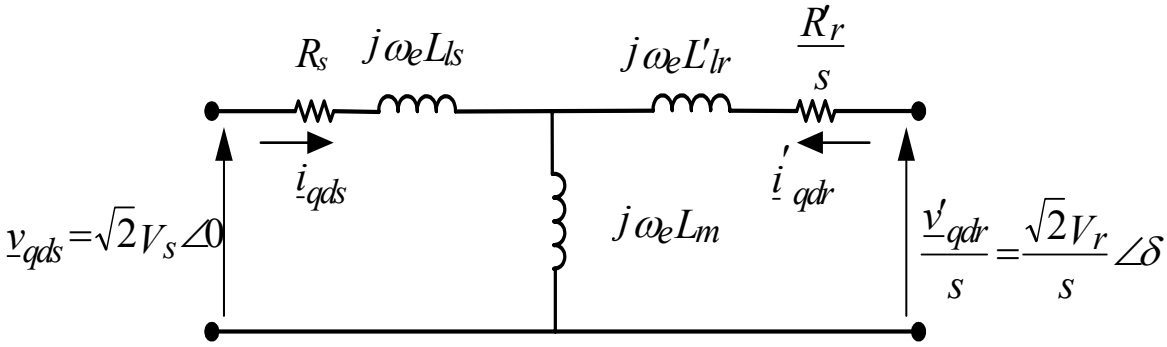

Figure 2-11: IDEA complex space vector equivalent circuit

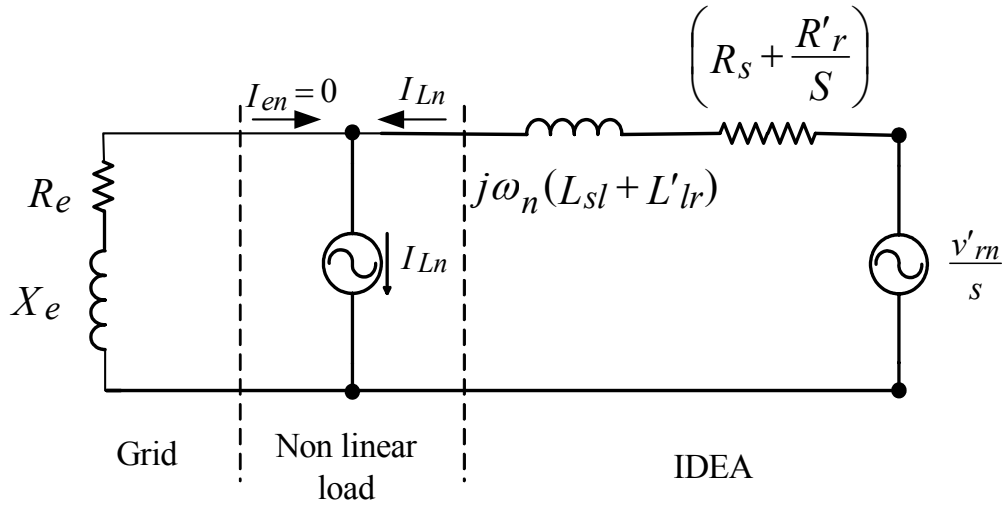

Figure 2-12: Harmonic equivalent circuit of the compensation system

Harmonic equivalent circuit of the compensation circuit is shown in Fig. 2-12. In this figure, v'_{rn} is the amplitude of harmonic n of rotor side power converter output voltage. Nonlinear load is modeled as current source with magnitude of I_{ln}. The equivalent circuit of the grid consists of a series resistor R_e and reactance of $X_e = n\omega_e L_e$ for a pure sinusoidal voltage waveform.

II.5.4. CONTROL OF ROTOR-SIDE POWER CONVERTER

Rotor side power converter is used to control excitation of IDEA and hence to control the generating active power, reactive power compensation and harmonic cancellation in the grid. A current regulated voltage source inverter is employed. In following an extended stator flux field oriented control is developed.

II.5.4.1. Stator flux oriented control

As it was discussed in the previous sections, all rotor and stator variables are transferred to two-phase synchronous reference frame. This simplifies the voltage equation and provides flexibility to develop the control law. In the following equations, the stator quantities are marked with subscript‘s’ and the rotor quantities are marked with subscript ‘r’. The scalar form of the stator and rotor voltages and flux linkages in the two-phase synchronous reference frame are developed. Stationary d-q reference frame and synchronous reference frame are shown in Fig. 2-13.

The flux linkages of stator and rotor in excitation reference frame can be written as:

$$\lambda_{qs}^{e} = L_s i_{qs}^{e} + L_m i_{qr}^{e} \tag{2-37}$$

$$\lambda_{ds}^{e} = L_s i_{ds}^{e} + L_m i_{dr}^{e} \tag{2-38}$$

$$\lambda'^{e}_{qr} = L'_r i'^{e}_{qr} + L_m i'^{e}_{qs} \tag{2-39}$$

$$\lambda'^{e}_{dr} = L'_r i^{e}_{dr} + L_m i'^{e}_{ds} \tag{2-40}$$

where:

$$L'_r = L'_{\ell r} + L_m$$

$$L_s = L_{\ell s} + L_m$$

Stator and rotor voltages in the d-q excitation reference frame in scalar form can be shown as:

$$v_{qs}^{e} = R_s i_{qs}^{e} + \omega_e . \lambda_{ds}^{e} + P . \lambda_{qs}^{e} \tag{2-41}$$

$$v_{ds}^{e} = R_s i_{ds}^{e} - \omega_e . \lambda_{qs}^{e} + P . \lambda_{ds}^{e} \tag{2-42}$$

$$v'^{e}_{qr} = R'_r i'^{e}_{qr} + (\omega_e - \omega_r) . \lambda'^{e}_{dr} + P . \lambda'^{e}_{qr} \tag{2-43}$$

$$v'^{e}_{dr} = R'_r i'^{e}_{dr} - (\omega_e - \omega_r) . \lambda'^{e}_{qr} + P . \lambda'^{e}_{dr} \tag{2-44}$$

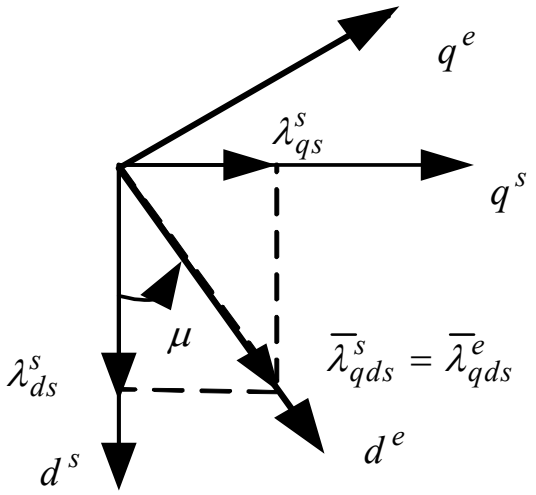

Figure 2-13: The d-q stationary and excitation reference frame for DFIG

If the stator flux vector is aligned with the d-axis in the synchronously rotating reference frame, then $\lambda^e_{qs} = 0$, and the rotor currents components can be shown as:

$$i^e_{qr} = -\frac{L_s}{L_m} \cdot i^e_{qs} \tag{2-45}$$

$$i^e_{dr} = -\frac{L_s}{L_m} \cdot i^e_{ds} + \frac{1}{L_m} \lambda^e_{ds} \tag{2-46}$$

Now, if we substitute these current components in the rotor flux linkage equations given by (2-37) and (2-38), we will get:

$$\lambda^e_{dr} = \sigma L_r i^e_{dr} + \frac{L_m}{L_s} \cdot \lambda^e_{ds} \tag{2-47}$$

$$\lambda^e_{qr} = \sigma L_r i^e_{qr} \tag{2-48}$$

where: $\sigma = 1 - \dfrac{L_m^2}{L_r L_s}$

If we substitute these equations into the rotor voltage equations in the excitation reference frame, (2-43) and (2-44), we have:

$$v_{qr}^{e} = r_r i_{qr}^{e} + \omega_{slp}\sigma L_r i_{dr}^{e} + \omega_{slp}\frac{L_m}{L_s}\lambda_{ds}^{e} + \sigma L_r \frac{d}{dt} i_{qr}^{e} \tag{2-49}$$

$$v_{dr}^{e} = r_r i_{dr}^{e} - \omega_{slp}\sigma L_r i_{qr}^{e} + \sigma L_r \frac{d}{dt} i_{dr}^{e} + \frac{L_m}{L_s}\frac{d}{dt}\lambda_{ds}^{e} \tag{2-50}$$

where: $\omega_{slp} = \omega_e - \omega_r$

It is clear that due to the presence of the rotational EMF terms, there are cross couplings between the d and q axes. The current loop dynamics along the two axes can be made independent of each other by compensating for these cross coupling terms. However, as the slip range is limited and the contributions of these terms are rather weak. Also the stator flux is influenced by the grid voltage and is constant. Therefore, the transformer EMF term depending on its derivative in (2-49) and (2-50) can be ignored. Control loop design can be proceed as follows:

$$v_{qr}^{e*} = \left(k_{pr} + k_{ir}\int\right)\left(i_{qr}^{e*} - i_{qr}^{e}\right) + \omega_{slp}\sigma L_r i_{dr}^{e} + \omega_{slp}\frac{L_m}{L_s}\lambda_{ds}^{e} \tag{2-51}$$

$$v_{dr}^{e*} = \left(k_{pr} + k_{ir}\int\right)\left(i_{dr}^{e*} - i_{dr}^{e}\right) - \omega_{slp}\sigma L_r i_{qr}^{e} \tag{2-52}$$

The Variables v_{qr}^{e*} and v_{dr}^{e*} are the rotor command voltages in two phase excitation reference frame applied to the rotor side power converter. Rotor current command components in excitation reference frame are denoted as i_{qr}^{e*} and i_{dr}^{e*}. Rotor current components in the excitation reference frame are regulated through the control loop.

Next task will be to calculate the command rotor currents in d-q excitation reference frame.

II.5.4.2. Quadrature and direct rotor current command

Quadreature and direct rotor current command can be derived from the active and reactive power references P*, Q* and harmonic currents needed for compensation of non-linear load current. Rotor currents command components in the excitation reference frame i_{qr}^{e*} and i_{dr}^{e*} can be derived as follow:

$$i_{qr}^{e*} = i_{qr-active}^{e*} + i_{qrh}^{e*} \tag{2-53}$$

$$i_{dr}^{e*} = i_{dr-reactive}^{e*} + i_{drh}^{e*} \tag{2-54}$$

Rotor current command in the d-axis is combination of two commands. Decoupled control of the active and reactive power is performed by the reference currents $i_{qr-active}^{e*}$, $i_{dr-reactive}^{e*}$ respectively, and harmonic compensation is controlled by i_{qrh}^{e*} and i_{drh}^{e*}. Quadrature and direct rotor harmonics currents demands can be found using (2-45) and (2-46) as follow:

$$i_{qrh}^{e*} = -\frac{L_s}{L_m} \cdot i_{qLh}^{e} \tag{2-55}$$

$$i_{dr}^{e*} = -\frac{L_s}{L_m} \cdot i_{dLh}^{e} + \frac{1}{L_m} \lambda_{ds}^{e} \tag{2-56}$$

where i_{qLh}^{e} and i_{dLh}^{e} are harmonics current drawn by the non-linear load transferred to the q-d excitation reference frame.

Electromagnetic torque in terms of stator variables in the synchronously rotating reference frame is:

$$T_{em} = \frac{3}{2}\frac{P}{2}\mathrm{Im}\left\{\bar{i}^{e}_{qds}\,\overline{\Lambda}^{e*}_{qds}\right\} = \frac{3}{2}\frac{P}{2}\left(\lambda^{e}_{ds} i^{e}_{qs} - \lambda^{e}_{qs} i^{e}_{ds}\right) \tag{2-57}$$

If the stator flux vector is aligned with the d-axis in the synchronously rotating reference frame, then $\lambda^{e}_{qs} = 0$ and the torque controller can be summarized as:

$$T_{em} = \frac{3}{2}\frac{P}{2}\lambda^{e}_{ds} i^{e}_{qs} \tag{2-58}$$

Stator active and reactive powers are calculated in terms of space vectors by the stator voltage and current in a general reference frame (a) as:

$$P_s = \frac{3}{2}\left(v^{a}_{ds} i^{a}_{ds} + v^{a}_{qs} i^{a}_{qs}\right) \tag{2-59}$$

$$Q_s = \frac{3}{2}\left(v^{a}_{qs} i^{a}_{ds} - v^{a}_{ds} i^{a}_{qs}\right) \tag{2-60}$$

Now, as IDEA has been connected to grid, we can consider a sinusoidal voltage source for stator. So in excitation reference frame we have: v^{e}_{ds}=0 and v^{e}_{qs}=v_m where v_m is the peak magnitude of grid voltage. Applying these constraints and substituting for them in active and reactive power (2-59) and (2-60) in excitation reference frame we will get:

$$P^{*}_{s} = \frac{3}{2}\left(v_m i^{*e}_{qs}\right) \tag{2-61}$$

$$Q^{*}_{s} = -\frac{3}{2}\left(v_m i^{*e}_{ds}\right) \tag{2-62}$$

If we substitute (2-45) and (2-46) for stator current components:

$$P_s^* = -\frac{3}{2}\left(v_m \frac{L_m}{L_s} i_{qr-active}^{*e} \right) \tag{2-63}$$

$$Q_s^* = -\frac{3}{2} v_m \left(\frac{\lambda_{ds}^e - L_m i_{dr-reactive}^{*e}}{L_s} \right) \tag{2-64}$$

Then we have achieved decoupled control of active and reactive power of the stator In case of wind-power generation, P_s^* is derived in regard to wind speed and turbine characteristics with applying optimum operating point tracking to provide maximum power capture from the wind energy. The methods for optimum operating point tracking will be discussed in the next section. Reactive power command Q_s^* is set by the grid demand.

II.5.4.3. Optimum power point tracking operation of IDEA

The mechanical power and mechanical torque extracted from the wind was modeled in section II.3.1 and is repeated here for convenience:

$$P_{mech} = \frac{\rho}{2} \cdot \pi \cdot R^2 \cdot C_p(\lambda, \beta) \cdot v_w^3 \tag{2-65}$$

$$T_{mech} = \frac{\rho}{2} \cdot \pi \cdot R^3 \cdot C_t(\lambda, \beta) \cdot v_w^2 \tag{2-66}$$

A family of characteristics representing output power and developed torque as function of turbine speeds can be deduced from aerodynamic efficiency $Cp(\beta,\lambda)$ and tip speed ratio λ. It is obvious that the captured power can be maximized at any wind speed if the aerodynamic efficiency $Cp(\beta,\lambda)$ is constrained to remain at its maximum value.

The output energy of wind turbine depends on the method of tracking the peak power points on the turbine characteristics due to fluctuating wind conditions. Optimal power point tracking to capture maximum energy of wind is derived from the power-speed characteristics of a given turbine. The turbine blade is characterized by particular Cp -λ and β. The role of optimum power operating tracking system is to maintain the optimal operation. The conventional method is to generate control law for the target generator power as cubic function of the angular velocity of turbine shaft ω_t:

$$P_{opt} = K_{opt}\omega_t^3 \tag{2-67}$$

The generated power is controlled by field-oriented control as discussed previously. The parameter K_{opt} is given by the following equation:

$$K_{opt} = 0.5.C_{p\max}.\rho.A.\left(\frac{R}{\lambda_{opt}}\right)^3 \tag{2-68}$$

where ρ is the air density, A is the swept area of the turbine and R is the radius of turbine blade. The P_{opt} defines the maximum energy capture shown in Fig. 2-9 and the objective of a tracking control is to keep the turbine operating to satisfy maximum captured power as the wind varies. For wind velocities higher than rated, the capturing energy by turbine must be limited by applying pitch control or driving the machine to the stall points. A general method for achieving optimum operating point tracking is called current-mode control. Given a shaft speed measurement, an electrical torque or electrical power can be imposed on the IDEA according to (2-68) after compensation for transmission friction losses:

$$P_{opt}^{*} = K_{opt}\,\omega_t^3 - B\,\omega_t^2 \tag{2-69}$$

$$i_{qr-active}^{*} = -\frac{2}{3}\frac{L_s}{L_m v_m} P_{opt}^{*} \tag{2-70}$$

As it was illustrated in previous section, the variable $i_{qr-active}^{*}$ will be imposed on control method of rotor-side power converter. But when the output power of IDEA falls bellow P_{min} shown in Fig. 2-9 corresponding to the maximum power point at wind velocity V1 m/s, the system goes to speed mode control. This method has been explained in [31-32]. The author [31] has shown that designing a speed observer is feasible and that significantly improved power point tracking may be obtained over the current-control method. In [32], a method of tracking the peak power in a wind energy conversion system has been proposed, which is independent of the turbine parameters and air density. The algorithm searches for the peak power varying the speed in the desired direction.

In this dissertation, as it was previously explained, the optimum power point tracking is based on current mode control if the power of turbine is greater than P_{min} in Fig. 2-10. And if the power of turbines falls below of P_{min}, the system goes to speed mode control method.

II.5.4.4. Block diagram of quadrature and direct rotor current commands generation

The block diagram of quadarature and direct rotor currents commands generation is shown in Fig. 2-14. In this method, wind velocity is measured and if it is higher than

the cut-in value the system goes to current mode control. Reference active power, P* is generated by a look-up table in regard to turbine characteristics. This will generate the active power command $i^*_{qr-active}$. If the wind turbine power falls below P_{min}, the speed control mode is activated and using speed regulator, the active power command is obtained.

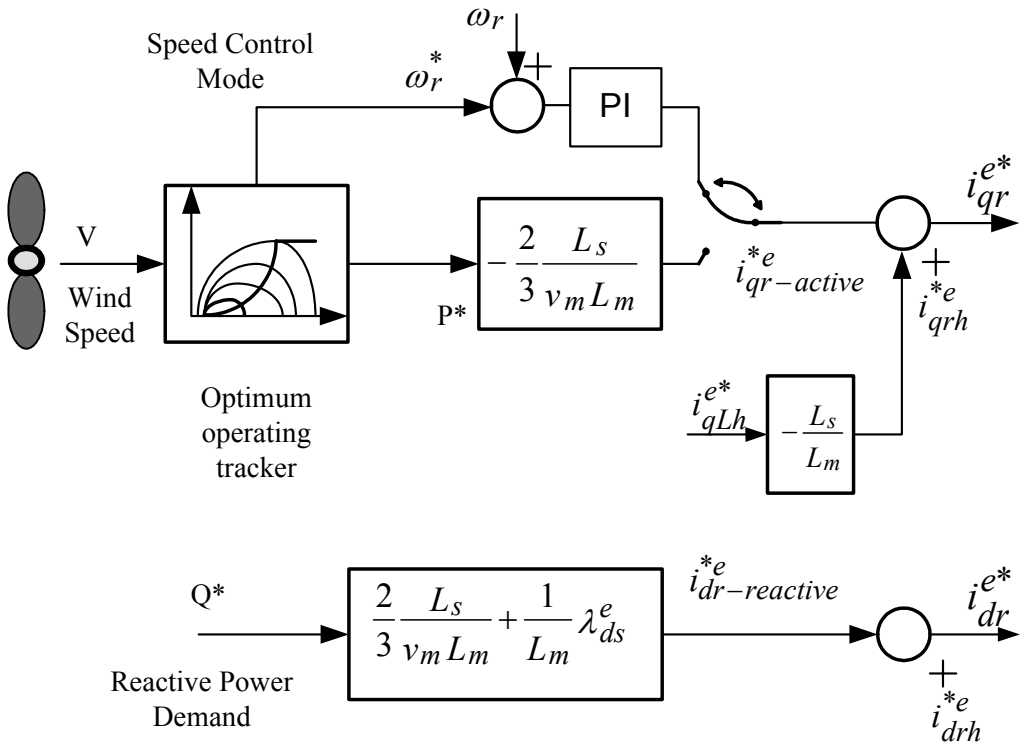

Figure 2-14: Quadrature and direct rotor currents commands generation

II.5.4.5. Stator flux angle calculator

The stator flux linkages components in the stationary reference frame can be calculated by:

$$\lambda_{qs}^{s} = \int (v_{qs}^{s} - r_s i_{qs}^{s}) dt \tag{2-71}$$

$$\lambda_{ds}^{s} = \int (v_{ds}^{s} - r_s i_{ds}^{s}) dt \tag{2-72}$$

Hence, the stator flux vector and the stator flux angle are given by:

$$\lambda_{ds}^{e} = \lambda_{qds}^{s} = \sqrt{(\lambda_{qs}^{s})^2 + (\lambda_{ds}^{s})^2} \tag{2-73}$$

$$\mu = \tan^{-1} \frac{\lambda_{qs}^{s}}{\lambda_{ds}^{s}} \tag{2-74}$$

II.5.4.6. Block diagram of the proposed control method for rotor–side power converter of IDEA

The block diagram of the proposed field oriented control method for the rotor side converter of the IDEA is shown in Fig. 2-15. The rotor side converter is a current regulated voltage source inverter. Active power reference is being generated with respect to the wind speed and turbine characteristics in response to maximum power point tracking method. Command current $i_{qr-active}^{*e}$ calculated by (2-70) is generated with respect to active power reference P*. The reactive power rotor current command is also generated using (2-64) with knowing reactive power demands Q*. Nonlinear load currents are sampled through current sensors and harmonic portion of them are extracted

by band rejection filter. These currents are transformed to two-phase excitation reference frame and will generate quadrature and direct rotor harmonics currents demands with employing (2-55) and (2-56). The commanded rotor d-q currents in the excitation reference frame are obtained by adding two components, one component is obtained by active and reactive power references and the other component is generated by harmonics components of the nonlinear load current which is induced in the rotor in the excitation reference frame. In this topology, while direct axis and quadrature axis are used to control the reactive power and active power generation respectively, the ac signal rides on the quadrature and the direct rotor current components and controls the harmonic compensation of the arbitrary non-linear load. Hence, decoupled controls of active power, reactive power and harmonic compensation are achieved.

In block diagram shown in Fig. 2-15 the rotor angular displacement θ_r is measured by a speed sensor.

II.5.4.7. Sensorless rotor position detection

Proper rotor current orientation with respect to the stator flux requires transformations between the stator and rotor coordinates. It means that the information of the instantaneous rotor position is necessary to implement correct field orientation. The following method is based on the simple trigonometric computations; therefore the estimation is possible instantaneously and the control on the fly is enforceable without any appreciable transient [34-36].

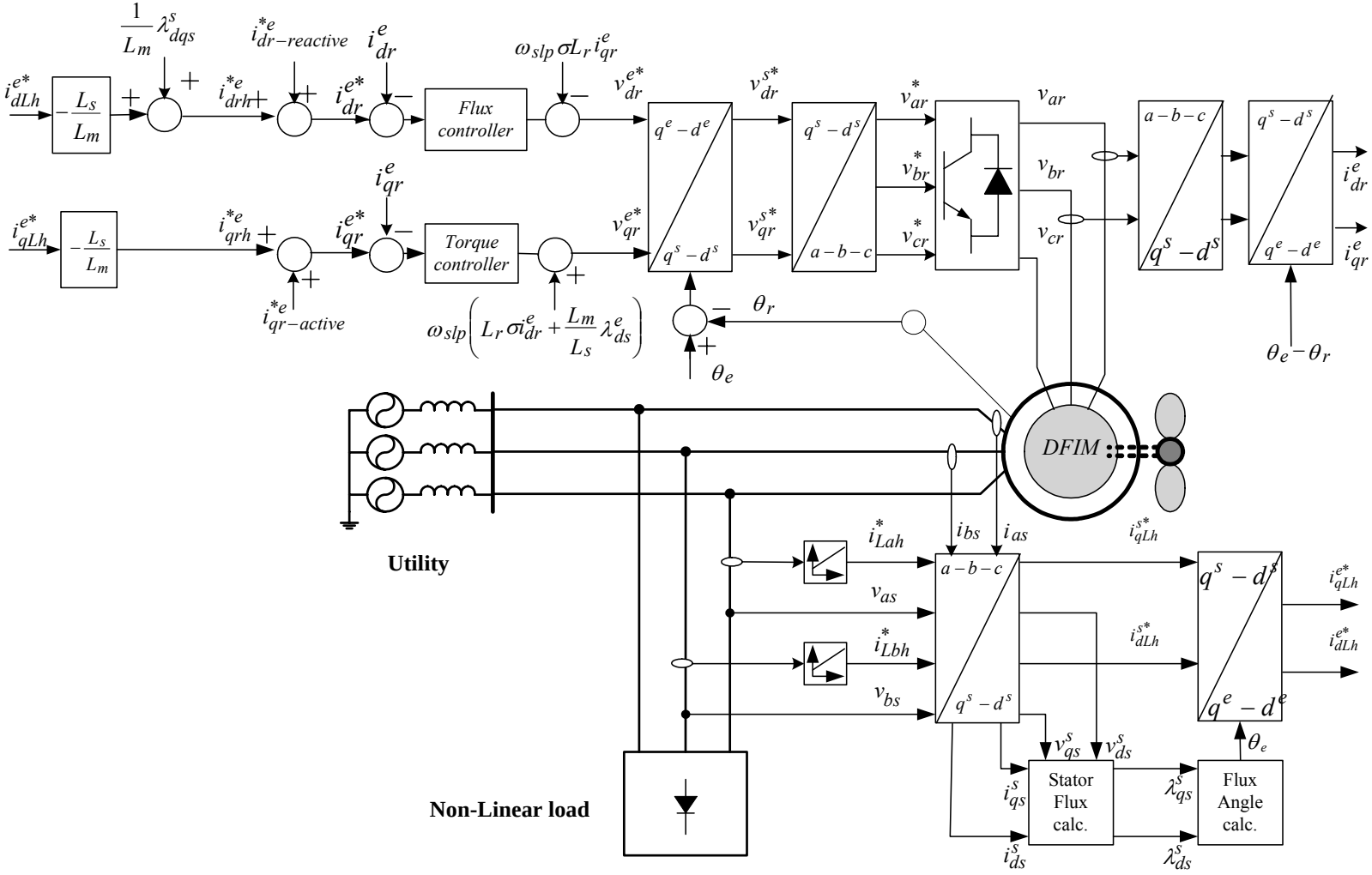

Figure 2-15: Proposed rotor side converter control of IDEA

The stator flux depends on the stator voltage and frequency of excitation. The d-q components of rotor current in the stationary reference frame can be obtained from:

$$i_{dr}^{s} = \frac{1}{L_m}\left(\int\left(v_{ds}^{s} - r_s i_{ds}^{s}\right)dt - (L_m + L_{ls}).i_{ds}^{s}\right) \tag{2-75}$$

$$i_{qr}^{s} = \frac{1}{L_m}\left(\int\left(v_{qs}^{s} - r_s i_{qs}^{s}\right)dt - (L_m + L_{ls}).i_{qs}^{s}\right) \tag{2-76}$$

These equations can be rewritten as follow:

$$i_{dr}^{s} = i_{dm}^{s} - (1+\sigma_s)i_{ds}^{s} \tag{2-77}$$

$$i_{qr}^{s} = i_{qm}^{s} - (1+\sigma_s)i_{qs}^{s} \tag{2-78}$$

Where, i^{s}_{dm} and i^{s}_{qm} are the magnetizing current in the stator reference frame. The absolute value of rotor vector current in the stator reference frame can be calculated as:

$$i_r = \sqrt{{i_{dr}^{s}}^{2} + {i_{qr}^{s}}^{2}} \tag{2-79}$$

$$\theta 1 = \tan^{-1}\frac{i_{qr}^{s}}{i_{dr}^{s}} \tag{2-80}$$

On the other hand, all the rotor currents are measurable. If we project these currents into two-phase orthogonal reference frame fixed on the rotor, we can write:

$$i_r = \sqrt{{i_{dr}^{r}}^{2} + {i_{qr}^{r}}^{2}} \tag{2-81}$$

$$\theta 2 = \tan^{-1}\frac{i_{qr}^{r}}{i_{dr}^{r}} \tag{2-82}$$

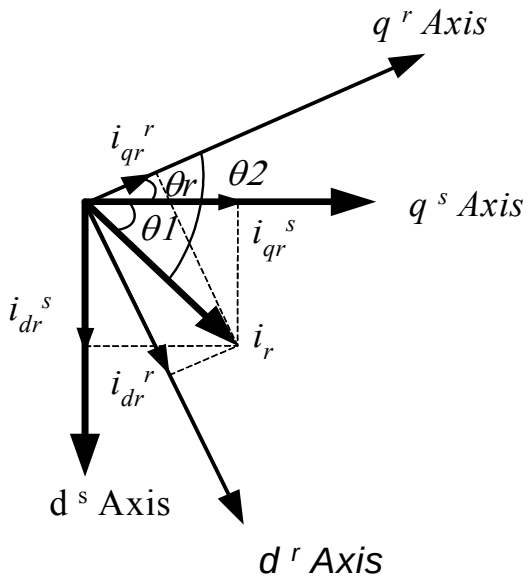

Figure 2-16: Rotor current vectors in the rotor and stator coordinates

The rotor current vectors in orthogonal d-q stationary and rotary reference frames are figured in Fig. 2-16. It can be inferred that the rotor current vector in the stationary reference frame rotates with the synchronous speed. However in the rotor reference frame this vector rotates with slip angular velocity ω_s. It is obvious that the rotor position angle can be calculated from:

$$\theta_r = \theta_1 - \theta_2 \tag{2-83}$$

The accuracy of this method depends on the value of stator flux or magnetizing current, i_m^s, since the other quantities can be directly measured. i_m^s is computed by stator voltage integration therefore variations in ac bus voltage and frequency are taken into account. However, it is also observed that at rated voltage, because of magnetic circuit saturation, there is a slight boost in the i_m^s value when reactive current are injected from

the rotor side. So the following method is proposed to estimate i_m^s. At the first step, i_m^s is computed by transforming the present rotor current from the rotor reference frame to the stationary reference frame for the current sampling interval, using the rotor position obtained in previous interval. This calculation can be shown below:

$$i_{dr}^{s}[k] = i_{dr}^{r}[k].\cos\theta_{r[k-1]} - i_{qr}^{r}[k].\sin\theta_{r[k-1]} \tag{2-84}$$

$$i_{qr}^{s}[k] = i_{dr}^{r}[k].\sin\theta_{r[k-1]} + i_{qr}^{r}[k].\cos\theta_{r[k-1]} \tag{2-85}$$

$$i_{dqm}^{s}[k] = (1+\sigma_s).i_{dqs}^{s}[k] + i_{dqr}^{s}[k] \tag{2-86}$$

Subsequently, i_m^s is recomputed using (2-78) to (2-80).

Therefore, the computation for the first few sampling intervals starts with the nominal value of i_m^s and then switches over to re-computation method. Thus, the estimation process becomes independent of variations in the stator voltage and frequency as well as machine parameters.

The procedure of calculation of rotor angular displacement θ_r without using a speed sensor has been shown in the block diagram depicted in Fig. 2-17.

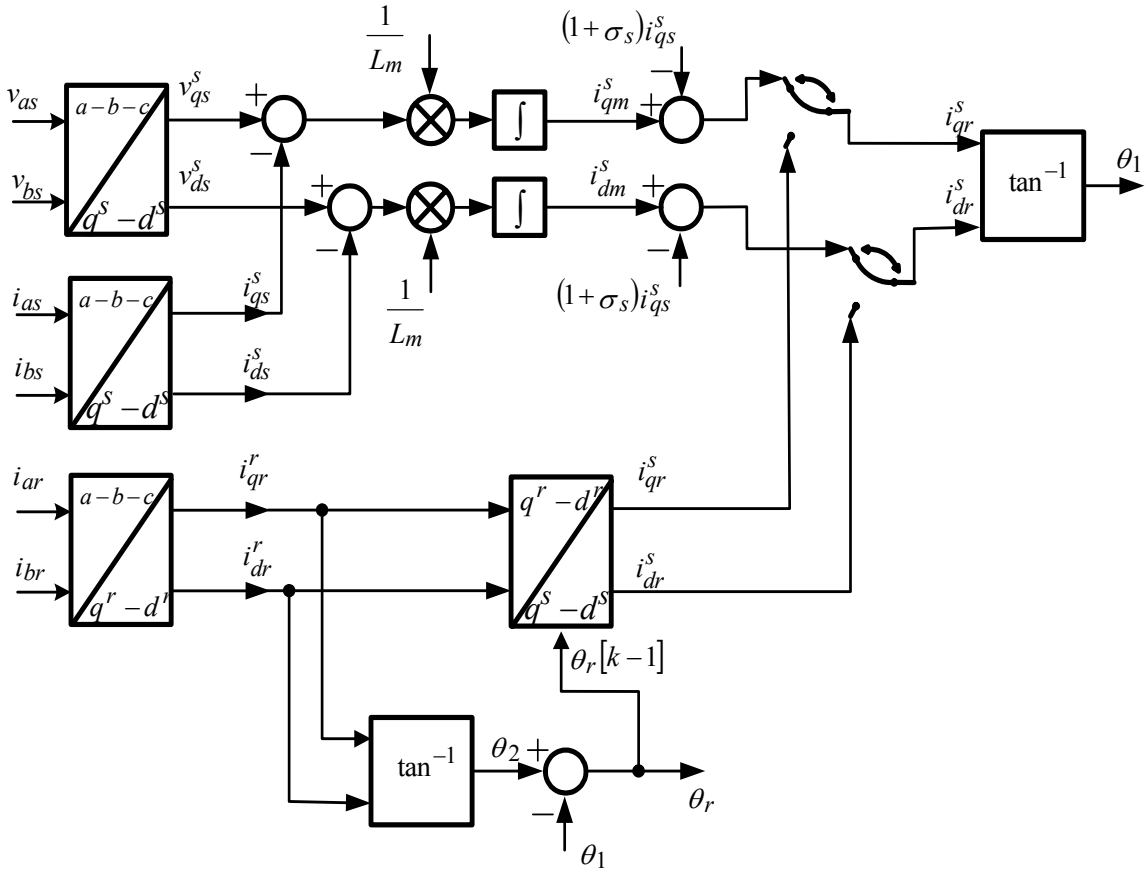

Figure 2-17: Block diagram of speed sensoreless method

II.5.5. FRONT END CONVERTER CONTROL

The objective of the front-end converter (FEC) is to keep the dc-link voltage constant regardless of direction and power flow of the rotor. A field oriented control similar to the rotor side converter is used, with a reference frame oriented along the stator or supply voltage vector position, enabling independent control of the active and reactive power flowing between the supply and FEC. FEC is current regulated, with the direct axis current used to regulate the reactive power and the quadrature axis current used to regulate the dc-link voltage. Figure 2-18 shows the schematic of FEC. The voltage equation across inductor can be written as follows:

$$\begin{bmatrix} v_a \\ v_b \\ v_c \end{bmatrix} = R.\begin{bmatrix} i_a \\ i_b \\ i_c \end{bmatrix} + L\frac{d}{dt}\begin{bmatrix} i_a \\ i_b \\ i_c \end{bmatrix} + \begin{bmatrix} v_{ai} \\ v_{bi} \\ v_{ci} \end{bmatrix} \tag{2-87}$$

L and R are the inductance and resistance of the input filter, respectively. Using transformation mentioned in (2-20) and (2-21), this equation is transformed to two-phase reference frame with q-axis attached to the stator voltage.

$$v_q^e = R\,i_q^e + L\frac{d}{dt}i_q^e + \omega_e L\,i_d^e + v_{qi}^e \tag{2-88}$$

$$v_d^e = R\,i_q^e + L\frac{d}{dt}i_d^e - \omega_e L\,i_q^e + v_{di}^e \tag{2-89}$$

Aligning the q-axis of the reference frame along the stator voltage vector, $v^e_d=0$ and $v^e_q=v_m$ where v_m is the peak magnitude of supply voltage.

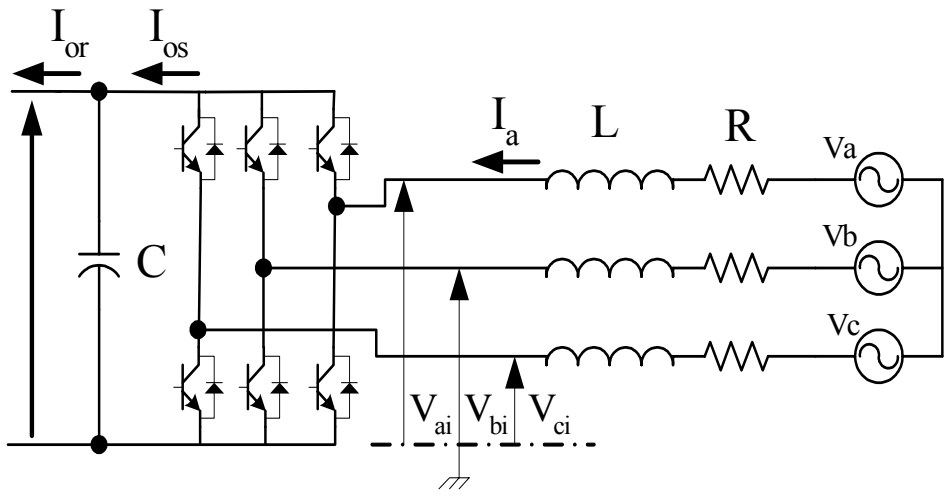

Figure 2-18: Front-end converter arrangement

Similar to (2-61) and (2-62), the active and reactive power will be proportional to i^e_q and i^e_d, respectively as it is shown in the following:

$$P = \frac{3}{2} v^e_q i^e_q \tag{2-90}$$

$$Q = -\frac{3}{2} v^e_q i^e_d \tag{2-91}$$

Neglecting harmonics due to switching and the losses in the inductor resistance and converter, we have:

$$\begin{aligned} E.i_{os} &= \frac{3}{2} v^e_q i^e_q \\ v^e_q &= \frac{m}{2\sqrt{2}} E \\ ios &= \frac{3}{4\sqrt{2}} m i^e_q \\ C\frac{d}{dt}E &= i_{os} - i_{or} \end{aligned} \tag{2-92}$$

From above equations, it is obvious that dc-link voltage can be controlled via i^e_q. Thus, the control scheme can be developed for i^e_d and i^e_q, with i^e_q command being derived from the dc-link voltage error through a PI controller. The i^e_d command determines the displacement factor on the supply-side of the inductors. Commanded direct and quadrature FEC voltages in exaction reference frame can be derived as follows:

$$v^{e*}_{qi} = v^e_q - \omega_e L i^e_d - v'^e_q \tag{2-93}$$

$$v^{e*}_{di} = \omega_e L i^e_q - v'^e_d \tag{2-94}$$

where:

$$v'^e_q = R i^e_q + L \frac{d}{dt} i^e_q \tag{2-95}$$

$$v'^e_d = R i^e_d + L \frac{d}{dt} i^e_d \tag{2-96}$$

The plant for the current control loops is given by:

$$F(s) = \frac{i^e_q(s)}{v'^e_q(s)} = \frac{i^e_d(s)}{v'^e_d(s)} = \frac{1}{Ls + R} \tag{2-97}$$

In (2-93) and (2-94), v^{e*}_{qi} and v^{e*}_{di} are the reference values for the front-end converter $\omega_e L i^e_{di}$ and $\omega_e L i^e_{qi}$ are compensation terms for cross coupling effect. The block diagram of the control system has been shown in Fig. 2-19.

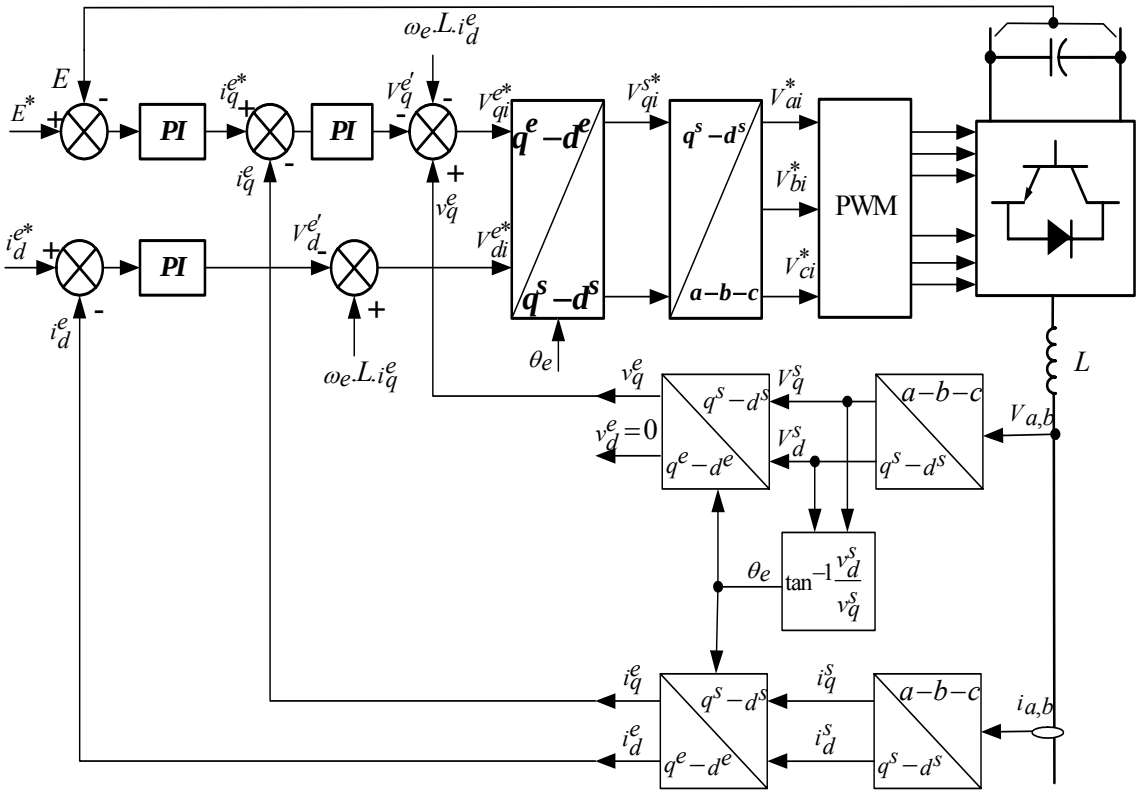

Figure 2-19: Block diagram of vector control method of front-end converter.

II.6. SIMULATION MODULES

In previous sections the mathematical model of system and control method for power converters was developed. To arrive at useful and conclusive results, the system performance needs to be investigated under both steady state and transient conditions for different operating conditions and constraints.

This section presents the digital computer simulation of the system equations, which provides for the numerical determination of the overall system performance. The subject has been treated in detail covering all aspects of the simulation procedure. To show the effectiveness of the proposed method, the proposed system has been simulated using MATLAB SIMULINK package on a 7.5 kW, 60Hz, and 230V wound rotor induction machine. The nonlinear load is modeled by a rectifier, which draws a non-linear current from ac lines. The rotor side controller based on the proposed method has been developed to control the rotor side power converter. Wind speed pattern is such that to allow the IDEA to work in both sub-synchronous and super-synchronous modes of operation.

Schematic diagram of simulated circuit is shown in Fig. 2-20. A software package representing the simulation has been developed. Each part of the system has been modeled very accurately. The software package has been structured in the form of modules and it has been capable of being used to study the system under various operating strategies and conditions. In following the main computer simulation modules are explained.

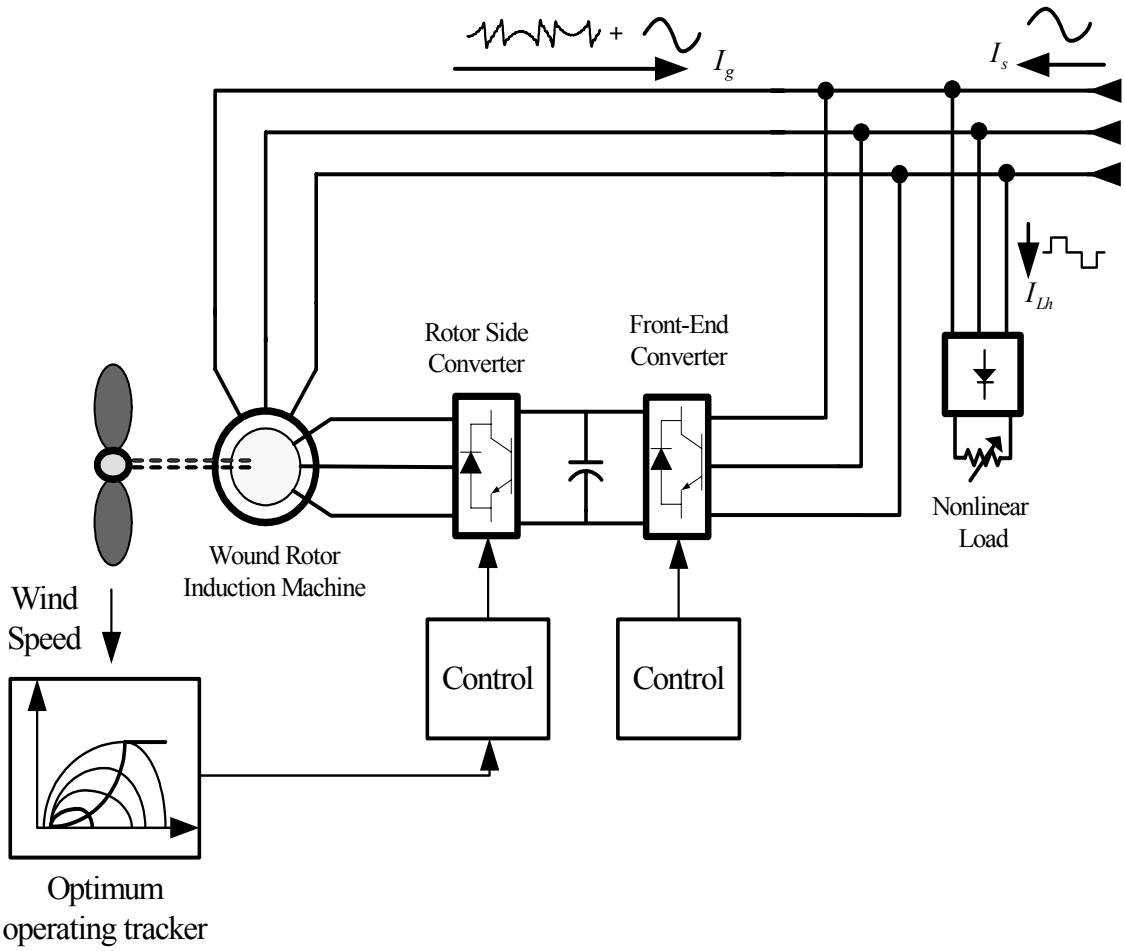

Figure 2-20: Schematic diagram of the simulated system

II.6.1. FIELD ORIENTED CONTROL TRANSFORMATIONS

As it was discussed, the control strategy of the rotor side power converter and front-end converter are based on field oriented control method. In the developed field oriented control methods, control topologies are performed in a two-phase reference frame fixed to the excitation reference frame $(q^e\text{-}d^e)$. As it was shown in the block diagram control of power converters, these transformations are done in two stages. In the first stage, we wish to transform all the variables from three-phase abc system to two-phase stationary reference frame and then retransform these variables from stationary reference frame to a rotary reference frame with arbitrary angular velocity of ω_e. These transformations are usually cascaded. The block diagram of this procedure is shown in Fig. 2-21.

In this figure, f is denoted as the currents or voltages and $q^e\text{-}d^e$ represents the arbitrary rotating reference frame with angular velocity ω_e and $q^s\text{-}d^s$ is representation of stationary reference frame. In vector control method, after applying field oriented control law, it is needed to transform the variables to the stationary a-b-c system to control the power converters.

This can be achieved by inverse transformation of variables from the arbitrary rotating reference frame to the stationary reference frame and then to a-b-c system. The block diagram of this procedure is shown in Fig. 2-22. In this block diagram, * is a representation of the commanded or desired values of variables.

Park's transformation or transformation of variables from three-phase stationary circuit to two-phase arbitrary reference frame was explained in (2-20) and (2-21) and it is depicted in Fig. 2-23.

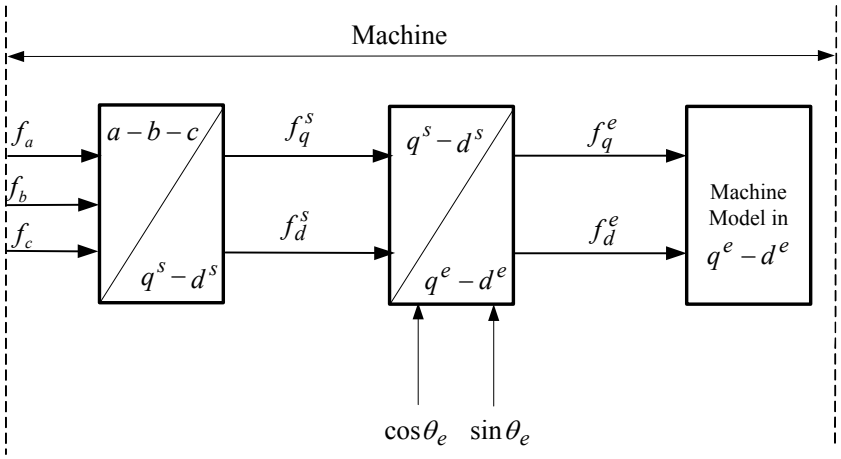

Figure 2-21: Machine side transformation in field oriented control

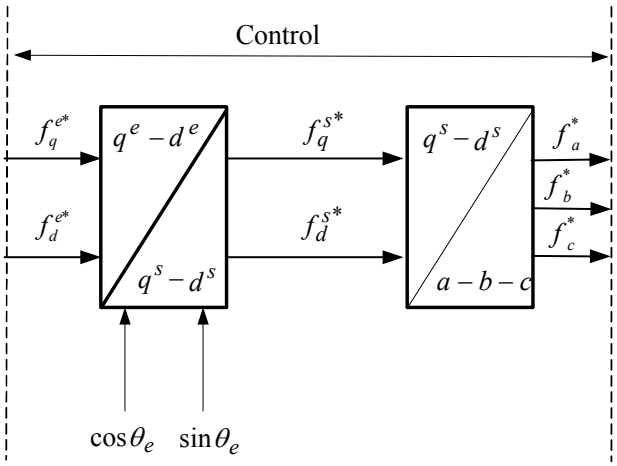

Figure 2-22: Variable transformation in the field oriented control

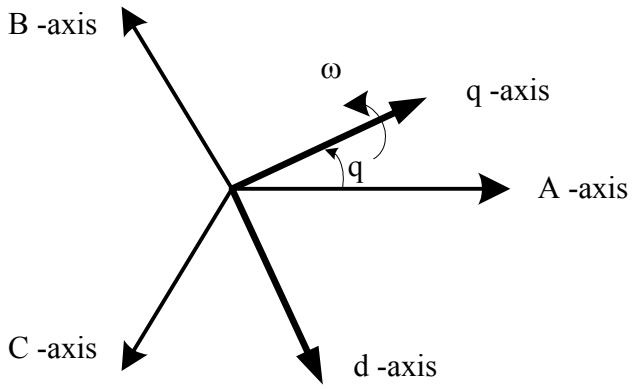

Figure 2-23: Park's transformation

It can be shown that for the inverse transformation we can write:

$$\left[f_{abcs}\right] = \left[T_{qd0}(\theta)\right]^{-1} \cdot \left[f_{qd0s}\right] \tag{2-98}$$

where the inverse Park's transformation matrix is given by:

$$\left[T_{qd0}(\theta)\right]^{-1} = \begin{bmatrix} \cos(\theta) & \sin(\theta) & 1 \\ \cos(\theta - \frac{2\pi}{3}) & \sin(\theta - \frac{2\pi}{3}) & 1 \\ \cos(\theta + \frac{2\pi}{3}) & \sin(\theta + \frac{2\pi}{3}) & 1 \end{bmatrix} \tag{2-99}$$

In the above equations, *f* can represent voltage, current, flux linkages or electric charge. The subscript s indicates the variables, parameters, and transformation associated with stationary circuits. The angular displacement θ must be continuous; however, the angular velocity associated with the change of variables is unspecified. The frame of reference may rotate at any constant or varying angular velocity or it may remain stationary. The angular velocity of the transformation can be chosen arbitrary to best fit for system equation solution or to satisfy the system constraints. The change of variables

may be applied to variables of any waveform and time sequence; however, we will find that transformation given above is particularly appropriate for an a-b-c sequence.

In order to establish any transformation between any two reference frames (in our case from stationary reference frame to rotation reference frame), we can denote *y* as new reference frame and *x* as old reference frame or the frame that the variables are being to be transformed.

In this regard, we can rewrite the transformation equation as:

$$\left\lfloor f^{y}_{qd0s} \right\rfloor = \left\lfloor T^{x\to y}_{qd0s} \right\rfloor \cdot \left\lfloor f_{qd0s} \right\rfloor \tag{2-100}$$

Then, the desired transformation can be expressed by the following matrix:

$$\left[T_{qd0_s}{}^{x \to y} \right] = \begin{bmatrix} \cos(\theta_y - \theta_x) & -\sin(\theta_y - \theta_x) & 0 \\ \sin(\theta_y - \theta_x) & \cos(\theta_y - \theta_x) & 0 \\ 1 & 1 & 1 \end{bmatrix} \tag{2-101}$$

In the developed computer simulation package, there are four different modules for transformation of variables that are explained in the following.

II.6.1.1. Transformation of 3-phase to 2-phase stationary reference frame

$$\left[(a-b-c) \to (q^s - d^s) \right]$$

This transformation transfers the three-phase stationary parameters, f_a, f_b, and f_c from a-b-c system to two-phase orthogonal stationary reference frame. If we substitute θ=0 in (2-10) and assuming that the system is balanced, we get:

$$f^{s}_{q} = f_a \tag{2-102}$$

$$f_d^s = -\frac{1}{\sqrt{3}}\left(2f_b + f_a\right) \tag{2-103}$$

II.6.1.2. Transformation from stationary reference frame to arbitrary rotary reference frame $\left[\left(q^s - d^s\right) \rightarrow \left(q^e - d^e\right)\right]$

This transformation converts vectors in balanced 2-phase orthogonal stationary system into orthogonal rotary reference frame. The inputs are f_q^s and f_q^s and θ_e and the outputs are f_q^e and f_d^e. This is the transformation between stationary reference frame and arbitrary reference frame rotating with the angular velocity of ω_e. If we substitute $\theta_x = 0$ and $\theta_y = \theta_e$ in (2-101) we obtain:

$$\begin{aligned} f_q^e &= \cos\theta_e . f_q^s - \sin\theta_e \cdot f_d^s \\ f_d^e &= \sin\theta_e . f_q^s + \cos\theta_e \cdot f_d^s \end{aligned} \tag{2-104}$$

II.6.1.3. Transformation of arbitrary rotary reference frame to stationary reference frame $\left[\left(q^e - d^e\right) \rightarrow \left(q^s - d^s\right)\right]$

This transformation projects vectors in orthogonal rotating reference frame into two-phase orthogonal stationary frame. From (2-73) we will get:

$$\begin{aligned} f_q^s &= \cos\theta_e f_q^e + \sin\theta_e f_d^e \\ f_d^s &= -\sin\theta_e f_q^e + \cos\theta_e \cdot f_d^e \end{aligned} \tag{2-105}$$

II.6.1.4. 2-phase to 3-phase transformation $\left[\left(q^s - d^s\right) \rightarrow \left(a - b - c\right)\right]$

This transformation transforms the variables from stationary two-phase q^s-d^s to stationary a-b-c system.

If we substitute θ=0 in (2-71) and assuming a balanced system we will get:

$$f_a = f_q^s$$
$$f_b = \frac{-f_q^s - \sqrt{3} * f_d^s}{2} \qquad (2\text{-}106)$$
$$f_c = \frac{-f_q^s - \sqrt{3} * f_d^s}{2}$$

II.6.2. COMPUTER SIMULATION MODEL OF DFIM

Mathematical model of DFIM was developed in section II.5.2. The computer simulation model suitable for SIMULINK solver is generated by reconfiguration of voltage and flux linkages equations. DFIM computer simulation module is shown in Fig.2-24. The inputs to this module are three phase stator voltages, three phase rotor voltages and load torque or torque of prime mover.

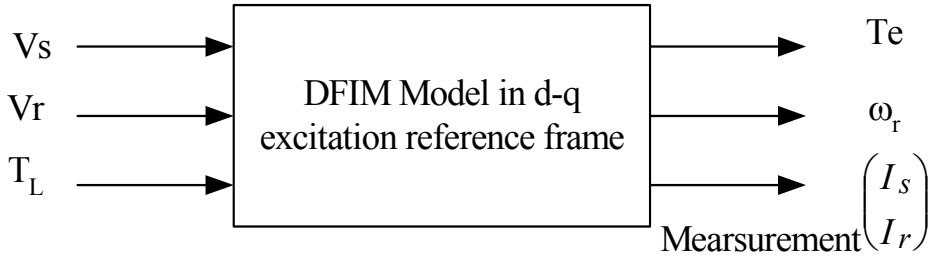

Figure 2-24: Computer simulation module for DFIM

The outputs are angular velocity of the rotor ω_e and electromagnetic torque T_e. The simulation model of the doubly fed induction machine is developed in the d-q excitation reference frame form. Proper transformations are done according to previous section to transform the stator and rotor voltages from three-phase stationary reference frame to two-phase excitation reference frame. Inverse transformation is also needed to transform current of stator and current of rotor from excitation reference frame to three-phase system. The mathematical model of DFIM used in the computer simulation module of DFIM is expressed in the following:

$$\begin{bmatrix} \lambda^e_{qs} \\ \lambda^e_{ds} \\ \lambda'^e_{qr} \\ \lambda'^e_{dr} \end{bmatrix} = \frac{1}{D}\left(\begin{bmatrix} v^e_{qs} \\ v^e_{ds} \\ v'^e_{qr} \\ v'^e_{dr} \end{bmatrix} - \begin{bmatrix} R_s & 0 & 0 & 0 \\ 0 & R_s & 0 & 0 \\ 0 & 0 & R'_r & 0 \\ 0 & 0 & 0 & R'_r \end{bmatrix} \begin{bmatrix} i^e_{qs} \\ i^e_{ds} \\ i'^e_{qr} \\ i'^e_{dr} \end{bmatrix} \right) + \frac{1}{D}\left(\begin{bmatrix} \omega_e & 0 & 0 & 0 \\ 0 & -\omega_e & 0 & 0 \\ 0 & 0 & (\omega_e - \omega_r) & 0 \\ 0 & 0 & 0 & -(\omega_e - \omega_r) \end{bmatrix} \begin{bmatrix} \lambda^e_{qs} \\ \lambda^e_{ds} \\ \lambda'^e_{qr} \\ \lambda'^e_{dr} \end{bmatrix} \right) \tag{2-107}$$

$$\begin{bmatrix} i^e_{qs} \\ i^e_{qs} \\ i'^e_{qr} \\ i'^e_{dr} \end{bmatrix} = \begin{bmatrix} L_s & 0 & L_m & 0 \\ 0 & L_s & 0 & L_m \\ L_m & 0 & L'_r & 0 \\ 0 & L_m & 0 & L'_r \end{bmatrix}^{-1} \begin{bmatrix} \lambda^e_{qs} \\ \lambda^e_{ds} \\ \lambda'^e_{qr} \\ \lambda'^e_{dr} \end{bmatrix} \tag{2-108}$$

$$T_e = \frac{3}{2}\frac{P}{2}\left(\lambda^e_{ds} i^e_{qs} - \lambda^e_{qs} i^e_{ds}\right) \tag{2-109}$$

$$\omega_r = \frac{1}{D}\left(\frac{P}{2J}\left(T_e - T_L\right)\right) \tag{2-110}$$

II.6.3. WIND TURBINE MODULE

The proposed system is based on variable speed constant frequency concept which requires the system to operate along the maximum power locus. It is therefore, necessary to obtain the torque-speed characteristics of the turbine corresponding to maximum power locus. This will enable the control mechanism to allocate the operating point along this trajectory to adjust the angular velocity of the rotor.

The characteristics of a wind turbine are derived from aerodynamic efficiency C_p that depends on the particulars of the turbine blade design. As it was shown previously, the aerodynamic efficiency coefficient varies with the tip speed ratio λ.

The turbine characteristics are usually provided by manufacturers. In this simulation module, C_p has been considered as follows [37]:

$$C_p(\lambda) = 0.043 - 0.108\lambda + 0.146\lambda^2 - 0.0602\lambda^3 + 0.0104\lambda^4 - .0006\lambda^5 \qquad (2\text{-}111)$$

The aerodynamic efficiency has been plotted versus tip speed ratio λ in Fig.2-25. To get maximum energy conversion, system should always operate at optimal value of aerodynamic efficiency C_{pmax} corresponding to optimal value of tip speed ratio λ_{opt}. For a given wind speed of v_w, the tip speed ratio λ of a wind turbine with blade radius r is expressed as:

$$\lambda = \frac{\omega_r . r}{v_w} \qquad (2\text{-}112)$$

As it is clear at each wind speed, adjusting the angular velocity of rotor of wind turbine ω_r is essential to achieve the optimal value of tip speed ratio λ_{opt}.

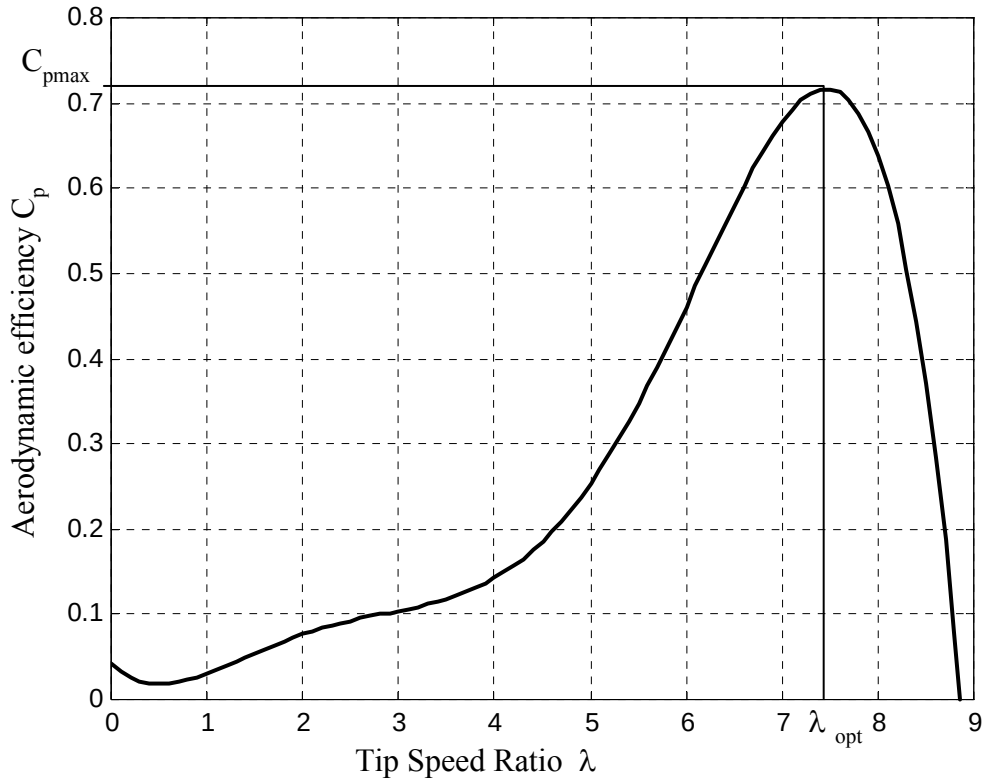

Figure 2-25: Aerodynamic efficiency C_p versus tip speed ratio

For wind speed v_w the maximum power of turbine and corresponding torque can be calculated as follows:

$$P_{mech} = \frac{\rho}{2} \cdot \pi \cdot R^2 \cdot C_{p\max}(\lambda) \cdot v_w^3 \tag{2-113}$$

$$T_{mech} = \frac{\rho}{2} \cdot \pi \cdot R^3 \cdot \frac{C_{p\max}(\lambda)}{\lambda_{opt}} \cdot v_w^2 \tag{2-114}$$

These data can be stored as a look-up table. The block diagram of wind turbine module is shown in Fig. 2-26.

II.6.4. NON-LINEAR LOAD MODULE

The nonlinear load is modeled by a controlled rectifier, which draws a non-linear current with controllable amplitude and phase. The schematic diagram of non-linear load is shown in Fig.2-27.

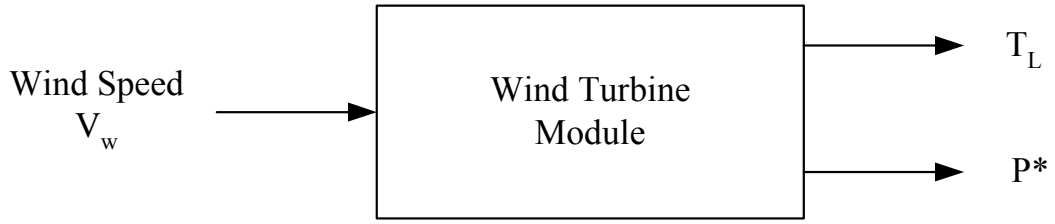

Figure 2-26: Wind turbine module

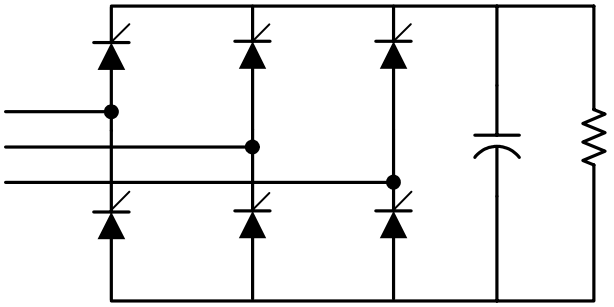

Figure 2-27: Schematic diagram of non-linear load

Switching converter functions are employed to model controllable rectifier. The operation of three-phase controllable rectifier with balanced inputs can be described by the expression:

$$V_o = F(\omega t).\begin{bmatrix} v_a \\ v_b \\ v_c \end{bmatrix} \tag{2-115}$$

where:

$$\begin{aligned} v_a &= v_m \sin(\omega t) \\ v_b &= v_m \sin\left(\omega t - \frac{2\pi}{3}\right) \\ v_c &= v_m \sin\left(\omega t - \frac{4\pi}{3}\right) \end{aligned} \tag{2-116}$$

$F(\omega t)$: Switching converter function

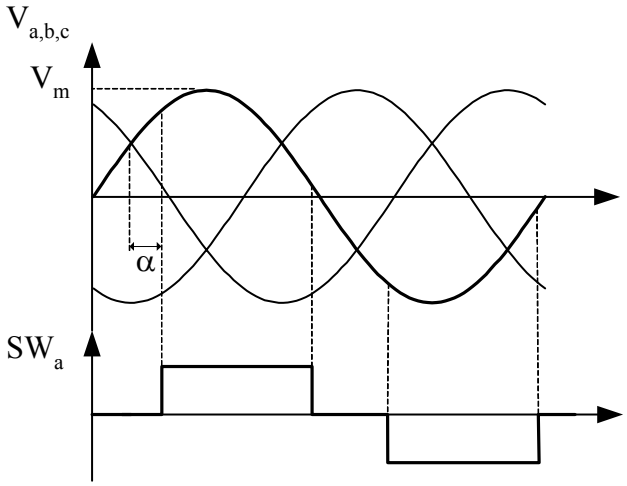

Figure 2-28: Switching converter function definition

The switching converter function has been shown in Fig.2-28 and can be expressed as:

$$F(\omega t)=\begin{bmatrix} sw_a \\ sw_b \\ sw_c \end{bmatrix}^T = \frac{2\sqrt{3}}{\pi}\begin{bmatrix} \sum_{n=1}^{\infty}\sin(n\omega t-\alpha) \\ \sum_{n=1}^{\infty}\sin\left(n\omega t-\frac{2\pi}{3}-\alpha\right) \\ \sum_{n=1}^{\infty}\sin\left(n\omega t-\frac{4\pi}{3}-\alpha\right) \end{bmatrix}^T \qquad (2\text{-}117)$$

where, n is an odd integer number.

For the input currents of rectifier we have:

$$\begin{bmatrix} i_a \\ i_b \\ i_c \end{bmatrix} = \begin{bmatrix} sw_a \\ sw_b \\ sw_c \end{bmatrix} . i_o \qquad (2\text{-}118)$$

where:

$$i_o = \frac{v_o}{Z} \tag{2-119}$$

Then we get:

$$\begin{bmatrix} i_a \\ i_b \\ i_c \end{bmatrix} = \frac{1}{Z} \begin{bmatrix} sw_a \\ sw_b \\ sw_c \end{bmatrix} \cdot \begin{bmatrix} sw_a & sw_b & sw_c \end{bmatrix} \cdot \begin{bmatrix} v_a \\ v_b \\ v_c \end{bmatrix} \tag{2-120}$$

$$\begin{bmatrix} i_a \\ i_b \\ i_c \end{bmatrix} = \frac{1}{Z} \begin{bmatrix} sw_a \\ sw_b \\ sw_c \end{bmatrix} \cdot \begin{bmatrix} sw_a{}^2 & sw_a sw_b & sw_a sw_c \\ sw_a sw_b & sw_b{}^2 & sw_b sw_c \\ sw_a sw_c & sw_b sw_c & sw_c{}^2 \end{bmatrix} \cdot \begin{bmatrix} v_a \\ v_b \\ v_c \end{bmatrix} \tag{2-121}$$

II.6.5. BACK-TO-BACK POWER CONVERTERS MODULES

A back-to back power converter is used to control the excitation of the rotor of IDEA. Both rotor side converter and front-end converter are current regulated voltage source inverter. Each power converter includes six switches. In sections II.5.4 and II.5.5 the control method of the rotor side power converter and front-end converter method were explained. As it was illustrated, the reference voltages are generated based on the commands. Space Vector PWM (SVPWM) technique is used to determine the switching sequence of the upper three power switching transistors, such as IGBTs and Power MOSFETs, of a three-phase Voltage Source Inverter (VSI) in regards to voltage commands. It has been shown that SVPWM technique generates less harmonic distortion in the output voltages, in comparison to direct sinusoidal modulation technique.

The structure of a typical three-phase voltage source inverter is shown in Fig. 2-29. Va, Vb and Vc are the output voltages applied to the windings of the rotor. T1 through T6 are the six power transistors that shape the output, which are controlled by gates signals. When an upper switch is on, the corresponding lower transistor is switched off.

II.6.5.1. Switching patterns and the basic space vectors

There are eight possible combinations of on and off states for the three upper power transistors. The on and off states of the lower power transistors are opposite to the upper ones and so the states of bottom switches are determined based on the upper switches states. The eight combinations and the derived output line-to-line and phase voltages with respect to dc supply voltage are shown in Table 2-4.

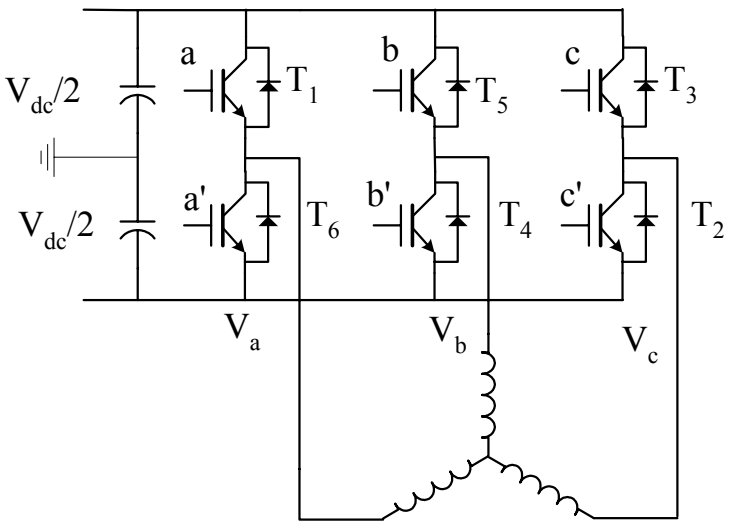

Figure 2-29: Three-phase power inverter supplying a three-phase inductive load

The relationship between the switching gate signals $[a, b, c]^t$ and the line-to-line voltage vector $[V_{ab}, V_{bc}, V_{ca}]^t$ is given by the following relationship:

$$\begin{bmatrix} V_{ab} \\ V_{bc} \\ V_{ca} \end{bmatrix} = V_{dc} \begin{bmatrix} 1 & -1 & 0 \\ 0 & 1 & -1 \\ -1 & 0 & 1 \end{bmatrix} \begin{bmatrix} a \\ b \\ c \end{bmatrix} \tag{2-122}$$

Similarly, the phase voltage (line-to-neutral) can be obtained as:

$$\begin{bmatrix} V_a \\ V_b \\ V_c \end{bmatrix} = \frac{1}{3} V_{dc} \begin{bmatrix} 2 & -1 & -1 \\ -1 & 2 & -1 \\ -1 & -1 & 2 \end{bmatrix} \begin{bmatrix} a \\ b \\ c \end{bmatrix} \tag{2-123}$$

The phase voltages corresponding to the eight combinations of switching patterns can be mapped into the d-q plane by the same d-q transformation (Table 2-5). Transformation of the three-phase variables to two-phase stationary reference frame is shown by (2-96).

Table 2-4: Switching patterns and output voltages of a 3-phase power inverter

a	b	c	V_a	V_b	V_c	V_{ab}	V_{bc}	V_{ca}
0	0	0	0	0	0	0	0	0
1	0	0	$2/3$	$-1/3$	$-1/3$	1	0	-1
1	1	0	$1/3$	$1/3$	$-2/3$	0	1	-1
0	1	0	$-1/3$	$2/3$	$-1/3$	-1	1	0
0	1	1	$-2/3$	$1/3$	$1/3$	-1	0	1
0	0	1	$-1/3$	$-1/3$	$2/3$	0	-1	1
1	0	1	$1/3$	$-2/3$	$1/3$	1	-1	0
1	1	1	0	0	0	0	0	0

This mapping results in six non-zero vectors and two zero vectors. The non-zero vectors form the axes of a hexagonal as shown in Fig. 2-30. The angle between any two adjacent non-zero vectors is 60 degrees. The two zero vectors are located at the origin. The group of the eight vectors are referred to as the basic space vectors and are denoted by V_0, V_1, V_2, V_3, V_4, V_5, V_6 and V_7.

$$\begin{bmatrix} V_q \\ V_d \end{bmatrix} = \frac{2}{3}\begin{bmatrix} 1 & -\frac{1}{2} & -\frac{1}{2} \\ 0 & \frac{\sqrt{3}}{3} & -\frac{\sqrt{3}}{2} \end{bmatrix}\begin{bmatrix} V_a \\ V_b \\ V_c \end{bmatrix} \tag{2-124}$$

II.6.5.2. Determination of output voltages with basic space vectors

The objective of the space vector PWM technique is to determine the reference voltage vector V_{out} by a combination of the eight switching patterns. One simple means of calculation is to require the average output voltage of the inverter (in sampling period, *T*) to be the same as the average of V_{out} in the same period. This is shown in (2-125) for the output voltage in the sector 0, where T_4 and T_6 are duration of switching patterns V_4 and V_6.

$$\frac{1}{T}\int_{nT}^{(n+1)T} V_{out}\, dt = \frac{1}{T}(T_4 V_4 + T_6 V_6) \qquad n = 0,1,2,\cdots, \textit{where} \quad T_4 + T_6 \le T \tag{2-125}$$

Table 2-5: The eight switching states and corresponding d-q voltages

a	b	c	V_q	V_d	V_{dq}
0	0	0	0	0	$V_0 = 0$
0	0	1	$-\frac{1}{3}V_{dc}$	$\frac{1}{\sqrt{3}}V_{dc}$	$V_1 = \frac{2}{3}V_{dc}$
0	1	0	$-\frac{1}{3}V_{dc}$	$-\frac{1}{\sqrt{3}}V_{dc}$	$V_2 = \frac{2}{3}V_{dc}$
0	1	1	$-\frac{2}{3}V_{dc}$	0	$V_3 = \frac{2}{3}V_{dc}$
1	0	0	$\frac{2}{3}V_{dc}$	0	$V_4 = \frac{2}{3}V_{dc}$
1	0	1	$\frac{1}{3}V_{dc}$	$\frac{1}{\sqrt{3}}V_{dc}$	$V_5 = \frac{2}{3}V_{dc}$
1	1	0	$\frac{1}{3}V_{dc}$	$-\frac{1}{\sqrt{3}}V_{dc}$	$V_6 = \frac{2}{3}V_{dc}$
1	1	1	0	0	$V_7 = 0$

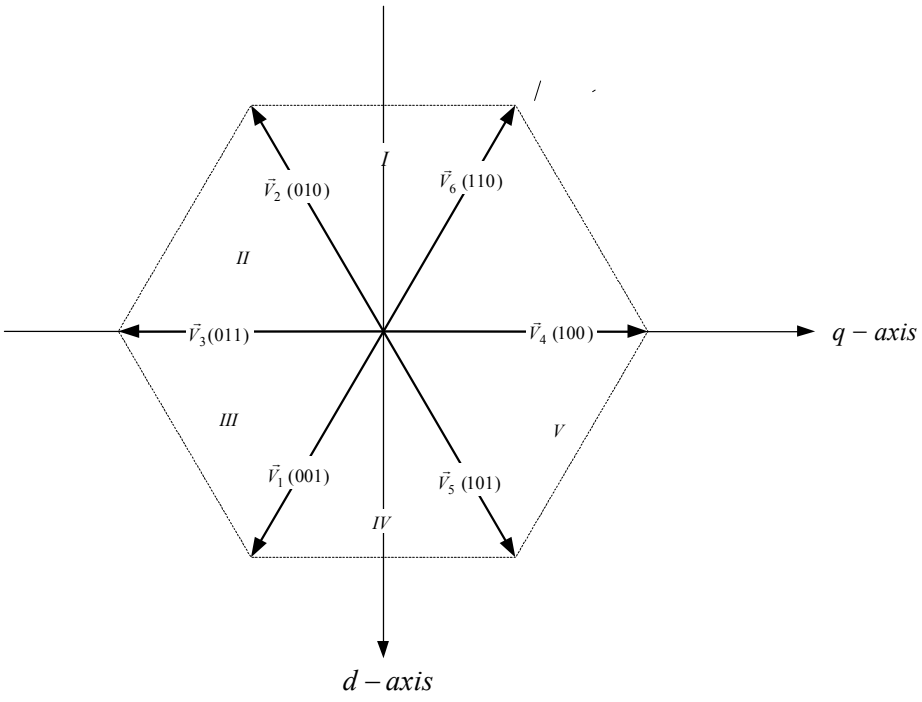

Figure 2-30: Space vector diagram

Assuming the PWM period, T_{pwm}, is small and the change of V_{out} is relatively slow, then we get:

$$\int_{nT_{PWM}}^{(n+1)T_{PWM}} V_{out}\,dt = T_{PWM}V_{out} = (T_4V_4 + T_6V_6) \quad n = 0,1,2,\cdots, \ where\ T_4 + T_6 \le T_{PWM} \tag{2-126}$$

It is clear that the reference voltage V_{out} can be determined by switching patterns of V_4 and V_6 for T_4 and T_6 periods of time, respectively. Since the sum of T_4 and T_6 is less than or equal to T_{pwm}, the inverter needs to have a zero vector ((000) V_0 or (111) V_7) pattern inserted for the rest of the period. Therefore, we can write:

$$T_{PWM}V_{out} = T_4V_4 + T_6V_6 + T_0(V_0\ or\ V_7) \tag{2-127}$$

where

$$T_1 + T_2 + T_0 = T_{pwm} \tag{2-128}$$

The reference voltage vector V_{out} is obtained by mapping the desired three phase output voltages to the d-q reference frame. In balanced three-phase system, V_{out} becomes a vector rotating around the origin of the d-q plane with angular velocity of ω. The maximum locus of V_{out} is limited by the hexagon formed by the basic vectors. Therefore, the magnitude of V_{out} must be limited to the shortest radius of this envelope. This gives a maximum magnitude of $V_{dc}/\sqrt{2}$ for V_{out}. Correspondingly, the maximum RMS values of the fundamental line-to-line and line-to-neutral output voltages are $V_{dc}/\sqrt{2}$ and $V_{dc}/\sqrt{6}$.

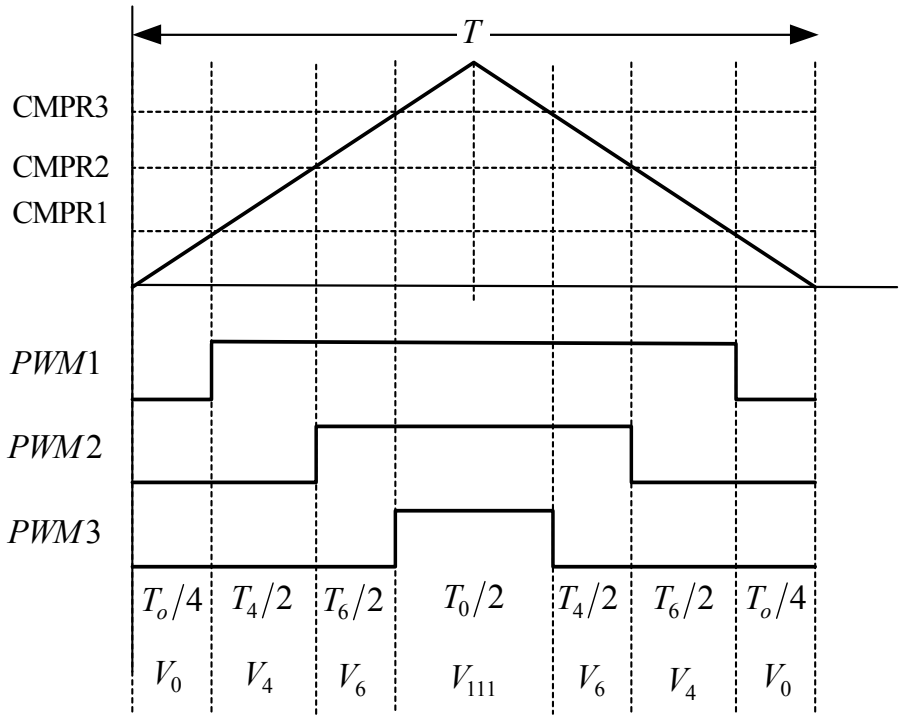

Figure 2-31: A symmetric space vector PWM switching pattern

Notice that these values are $2/\sqrt{3}$ times higher than what a standard sinusoidal PWM technique can generate. An example of a symmetric space vector PWM waveform is shown in Fig. 2-31. It is assumed that the reference voltage V_{out} lies in Sector 0, which is bordered by vectors V_4 and V_6.

II.6.5.3. Calculation the time periods of the switching states

The output voltage V_{out} can be located in any sector from sectors0 to sectors5. Equation (2-100) shows that for every PWM period V_{out} is determined by switching between the two non-zero basic vectors that boarder the sector of the current output

voltage V_{out}. For instance, if V_{out} is in sector 1, it can be approximated by switching the inverter between states V_2 and V_6 for periods of time T_2 and T_6 respectively. Because the sum of T_2 and T_6 should be less than or equal to T_{pwm}, the inverter should remain in T_0 or T_7 for the rest of the period.

$$\begin{bmatrix} T_4 \\ T_6 \end{bmatrix} = T_{PWM} \begin{bmatrix} V_{4q} & V_{6q} \\ V_{4d} & V_{6d} \end{bmatrix}^{-1} \begin{bmatrix} V_{outq} \\ V_{outd} \end{bmatrix} \tag{2-129}$$

Or we can write:

$$\begin{bmatrix} T_4 \\ T_6 \end{bmatrix} = T_{PWM} M_0 \begin{bmatrix} V_{outq} \\ V_{outd} \end{bmatrix} \tag{2-130}$$

where M_0 is the normalized decomposition matrix for sector 0. By substituting the values of V_{4q}, V_{4d}, V_{6q} and V_{6d}, we obtain:

$$\begin{bmatrix} T_4 \\ T_6 \end{bmatrix} = T_{PWM} \begin{bmatrix} 2/3 & 1/3 \\ 0 & -1/\sqrt{3} \end{bmatrix}^{-1} \begin{bmatrix} V_{outq} \\ V_{outd} \end{bmatrix} \tag{2-131}$$

Table 2-6 shows the sector numbers and the associated normalized decomposition matrix.

II.6.5.4. Finding the sector number

It is necessary to know which sector the output voltage is located in to determine the switching time periods and switching sequence. The algorithm below can be used if the reference output voltage is in a-b-c plane. If the output voltage is given in the d-q plane, we must first transform the vector to the a-b-c plane before using the algorithm.

First, calculate the values of A, B and C by as following:

$$\begin{aligned} A &= sign(ref_1 - ref_2) \\ B &= sign(ref_2 - ref_3) \\ C &= sign(ref_3 - ref_1) \end{aligned} \tag{2-132}$$

where:

$$sign(x) = \begin{cases} 1 & x > 0 \\ undef & x = 0 \\ -1 & x < 0 \end{cases} \tag{2-133}$$

and ref_1, ref_2 and ref_3 are the output a, b and c voltages. Secondly, finding the value of N from following equation:

$$N = \left| A + 2B + 4C \right| \tag{2-134}$$

From Table 2-7 the sector number can be found.

II.6.5.5. SVPWM switching pattern

The order of the non-zero vectors and zero vectors in each PWM period must be determined. Different switching orders result in different waveform patterns. Figure (2-32) shows the waveform produced for each sector of a symmetric switching scheme.

Table 2-6: Normalized decomposition matrix versus sector

Sector	Duration Calculated	Decomposition Matrix
0	T_4 *and* T_6	$M_0 = \begin{bmatrix} \sqrt{3}/2 & 1/2 \\ 0 & -1 \end{bmatrix}$
1	T_2 *and* T_6	$M_1 = \begin{bmatrix} -\sqrt{3}/2 & -1/2 \\ \sqrt{3}/3 & -1/2 \end{bmatrix}$
2	T_2 *and* T_3	$M_2 = \begin{bmatrix} 0 & -1 \\ -\sqrt{3}/3 & 1/2 \end{bmatrix}$
3	T_1 *and* T_3	$M_2 = \begin{bmatrix} 0 & 1 \\ -\sqrt{3}/3 & -1/2 \end{bmatrix}$
4	T_1 *and* T_5	$M_4 = \begin{bmatrix} -\sqrt{3}/2 & 1/2 \\ \sqrt{3}/3 & 1/2 \end{bmatrix}$
5	T_5 *and* T_4	$M_5 = \begin{bmatrix} -\sqrt{3}/2 & -1/2 \\ 0 & 1 \end{bmatrix}$

Table 2-7: N versus sector number

N	1	2	3	4	5	6
Sector	1	5	0	3	2	4

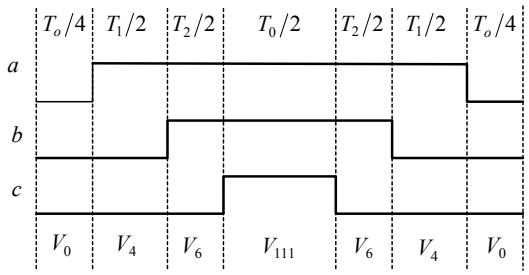

V_{out} in sector 0

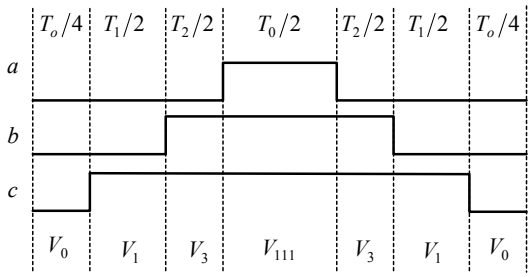

V_{out} in Sector 3

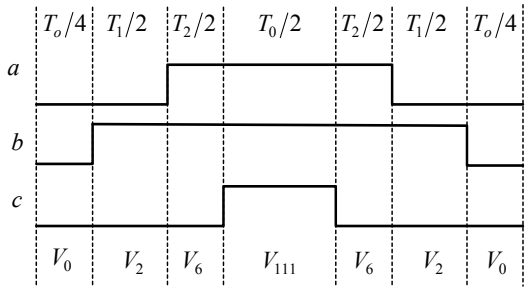

V_{out} in sector 1

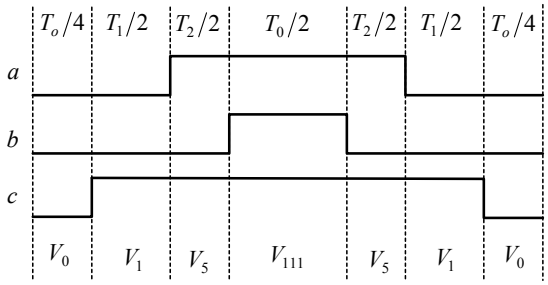

V_{out} in sector 4

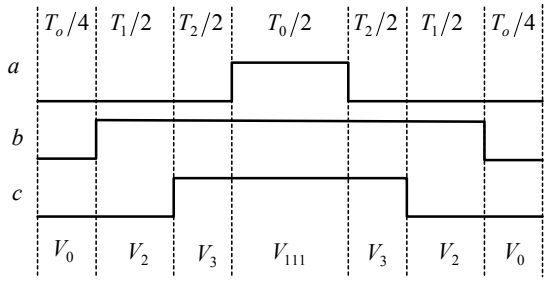

V_{out} in sector 2

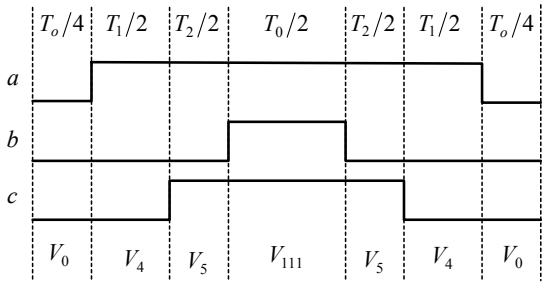

V_{out} in sector 5

Figure 2-32: A symmetric space vector PWM switching pattern in different sectors

II.6.6. SIMULATION EXAMPLES

The necessary platform for the analytical investigation on the grid-connected variable speed wind turbine equipped with IDEA has been established in previous sections. The simulation software has been developed in MATLAB SIMULINK environment. Software is modular and each module was developed accurately in previous section. Behavior of the proposed scheme under both steady state and transient conditions are examined in this section. A few examples will be explained in the following.

To show the effectiveness of the proposed method, the system has been simulated package on a 7.5 kW, 60Hz, and 230V wound rotor induction machine. The rotor side controller based on the proposed method has been developed to control the rotor side converter. Wind speed is varied to allow the IDEA works in both sub-synchronous and super-synchronous modes.

II.6.6.1. Case study 1

In this case study, response of system in generation mode without harmonic compensation is investigated. The wind speed is set at 8 m/s which from turbine characteristics look-up table, it determines that $i_{qr}^{e*} = -9.7$.

At the time t=1.1 s there is a step change in wind speed and it increases to 12 m/s which corresponds to $i_{qr}^{e*} = -24.5$. Turbine shaft torque transferred to the shaft of IDEA also increases accordingly to 29.5 N.m.

Reactive power compensation is also activated in both operations and to achieve to unity power factor. Step change in wind speed results in step change in command power and accordingly to i_{qr}^{e*}.

In Fig. 2-33 (a), the turbine shaft torque transferred to the rotor of IDEA in response to step change in power command at t=1.1s has been shown. In Fig. 2-33 (b) and (c), rotor speed and actual rotor in quadrature axis in excitation reference frame has been depicted, respectively. Current of phase a of stator and current of the rotor phase have plotted respectively in Fig. 2-34 (a) and Fig. 2-34 (b). In Fig. 2-35 flux of stator and rotor in d-q form in excitation reference frame is shown. As it is clear the flux of stator in q-axis of excitation reference frame is kept zero due to stator flux field oriented control.

Command reactive power is kept zero $i_{dr}^{e*} = 0$, to maintain unity power factor for stator current. Current of stator and voltage of stator both in phase (a) have been plotted in Fig. 2-36.

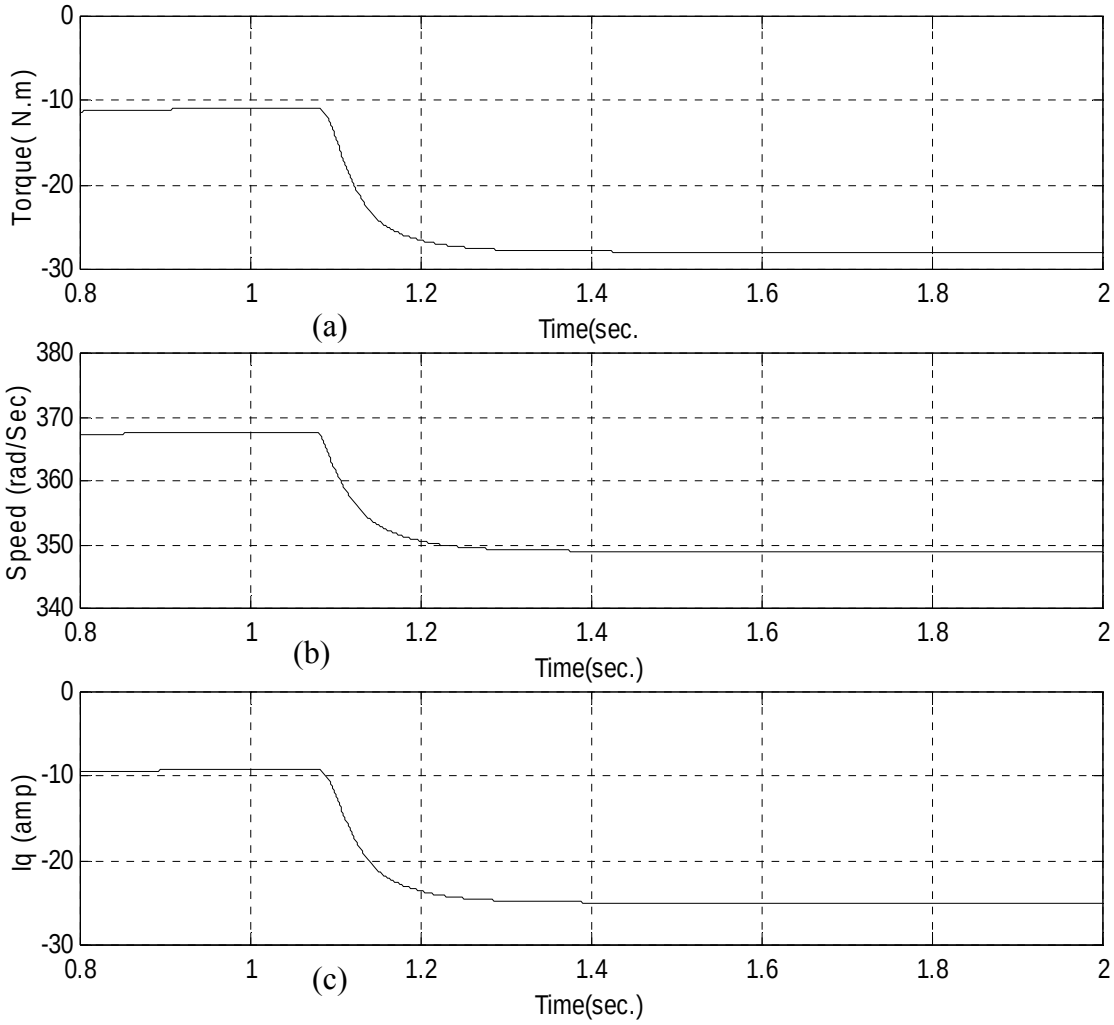

Figure 2-33: Simulation result for case study 1, step change in wind speed. (a) Turbine shaft torque transferred to IDEA, (b) Speed of rotor of IDEA(Rad./sec) and (c) Quadearature-axis rotor current in excitation reference frame

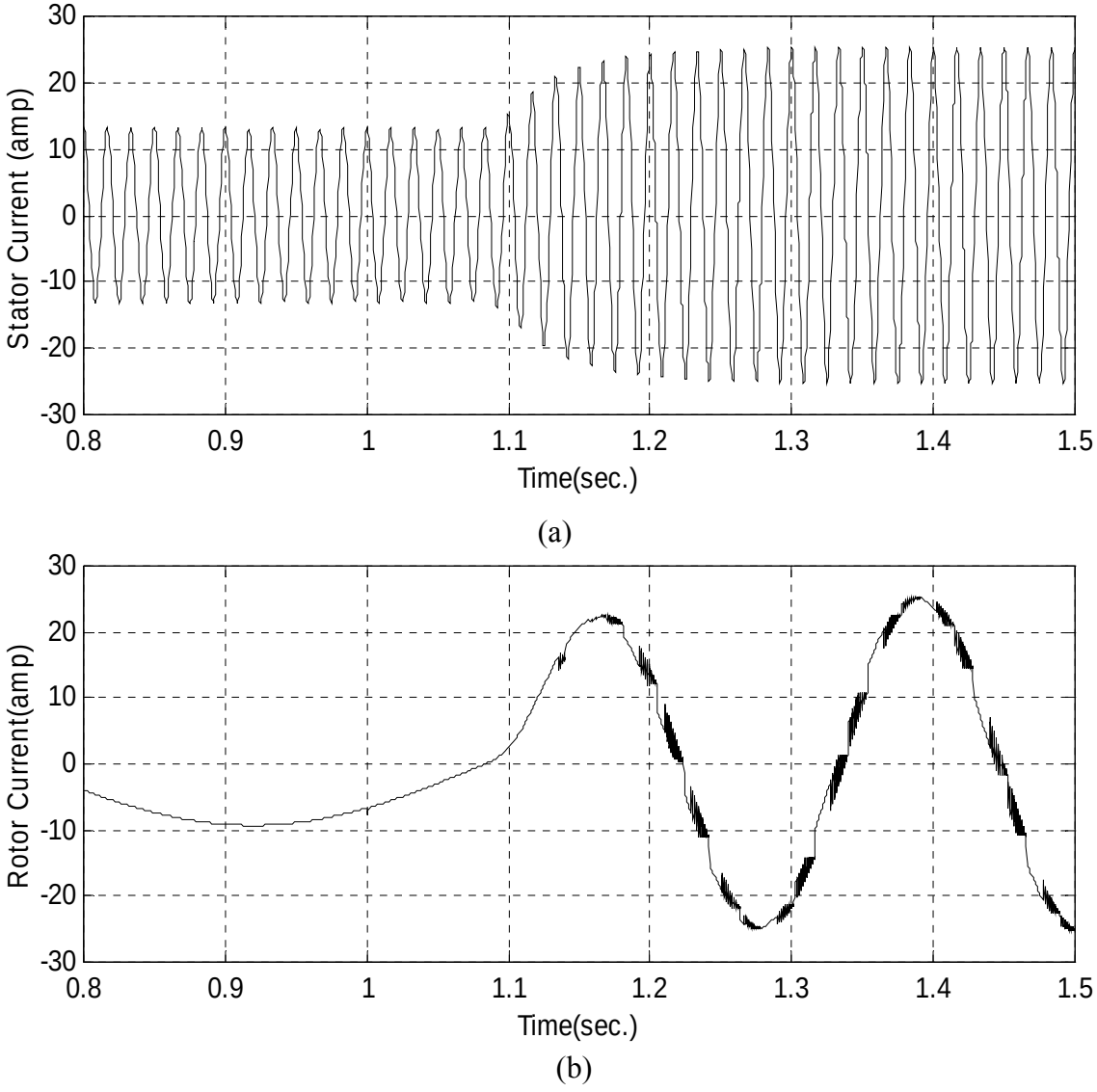

Figure 2-34: Simulation result for case study 1, step change in wind speed. (a) Stator current of IDEA and (b) Rotor current of IDEA

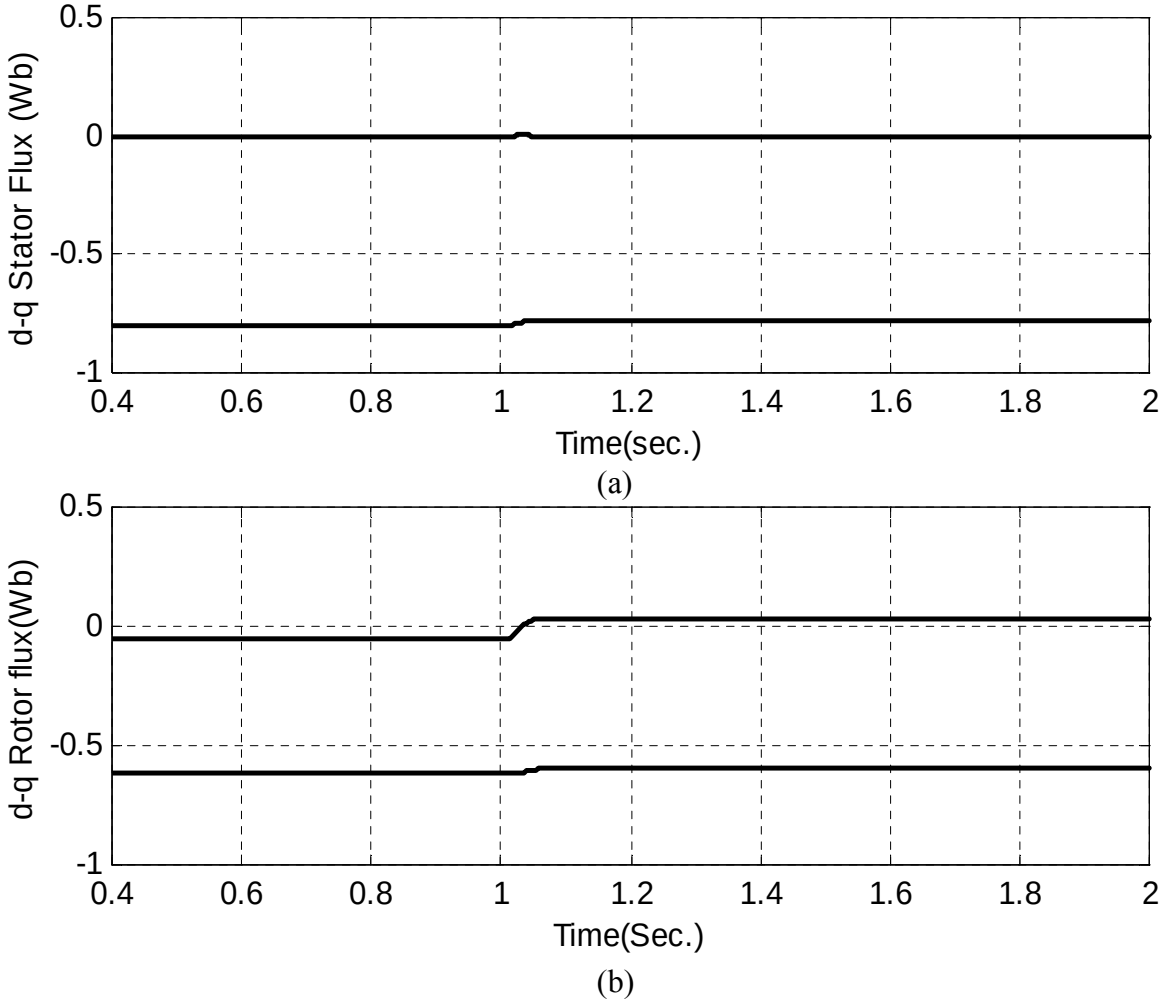

Figure 2-35: Simulation result for case study 1, step change in wind speed. (a) The d-q stator flux in excitation reference frame and (b) The d-q stator flux in excitation reference frame

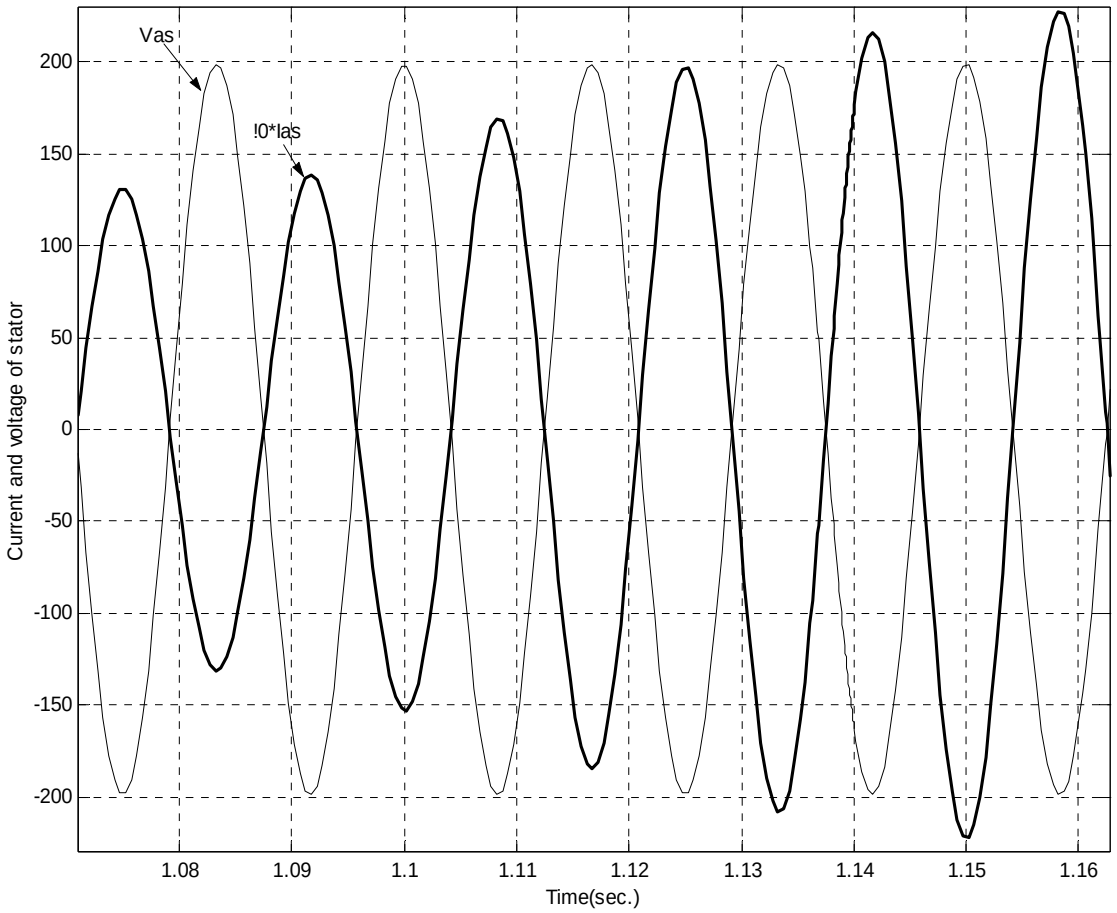

Figure 2-36: Simulation result for case study 1, step change in wind speed, stator phase a voltage and stator current corresponding to pf=1

II.6.6.2. Case study 2

In this case study, harmonic compensation system is also activated. The nonlinear load is modeled by a rectifier, which draws a non-linear current with amplitude of 10A. Then, the rotor side controller based on the proposed method has been developed to control the rotor side converter. Wind speed is varied to allow the IDEA works in both sub-synchronous and super-synchronous modes. The command wind speed has been shown in Fig. 2-37 (a). Then command active power reactive powers are generated upon wind speed command utility demand. The command active power and reactive power and their actual values have been plotted in Fig. 2-37 (b).

It is observed that harmonics have been removed from the grid lines and the utility current is pure sinusoidal. Response of system is fast enough for variation of wind speed. Current of nonlinear load and its spectrum and current of IDEA and utility current with variation of wind speed are shown in Fig. 2-38. Front-end converter and dc-bus are also simulated. The utility voltage and input current to front-end converter are shown in Fig.2-39. The reactive power command has been set to zero $i_d^{e*} = 0$ for unity power factor. The dc-bus voltage has been set to Vdc=300V.The variation of dc-bus voltage in corresponding to the wind speed pattern is depicted in Fig. 2-40.

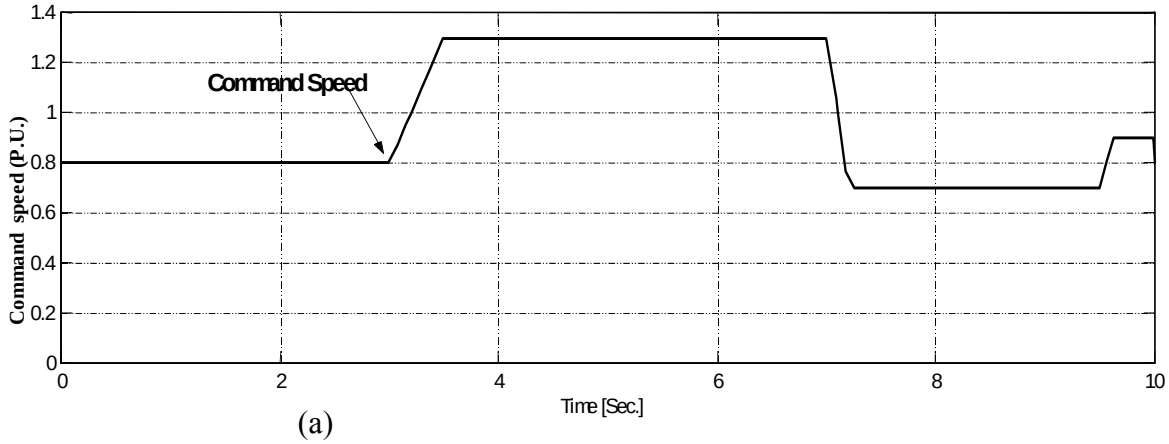

(a)

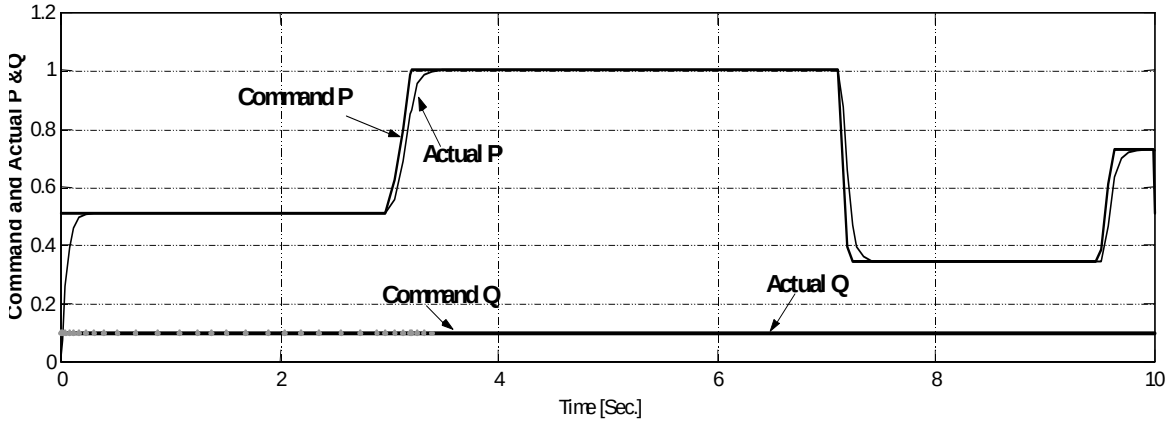

(b)

Figure 2-37: Simulation result for case study 2. (a) Command speed (pu) and (b) Command and actual active and reactive power (pu)

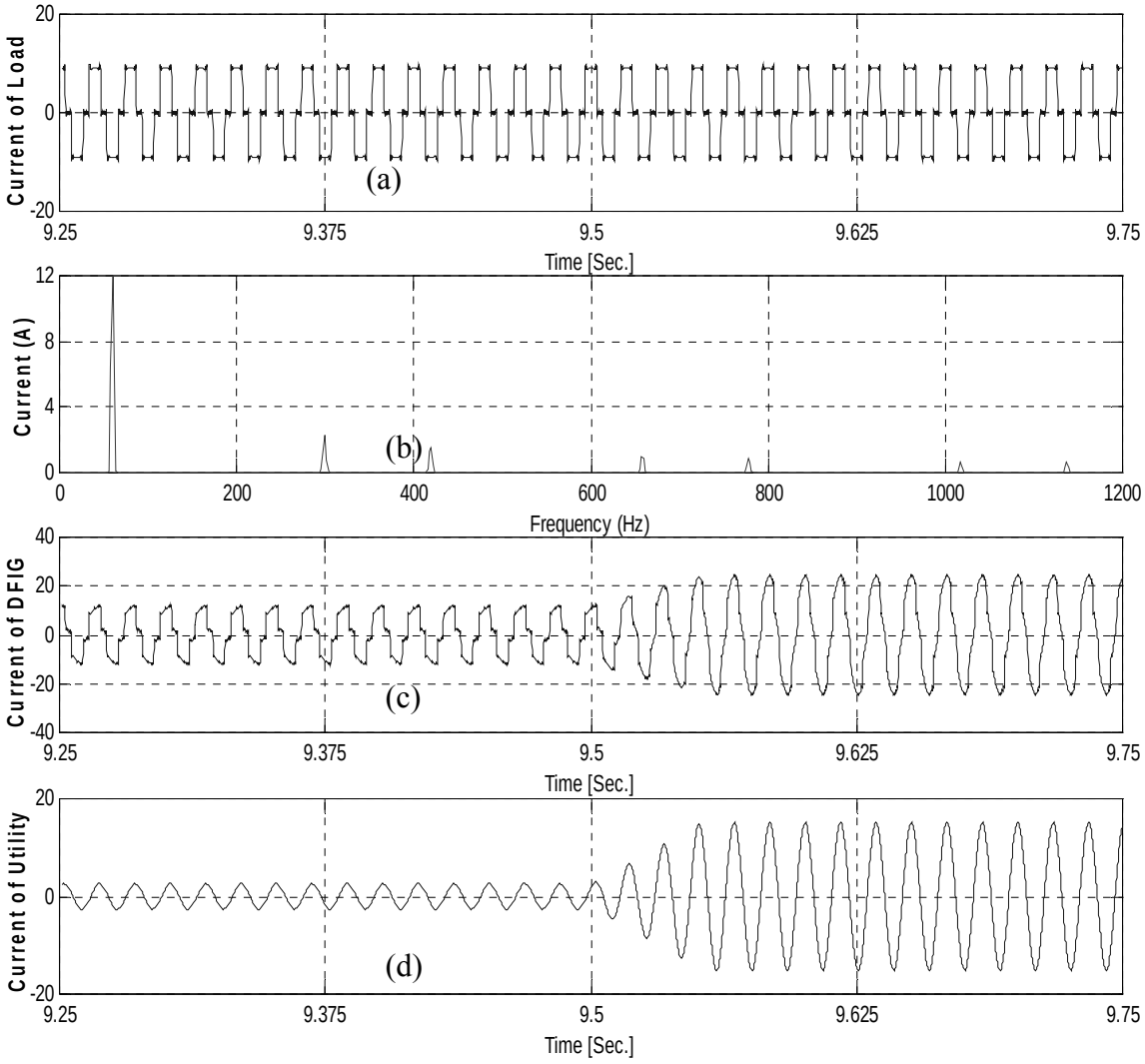

Figure 2-38: Simulation result for case study 2. (a) Nonlinear load current, (b) Frequency spectrum of nonlinear load current, (c) Current of IDEA and (d) Current of utility

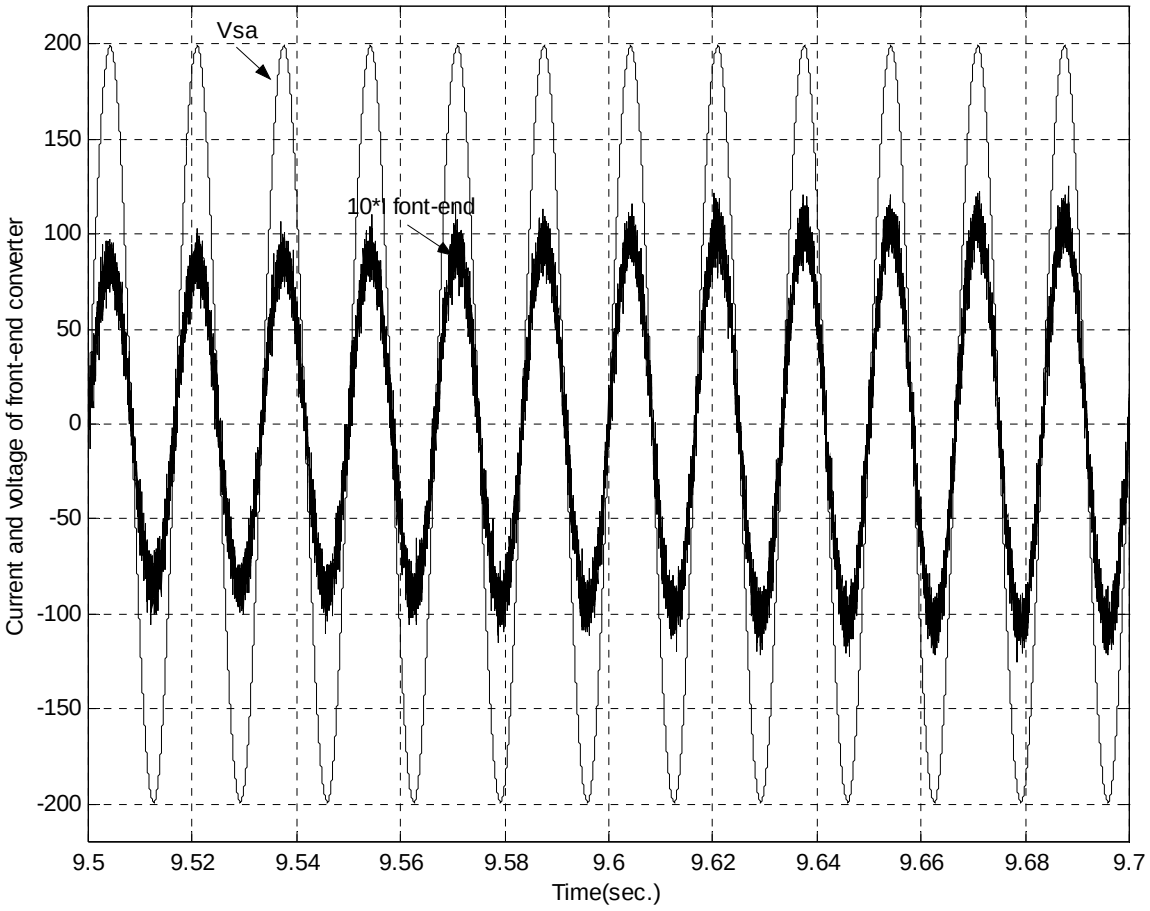

Figure 2-39: Simulation result for case study 2, current and voltage of front-end converter with, $i_d^{e*} = 0$ for unity power factor (current has been scaled up by 10 times)

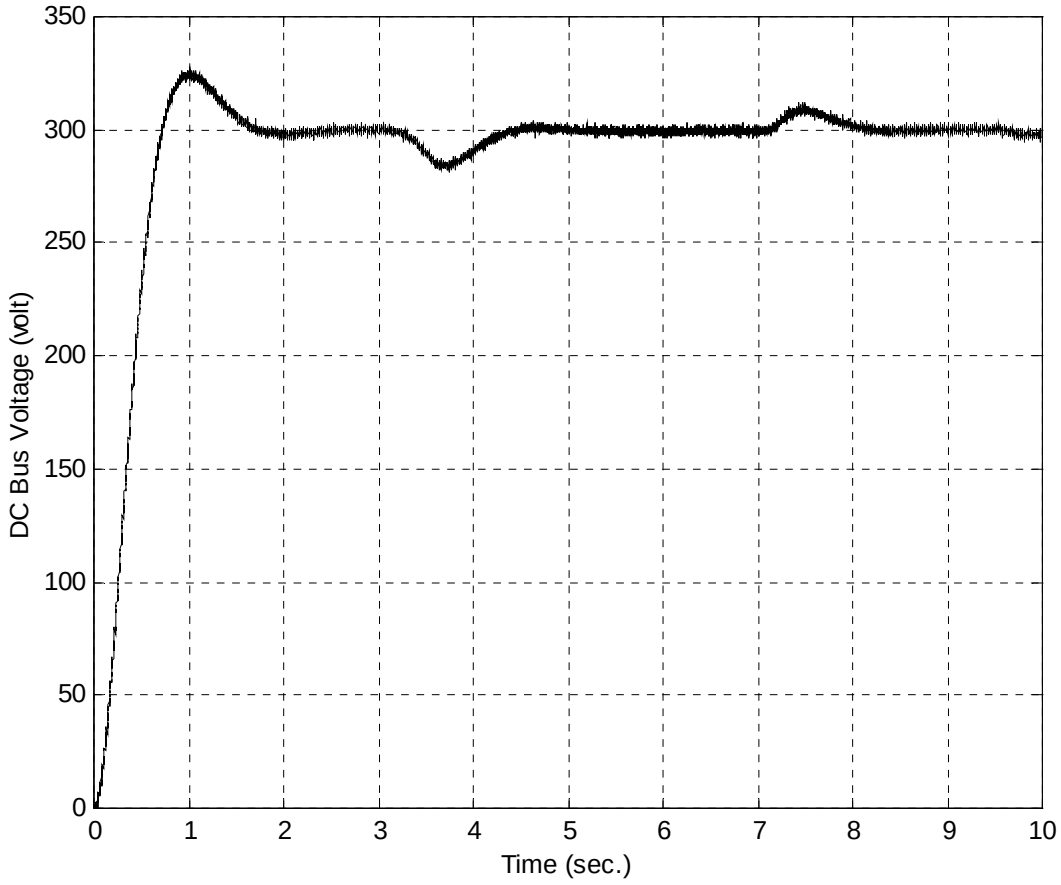

Figure 2-40: Simulation result for case study 2, dc-bus voltage (volts)

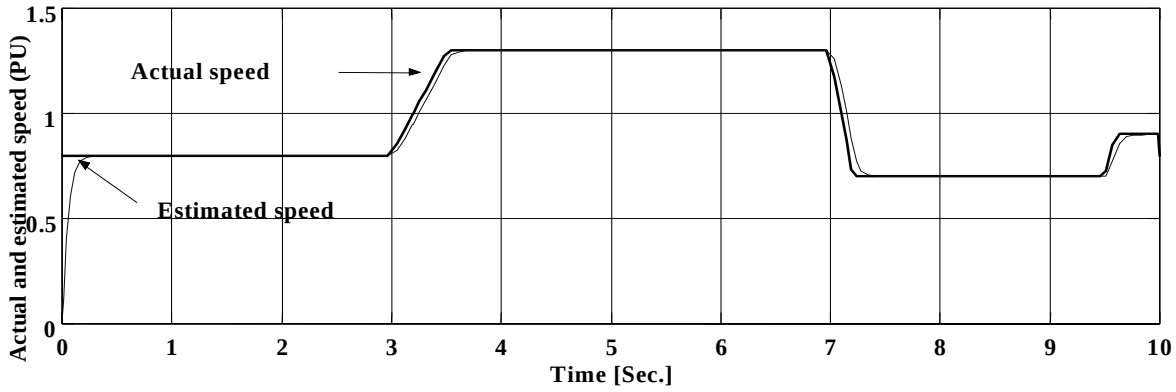

(a)

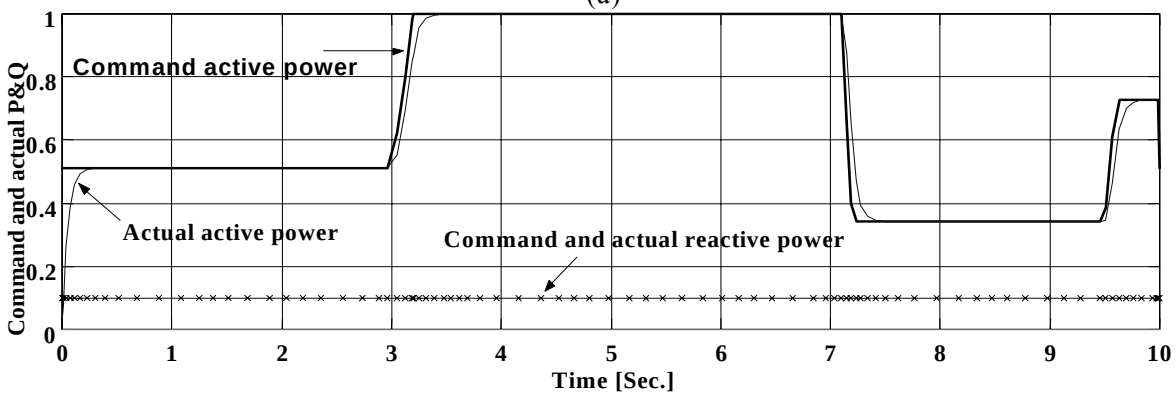

(b)

Figure 2-41: Simulation result for case study 3. (a) Actual and estimated speed (pu) and (b) Command and actual active and reactive power (pu)

II.6.6.3. Case study 3

In this case study, the response of sensoreless rotor position estimator is investigated. The same wind speed command for case study 2 is used. Active power and reactive commands are being generated in regard to wind speed. The speed of the rotor of IDEA is estimated with using the method illustrated in section II.5.4.7. The actual rotor speed and estimated rotor speed is depicted in Fig. 2-41 (a). Actual and command active and reactive powers have been plotted in Fig. 2-41 (b). It is observed that the performance of the system in sensoreless method is similar to the sensored method.

II.7. EXPERIMENTAL SETUP

A laboratory prototype wind energy conversion system equipped with the proposed IDEA has been designed and fabricated to test the proposed system configuration. Wind turbine characteristics are emulated with a controllable speed dc motor. The control topology has been implemented using Texas Instruments DSP based digital control platform. In the following the hardware and software configurations are explained. Several experiments are illustrated. The pictures of laboratory setup are shown in Fig. 2-42 and Fig. 2-43.

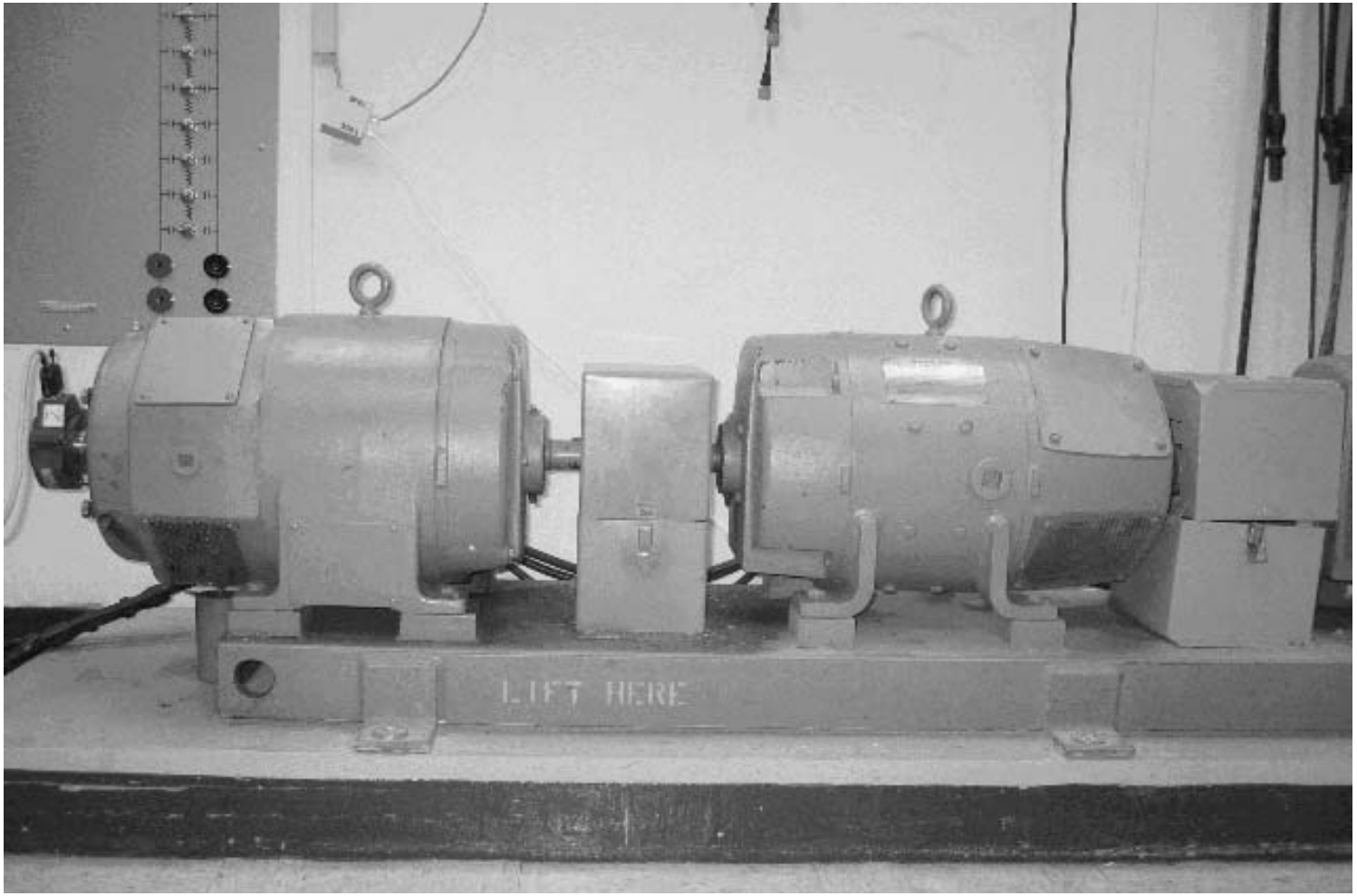

Figure 2-42: Laboratory setup

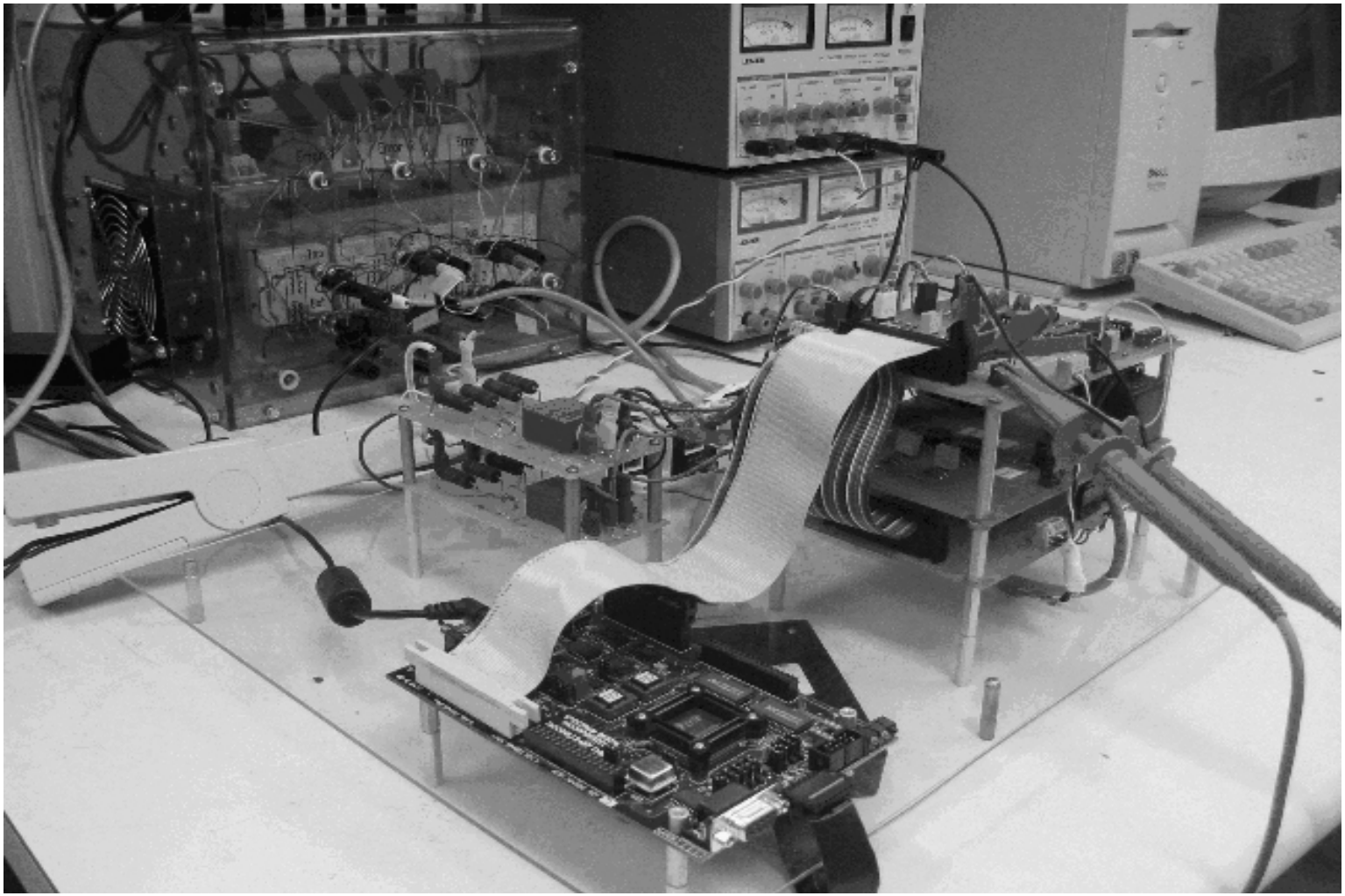

Figure 2-43: Laboratory setup, control boards

II.7.1. HARDWARE CONFIGURATION

In this section, the hardware configuration of the laboratory setup is explained. It is beneficial to detail power circuit configuration and control hardware arrangement separately.

II.7.1.1. Power circuit configuration

The schematic block diagram of the laboratory experimental setup is given in Fig. 2-44. It consists of 7.5 kW wound rotor induction machine with its stator connected to 230 V, 60 Hz, 3-phase power grid, and the rotor being fed by IGBT-based PWM power converter and diode rectifier. The setup is organized for generation operation where the torque-speed characteristics of the wind turbine are emulated by a controllable speed 7.5kW dc motor, which is coupled with IDEA shaft and is driven using a controlled diode rectifier.

A diode rectifier feeding a variable resistor has been connected to the grid in parallel to IDEA and acts as a nonlinear load. A Semikron power converter has been used to control the excitation of IDEA.

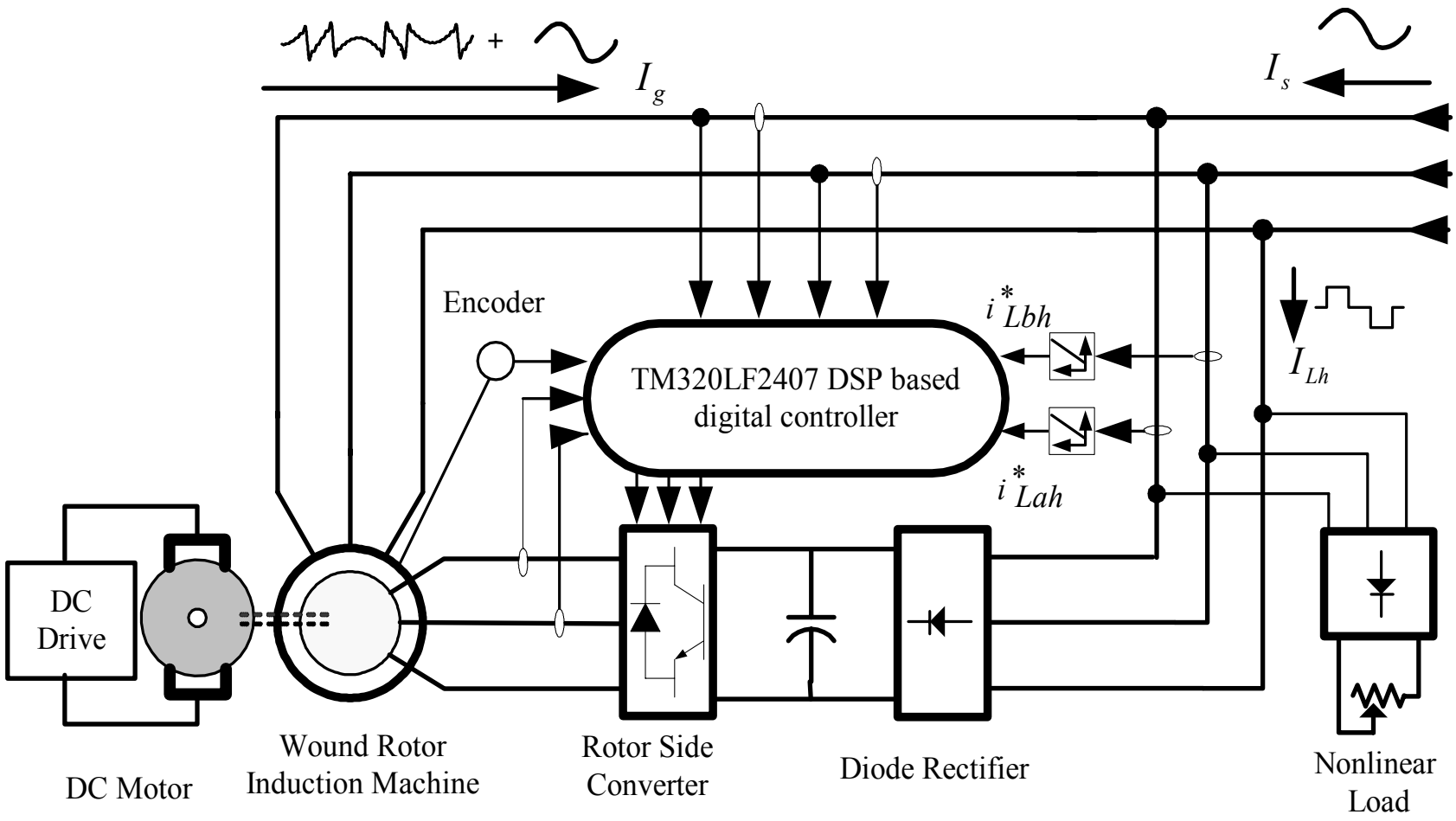

Figure 2-44: Schematic block diagram of the experimental setup

II.7.1.2. Control circuit configuration

A TMS320F2407 fixed point TI DSP based digital control platform is designed and employed for implementing the proposed field oriented control method of the IDEA. The processor runs at a clock frequency of 30 MHz and the sampling frequency used is 50 μs. The software is assembly coded for fast real-time execution.

Currents of stator and rotor of IDEA and current of nonlinear load are measured. The system is three-wire system without neutral connection so the sum of the currents is zero, this make it possible to use just two current sensors per each current measurement. A total of eight current sensors have been employed; two of them are used to sample the stator current of IDEA, another two to sense the rotor current of IDEA and the other two to measure the nonlinear load currents. Utility voltages are sensed through two voltage sensors. An optical speed sensor with resolution 1024 pulse per revolution has been installed on the shaft of IDEA, which provides very good accuracy on speed measurement. Two analog band rejection filter have been designed and fabricated to filter out the fundamental current from the nonlinear load current which make the command current for harmonic compensation system. Interfaces circuit boards for signal conditioning for DSP controller and derive of power converter have been designed and fabricated. The control hardware's configurations have been shown in Fig. 2-45.

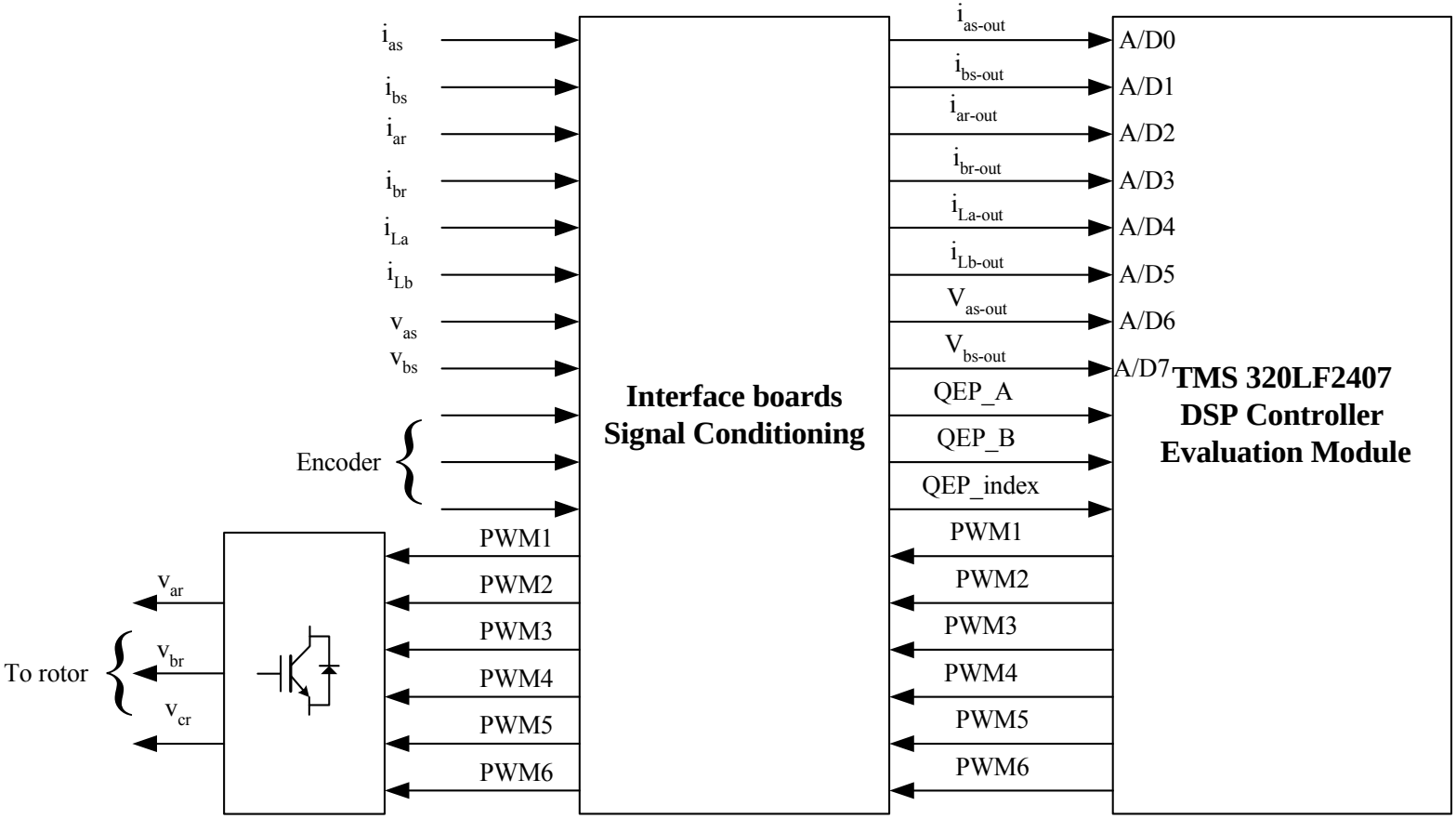

Figure 2-45: Control hardware configuration

II.7.2. A SOFTWARE MODULARITY STRATEGY FOR DIGITAL CONTROL SYSTEM OF IDEA

A software modular to use with TI DSP controller TMS320LF2407 has been developed in assembly code for digital control of IDEA. The benefits of structured modular software are well known. The software is included different independent modules where each module can be debugged and tested separately while they can be connected to other modules for software development. Well-defined module input/output variables provide clear probe/debug points within the software. The inputs and outputs of each module can be addressed in program memory. This makes possible connecting the inputs and outputs of modules easily. All numbers are represented in fixed-point representation numbers for further accuracy. In the following, the fixed point arithmetic and representation of the numbers are explained.

II.7.2.1. Fixed-point arithmetic, representation of numbers

In binary format, a number can be represented in signed magnitude, where the left-most bit represents the sign and the remaining bits represent the magnitude. Two's complement is an alternative form of representation used in most processors, including the TMS320 series. The representation of a positive number is the same in two's complement and in signed magnitude. However, the representation of a negative number is different. The TMS320F2407 is part of the TMS320C2xx 16bit fixed-point DSP family of TI. The native length of a word is 16bit in this family.

To represent real numbers on this fixed-point architecture, a Q*k* format has to be chosen by the user. Q*k* numbers can be represented by the following general formula:

$$Z = -b_{15-k} * 2^{15-k} + b_{14-k} * 2^{14-k} + ...b_0 + b_{-1} * 2^{-1} + b_{-2} * 2^{-2} + ... + b_{-k} * 2^{-k}$$

(2-135)

An implied dot separates the integer part from the fractional part of the Q*k* number where *k* represents the quantity of fractional bit. For instance, the real number π (3.14159) can be represented in Q*13* with finite precision as follows:

$$011.001001000011112 = 0*2^2 + 1*2^1 + 1*2^0 + 0*2^{-1} + 0*0^{-2} + 1*2^{-3} + 0*2^{-4} + 0*2^{-5} + 1*2^{-6} + 0*2^{-8} + 0*2^{-9} + 0*2^{-10} + 1*2^{-11} + 1*2^{-12} + 1*2^{-13}$$

(2-136)

The number of bits dedicated to the fractional part affects the accuracy of the result while the integer part affects the dynamic range of values that can be represented. The Q*15* format offers the best precision but only real numbers comprised between –1 and +1 can be represented.

The Q*k* format offers a compromise between dynamic range and precision. The Q*12* numeric format is used in the major parameters: 4 bits are dedicated to the integer part and 12 bits are dedicated to the fractional part. The precision of this format is 2^{-12} (0.00024414). The represented numbers are in the range of [-8 to 8] to ensure that values can handle each drive control quantity, not only during steady state operation but also during transient operation.

II.7.2.2. Arithmetic operations

II.7.2.2.1. Multiplaction

Figure 2-46 shows an example how two real numbers (X and Y) coded in Q*12* are multiplied.

X = -1.12510 is represented as 1110**.** 1110 0000 00002 in Q*12*
Y = +1.37510 is represented as 0001**.** 0110 0000 00002 in Q*12*
0001 011(0 0000 0000) (+1.375)
1110 111(0 0000 0000) (-1.125)

0001 011
0 0010 11 SUM1= 00100001+(zeroes)
00 0101 1 **..** SUM2=001001101+(zeroes)
000 0000 **...** SUM3=0001001101+(zeroes)
0001 011 **....** SUM4=00011111101+(zeroes)
1 1101 01 **.....**
z = 1 1111 0**.**011 101(00…00) (-1.546875)
18 zeroes

Figure 2-46: An example on mulitiplication of two real numbers in Q12 format

The multiplication of a Q_k (2^k) number by a Q_p (2^p) number results in a Q_{k+p} (2^{k+p}) number (the same rule also exists in base 10. ex : $10^3 * 10^5 = 10^8$). In the case of a Q_{12} by Q_{12} multiplication, the virtual dot is shifted and the 24 least significant bits of the 32-bit accumulator represents the fractional part of the result ($Q_{12} * Q_{12} = Q_{24}$).

As the result of the multiplication gives a 30bit number, the SXM bit (sign extension mode) is set to propagate the sign to the two most significant bits of the accumulator.

Z will be stored back in Q_{12} format. To do so, the content of the accumulator is left shifted four times and the upper word of the accumulator is stored in Z. Z is stored as 1110. 0011 1010 00002 in Q*12* = -1.546875 (decimal).

II.7.2.2.2. Addition

The following example shows how two real numbers (X and Y) coded in Q_{12} are added.

X = +1.12510 is represented as 0001**.** 0010 0000 00002 in Q_{12}

Y = +1.37510 is represented as 0001**.** 0110 0000 00002 in Q_{12}

Z is stored as 0010. 1000 0000 00002 in Q_{12} = 2.5 (decimal).

II.7.2.3. PU model and base values

The Per Unit model (PU) is associated with reduced value notion. As the TMS320F240 is a fixed-point DSP, it has been shown that the greatest precision is obtained in Q^{15} format but the dynamic range of this format is small: it is comprised between –1 and +1 only. Using a fixed-point DSP, it is necessary to reduce the amplitude of the variables in order to get a fractional part with a maximum precision. The notion of Per Unit model is introduced to use this fixed-point feature. It is usually associated with the nominal values of the motor. The per-unit current is usually defined as I pu = I / $I_{nominal}$. This equation shows that I pu = 1 when the current reaches its

nominal value. Instead of using the nominal value as reference, a base value is preferred. For currents and voltages, the reason to choose a base different from the nominal values is that nominal values usually given by the motor manufacturer are RMS (root mean square). Then, the preferred per unit model for the current is given by:

$$i = \frac{I}{I_{base}} \tag{2-137}$$

where:

$$I_{base} = I_{no\min al} * \sqrt{2} \tag{2-138}$$

and the pu model for voltage is given by:

$$v = \frac{V}{V_{base}} \tag{2-139}$$

where: $V_{base} = V_{no\min al} * \sqrt{2}$ (2-140)

As mentioned earlier, transient currents (for instance) might reach higher values than their nominal values. Furthermore, the motor speed range might be extended above the nominal speed, then each per unit value might be greater than one. This remark forces the implementation to handle these situations and thus the suited numerical format chosen was Q12 for the pu models. The Q12 representation of 1 is 1000h. The pu value is equal to 1 when the value is equal to its base. The software module configuration is shown in Fig. 2-47. As it was discussed the parameters and variables are defined in pu system for more accuracy. The input and output of each module is in Q15 format for better precision.

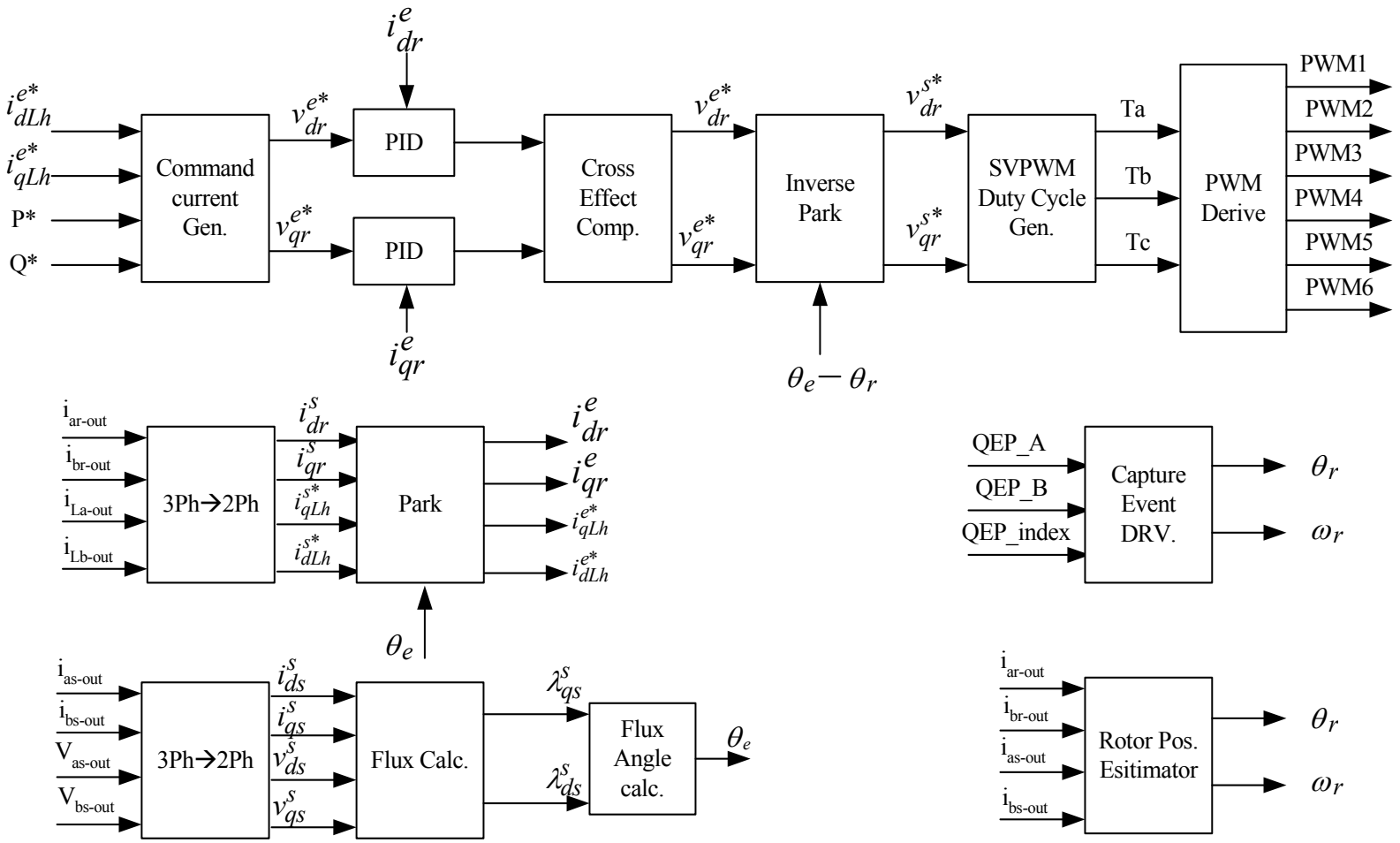

Figure 2-47: Software modules configuration

II.7.3. EXPERIMENTAL RESULTS

Several experiments have been conducted in different conditions that in following several case studies are explained.

II.7.3.1. Case study 1

Non-linear load current is generated by a diode rectifier feeding a variable resistor. The magnitude and phase of nonlinear load are changed to evaluate the performance of the proposed IDEA. In this case study, all the generation, reactive power compensation and harmonic cancellation features are activated. Diode rectifier has been connected to utility and draws a non-linear load current where phase A current is shown in Fig. 2-48 (a). Fundamental current is extracted and harmonics reference current in phase A is generated which is given in Fig. 2-48 (b). These reference currents are transferred to two-phase stationary reference frame which harmonics currents in d-axis and q-axis in stationary reference frame have been depicted in Fig. 2-48 (c) and (d). Active power and reactive power commands are set to 40% pu and 0.05 pu respectively. Command rotor harmonic currents in d and q-axes in stationary reference frame have been shown in Fig.2-49 (a) and (b) respectively. Then, the active and reactive commands are added to these values and make the total rotor quadrature and direct axes commands currents in the excitation reference frame for rotor side power converter which are plotted in Fig. 2-49 (c) and (d).

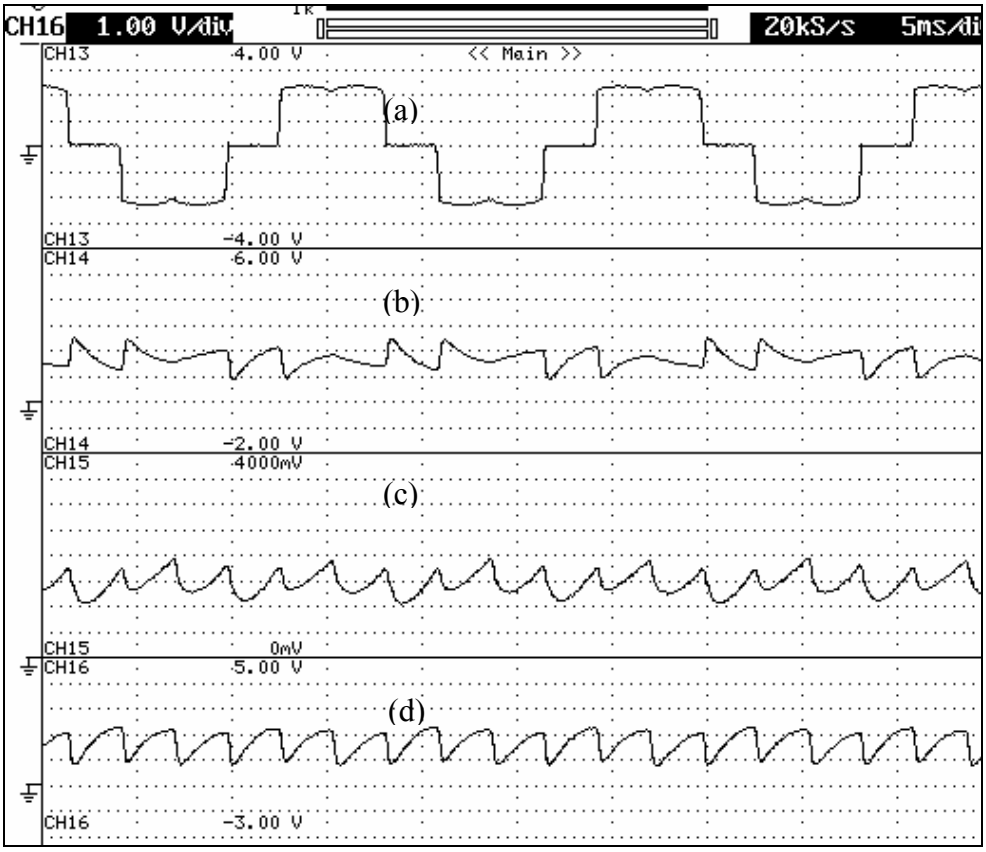

Figure 2-48: Case study 1. (a) Nonlinear load current, (b) Harmonic reference current, (c) The d-axis harmonic current command in stationary reference frame and (d) The q-axis harmonic current command in the stationary reference frame

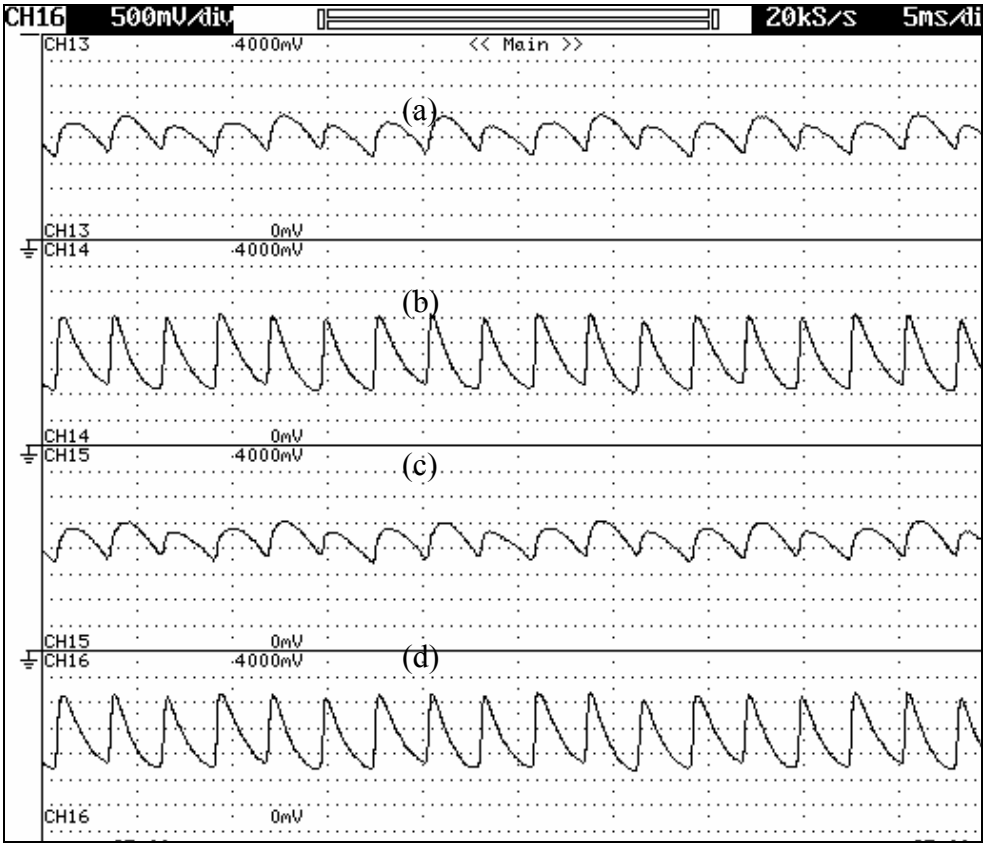

Figure 2-49: Case study 1. (a) The d-axis harmonic rotor current command in the excitation reference frame, (b) The q-axis harmonic rotor current command in the excitation reference frame, (c) Total d-axis rotor current command in the excitation reference frame and (d) Total d-axis rotor current command in the excitation reference frame

The angular position of the rotor is obtained by optical encoder. With having angular position of stator flux and rotor position, angular position of slip is generated which is shown in Fig. 2-50 (d). Cross effect compensation in d and q axes are performed and voltage command for rotor side power converter in excitation reference frame is calculated. Using inverse park transformation and angular position of slip, rotor command voltage components in stationary reference frame is produced, which are shown in Fig. 2-50 (c) and Fig.2-50 (b). Using SVPWM modules, the gates drive of the IGBT's of rotor side power converter are generated. The applied voltage to rotor circuitry in phase A is illustrated in Fig. 2-50 (a). In Fig. 2-51 voltage of the grid and current of IDEA are shown. The nonlinear portion of the current of the IDEA compensates the harmonics currents of the non-linear load while some active power to the grid is also injected. The power factor is maintained at unity.

II.7.3.2. Case study 2, power generation only

In this case study, harmonic compensation system is deactivated and only power generation module is evaluated.

In this exercise, active power command is set to 0.8 pu and reactive power command is set to 0.1 pu. Angular rotor slip position is generated and has been captured in Fig. 2-52 (d). Command rotor voltages in d and q axis in stationary reference frame are shown in Figs. 2-52 (b) and 2-52 (c). Applied rotor voltage and rotor current both in phase A are shown in Fig. 2-52 (a).

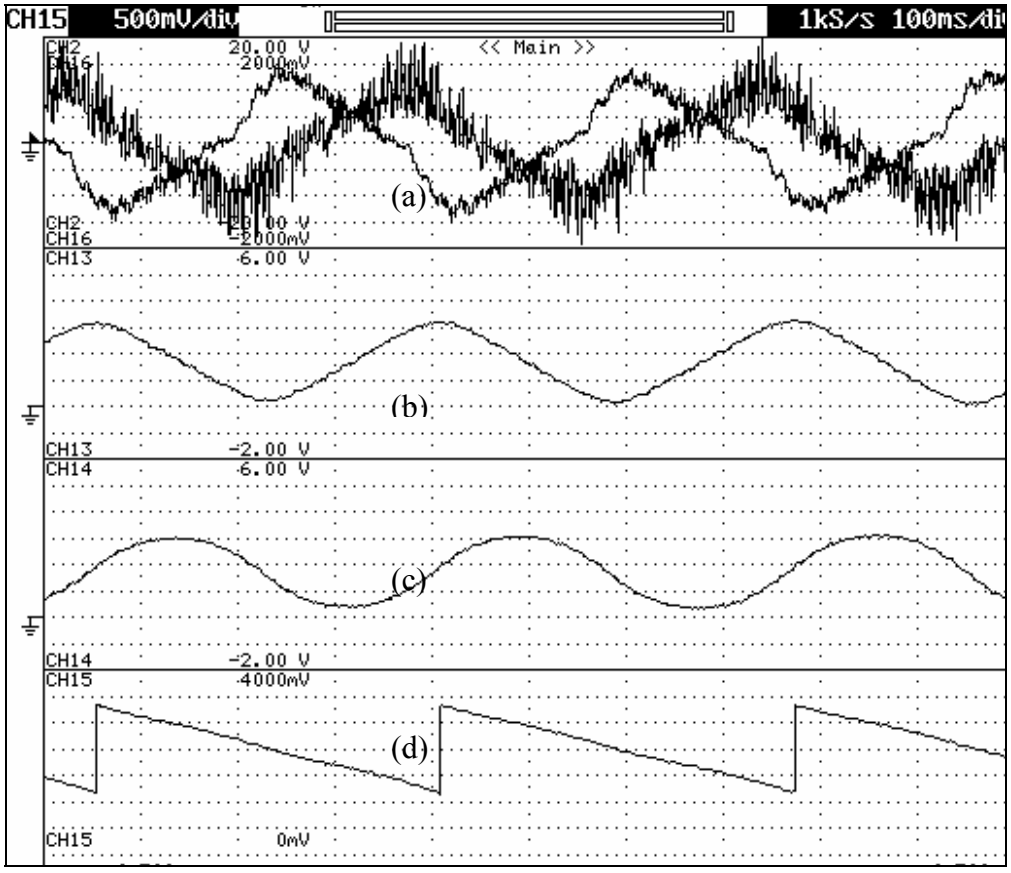

Figure 2-50: Case study 1. (a) Applied voltage to the rotor, (b) The d-axis command rotor voltage in the stationary reference frame, (c) The q-axis command rotor voltage in stationary reference frame and (d) Angular position of slip frequency

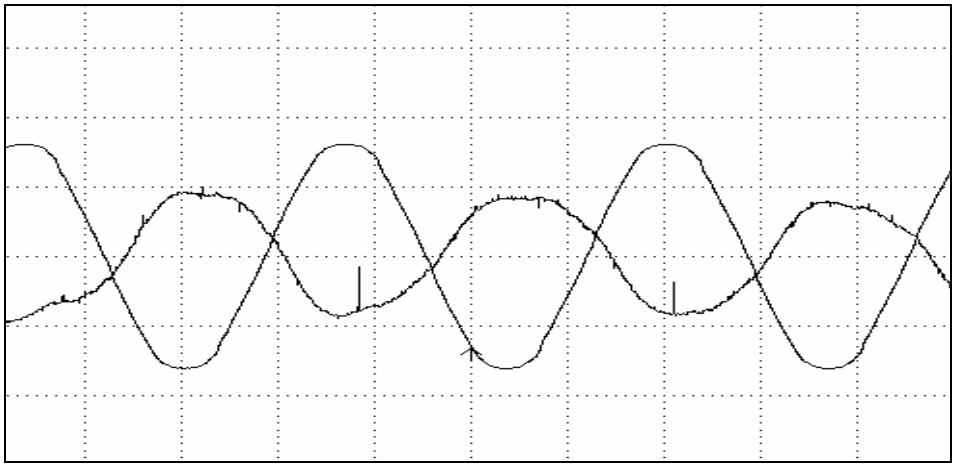

Figure 2-51: Voltage of the grid and current of IDEA

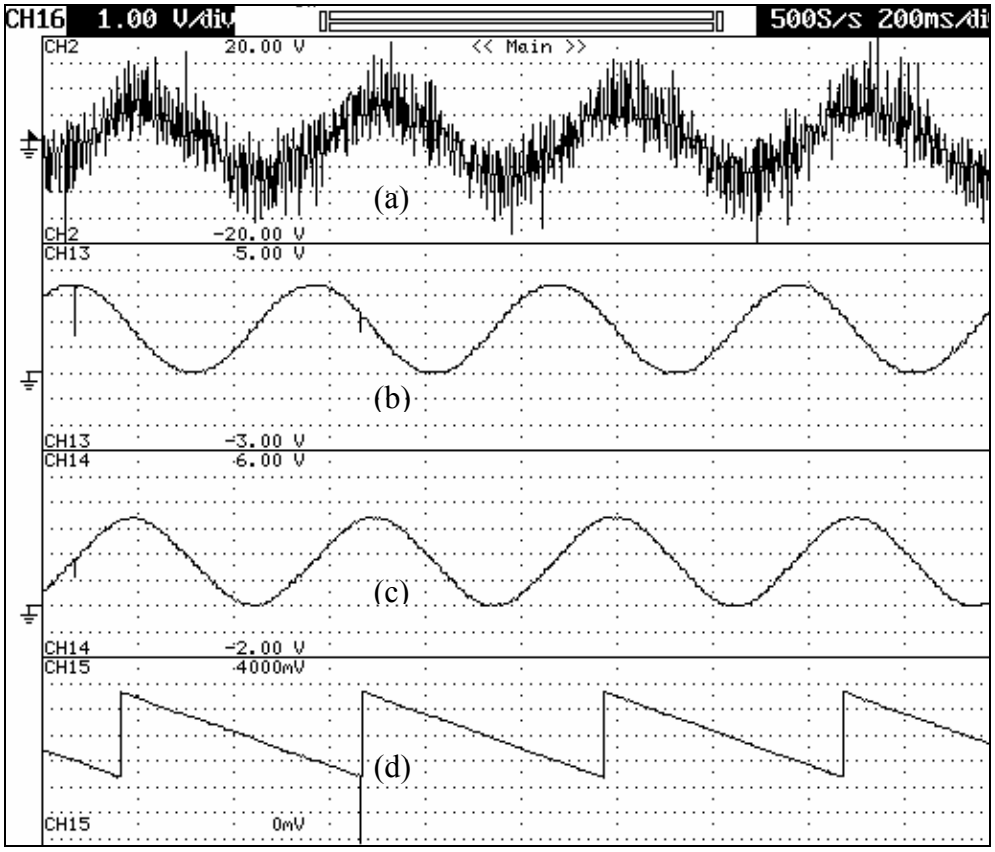

Figure 2-52: Case study 2, power generation only. (a) Applied voltage to the rotor and current of the rotor, (b) The d-axis command rotor voltage in stationary reference frame, (c) The q-axis command rotor voltage in stationary reference frame and (d) Angular position of slip frequency

The current of IDEA and voltage of utility are shown in Fig. 2-53.

II.7.3.3. Case study 3

In this case study, the amount of power generation command is decreased to 20% pu but the reactive current command is maintained at 5% pu. It is predicted that slip frequency will increase.

Diode rectifier has been connected to utility and draws a non-linear load that current in phase A has been shown in Fig. 2-54 (a). Fundamental current is extracted and harmonics reference current in phase A is generated which is given in Fig. 2-54 (b). These reference currents are transferred to two-phase stationary reference frame which harmonics currents in d-axis and q-axis in stationary reference frame is shown in Fig. 2-54 (c) and (d). Angular position of slip is calculated which is shown in Fig. 2-55 (d). Cross effect compensation in d and q axis are performed and voltage command for rotor side power converter in excitation reference is calculated. Using inverse park transformation and angular position of slip, rotor command voltage components in stationary reference frame are produced; these are shown in Fig. 2-55 (c) and Fig. 2-55 (b). Using SVPWM modules the gates derive of the IGBT's of rotor side power converter are generated. The applied voltage to rotor circuitry in phase A and current of the rotor in phase A are depicted in Fig. 2-55 (a). In Fig. 2-56 voltage of the grid and current of IDEA are shown.

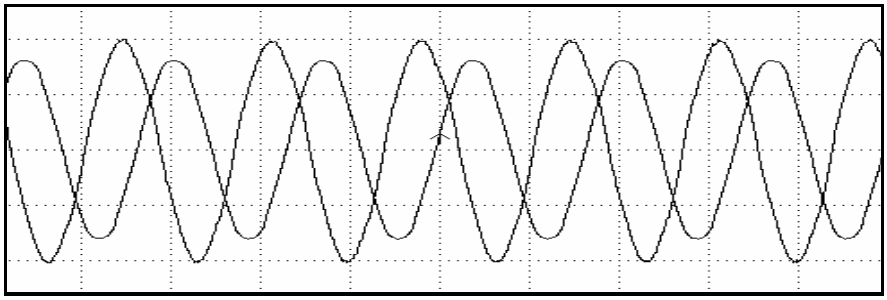

Figure 2-53: Case study 2, power generation only, grid voltage and current of IDEA

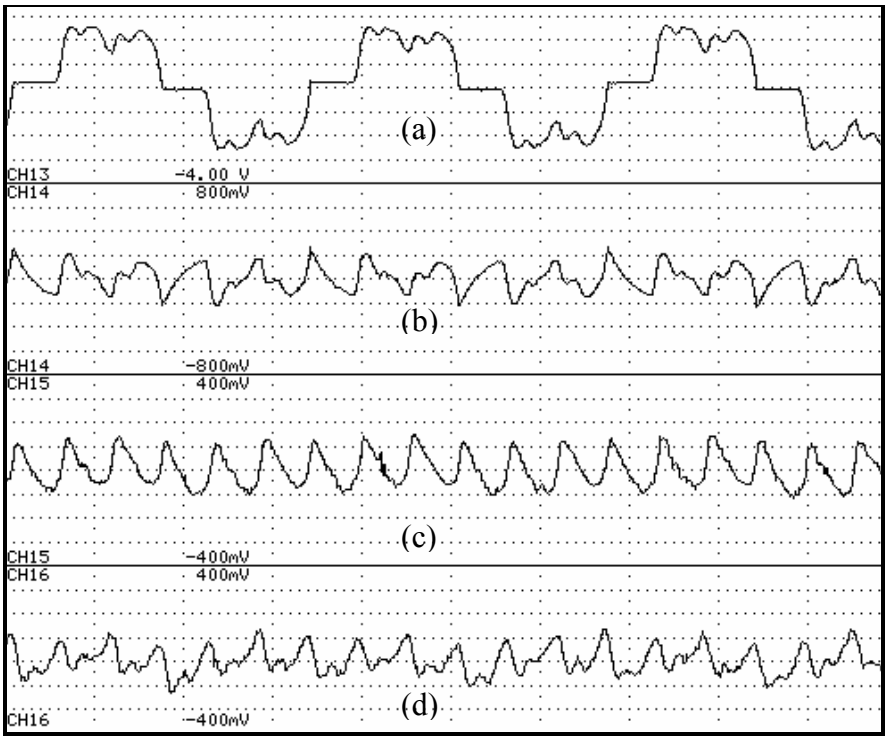

Figure 2-54: Case study 3. (a) Nonlinear load current, (b) Harmonic reference current, (c) The d-axis harmonic current command in stationary reference frame and (d) The q-axis harmonic current command in stationary reference frame

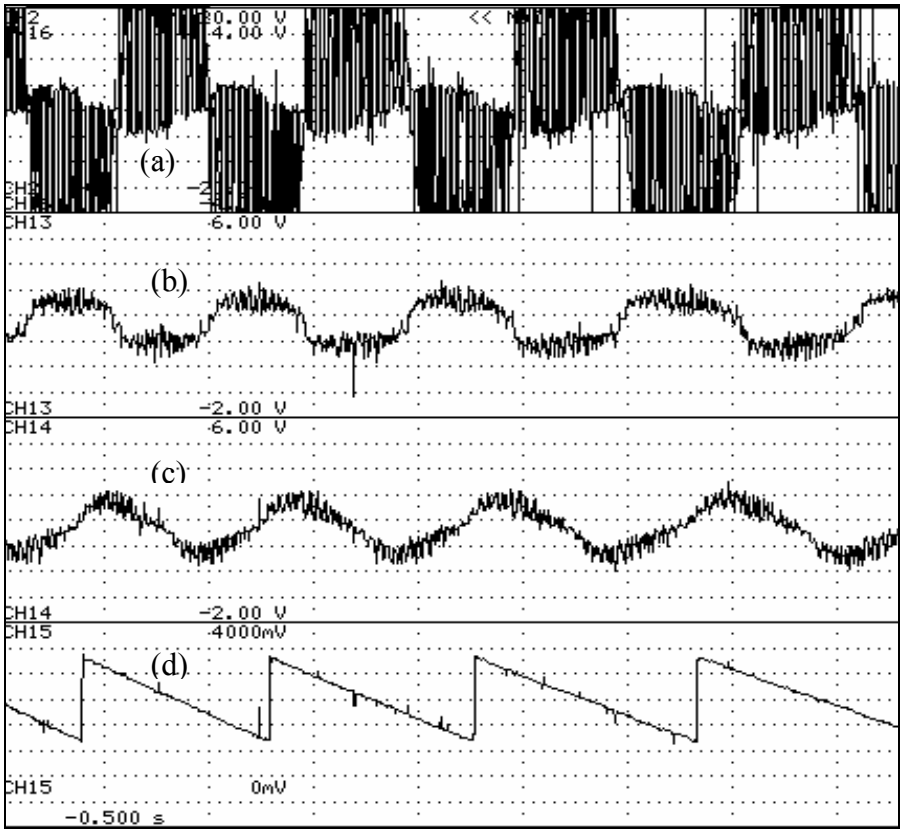

Figure 2-55: Case study 3. (a) Applied voltage to the rotor and current of the rotor, (b) The d-axis command rotor voltage in stationary reference frame, (c) The q-axis command rotor voltage in stationary reference frame and (d) Angular position of slip frequency

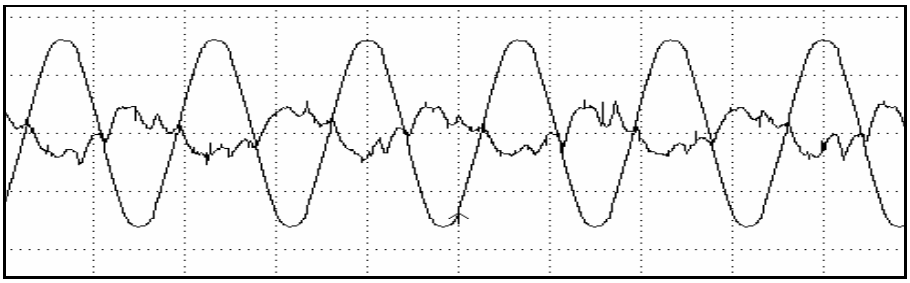

Figure 2- 56: Case study 3, voltage of utility and current of IDEA

II.7.3.4. Case study 4

In this experiment the power command is set to 30% pu and reactive power command is set to zero. Harmonic command current in phase A and B are shown in Fig. 2-57 (a) and Fig. 2-57 (b), respectively. Command rotor harmonic currents in d and q axes in excitation reference frame are given in Fig. 2-57 (c) and (d) respectively. Slip frequency angular position is calculated and has been plotted in Fig.2-58 (d). Command rotor voltage components in two-phase stationary reference are given in Fig.2-58 (b) and (c). Output voltage of rotor side power converter and current of the rotor are given in Fig.2-57 (a). In Fig. 2-59, voltage of utility and current of IDEA have been captured. Current of IDEA is enough to compensate the harmonics of rectifier load and correspond to 20% pu active power generation.

II.7.3.5. Case study 5, sensorless rotor position estimation

In this experimental study, the performance of sensorless rotor position estimator is evaluated. The rotor position estimator module is tested over a wide range of rotor speed variation. Measured rotor position by using optical encoder and estimated rotor position are compared in Fig. 2-60. Estimated rotor angle current in the stationary reference frame ($\theta 1$) and in the rotary reference frame ($\theta 2$) and estimated rotor angle position (θr) are depicted in Fig.2-61 (a-c), respectively.

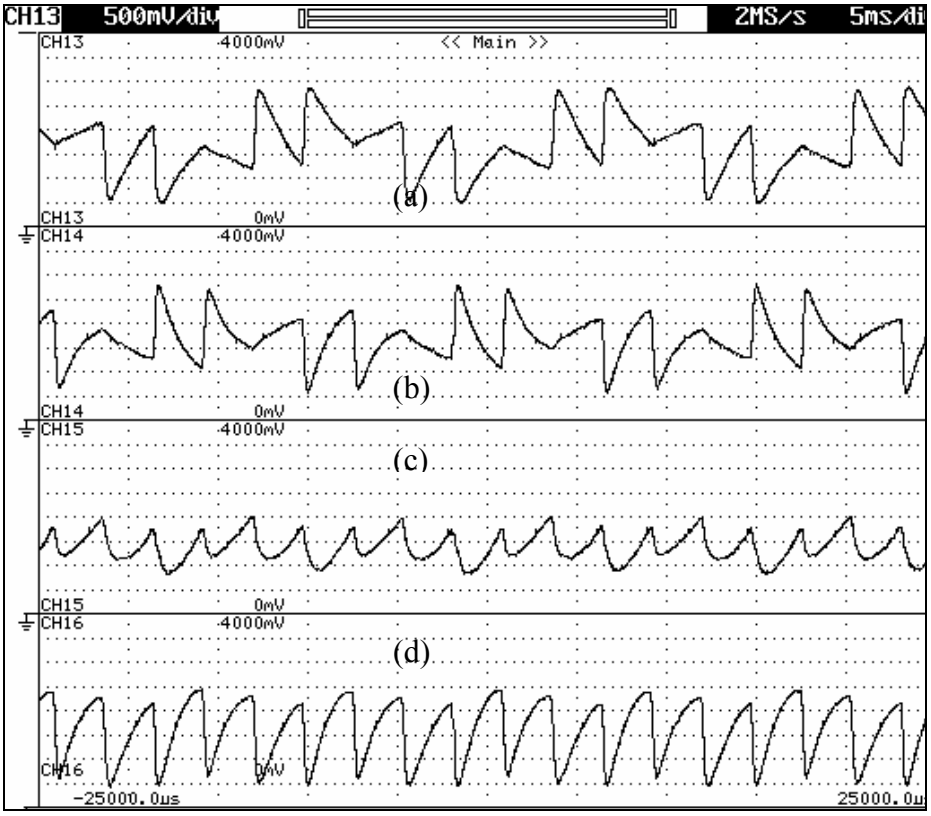

Figure 2-57: Case study 4. (a) Harmonic current command in phase A, (b) Harmonic current command in phase B, (c) Harmonic current command in d-axis excitation reference frame, (d) Harmonic current in q-axis in excitation reference frame

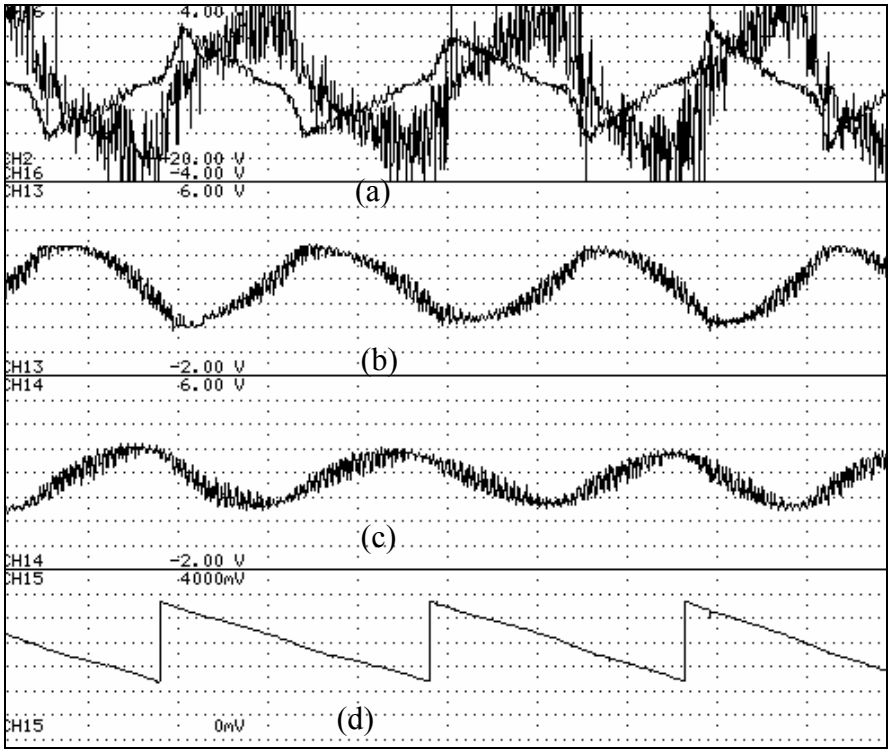

Figure 2-58: Case study 4. (a) Applied voltage to the rotor and current of the rotor, (b) The d-axis command rotor voltage in stationary reference frame, (c) The q-axis command rotor voltage in stationary reference frame and (d) Angular position of slip frequency

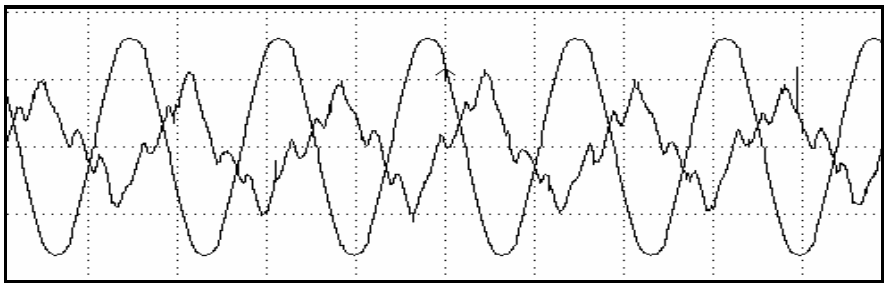

Figure 2-59: Case study 4, voltage of utility and current of IDEA

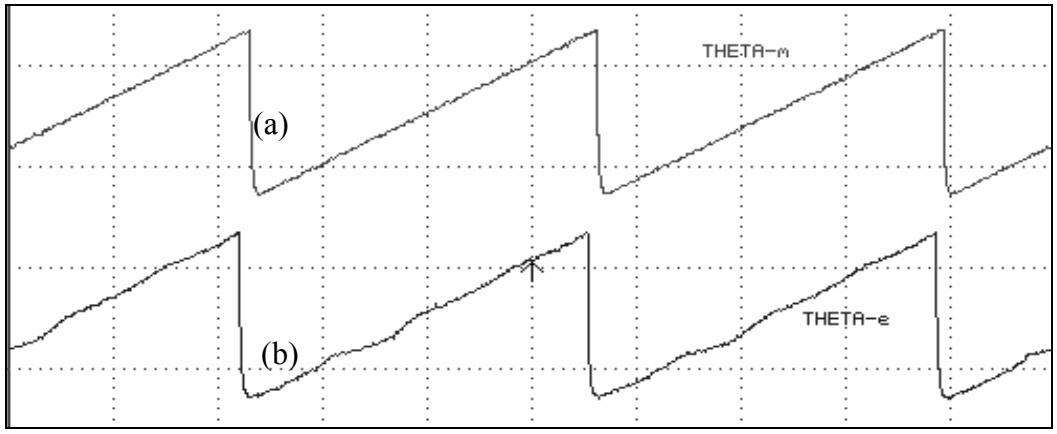

Figure 2-60: Case study 5. (a) Actual rotor angle position and (b) Estimated rotor angle position

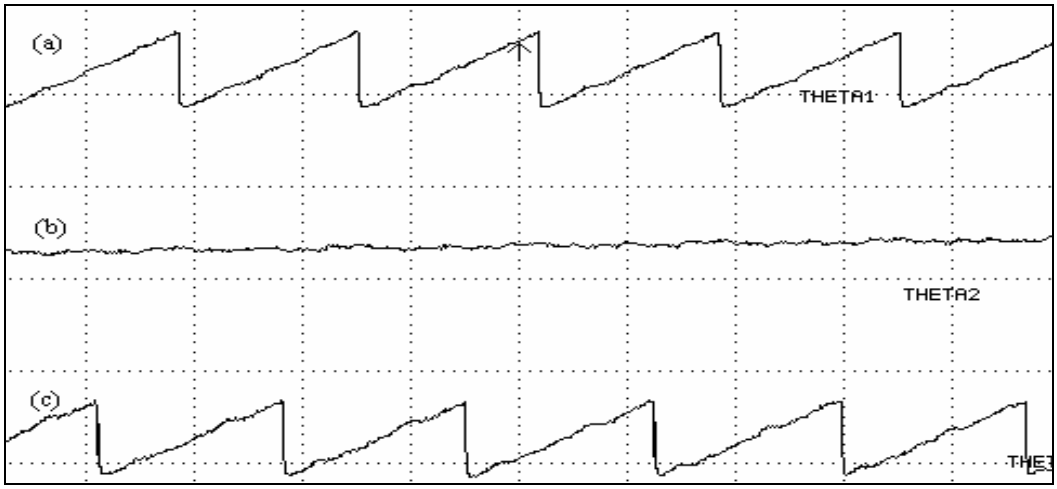

Figure 2-61: Case study 5. (a) Rotor current angle position in stationary refrence frame, (b) Rotor Current angle position in rotor refrence and (c) Esimated rotor angle position

Figure 2-62 shows the estimated rotor angular velocity, slip angular velocity and rotor current angle position in the rotor reference frame.

Stator flux position is calculated based on illustrated method in previous sections and is shown in Fig. 2-63 (a). The rotor position is estimated using the proposed sensoreless method and is captured in Fig. 2-63 (b). Subtraction of stator flux position and rotor position will give the rotor current position rotor reference frame which is shown in Fig.2-63(c)

In Fig. 2-64, the performance of sensoreless rotor position in both sub-synchronous and super synchronous is evaluated. The estimated rotor speed and measured rotor speed using the optical encoder are shown in Fig. 2-64 (a) and (b), respectively. The rotor current position in rotor reference frame is given in Fig 2-64 (c). As it is shown, the direction of rotor current position changes with crossing synchronous speed. As the comparisons in Figs. 2-60 to 2-64 clarify, performance of IDEA at both sensoreless method and sensored using optical encoder is the same. All angles are shown in the range of 0 to 2π.

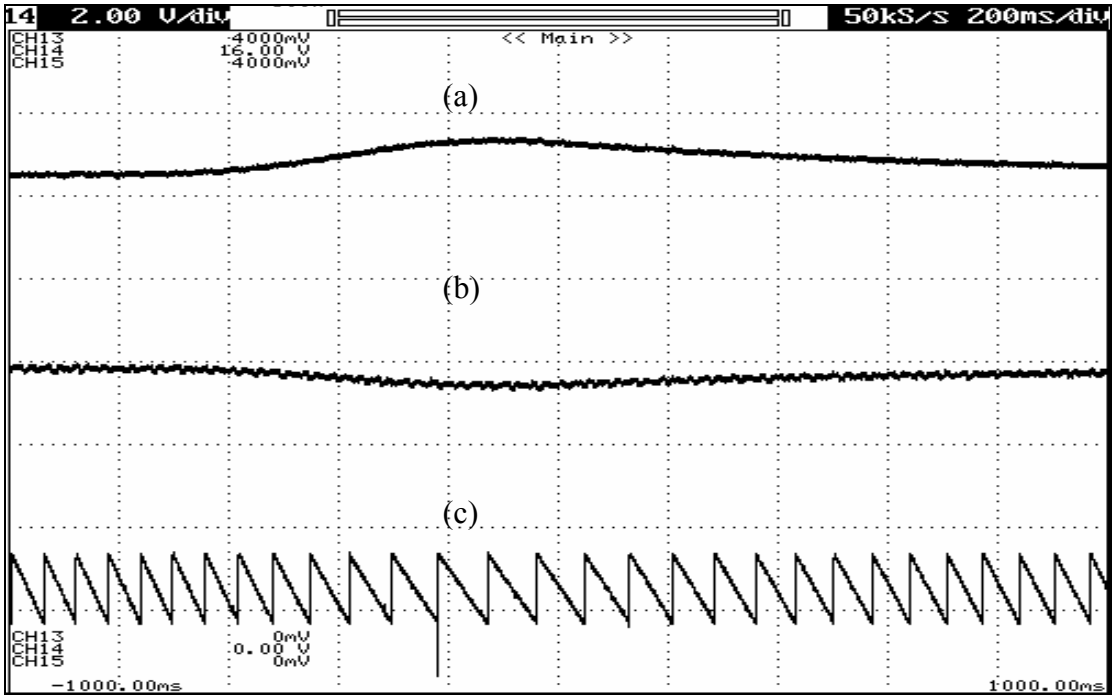

Figure 2-62: Case study 5. (a) Rotor angular velocity, (b) Slip angular velocity and (c) Rotor current angle position in rotor reference frame

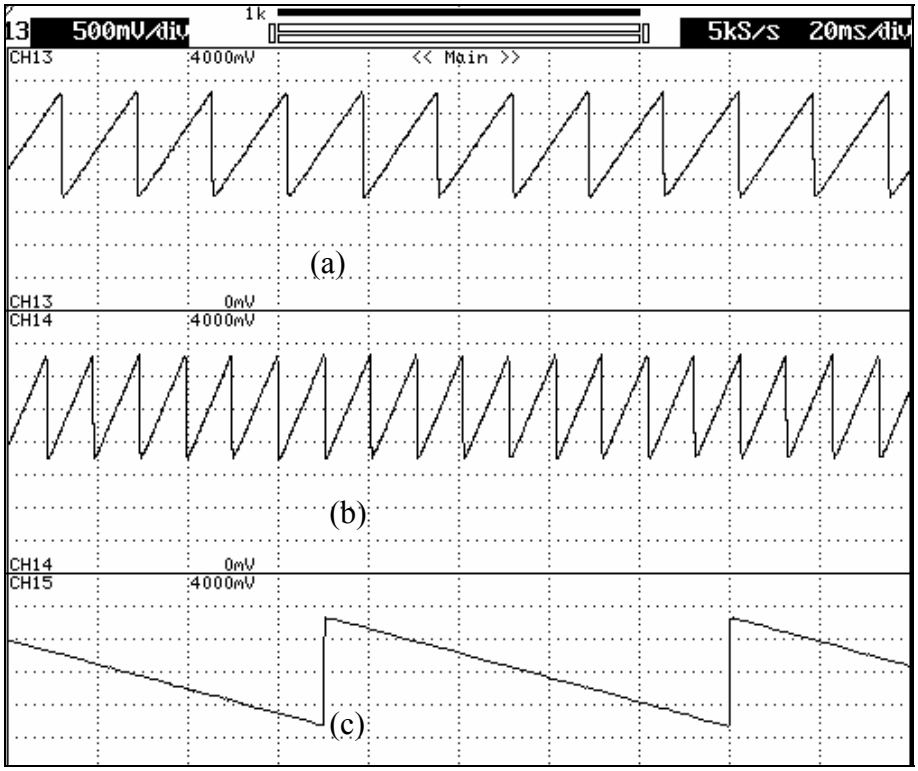

Figure 2-63: Case study 5. (a) Stator flux angle position, (b) Estimated rotor position and (c) Rotor current angle position in rotor reference frame

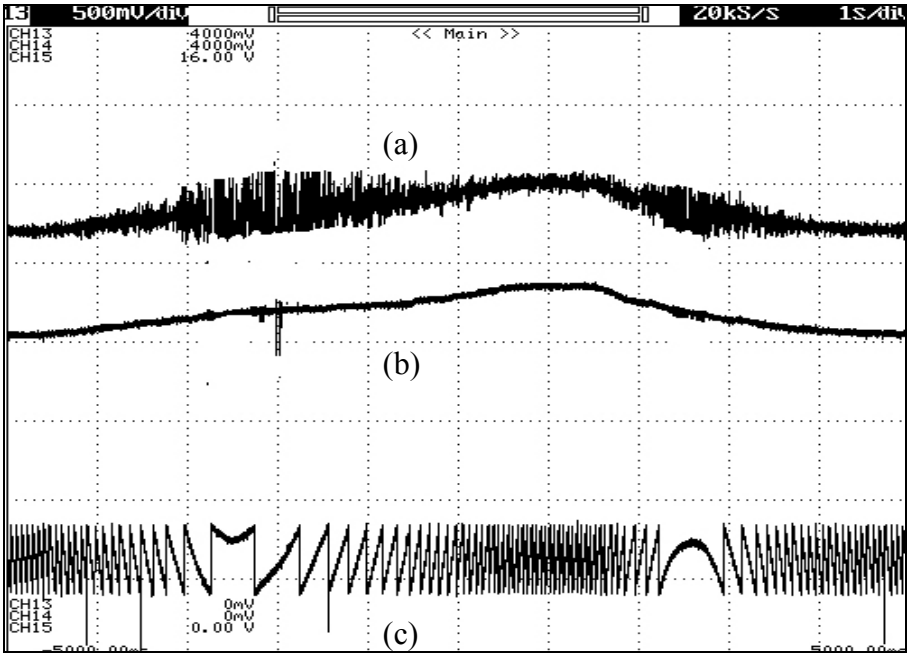

Figure 2-64: Case study 5. (a) Estimated rotor speed, (b) Actual rotor speed and (c) Rotor current angle position in rotor reference frame

II.8. CONCLUSIONS

A sensoreless integrated doubly-fed alternator/active filter IDEA for grid connected variable speed wind energy conversion system has been developed. With the proposed method, it is possible to capture the maximum wind power while harmonics current of utility can be compensated simultaneously. A sensoreless stator flux field oriented control was developed to control the rotor side converter of IDEA where the control strategy is capable of controlling the generated active and reactive power as well as the amount of harmonic compensation in the grid independently. Vector control method for front-end converter for allowing bi-directional power flow in rotor circuit has also been developed. Simulation result as well experimental results have proved the effectiveness of the proposed method.

CHAPTER III

AN INTEGRATED SYNCHRONOUS MACHINE/ACTIVE FILTER

III.1. INTRODUCTION

In the recent years, use of electronic equipment, adjustable speed derives and other nonlinear loads especially in large energy consuming plants have been rapidly increased. It is well known that nonlinear loads demand a non-sinusoidal currents from the utility and contribute to numerous power system problems. The current drawn from the ac lines are rich in harmonics, this results in lower power factor, overheating and interference. With the widespread use of harmonic-producing equipment, the control of harmonic currents to maintain a high level of power quality is becoming important.

The relatively large 5^{th} and 7^{th} harmonics generated by the nonlinear loads are one of the major concerns in electric power distribution systems. Current practice to address this issue is to install passive harmonic filters. However, passive 5^{th} and 7^{th} harmonic filters are known to cause resonance and cannot adapt to changing load conditions.

Conventional ac machines are designed to have sinusoidal voltage and current waveforms to reduce flow of harmonics currents in the utility lines. It appears possible to develop various types of ac machines having a non-sinusoidal winding distribution in which a prescribed non-sinusoidal current can flow [38-43].

In response to these concerns, an integrated synchronous machine/active filter is proposed. The proposed technology can be used as conventional electric generator or electrical motor with featuring of power conditioning of the utility, by means of

compensation of 5^{th} and 7^{th} harmonics currents of the grid. The proposed approach consists of a conventional synchronous machine with modification to its field excitation. It is shown that if proper ac excitation is added to field of conventional synchronous machine, 5^{th} and 7^{th} harmonics of the grid can be compensated.

The proposed approach allows for independent control of 5^{th} and 7^{th} harmonics compensation both in magnitude and in phase. The ac field excitation including controllable 2^{nd}, 4^{th} and 6^{th} harmonics is performed by means of a switching power converter. The dc excitation controls active power and reactive power while ac field excitation adjusts the amount of harmonic cancellation.

The advantages of the proposed approach are:

- A standard synchronous generator can be modified to perform the function of an active harmonic compensator.
- The approach is rugged and can be adapted to low and medium voltage systems.
- The system can be controlled to simultaneously transfer active power to the mechanical load, compensate for reactive power and cancel 5^{th} and 7^{th} harmonic currents generated by nonlinear loads in an industrial plant.

III.2. DESCRIPTION OF THE PROPOSED METHOD

The block diagram of the proposed integrated synchronous machine/ active filter is shown in Fig.3-1 and Fig. 3-2. It is assumed that the combination of nonlinear loads are connected to the utility line and are demanding a nonlinear load current that contains 5^{th} and 7^{th} harmonics.

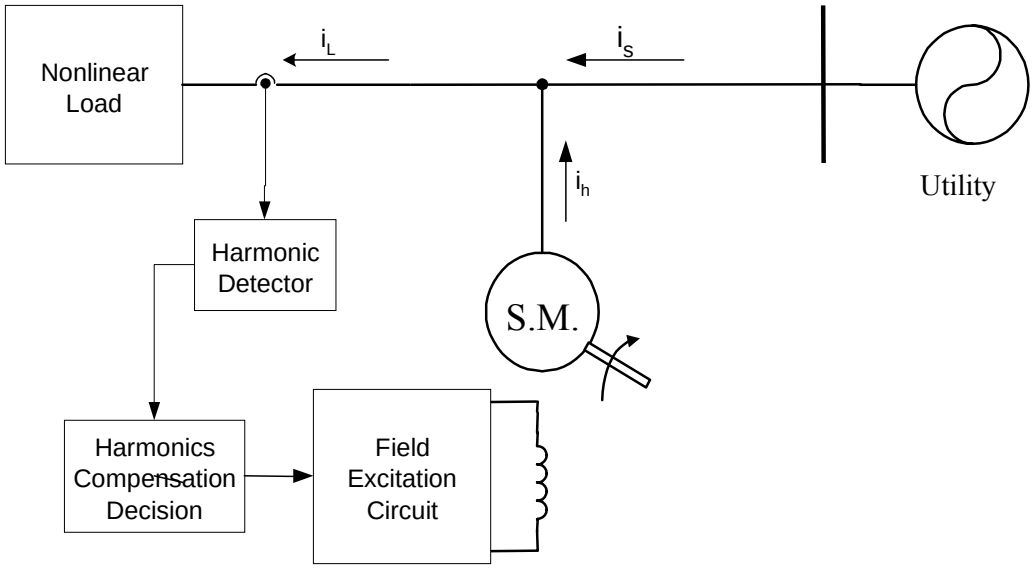

Figure 3-1: Block diagram of the proposed integrated synchronous machine/active filter

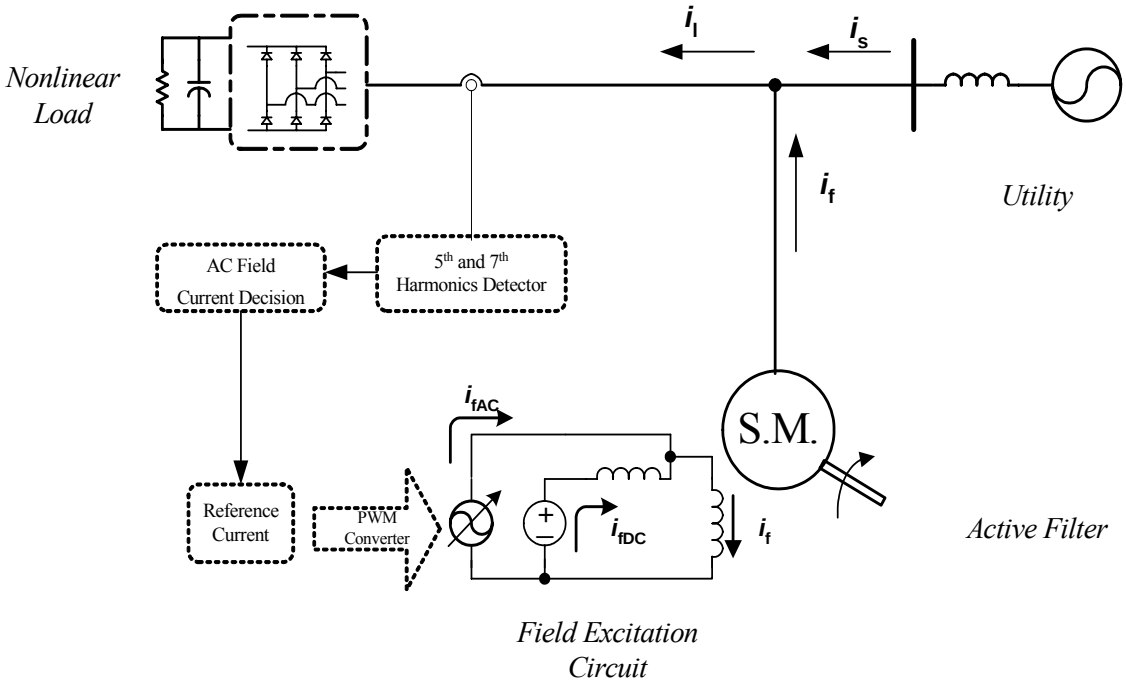

Figure 3-2: The detail schematic of the integrated synchronous machine/active filter

The integrated synchronous machine/active filter is connected to the utility line and is in parallel with the non-linear load. The system can be allowed to operate either in motoring mode or generating mode. The "*Harmonic Detector Block"* detects the amplitude and phase of the 5^{th} and 7^{th} harmonics generated by the non-linear load. This can be performed by sampling the current of nonlinear load through the current sensors and after passing through an analog band pass filter, the fifth and seventh harmonics currents of the nonlinear load are determined. This signal goes to the "*AC Field excitation Decision"*. In this block, the required excitation current for canceling these harmonics components is calculated and then the required excitation current will be made using a power electronic converter.

The illustrated method is for controlling the excitation of a rotating magnetic field of synchronous machine connected to an electric power system as it is shown in Fig. 3-1. This includes the steps for detecting the 5^{th} and 7^{th} harmonics components generated by the nonlinear load with performing fast Fourier transform (FFT) of the nonlinear load current and signal conditioning. This step is followed by detecting the amplitude and phase of 5^{th} and 7^{th} harmonics, finding the required excitation current and regulating it to completely canceling the 5^{th} and 7^{th} harmonics components of the nonlinear load current. Developing the reference current for the current regulated PWM inverter to generate the needed excitation current combination of 2^{nd}, 4^{th}, and 6^{th} harmonics is performed in the next stage. With this strategy, the exact excitation for compensation of 5^{th} and 7^{th} components of the nonlinear load current will be made.

III.3. ANALYSIS OF THE PROPOSED INTEGRATED SYNCHRONOUS MACHINE/ACTIVE FILTER

III.3.1. MMF DISTRIBUTION IN SYNCHRONOUS MACHINE

The MMF distribution in cross section of the synchronous machine is shown in Fig.3-3. If an even harmonic current i_h flows into the field winding of synchronous generator, an electromagnetic flux φ_h links the field winding, which rotates with speed of the rotor. This flux links the stator winding and builds up two opposing MMF inside the airgap which are rotating in forward and backward directions.

The produced forward MMF rotates with the speed of $[(h+1)\omega]$, and the backward MMF rotates with the speed of $[(h-1).\omega]$. From rotor point of viewpoint, both these MMFs are revolving at speed of $[h.\omega]$. The forward MMF causes harmonic current $i_{(h+1)}$ to flow in the stator windings. The backward MMF causes the flow of harmonic current $i_{(h-1)}$ which the phase displacement between $i_{(h+1)}$ and $i_{(h-1)}$ is 180°. Notice that the amplitude and phase of $i_{(h+1)}$ and $i_{(h-1)}$ flowing in the stator windings can not be controlled independently with regulating just i_h. In this chapter, in order to control the amplitude and phase of developed harmonics currents by the field winding and complete cancellation of 5^{th} and 7^{th} harmonics, it is proposed to inject 2^{nd}, 4^{th} and 6^{th} harmonics currents in the field winding. Injecting 6^{th} harmonics in the field winding generates two rotating MMFs in the airgap, where one rotates with speed of 7ω in forward direction, and the other one revolves with speed of 5ω in the backward direction.

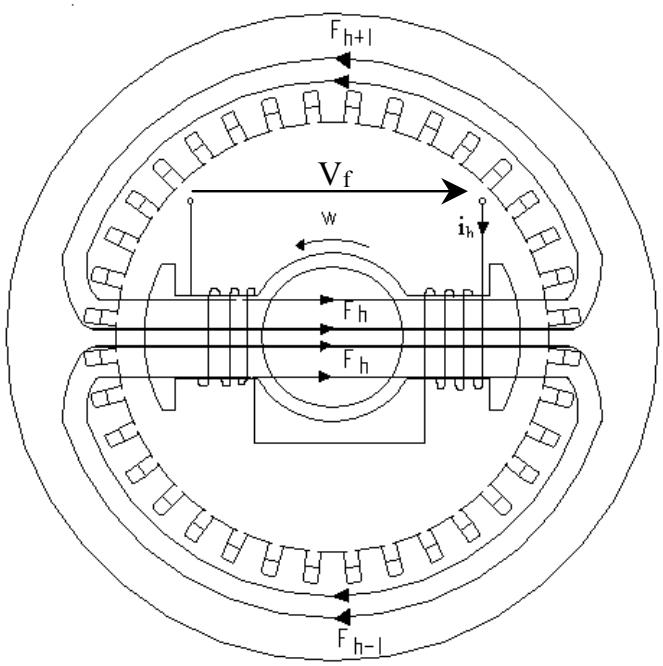

Figure 3-3: MMF distribution in cross section of synchronous machine

These two MMFs cause the flow of 5^{th} and 7^{th} harmonics currents in the stator windings, where the phase displacement between them is 180°. The harmonic flux in the rotor changes with speed of 6ω, which also rotates, with speed of the rotor. The flux lines close their paths in two opposing direction as it is shown in Fig. 3-3. These flux lines link the stator winding and generated to MMF components in the stator windings, one in forward direction with the angular frequency 7ω and the other in back ward direction or with 180 degree phase shift with angular frequency 5ω. As the MMF is derivative of flux linkage, the magnitude of 7^{th} harmonic MMF is 7/5 times of 5^{th} MMF harmonics. For example in a rectifier load, the amplitude of 5^{th} harmonics is more than 7^{th} harmonics, then for completely compensation of the 5^{th} harmonic current, it is needed

to boost the 5th harmonic of MMF in the air gap in order to increase the amplitude of 5th harmonic current.

As it is shown in Table 3-1, for this purpose, it is considered adding 4th harmonic current in the field winding. With controlling amplitude and phase of the injected 4th harmonic, it is possible to increase the 5th harmonic rotating MMF in the air gap. For canceling the 3rd harmonic produced by the rotating MMF in the air gap, it is needed to add the 2nd harmonic current in the field winding excitation circuit. With this strategy, the final developed MMFs inside the air gap are fundamental, 5th and 7th harmonics. Which are independently controllable in phase and magnitude.

Following equation describes the total field excitation current:

$$i_f = I_{dc} + i_{m2}\sin(2\omega t + \varphi_2) + i_{m4}\sin(4\omega t + \varphi_4) + i_{m6}\sin(6\omega t + \varphi_6) \qquad (3\text{-}1)$$

Where I_{dc} indicates the dc component of the field current and $i_{m2,}$ i_{m4} and i_{m6} denote the 2nd, 4th and 6th ac excitation components. The phase angles φ_2, $\varphi_{4,}$ and φ_6 indicate phase of the 2nd, 4th, and 6th harmonics currents respectively.

Table 3-1: Combination of the injected harmonics to the field and produced MMFs

AC field excitation	Produced MMF		Produced Currents
	Forward	Backward	
6th	7th	5th	i_5, i_7
4th	5th	3rd	i_5, i_3
2nd	3rd	1st	i_3, i_1
Total	7th , 5th , 1st		i_1 , i_5 , i_7

The dc current will furnish the active power and reactive power control and ac components are used to cancel the harmonics current of the utility.

III.3.2. REDUCING THE OPERATIONAL INDUCTANCE WITH RESONANCE CIRCUIT

With the increased use of adjustable speed drives in recent years harmonic modeling of synchronous machine has received many researchers attentions and several harmonic models have been developed [38]. The configuration of field winding excitation circuitry of synchronous generators in this electromechanical compensatory method has been shown in Fig. 3-4. An ac harmonic source is connected across the field winding through an ac capacitor. The dc power source is connected in series with an inductor, $L_{bl.}$. The inductor L_{bl} blocks the flow of ac harmonics currents through the dc power supply. The role of the capacitor C_{ac} is to decrease the operational inductance of the machine at frequency (h.ω).

The voltage equations in the rotor reference frame with all rotor quantities referred to the stator is given below:

$$v_{qs}^{r} = -r_s i_{qs}^{r} + \omega_r \lambda_{ds}^{r} + \frac{d\lambda_{qs}^{r}}{dt} \tag{3-2}$$

$$v_{ds}^{r} = -r_s i_{ds}^{r} - \omega_r \lambda_{qs}^{r} + \frac{d\lambda_{ds}^{r}}{dt} \tag{3-3}$$

$$v'^{r}_{fd} = r'_{fd} i'^{r}_{fd} + \frac{d\lambda'^{r}_{fd}}{dt} \tag{3-4}$$

where the flux linkages are given by:

$$\lambda^{r}_{qs} = -L_q i^{r}_{qs} \tag{3-5}$$

$$\lambda^{r}_{ds} = -L_d i^{r}_{ds} + L_{md} i''^{r}_{fd} \tag{3-6}$$

$$\lambda''^{r}_{fd} = L'_{fd} i''^{r}_{fd} - L_{md} i''^{r}_{ds} \tag{3-7}$$

where:

$$L_q = L_{ls} + L_{mq}$$

$$L_d = L_{ls} + L_{md}$$

$$L'_{fd} = L'_{lfd} + L_{md}$$

r_s : stator winding resistance

r_{fd}': field winding resistance

L_q: q-axis synchronous inductance

$L_{d:}$ d-axis synchronous inductance

L_{md}: d-axis stator magnetizing inductance

L_{mq}: q-axis stator magnetizing inductance

L_{ls}: stator leakage inductance

L_{lf}': field winding leakage inductance.

In above equations it is assumed that there is no damper winding in the machine. The inductance of L_{bl} in Fig. 3-4 is chosen high, so that the ac current through the L_{bl} is negligible. Using superposition law and assuming only ac source with frequency of $(h.\omega)$ and rewriting the rotor voltage equation in angular frequency of $(h.\omega)$, we get:

$$v''^{r}_{fdh} = r'_{fd} i''^{r}_{fdh} + jh\omega \lambda''^{r}_{fdh} \tag{3-8}$$

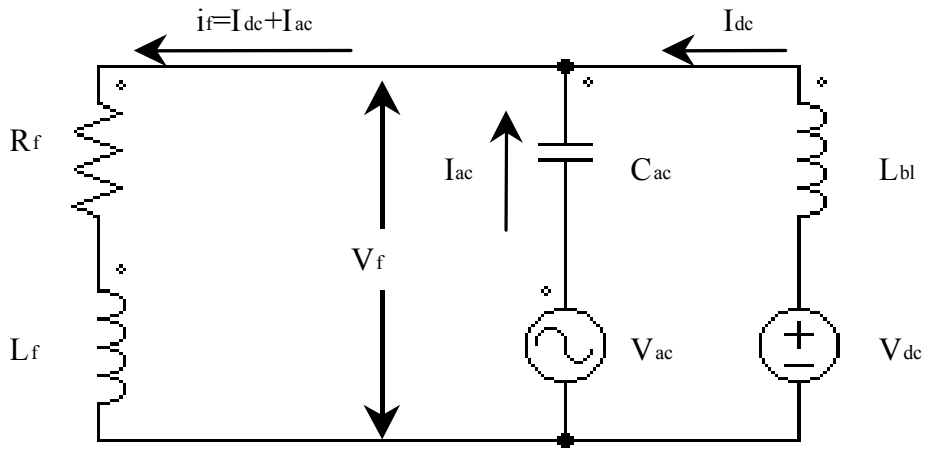

Figure 3-4: Configuration of field excitation

where v'^{r}_{fdh} , i'^{r}_{fdh} and λ'^{r}_{fdh} are voltage, current, and flux of field winding at frequency of $(h.\omega)$ respectively. Rotor field winding current, i'^{r}_{fdh}, can also be obtained using the following equation:

$$i'^{r}_{fdh} = -jh\omega C'_{ac}(v'^{r}_{fdh} - v'_{ach}) \tag{3-9}$$

where, v'_{ach} and C'_{ac} are the harmonic voltage source at frequency $(h.\omega)$ and the capacitor value used in the field winding excitation circuit, both referred to the stator side and are defined as following:

$$v'_{ach} = \left(\frac{N_s}{N_{fd}}\right) \cdot v_{ach} \tag{3-10}$$

$$C'_{ac} = \frac{2}{3} \cdot \left(\frac{N_{fd}}{N_s}\right)^2 \cdot C_{ac} \tag{3-11}$$

By substituting (3-8) and (3-9) in (3-6) at frequency of $(h.\omega)$ we obtain:

$$\lambda^{r}_{dsh} = L_{oh} i^{r}_{dsh} + A v'_{ach} \tag{3-12}$$

where λ^{r}_{dsh} and i^{r}_{dsh} are the d-axis stator flux and current in rotor reference frame at frequency of $(h.\omega)$ respectively, and L_{oh} is defined as the operational inductance at frequency of $(h.\omega)$ and A is a constant value. L_{oh} and A are given by:

$$L_{oh} = \frac{1-(h\omega)^2 C'_{ac} L'_{fm} + jh\omega C'_{ac} r'_f}{1-(h\omega)^2 C'_{ac} L'_{ff} + jh\omega C'_{ac} r'_f} \cdot L_d \tag{3-13}$$

$$A = \frac{jh\omega C'_{ac} L_{md}}{1-(h\omega)^2 C'_{ac} L'_{ff} + jh\omega C'_{ac} r'_f} \tag{3-14}$$

where :

$$L'_{ff} = L'_{lfd} + L_{md} \tag{3-15}$$

$$L'_{fm} = \left(L'_{ff} - \frac{L^2_{md}}{L_d} \right) \tag{3-16}$$

In (3-12), v'_{ach} has a very small value because of stator to rotor windings turns ratio, and also $|A|$ is very small. Therefore, the effect of second term in (3-12) is negligible. Nonetheless, for flowing maximum d-axis stator current at frequency of $(h.\omega)$, it is sufficient to minimize the absolute value of operational inductance at frequency of $(h.\omega)$ which means *min* ($|L_{oh}|$). Minimum value of $|L_{oh}|$ will be obtained when C'_{ac} resonates with inductance L'_{fm} at the frequency of $(h.\omega)$. Then, the optimum value of C'_{ac} will be:

$$C'_{ac}(opt.) = \frac{1}{(h\omega)^2 \cdot L'_{fm}} \tag{3-17}$$

As it is clear, the operational inductance at frequency of *(h.ω)* can be decreased by adjusting of the C_{ac} in the field excitation circuit. Therefore the d-axis stator current at frequency of *(h.ω)* or stator winding current in frequency of *[(h±1).ω]* will increase for the same value of V_{ac} in the field.

III.3.3. THE MATHEMATICAL MODEL OF INTEGRATED SYNCHRONOUS MACHINE/ACTIVE FILTER

Using the motoring convention, the stator voltage and flux linkages of stator can be formulated as:

$$v_S = R_S \cdot I_S + \frac{d\,\lambda_S}{dt} \tag{3-18}$$

$$\lambda_S = L_{ss} \cdot I_S + L_{sf} \cdot I_f \tag{3-19}$$

where:

$$v_S = \begin{bmatrix} v_{as} \\ v_{bs} \\ v_{cs} \end{bmatrix} \quad , \quad Rs = \begin{bmatrix} rs & 0 & 0 \\ 0 & rs & 0 \\ 0 & 0 & rs \end{bmatrix}$$

$$I_S = \begin{bmatrix} i_{as} \\ i_{bs} \\ i_{cs} \end{bmatrix} \quad , \quad \frac{d\,\lambda_S}{dt} = \begin{bmatrix} \frac{d\,\lambda_{as}}{dt} \\ \frac{d\,\lambda_{bs}}{dt} \\ \frac{d\,\lambda_{cs}}{dt} \end{bmatrix}$$

$$L_{ss} = \begin{bmatrix} L_{saa} & L_{sba} & L_{sac} \\ L_{sba} & L_{sbb} & L_{sbc} \\ L_{sca} & L_{scb} & L_{scc} \end{bmatrix} \quad , \quad L_{sf} = \begin{bmatrix} L_{af} \\ L_{bf} \\ L_{cf} \end{bmatrix}$$

$$L_{ss}=\begin{bmatrix} L_{ls}+L_o-L_{ms}\cos 2\theta_{rm} & -\frac{1}{2}L_o-L_{ms}\cos 2\left(\theta_{rm}-\frac{\pi}{3}\right) & -\frac{1}{2}L_o-L_{ms}\cos 2\left(\theta_{rm}+\frac{\pi}{3}\right) \\ -\frac{1}{2}L_o-L_{ms}\cos 2\left(\theta_{rm}-\frac{\pi}{3}\right) & L_{ls}+L_o-L_{ms}\cos 2\left(\theta_{rm}-\frac{2\pi}{3}\right) & -\frac{1}{2}L_o-L_{ms}\cos 2(\theta_{rm}+\pi) \\ -\frac{1}{2}L_o-L_{ms}\cos 2\left(\theta_{rm}+\frac{\pi}{3}\right) & -\frac{1}{2}L_o-L_{ms}\cos 2(\theta_{rm}+\pi) & L_{ls}+L_o-L_{ms}\cos 2\left(\theta_{rm}+\frac{2\pi}{3}\right) \end{bmatrix}$$

$$L_{sf}=\begin{bmatrix} L_{sf}\sin(\theta_{rm}) \\ L_{sf}\sin\left(\theta_{rm}-\frac{2\pi}{3}\right) \\ L_{sf}\sin\left(\theta_{rm}+\frac{2\pi}{3}\right) \end{bmatrix}$$

where θ_{rm} is mechanical rotor position. Rotor voltages and flux linkages of rotor windings can be expressed as:

$$v_f = R_f \cdot I_f + \frac{d\lambda_f}{dt} \tag{3-20}$$

$$\lambda_f = L_{sf}^T \cdot I_s + L_{ff} I_f \tag{3-21}$$

From now we consider:

$$R_f = r_f \quad , \quad I_f = i_f \quad , \quad L_{ff} = L_{sff}$$

Now if we consider the series capacitor in field winding the new voltage equation is expressed as:

$$v_f = r_f \cdot i_f + \frac{d\lambda_f}{dt} + \frac{1}{C_f}\int i_f . dt \tag{3-22}$$

If we take the derivative from rotor voltage equation, we will obtain as follows:

$$v'_f = r_f i'_f + \lambda''_f + \frac{1}{C_f} i_f \tag{3-23}$$

The derivative of field winding flux linkage will be:

$$\lambda'_f = L'^T_{sf} \cdot I_s + L^T_{sf} \cdot I'_s + L'_{ff} i_f + L_{ff} i'_f \tag{3-24}$$

and we can get:

$$\lambda''_f = L''^T_{sf} \cdot I_s + 2L'^T_{sf} \cdot I'_s + L'^T_{sf} \cdot I''_s + L''_{ff} i_f + 2L'_{ff} i'_f + L_{ff} i''_f \tag{3-25}$$

But we have:

$$L_{ff} = Cons\tan t \quad \text{so} \quad L'_{ff} = L''_{ff} = 0$$

$$\theta_{rm} = \omega_{rm} t + \delta \quad \text{so} \quad \frac{d\theta_{rm}}{dt} = \omega_{rm}$$

If we substitute these to the equation (3-25) we can write:

$$\lambda''_f = \omega^2_{rm} \cdot \frac{d^2 L^T_{sf}}{d\theta^2_{rm}} \cdot I_s + 2\omega_{rm} \cdot \frac{d L^T_{sf}}{d\theta_{rm}} \cdot I'_s + L^T_{sf} \cdot I''_s + L_{ff} i''_f \tag{3-26}$$

Now from (3-23), we can get:

$$v'_f = r_f i'_f + L_{ff} i'_f + \frac{1}{C_f} i_f + \omega^2_{rm} \frac{d^2 L^T_{sf}}{d\theta^2_{rm}} I_s + 2\omega_{rm} \frac{d L^T_{sf}}{d\theta_{rm}} I'_s + L^T_{sf} I''_s \tag{3-27}$$

Similar for stator equation:

$$v_s = \left(R_s + \omega_{rm} \frac{d L_{ss}}{d\theta_{rm}} \right) \cdot I_s + \omega_{rm} \cdot \frac{d L_{sf}}{d\theta_{rm}} i_f + L_{ss} \cdot I'_s + L_{sf} I'_f \tag{3-28}$$

So the derivative of stator voltage will be:

$$v'_s = \left(R_s + 2\omega_{rm} \frac{d L_{ss}}{d\theta_{rm}} \right) \cdot I'_s + \omega^2_{rm} \cdot \frac{d^2 L^T_{ss}}{d\theta^2_{rm}} \cdot I_s + 2\omega_{rm} \cdot \frac{d L^T_{sf}}{d\theta_{rm}} \cdot i'_f + \omega^2_{rm} \cdot \frac{d^2 L^T_{sf}}{d\theta^2_{rm}} \cdot i_f + L_{ss} i''_s + L_{sf} i''_f \tag{3-29}$$

If we rearrange (3-27) and (3-29), we can obtain the state space representation model for integrated synchronous machine/active filter as following:

$$L_{ss}\,i''_s + L_{sf}\,i''_f = v'_s - \omega_{rm}^2 \cdot \frac{d^2 L_{ss}^T}{d\,\theta_{rm}^2} \cdot I_s - \omega_{rm}^2 \cdot \frac{d^2 L_{sf}^T}{d\,\theta_{rm}^2} \cdot i_f - \left(R_s + 2\omega_{rm} \frac{d\,L_{ss}}{d\,\theta_{rm}} \right) \cdot I'_s - 2\,\omega_{rm} \cdot \frac{d\,L_{sf}^T}{d\,\theta_{rm}} \cdot i'_f \qquad (3\text{-}30)$$

$$L_{ff}\,i'_f + L_{sf}^T \cdot I''_s + r_f \cdot i'_f = v'_f - \omega_{rm}^2 \cdot \frac{d^2 L_{sf}^T}{d\,\theta_{rm}^2} \cdot I_s - \frac{1}{C_f} I_f - 2\,\omega_{rm} \cdot \frac{d\,L_{sf}^T}{d\,\theta_{rm}} \cdot I'_s \qquad (3\text{-}31)$$

$$\begin{bmatrix} 1 & 0 & 0 & 0 \\ 0 & 1 & 0 & 0 \\ 0 & 0 & L_{ss} & L_{sf} \\ 0 & r_f & L_{sf}^T & L_{ff} \end{bmatrix} \cdot \begin{bmatrix} I'_s \\ i'_f \\ I''_s \\ i''_f \end{bmatrix} =$$

$$\begin{bmatrix} 0 & 0 & 1 & 0 \\ 0 & 0 & 0 & 1 \\ -\omega_{rm}^2 \cdot \dfrac{d^2 L_{ss}^T}{d\,\theta_{rm}^2} \cdot & -\omega_{rm}^2 \cdot \dfrac{d^2 L_{sf}^T}{d\,\theta_{rm}^2} & -\left(R_s + 2\omega_{rm} \dfrac{d\,L_{ss}}{d\,\theta_{rm}} \right) & -2\,\omega_{rm} \cdot \dfrac{d\,L_{sf}^T}{d\,\theta_{rm}} \\ -\omega_{rm}^2 \cdot \dfrac{d^2 L_{sf}^T}{d\,\theta_{rm}^2} & -\dfrac{1}{C_f} & -2\,\omega_{rm} \cdot \dfrac{d\,L_{sf}^T}{d\,\theta_{rm}} & 0 \end{bmatrix} \begin{bmatrix} I_s \\ i_f \\ I'_s \\ i'_f \end{bmatrix} + \begin{bmatrix} 0 \\ 0 \\ v'_s \\ v'_f \end{bmatrix} \qquad (3\text{-}32)$$

This equation is in form of:

$$AX' = BX + U \tag{3-33}$$

If we multiply the (3-33) by A^{-1} the state space model will be:

$$X' = A^{-1}BX + A^{-1}U \tag{3-34}$$

III.3.4. GAIN OF THE PROPOSED COMPENSATORY METHOD

Gain of this compensation method is the ratio of the generated 5^{th} and 7^{th} harmonics current to the ac excitation current. As it is known, the number of turns in the field winding of a synchronous machine is much higher than the number of turns in the stator windings, therefore the rotor to stator windings turns ratio in synchronous machine has a large value. It is shown that the gain of the proposed compensation method is reasonable and comparable with windings turns ratio. In the simulation study, it will be shown that the gain of compensation is about 8 times.

The proposed system is connected to the grid so the voltage of utility can be assumed three-phase, pure sinusoidal, balanced and stiff. If we neglect the resistance of the stator and space harmonics of the windings, the flux linkage of the stator is also distributed sinusoidally, because the stator flux is in influence of stator voltage and as it is clear from (3-18), stator flux is approximately equal to integral of stator voltage. Now if the stator flux is projected on the two-phase rotor reference frame, we will get the (3-5) and (3-6). Stator flux linkages components in two-phase rotor reference frame, λ_{ds}^{r} and λ_{qs}^{r}, will be dc values. So if a harmonic current is injected into the field winding,

which has been attached to d-axis in rotor reference frame, it will induce some harmonic flux component on equivalent stator winding in direct axis. But stator flux in d-axis in rotor reference frame has been forced to be constant by grid voltage. So this portion should be canceled out by stator direct axis current. This procedure is explained in following.

The stator flux in direct axis in rotor reference frame is:

$$\lambda_{ds}^{r} = -L_d i_{ds}^{r} + L_{md} i''^{r}_{fd} \tag{3-35}$$

Now consider that we inject a harmonic current with frequency $h\omega$ and magnitude i_{fhm} , i_{fhd} into the field winding:

$$i_{fhd} = i_{fhm}.\cos(h\omega t + \varphi) \tag{3-36}$$

But λ_{ds}^{r} has no ac components so we can write:

$$0 = -L_d i_{dhs}^{r} + L_{md} i'_{fhd} \tag{3-37}$$

where i'_{fhd} is the current i_{fhd} referred to stator circuit and we can write:

$$i'_{fhd} = \frac{2}{3}\frac{N_f}{N_s}.i_{fhd} \tag{2-38}$$

$$i'_{fhm} = \frac{2}{3}\frac{N_f}{N_s}.i_{fhm} \tag{2-39}$$

So from (3-37), we can obtain:

$$i_{dhs}^{r} = \frac{L_{md}}{L_d} i'_{fhd} \tag{3-40}$$

As the field winding is along the d-axis, so there is no induction in q-axis so:

$$i^r_{qhs} = 0 \tag{3-41}$$

In above equation, i^r_{qhs} and i^r_{dhs} are stator harmonic currents components in two-phase rotor reference frame.

Inverse Park transformation matrix is defined as:

$$(K_s)^{-1} = \begin{bmatrix} \cos\theta & \sin\theta & 1 \\ \cos(\theta - \frac{2\pi}{3}) & \sin(\theta - \frac{2\pi}{3}) & 1 \\ \cos(\theta + \frac{2\pi}{3}) & \sin(\theta + \frac{2\pi}{3}) & 1 \end{bmatrix} \tag{3-42}$$

where:

$$\theta = \omega t + \delta$$

where, δ is rotor angle.

Now we transfer the stator harmonic current components on rotor reference frame to stationary three phase system by following transformation:

$$\begin{bmatrix} i_{ahs} \\ i_{bhs} \\ i_{chs} \end{bmatrix} = (K_s)^{-1} \begin{bmatrix} i^r_{qhs} \\ i^r_{dhs} \\ i^r_{ohs} \end{bmatrix} \tag{3-43}$$

If we substitute equitation's (3-38) to (3-40) into (3-41) we will obtain:

$$\begin{bmatrix} i_{ahs} \\ i_{bhs} \\ i_{chs} \end{bmatrix} = \begin{bmatrix} \cos(\omega t + \delta) & \sin(\omega t + \delta) & 1 \\ \cos(\omega t + \delta - \frac{2\pi}{3}) & \sin(\omega t + \delta - \frac{2\pi}{3}) & 1 \\ \cos(\omega t + \delta + \frac{2\pi}{3}) & \sin(\omega t + \delta + \frac{2\pi}{3}) & 1 \end{bmatrix} \begin{bmatrix} 0 \\ \frac{L_{md}}{L_d} i'_{fhd} \\ 0 \end{bmatrix}$$

and then:

$$\begin{bmatrix} i_{ahs} \\ i_{bhs} \\ i_{chs} \end{bmatrix} = \frac{L_{md}}{L_d}.i'_{fhm} \begin{bmatrix} \sin(\omega t+\delta).\cos(h\omega t+\varphi) \\ \sin(\omega t+\delta-\frac{2\pi}{3}).\cos(h\omega t+\varphi) \\ \sin(\omega t+\delta+\frac{2\pi}{3}).\cos(h\omega t+\varphi) \end{bmatrix}$$

So, we have:

$$\begin{bmatrix} i_{ahs} \\ i_{bhs} \\ i_{chs} \end{bmatrix} = \frac{2N_f L_{md} i_{fhm}}{3N_s L_d} \left(\begin{bmatrix} \sin((h+1)\omega t+\delta+\varphi) \\ \sin((h+1)\omega t+\delta+\varphi-\frac{2\pi}{3}) \\ \sin((h+1)\omega t+\delta+\varphi+\frac{2\pi}{3}) \end{bmatrix} - \begin{bmatrix} \sin((h-1)\omega t+\delta-\varphi) \\ \sin((h+1)\omega t+\delta-\varphi-\frac{2\pi}{3}) \\ \sin((h+1)\omega t+\delta-\varphi+\frac{2\pi}{3}) \end{bmatrix} \right) \quad (3\text{-}44)$$

As it is clear, the generated harmonics current at angular frequencies of (h+1)ω and (h-1)ω in stator have the same magnitude. Equation (3-44) is used to control the amount of harmonics current compensation in the grid.

III.4. SIMULATION RESULTS

The proposed system has been simulated on a 4-pole, salient pole, 3-phase, 480 V, 60 Hz, 475 kVA synchronous generator. A software package has been developed, using MATLAB, SIMULINK package. In this package, the mathematical model and the state space equations developed in section III.3.3 have been used. Self-inductances of stator windings and field windings and mutual inductances between stator windings and field winding are developed using winding functions and inverse gap function. So, the effect of space harmonics and winding distribution are also considered. The simulated circuit has been shown in Fig. 3-5. It is assumed that the synchronous generator has been

connected to an infinite bus and is paralleled to a rectifier load. Current of diode rectifier is non-linear which includes 5^{th} and 7^{th} harmonics. The integrated synchronous generator/active filter is properly excited such that it generates the required 5^{th} and 7^{th} harmonics for harmonic compensation in the grid.

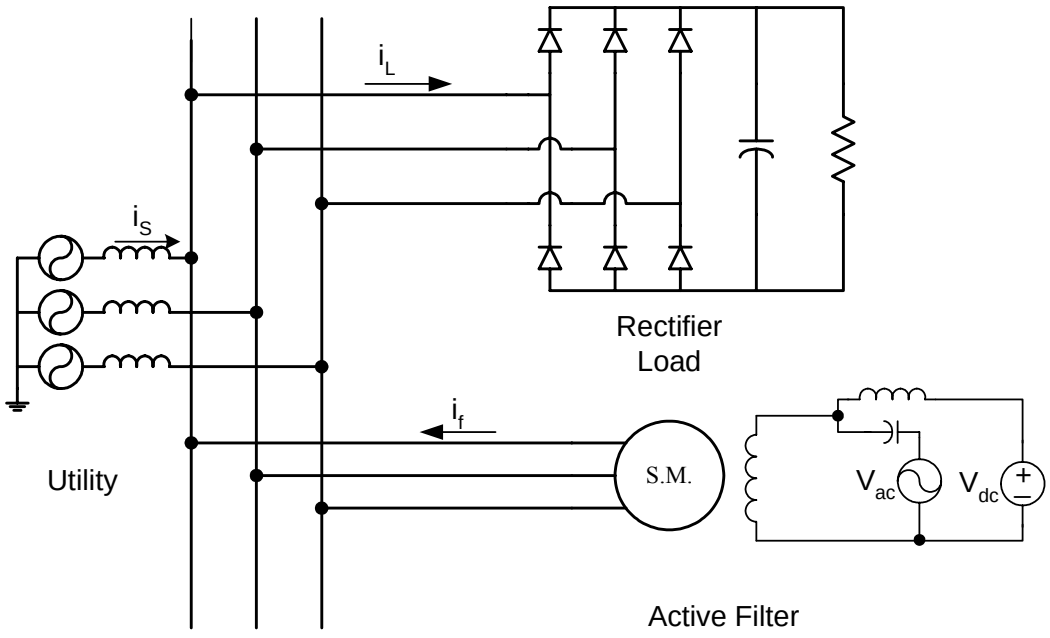

Figure 3-5: Simulated circuit

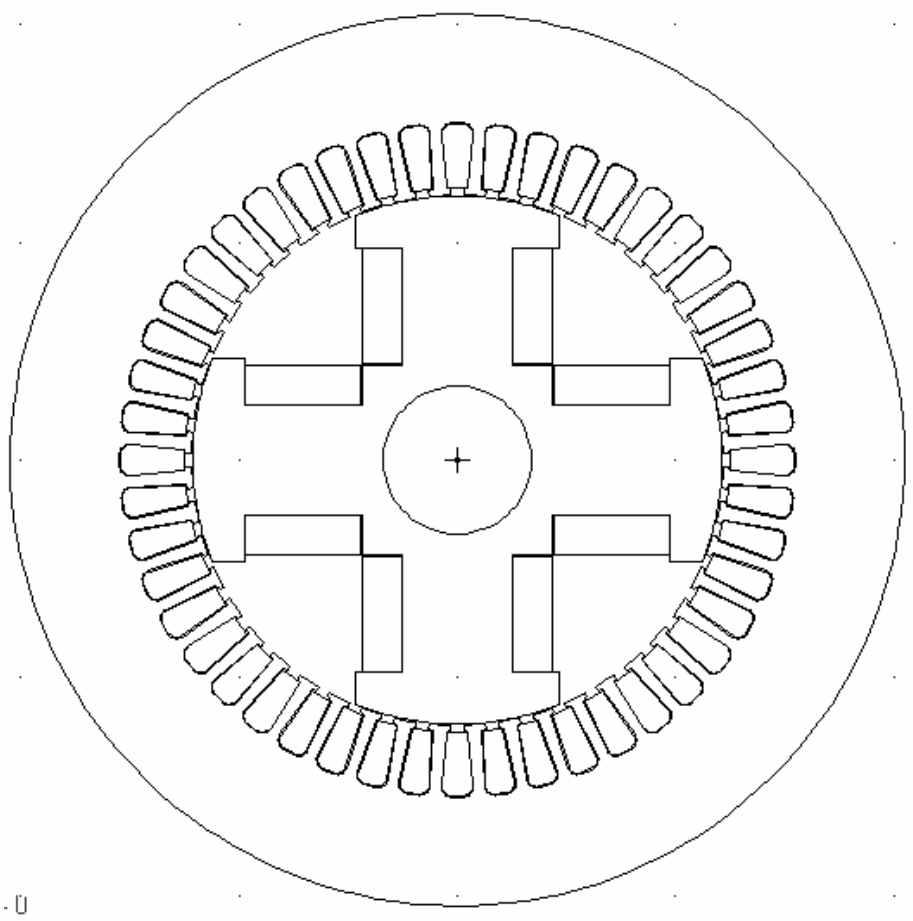

Figure 3-6: Cross section of simulated synchronous generator

The cross section of simulated synchronous generator is shown in Fig. 3-6. The stator has 48 slots with double layer winding which corresponds to 3 coils per pole per phase. As it was described in the previous section, the operational inductance of synchronous machine at frequency of $(h.\omega)$ can be reduced by the resonance capacitor C_{ac}. In this case, for the simulated synchronous machine the variation of the operational inductance at frequencies of 2ω, 4ω, and 6ω versus variation of the resonance capacitor value is shown in Fig. 3-7.

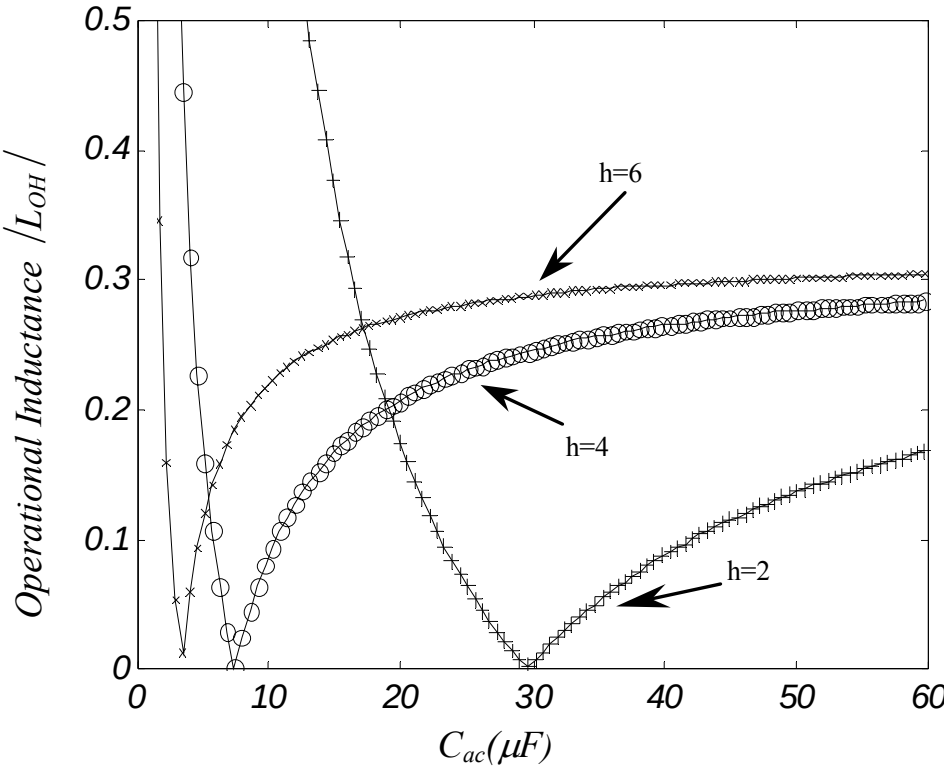

Figure 3-7: Variation of operational inductance with capacitor value

This figure shows that the variation of the operational inductance with capacitor value is like a V-curve where the left-hand side drops sharply but the right-hand side rise up smoothly. Without the series capacitor in the ac field excitation, the operational inductance for harmonics is high so it needs higher voltage for ac excitation.

In this simulation study, C_{ac} =25μF was chosen to reduce the operational inductance of the integrated synchronous machine/ active filter. The rectifier load needs a nonlinear current, which is shown in Fig. 3-8 (a) and its spectrum is illustrated in Fig. 3-8 (b).

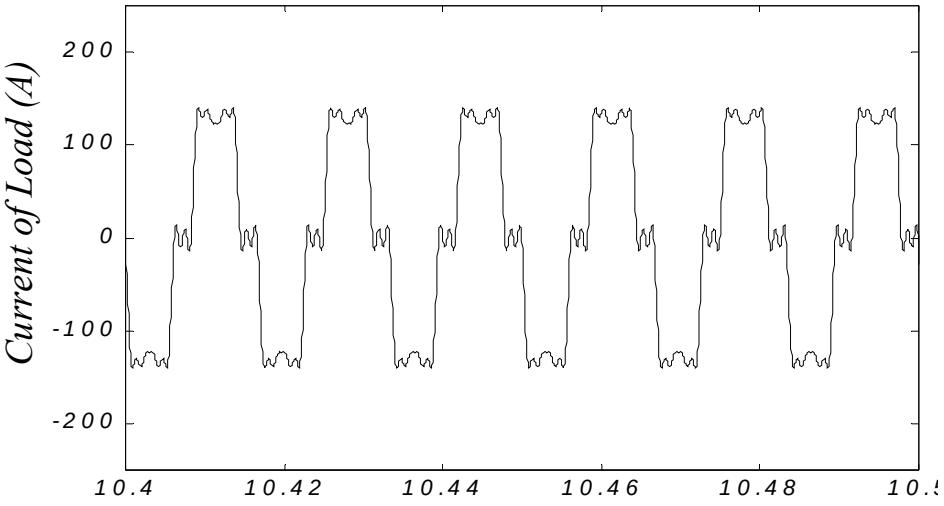

(a) Waveform

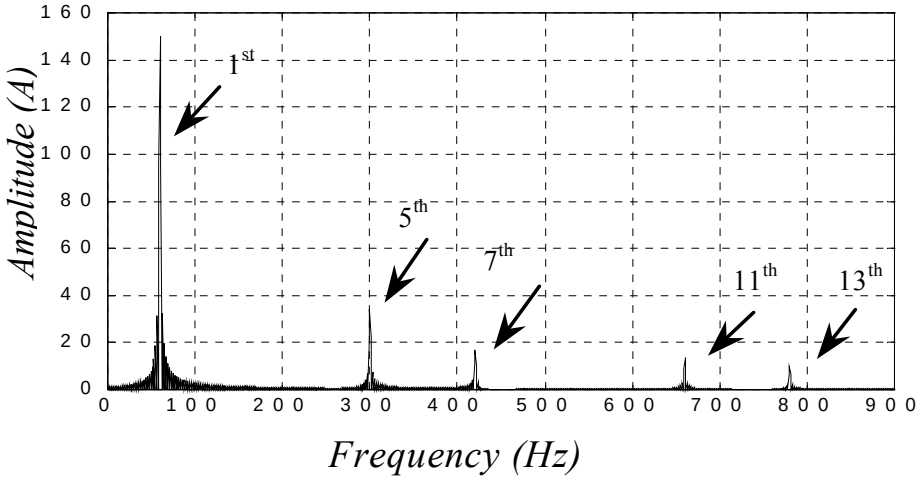

(b) FFT Spectrum

Figure 3-8: Current of nonlinear load. (a) Waveform and (b) FFT spectrum

If the synchronous machine is excited by dc field, the current of synchronous machine is almost sinusoidal. So, harmonics current of diode rectifier flows into the grid.

With adding ac excitation in the field that is combination of 2^{nd}, 4^{th} and 6^{th} harmonics components current and controlling the phase and magnitude of them, the 5^{th} and 7^{th} harmonics current have been generated as much as needed to feed the nonlinear load. The current of integrated synchronous machine/active filter and its power spectrum has been shown in Fig. 3-9 (a) and (b), respectively. As it is clear from Fig.3-9, the third harmonic component has been cancelled and 5^{th} and 7^{th} harmonics components have been produced as much as needed by the nonlinear load. Therefore, the generated 5^{th} and 7^{th} harmonics current compensate the harmonics of the nonlinear load current.

The supplied current by the utility and its frequency spectrum is shown in Fig. 3-10. The ac field winding current is depicted in Fig. 3-11. As it was shown, the proposed electromechanical compensation method successfully eliminated the 5^{th} and 7^{th} harmonics components from utility current. In this case study, the gain of electromechanical compensator is close to 8.

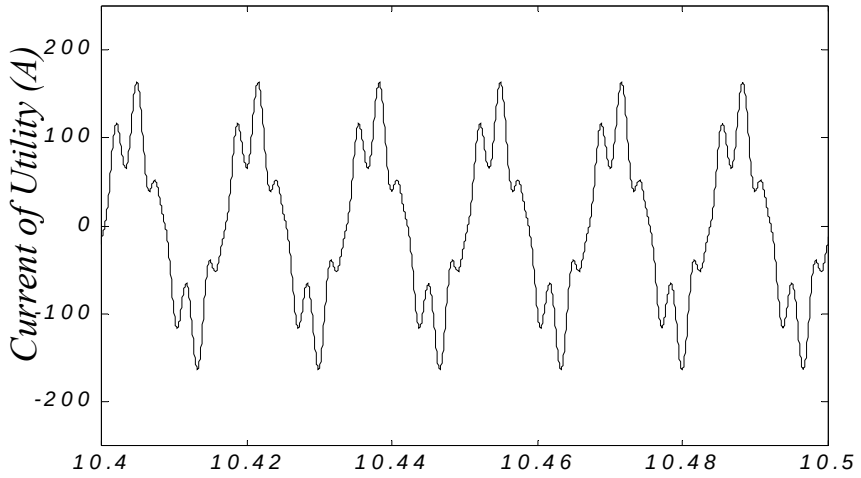

(a) Waveform

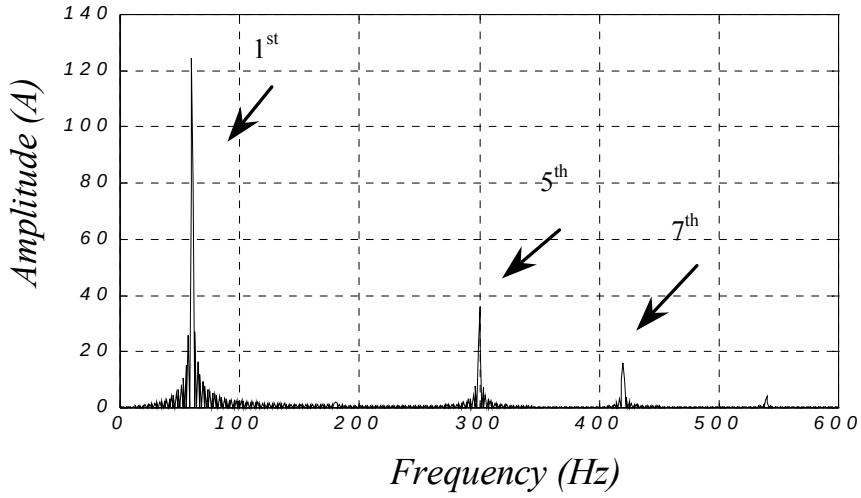

(b) FFT Spectrum

Figure 3-9: Current of synchronous generator. (a) Waveform and (b) FFT spectrum

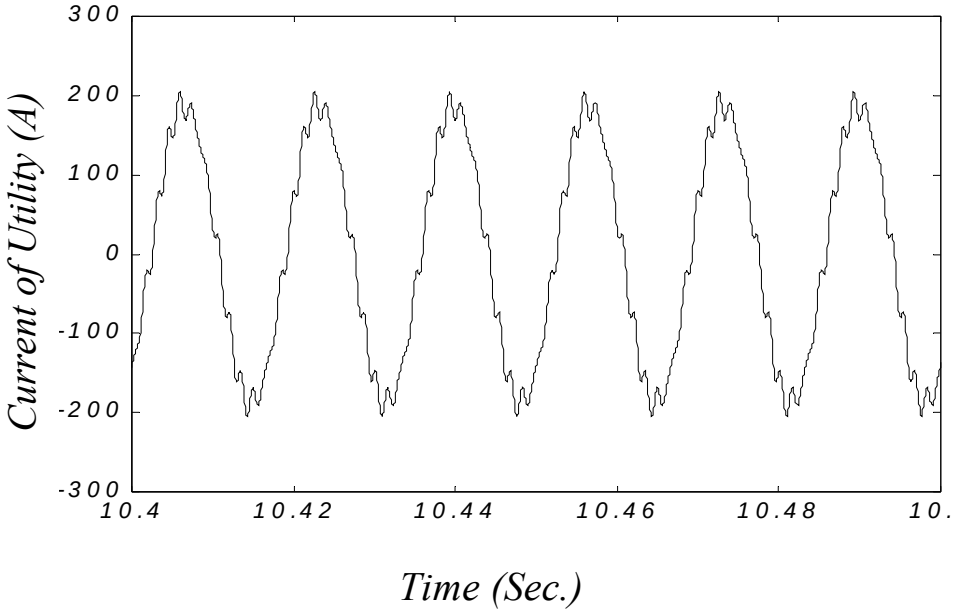

(a) Waveform

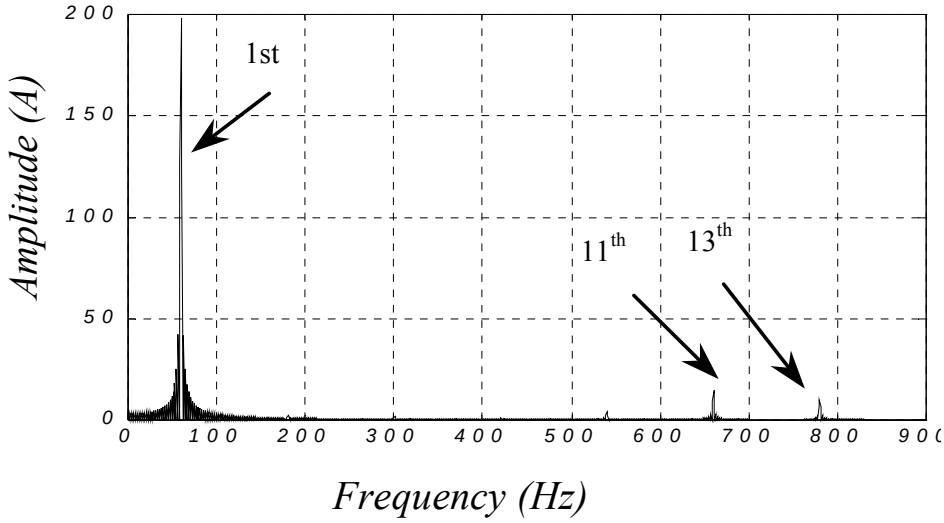

(b) FFT Spectrum

Figure 3-10: Current of utility. (a) Waveform and (b) Power spectrum

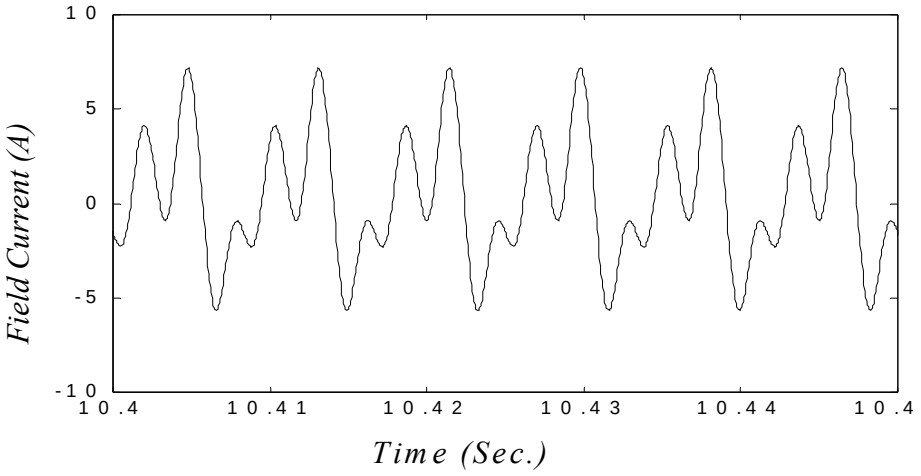

Figure 3-11: Current of field excitation

III.4.1.1. Finite element analysis

Finite element analysis has been conducted for the simulated integrated synchronous generator/active filter. The simulation has been performed using MAXWELL package from ANSOFT Co. The flux distribution paths in cross section of simulated synchronous machine is shown in Fig.3-12.

At the first, the field is excited by dc current. The back-emf is calculated from finite element solution, and is depicted in Fig.3-13. The spectrum analysis of it is also given in Fig.3-14. As it is clear, the back-EMF includes some higher harmonic because of slot harmonics and space harmonics. Then, the 6^{th} harmonics current with the amount of 10% of nominal field current is added to field current excitation. This ac current will contribute in 5^{th} and 7^{th} harmonics in back-emf voltage.

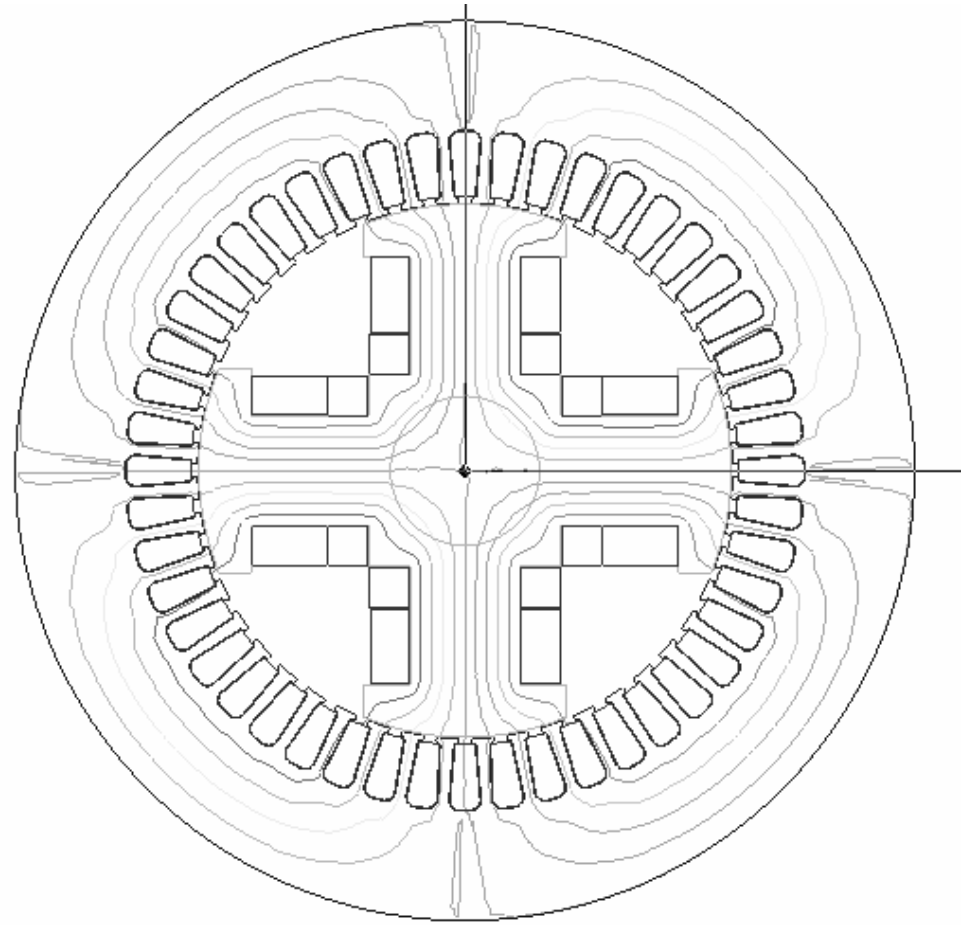

Figure 3-12: Flux line distribution in simulated synchronous machine

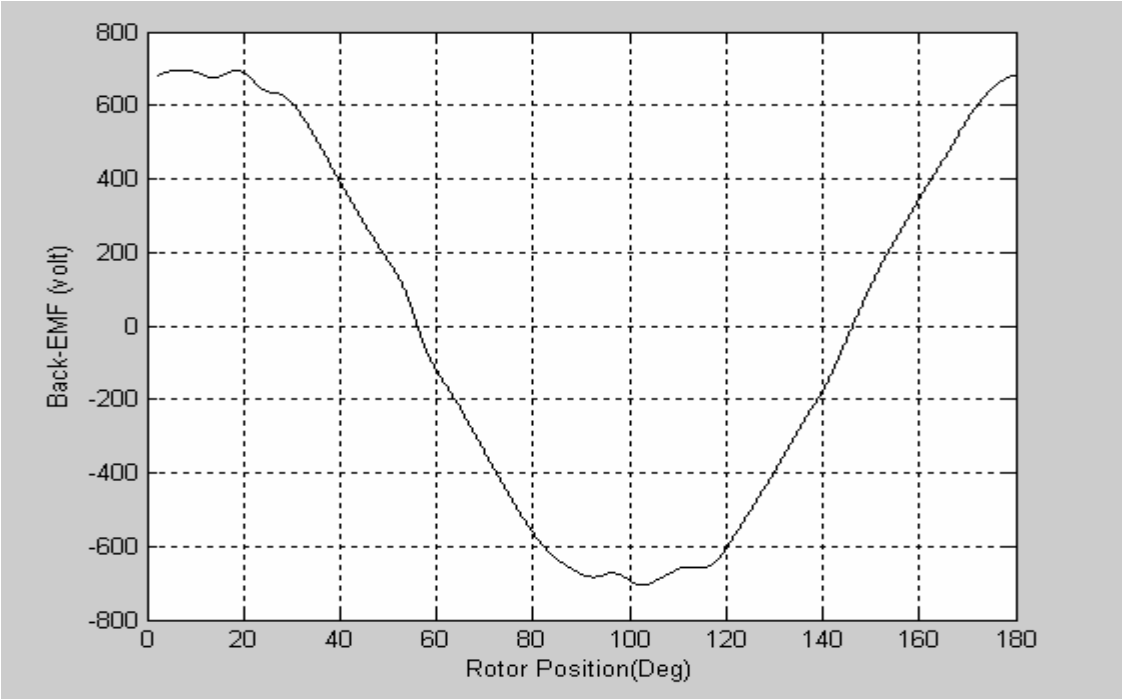

Figure 3-13: Back-emf with dc excitation

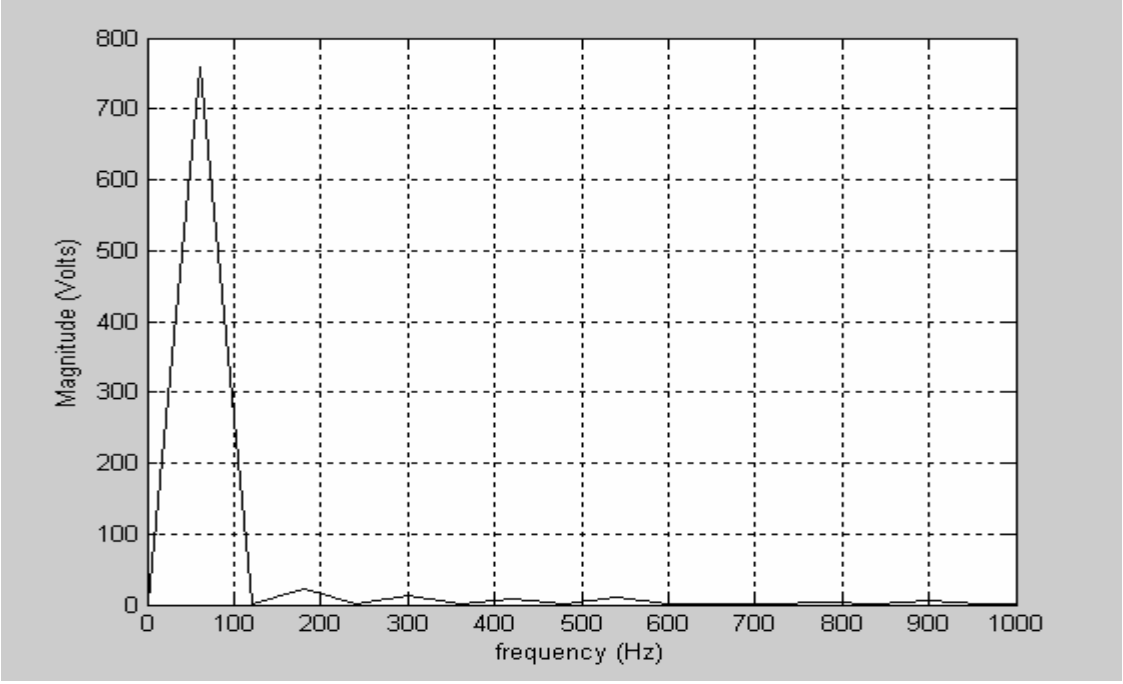

Figure 3-14: Spectrum analysis of back-emf with dc excitation

The generated back-emf in this case is depicted in Fig. 3-15 and spectrum analysis of it, is shown in Fig.3-16. To clearly understand the contribution of 6^{th} harmonics in 5^{th} and 7^{th} harmonics of back-emf, the dc excitation is removed and field is just excited with 6^{th} harmonics current with the same magnitude. The generated back-emf in case of 6^{th} harmonic excitation only, has been plotted in Fig. 3-17 and its spectrum analysis has been shown in Fig. 3-18.

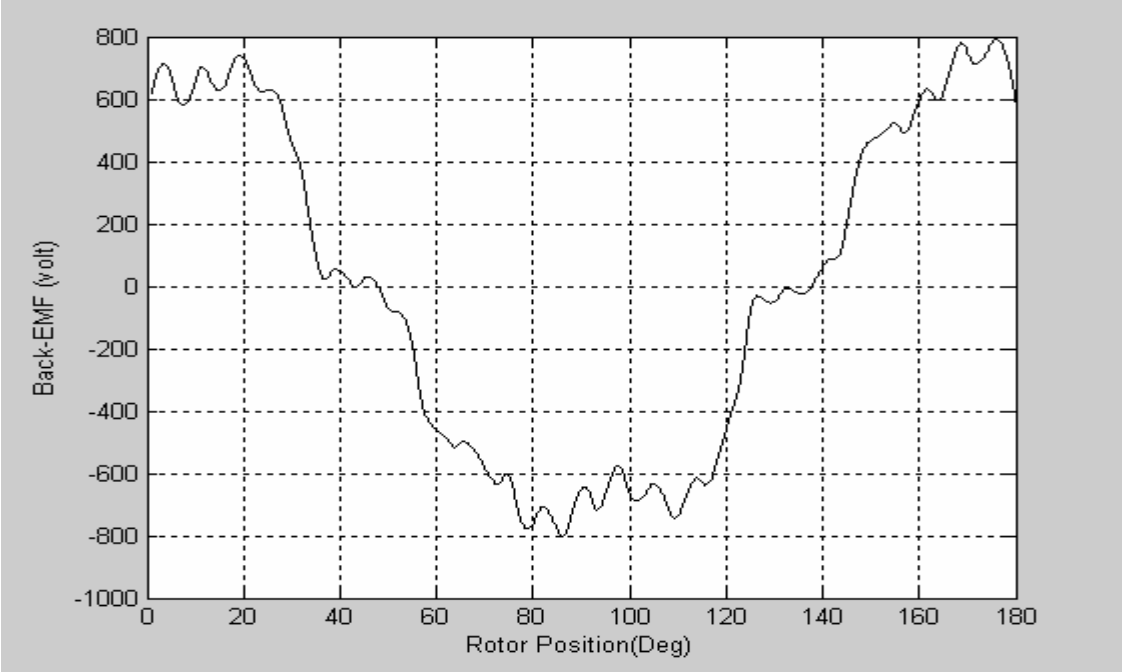

Figure 3-15: Back-emf with dc excitation plus 6^{th} harmonics

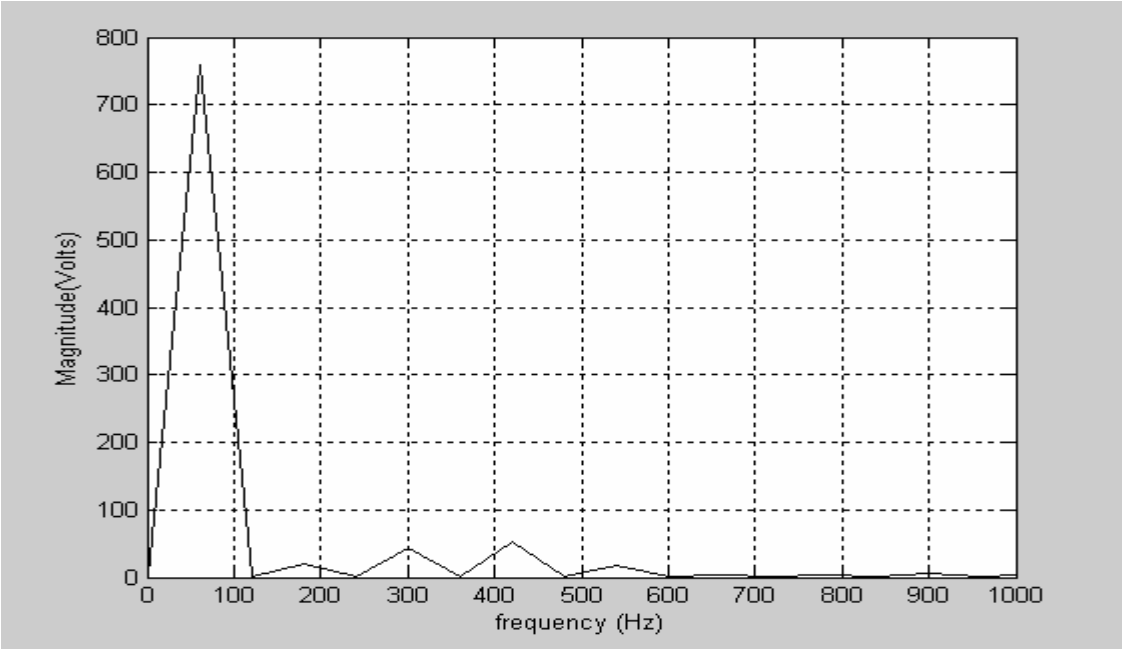

Figure 3-16: Spectrum analysis of back-emf with dc plus 6th harmonics excitation

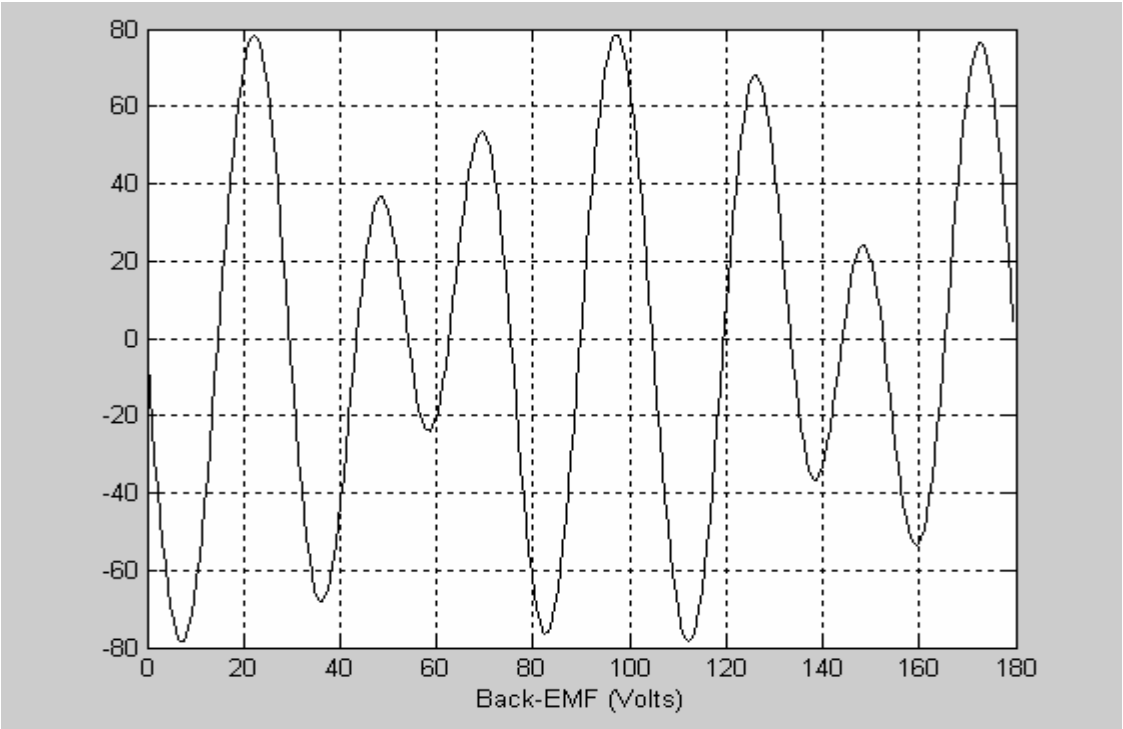

Figure 3-17: Back-emf with 6th harmonics excitation only

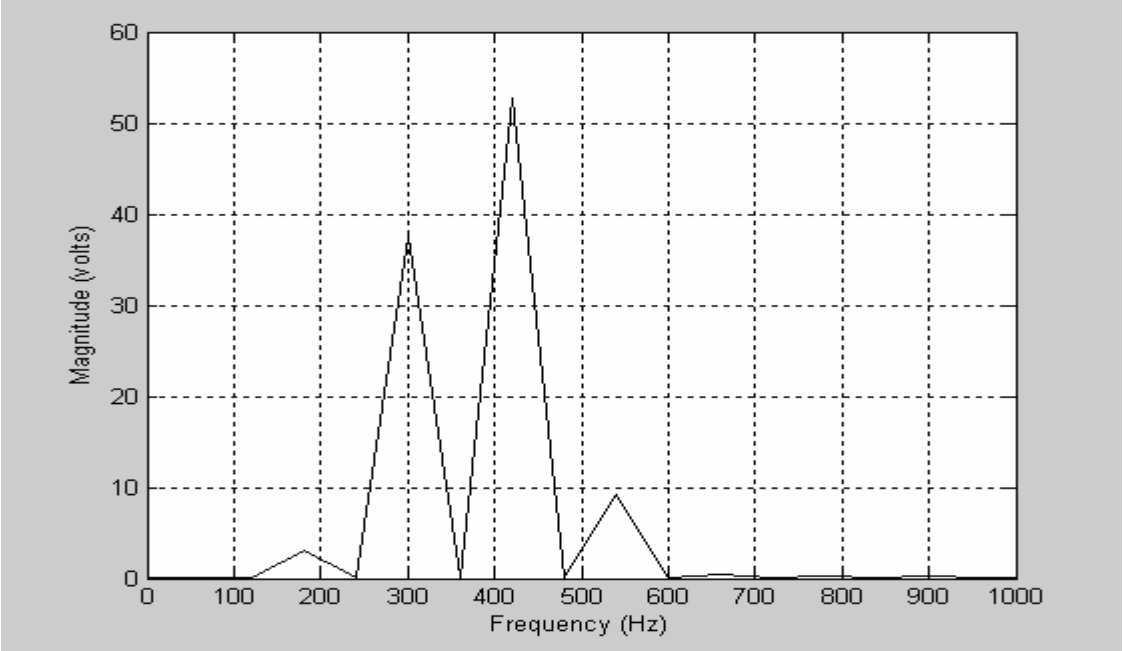

Figure 3-18: Spectrum analysis of back-emf with 6th harmonics excitation

III.5. EXPERIMENTAL RESULTS

An experiment has been performed on a round-rotor synchronous generator with both dc and ac excitation field in the rotor winding. The generator is a three- phase, 4 pole, 5 kVA, 240 V and 1800 rpm. As the voltage of the grid is assumed sinusoidal, there is no 5^{th} and 7^{th} harmonics voltage component in the utility voltage waveform. From super position point of the view, the higher harmonics are shorted in synchronous generator terminals. In this laboratory experiment, to avoid problem of synchronization with grid voltage, the terminal of synchronous generator is shorted through three small resistors with values of 2Ω.

The schematic of experimental setup is shown in Fig. 3-19. An ac capacitor is in series with the 6th harmonic voltage source. The dc voltage source is connected to the field winding through a large inductor. The amount of dc excitation is limited to 10% of nominal excitation current. The shaft of synchronous generator has been coupled with shaft of dc motor. The dc motor is controlled to run at 1800 RPM. In the first experimental study, the ac excitation is removed and field is excited just with 10% nominal excitation current. The current of phase A of generator is shown in Fig. 3-20.

As it is clear, the current of synchronous generator without adding any harmonics current into the field includes some harmonics.

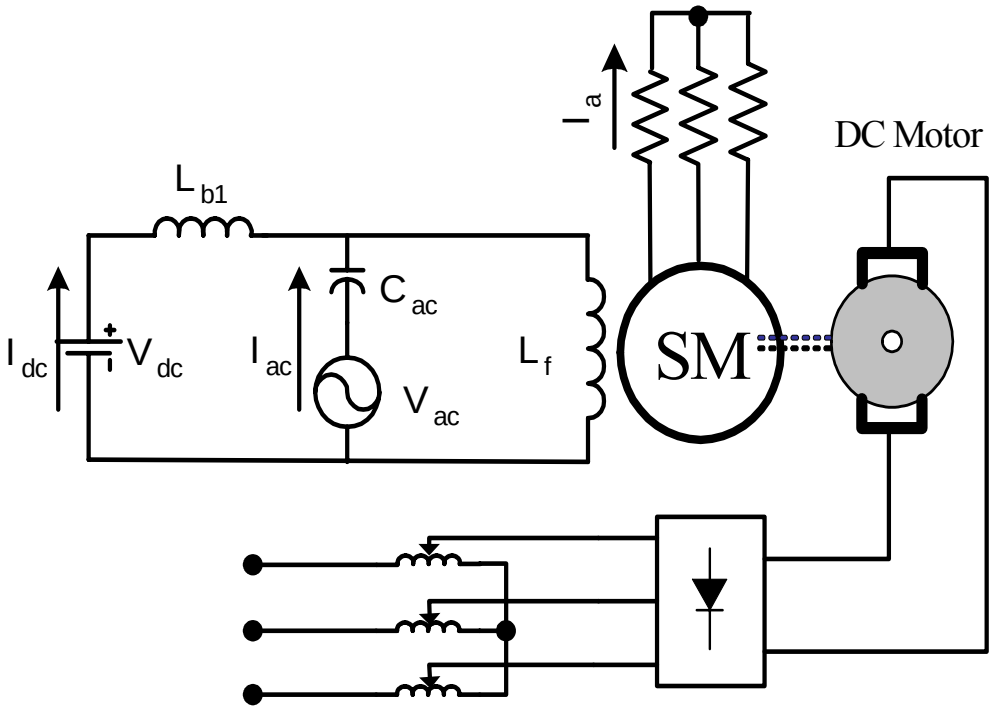

Figure 3-19: Experimental circuit

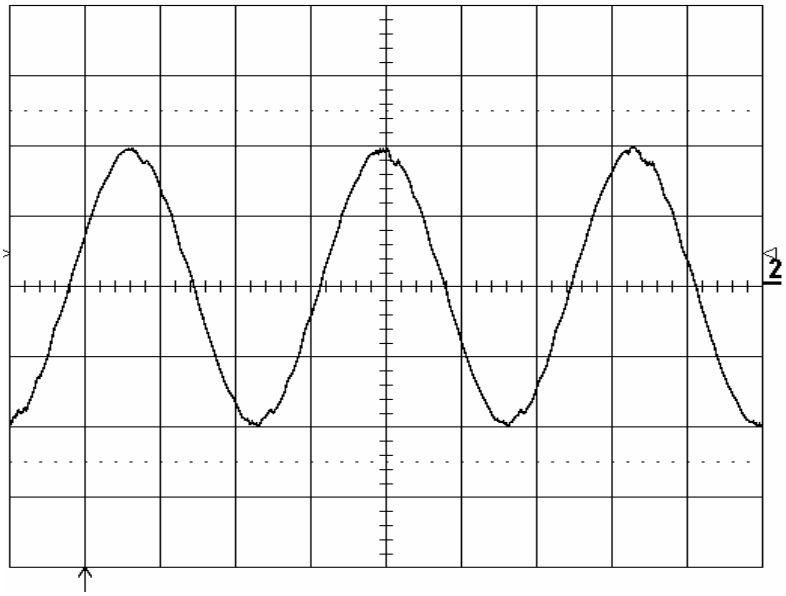

Figure 3-20: Current of synchronous generator with dc excitation

In case study 2, 6^{th} harmonic excitation is also added to the field winding. The ac power supply is controlled that the amount of the ac excitation current remains in 15% of nominal field current. In this case, the current of synchronous generator shows a non-sinusoidaly waveform. The current of generator in case of dc and 6^{th} harmonic excitation is shown in Fig. 3-21. The power spectrum analysis of this current is shown in Fig. 3-22. As it is shown the magnitude of 5^{th} and 7^{th} harmonics currents are almost equal. This confirms the gain calculation and developed mathematical model.

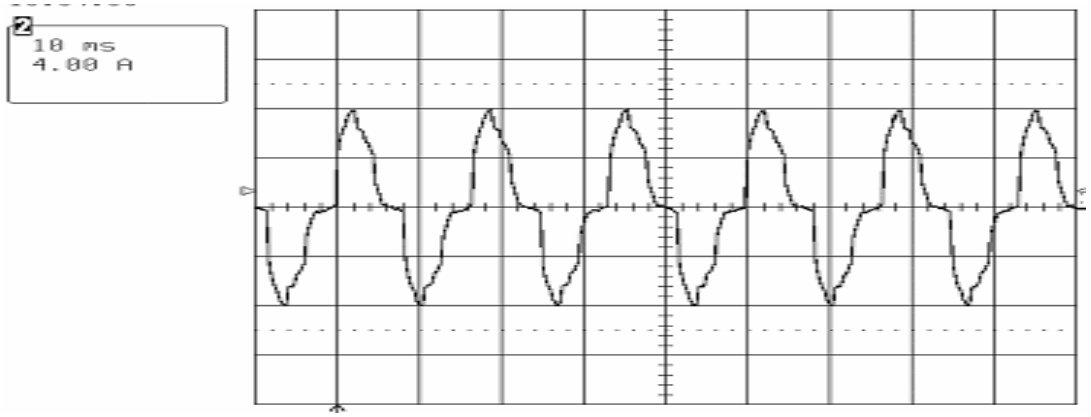

Figure 3-21: Current of synchronous generator with dc plus 6th harmonic excitation

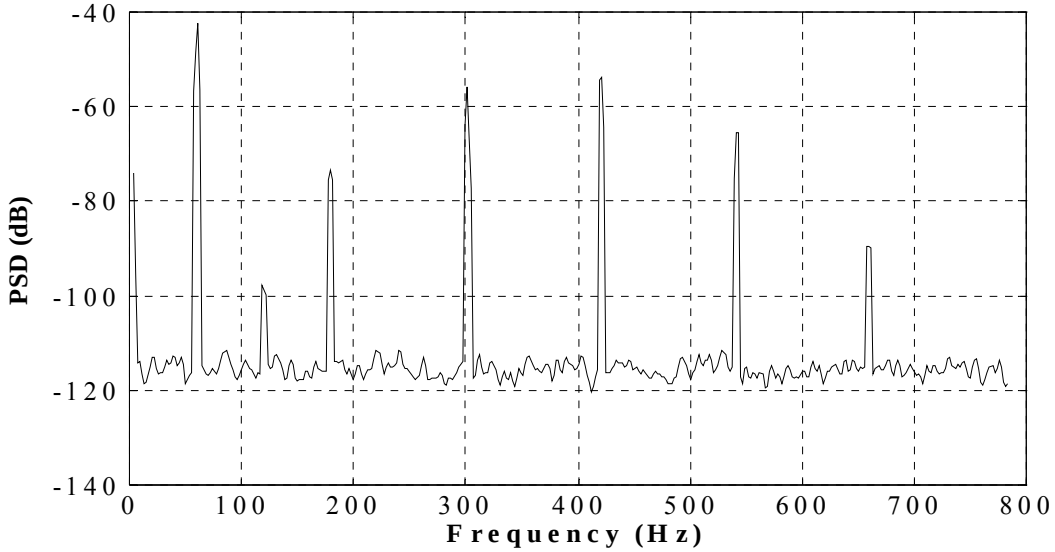

Figure 3-22: Power spectrum analysis of current of synchronous generator with dc plus 6th harmonics excitation

III.6. CONCLUSIONS

In this chapter, an integrated synchronous machine/active filter has been developed. By using this method, the 5^{th} and 7^{th} harmonics, the most troublesome harmonics, can be removed from utility line current while synchronous machine can work in generating or motoring mode of operation. This approach is based on adding an ac excitation circuit in the field of synchronous generator. It was shown that with adding ac signals to the field excitation circuit, the 5^{th} and 7^{th} harmonics would flow in the stator windings such that the phase and amplitude of each one can be controlled independently. This method can be applied to stand–by generators, which exist in various plants with small changes in excitation circuit. This chapter detailed the analysis and simulation as well as laboratory experiments of the proposed system. The experimental results also proved the effectiveness of the proposed harmonic compensation method.

CHAPTER IV

HARMONIC COMPENSATION USING ADVANCED ELECTRIC MACHINES

IV.1. INTRODUCTION

In this chapter an electromechanical active filter to cancel the most dominant harmonics generated by nonlinear loads is proposed. Specifically, 5^{th} and 7^{th} harmonics are suppressed and 11^{th} and 13^{th} harmonics are significantly reduced. The proposed approach consists of a new asymmetric air gap concentrated winding machine (AACWSM) with both ac and dc excitation field.

Conventional ac machines are designed to have sinusoidal voltage and current waveforms to reduce flow of harmonics currents in the utility lines. It appears possible to develop various types of ac machines having a non-sinusoidal winding distribution in which a prescribed non-sinusoidal current can flow [39-41]. Clearly, the iron in an ac machine would be utilized better and the power density will increase if a nearly rectangular distribution of flux as generally encountered in a dc machine is generated in the air-gap of ac machines. This could be achieved if the stator and rotor flux densities are nearly rectangular waves traveling in the air gap.

In this chapter, a new AACWSM with combined dc and ac excitation circuits to cancel the most significant current harmonics is developed. The proposed approach allows for independent control of 5^{th} and 7^{th} harmonics both in magnitude and in phase

and reduces 11^{th} and 13^{th} harmonics. The field excitation current with controllable 2^{nd}, 4^{th} and 6^{th} harmonics is generated by means of a switching power converter.

The advantages of the proposed approach are:

- Line current harmonics (5^{th} and 7^{th}) generated by non-linear load are cancelled, 11^{th} and 13^{th} harmonics are significantly reduced.
- The approach is rugged and can be adapted to low and medium voltage systems.
- The system can be controlled to simultaneously transfer active power to the mechanical load, compensate for reactive power and compensate harmonics generated by nonlinear loads in an industrial plant.

IV.2. DESCRIPTION OF THE PROPOSED METHOD

The block diagram of the proposed electromechanical harmonic filter is shown in Fig. 4-1. It is assumed that the combination of a nonlinear loads have been connected to the utility line and are demanding a nonlinear current which contains the 5^{th}, 7^{th}, 11^{th},13^{th} and etc. The AACWSM is connected to the utility line in parallel with the non-linear load. AACWSM with its unique design generates a non-linear current that includes fundamental, 5^{th}, 7^{th}, 11^{th}, and 13^{th} harmonics. In order to control the magnitude and phase 5th and 7^{th} harmonics, ac excitation along with dc excitation are employed.

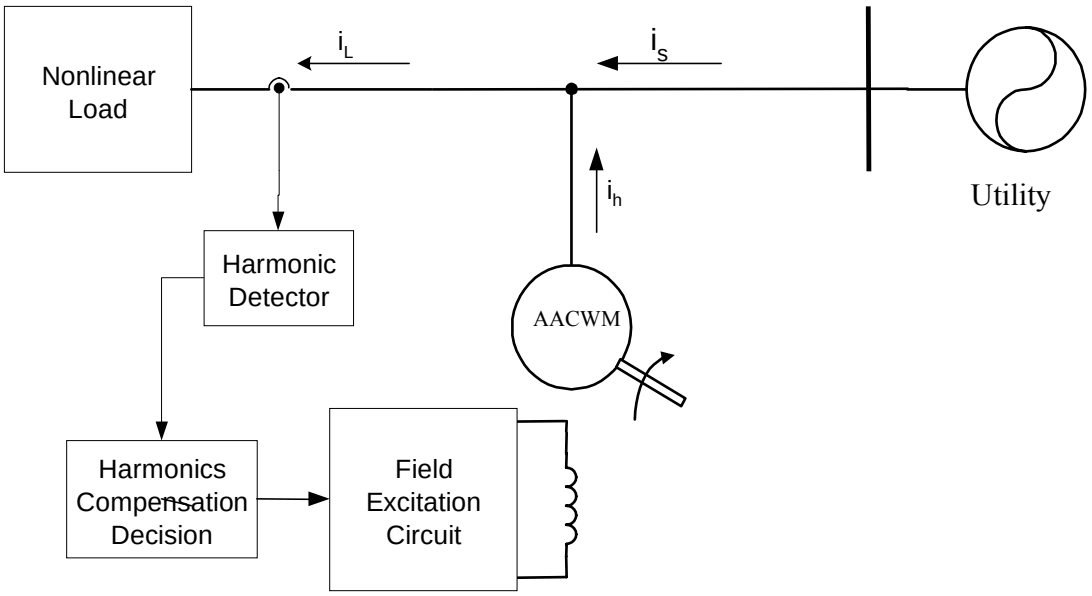

Figure 4-1: Block diagram of the proposed electromechanical harmonic filter

The ac excitation of field is proper combination of 2nd, 4th, and 6th harmonics to generate the 5th and 7th harmonics with specific magnitude and phase as needed for elimination of 5th and 7th harmonics currents of the non-linear load. Procedure of ac excitation is illustrated further. The "*Harmonic Detector Block"* detects the amplitude and phase of the harmonics currents drawn by the non-linear load. This signal goes to the "*Harmonic Compensation Decision Block"*. In this block, the excitation current for canceling these harmonics components is calculated and then the excitation current control is done in the "*Field Excitation Circuit Block*".

The illustrated method is for controlling the excitation of a rotating field of AACWSM connected to an electric power system as it is shown in Fig. 4-1. In this control strategy, the magnitude and phase of 5th and 7th harmonics currents of non-linear load is detected with performing fast Fourier transform on pattern of non-linear load

current. The proper ac excitation is calculated based on required 5^{th} and 7^{th} harmonics currents and applied to rotor winding using a PWM converter.

IV.2.1. ANALYSIS OF THE PROPOSED ELECTROMECHANICAL ACTIVE HARMONIC FILTER

IV.2.1.1. Analysis of AACWSM

This machine is designed to develop a rectangular rather than the more conventional sinusoidal back EMF in order to generate the harmonics needed for the parallel nonlinear load. The machine consists of a concentrated full-pitched winding having one slot per phase. The rotor employs a salient pole field structure with a pole arc of 120° (electrical) utilizing a specially designed asymmetrical pole face taper.

Because of the asymmetrical gap, the inductances between stator and rotor no longer retain the sinusoidal variation characteristic of conventionally designed synchronous and induction machines. Hence, the analysis of this type of machine becomes exceedingly complicated due to the fact that usual transformation no longer yields a simplification in the model.

A six pole AACWSM is shown in Fig. 4-2. It is clear that, this kind of machine with special construction can always be described by a set of differential equation of the form:

$$v = R * i + {}^{1}\!\!\diagup\!\!{}_{\omega_b} \cdot \frac{d}{dt}(X * i) \tag{4-1}$$

$$v = [v_a \quad v_b \quad v_c \quad v_f]^T \tag{4-2}$$

$$i = [i_a \quad i_b \quad i_c \quad i_f]^T \tag{4-3}$$

$$R = \begin{bmatrix} r_a & 0 & 0 & 0 \\ 0 & r_b & 0 & 0 \\ 0 & 0 & r_c & 0 \\ 0 & 0 & 0 & r_f \end{bmatrix} \tag{4-4}$$

$$X = \begin{bmatrix} x_{aa} & x_{ab} & x_{ac} & x_{af} \\ x_{ba} & x_{bb} & x_{bc} & x_{bf} \\ x_{ca} & x_{cb} & x_{cc} & x_{cf} \\ x_{fa} & x_{fb} & x_{fc} & x_{ff} \end{bmatrix} \tag{4-5}$$

The subscripts a, b and c correspond to the three phase stator windings, and f to field winding. ω_b is a constant selected as the base angular frequency. It is useful to consider the individual terms, which appear in (4-1) in more detail. In particular, the voltage of phase A can be solved from the first row of (4-1), that is:

$$v_a = r_a \cdot i_a + \frac{1}{\omega_b} x_{af} \cdot \frac{d\, i_f}{dt} + \frac{\omega_r}{\omega_b} \cdot \frac{d\, x_{af}}{dt} \cdot i_f + \frac{1}{\omega_b} \sum_{k=a,b,c} x_{ak} \cdot \frac{d\, i_k}{dt} + \frac{\omega_r}{\omega_b} \cdot \sum_{k=a,b,c} \frac{d\, x_{ak}}{dt} \cdot i_k \tag{4-6}$$

where:

$$\omega_r = \frac{d\, \theta_r}{dt} \tag{4-7}$$

ω_r is rotor angular speed. From (4-6), the effect of different components on voltage waveform can be observed. As it is clear, the voltage waveform is affected by five different components. The effect of these terms on voltage waveform can be checked by:

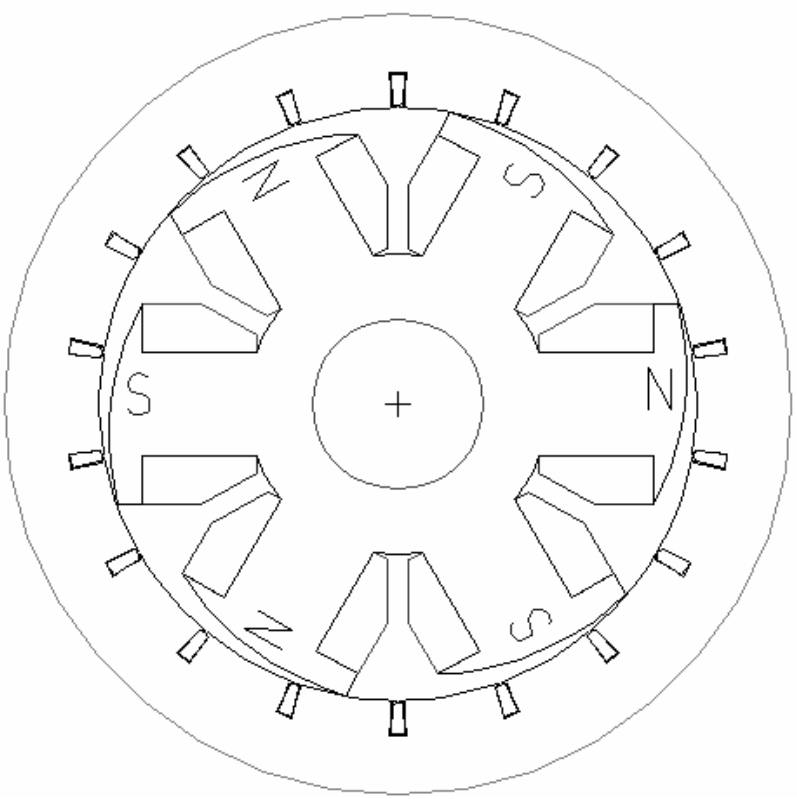

Figure 4-2: Cross section of six-pole AACWSM

1) $r_a \cdot i_a$

This term represents the resistive voltage drop which its value is small compared to other drops.

2) $\frac{1}{\omega_b} . x_{af} \cdot \frac{d i_f}{dt}$

This term is the back EMF produced by the variation of the field current. For a conventional synchronous machine this term is small and usually can be neglected. But for the developed AACWSM, however, its value due to variation of field current

because of the special structure of winding and pole result in time harmonics and also injection of extra harmonics to the field winding makes up for a great portion of voltage drop in the voltage waveform.

3) $\frac{\omega_r}{\omega_b} \cdot \frac{d\, x_{af}}{dt} \cdot i_f$

This term is the back EMF portion produced by variation of x_{af} in time. Because of non-sinusoidal shape of inductances this term has an important role in producing the harmonics in voltage waveform.

4) $\frac{1}{\omega_b} \sum_{k=a,b,c} x_{ak} \cdot \frac{d\, i_k}{dt}$

These components are the portion of induced armature reaction back EMF due to the time varition of phase current.

5) $\frac{\omega_r}{\omega_b} \cdot \sum_{k=a,b,c} \frac{d\, x_{ak}}{dt} \cdot i_k$

These components are the portion of induced armature reaction EMF due to time varition of mutual and self inductances.

It is clear that the presence of an asymmetric gap introduces a formidable complication in the analysis of these equations. In general, the AACWSM possesses sufficient symmetry such that $r_a=r_b=r_c$. In addition, conservation of energy implies that the reactance matrix X is symmetric so that $x_{ab}=x_{ba}$, etc. However, since the air gap is not symmetric the sinusoidal variation of mutual inductances inherent in the Park transformation approach to the analysis of synchronous machine is not applicable.

IV.2.1.2. MMF distribution in AACWSM

It is clear that if an even harmonic current i_h flows in the field winding of machine, a MMF F_h will be developed by the rotor field winding. This MMF is rotating with the mechanical speed ω. The developed MMF by the rotor filed winding generates two equal and opposing MMF inside the air gap which are rotating in forward and backward directions. Notice that the amplitude and phase of $i_{(h+1)}$ and $i_{(h-1)}$ flowing in the stator windings can not be controlled independently with regulating just i_h The developed forward MMF rotates with the speed of $[(h+1)\omega]$, and the backward MMF rotates with the speed of $[(h-1).\omega]$. From rotor point of view, both of these MMFs are revolving at speed of $(h.\omega)$. The forward MMF causes the harmonic current $i_{(h+1)}$ to flow in the stator windings. The backward MMF causes the harmonic current $i_{(h-1)}$ to flow, where the phase displacement between $i_{(h+1)}$ and $i_{(h-1)}$ is 180° degree.

IV.2.1.3. Controlling 5th and 7th harmonics in AACWSM

In this chapter, in order to control the amplitude and phase of developed harmonics currents by the field winding and complete cancellation of 5th and 7th harmonics, it is proposed to inject 2nd, 4th and 6th harmonics currents in the field winding. Injecting 6th harmonics in the field winding generates two equal MMFs in the air gap, where one rotates with speed of 7ω in forward direction, and the other one revolves with speed of 5ω in the backward direction. These two MMFs cause the flow of 5th and 7th harmonics currents in the stator windings, where the phase displacement between them is 180°.

Without considering space harmonics inside the air gap, the amplitude of 7th harmonic current is less than that of 5th harmonic because of the stator winding inductance. For example in a rectifier load, the amplitude of 5th harmonics is more than 7th harmonics, then for completely compensating the 5th harmonic, it is needed to boost the 5th harmonic of MMF in the air gap in order to increase the 5th harmonic current.

As it is shown in Table 4-1, for this purpose, it is considered adding 4th harmonic current in the field winding. With controlling amplitude and phase of the injected 4th harmonic, it is possible to increase the 5th harmonic rotating MMF in the air gap. For canceling the 3rd harmonic produced by the rotating MMF in the air gap, it is needed to add the 2nd harmonic current in the field winding excitation circuit. With this strategy, the final developed MMFs inside the air gap are fundamental, 5th and 7th harmonics.

Following equation describes the total field excitation current:

$$i_f = I_{dc} + i_{m2}\sin(2\omega t + \varphi_2) + i_{m4}\sin(4\omega t + \varphi_4) + i_{m6}\sin(6\omega t + \varphi_6) \qquad (4\text{-}8)$$

where, I_{dc} indicates the dc component of the field current and $i_{m2,}$ i_{m4} and i_{m6} indicate the 2nd, 4th and 6th harmonics of current injected in the field winding excitation circuitry, respectively. The phase angles φ_2, $\varphi_{4,}$ and φ_6 indicate phase of the 2nd, 4th, and 6th harmonics currents, respectively.

IV.2.1.4. Determination of self and mutual inductances

A traditional definition of inductance parameters of conventional synchronous machines typically employs the assumption that the air gap flux density is sinusoidal and that the stator has smooth surface. These assumptions are, however, no longer valid for

the AACWSM owing its novel construction. In order to obtain modified equation for these inductances one solution is to derive the winding function and inverse air gap function in case of asymmetric air gap. However, in this method the effect of saturation is neglected. Nonlinear finite element analysis can be used for obtaining the magnetic field in machine. Then, the flux linkage and inductances are calculated. Distribution of flux lines in cross section of a six pole AACWSM in case of field excitation is shown in Fig. 4-3. As it is clear, the flux paths are pushed to the side where the air gap is minimal.

Table 4-1: Controlling the 5^{th} and 7^{th} harmonics currents in AACWSM

AC Excitation	Produced MMF		Produced Currents
	Forward	Backward	
6^{th}	7^{th}	5^{th}	i_5, i_7
4^{th}	5^{th}	3^{rd}	i_5, i_3
2^{nd}	3^{rd}	1^{st}	i_3, i_1
Total	7^{th} , 5^{th} , 1^{st}		i_1 , i_5 , i_7

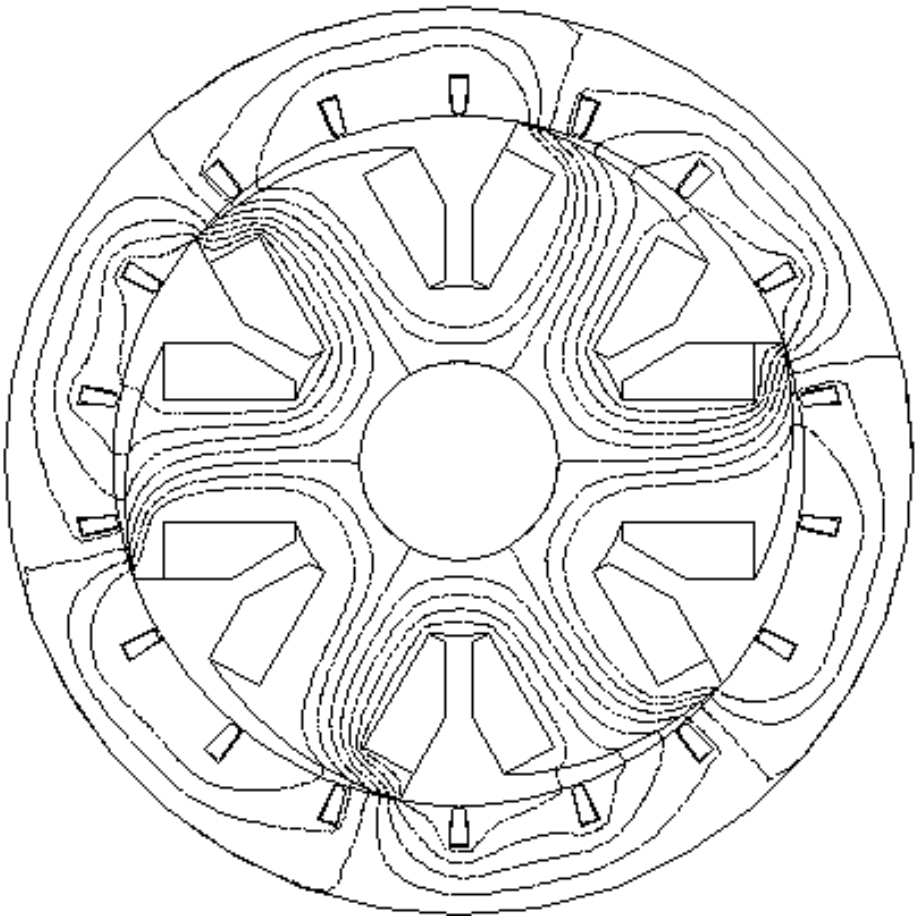

Figure 4-3: Flux path in cross section of a six-pole AACWSM

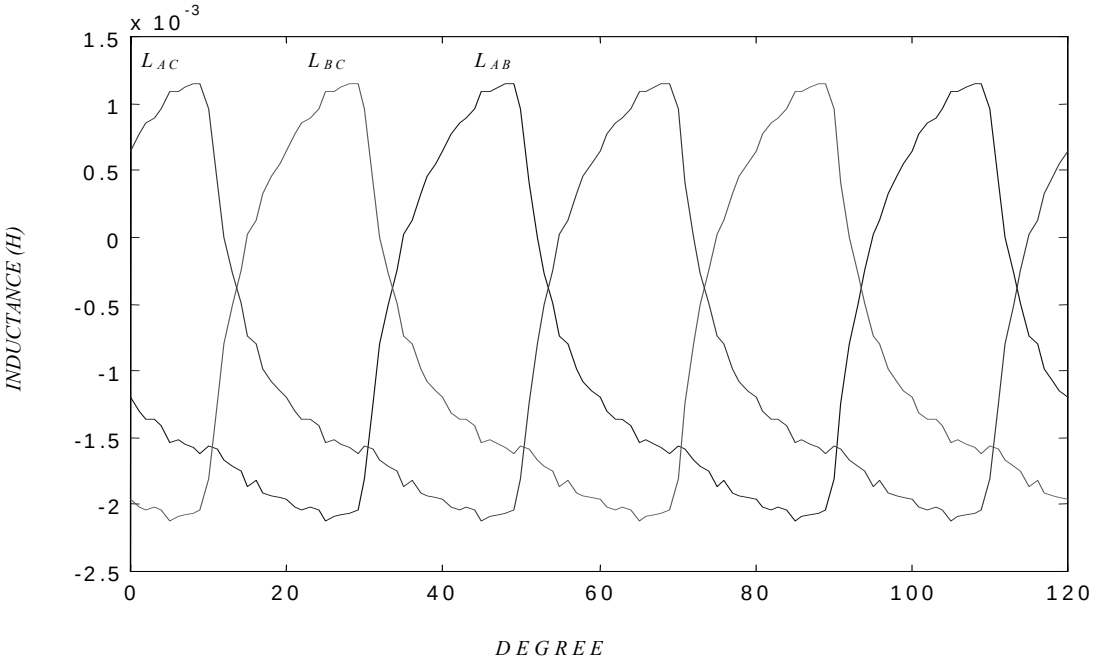

Figure 4-4: Mutual inductances between stator windings

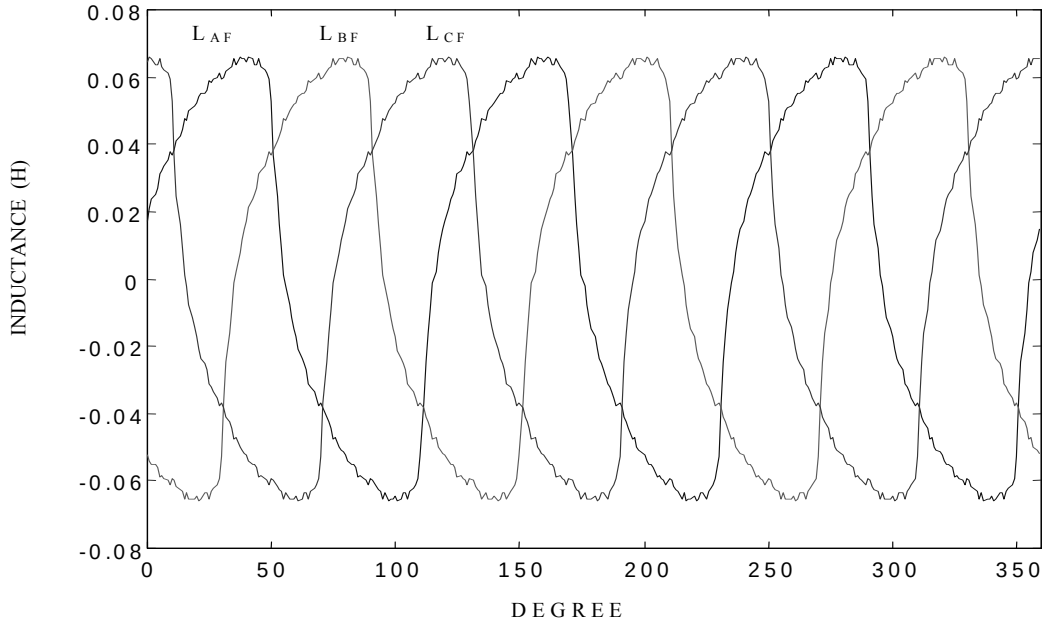

Figure 4-5: Mutual inductances between stator and rotor windings

A series of finite element analysis have been performed and self-inductances and mutual inductances between stator windings and field winding are calculated. The inductances of L_{ab}, L_{ac}, L_{bc} are plotted in Fig. 4-4 and the mutual inductances between rotor and stator are illustrated in Fig. 4-5. As it is shown the mutual inductances between stator windings and also mutual inductances between stator and rotor windings are not sinusoidal. It is crystal clear that the derivatives of these inductances are not sinusoidal too. The effect of these inductances in generating harmonic components in (4-6) is obvious. The self-inductances of stator and rotor windings are nearly constant so their effect in producing harmonics components in (4-6) is negligible.

IV.2.1.5. Calculating the gain of harmonic compensatory system

To find a relationship between the injected field current and the generated harmonics currents, (4-6) is used. For simplicity, we assume that r_a=0 and inductances vary sinusoidally. So we have:

$$r_a = 0 \tag{4-9}$$

$$L_{af} = L_{sfd}.\sin\theta_r = L_{sfd}.\sin\omega t \tag{4-10}$$

$$L_{asas} = L_A - L_B.\cos(2\omega t) \tag{4-11}$$

$$L_{asbs} = -1/2\, L_A - L_B.\cos 2(\omega t - \pi/3) \tag{4-12}$$

$$L_{ascs} = -1/2\, L_A - L_B.\cos 2(\omega t + \pi/3) \tag{4-13}$$

Assume the field current is given by:

$$i_f = i_6.Sin(6\omega t + \varphi_6) \tag{4-14}$$

and the stator current is represented by:

$$i_a = i_5 Sin5\omega t + i_7 Sin7\omega t \tag{4-15}$$

Substituting these values into (4-6), we can find the ratio of i_5 to i_6 and i_7 to i_6 using the following equations:

$$\frac{i_5}{i_6} = -\left(\frac{3\omega L_{sfd} + \omega^2 L_{sfd}}{-7.5 L_B \omega + 3\omega^2 L_B} \right) \tag{4-16}$$

$$\frac{i_7}{i_6} = \left(\frac{-3\omega L_{sfd} + \omega^2 L_{sfd}}{10.5 L_B \omega + 3\omega^2 L_B} \right) \tag{4-17}$$

For this example, $L_{sfd} = 65mH$ and $L_B = 1.65mH$ are calculated from finite element analysis so the ratio of $\frac{i_5}{i_6} = -13.3$ and the ratio of $\frac{i_7}{i_6} = 12.9$ are obtained. Using this method, the overall compensation gain can be computed.

IV.2.1.6. Calculation of the required field current

Field current is the combination of 6th, 4th, 2nd and dc currents. To find the amount of these values, we start with 6th harmonic current. If 6th harmonic current is injected into the field, 5th and 7th harmonics currents are produced according to (4-16) and (4-17). So we can adjust the 6th harmonics current to produce the needed 7th harmonic using (4-16). 4th harmonic current should be injected to the field to generate the remaining amount of required 5th harmonic current. After finding the required amount of the injected 4th harmonic, we can calculate 2nd harmonic needed to cancel the generated 3rd harmonic current.

IV.3. SIMULATION RESULTS

A six-pole 245 kVA, 460 V, 60 Hz, AACWSM shown in Fig. 4-2 has been simulated using MATLAB package to prove the effectiveness of the proposed method. This simulation has been performed in abc system according to developed mathematical model. The mutual inductances and self-inductances for the proposed AACWSM have been calculated using finite element analysis using MAXWELL package which have been plotted in Fig. 4-4 and Fig. 4-5, respectively. As it is observed these inductances are no longer sinusoidal and cause a non-sinusoidal voltage waveform in terminal of AACWSM. But the AACWSM has been connected to utility and stator voltage is assumed to be sinusoidal. So with controlling the AC excitation, the amount of harmonics current for compensation of non-linear load currents can be controlled.

The self-inductances are calculated but their variation with the rotor position is minimal and therefore it is assumed they are constant. Figure 4-6 illustrates the system used for simulation study. It is assumed that the AACWSM has been connected to an infinite bus and is paralleled with 240 kVA rectifier load.

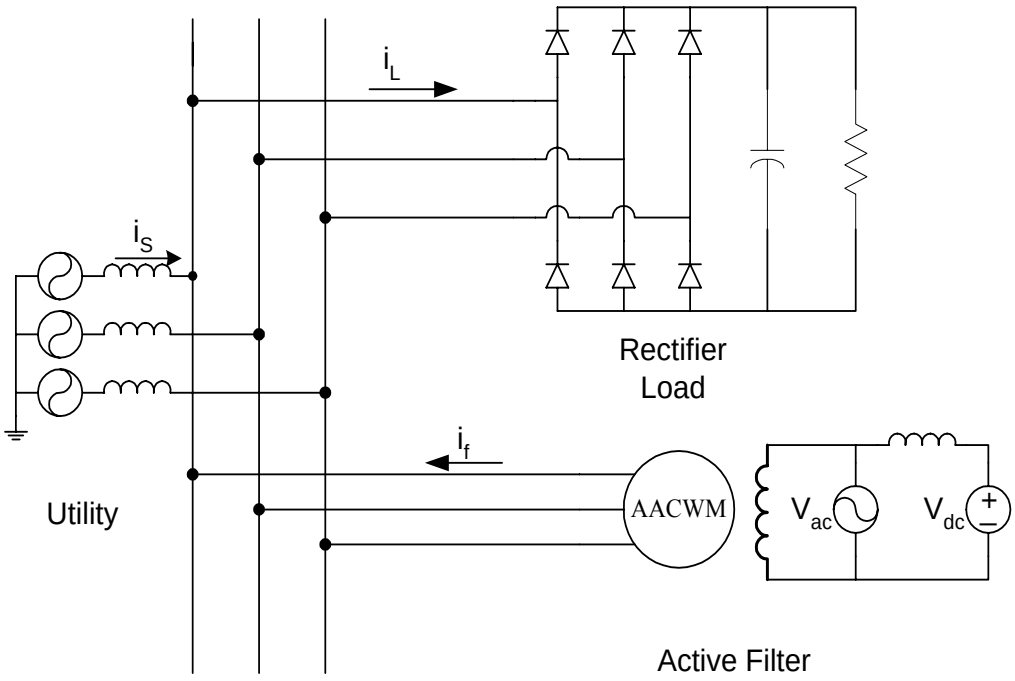

Figure 4-6: Simulated circuit

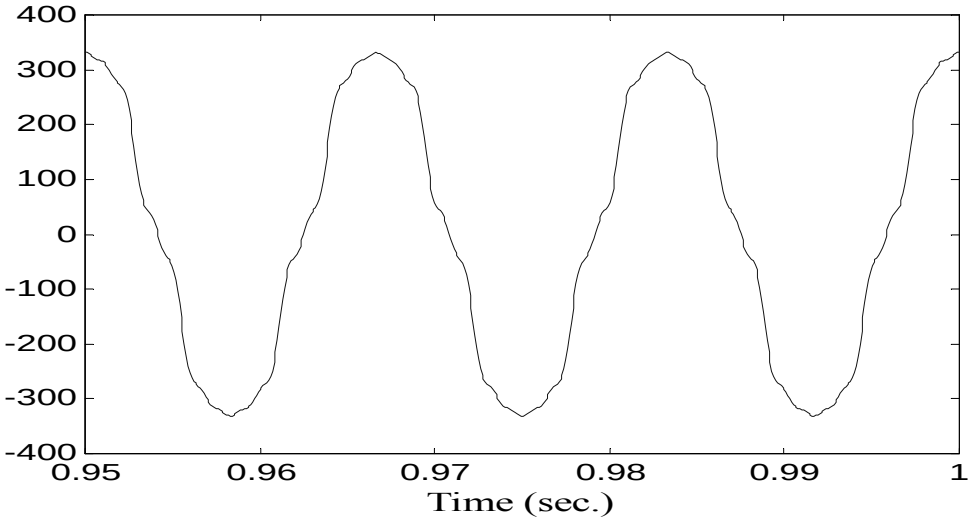

Figure 4-7: Current waveform of AACWSM with dc excitation

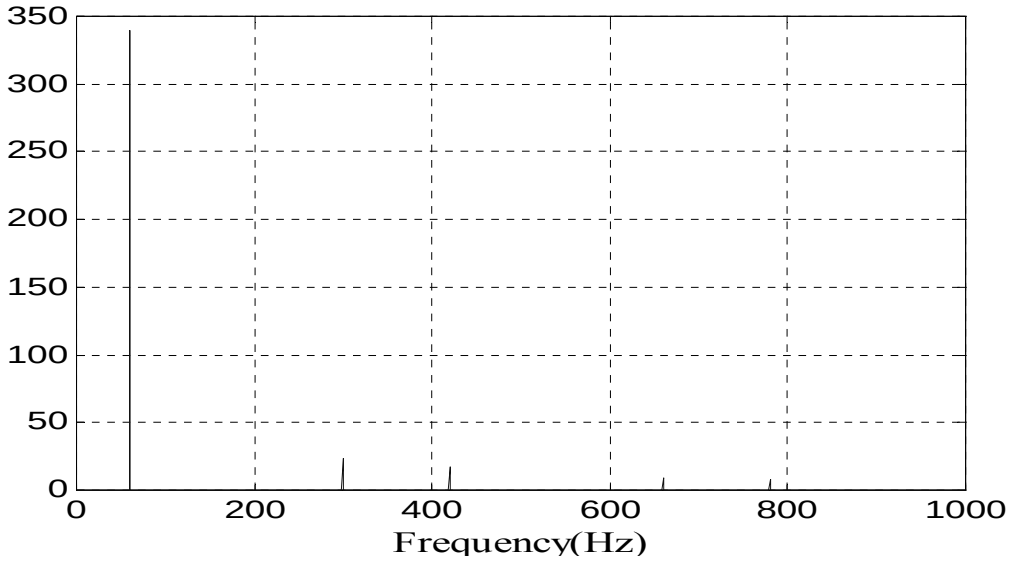

Figure 4-8: Current spectrum of AACWSM with dc excitation

In case of dc excitation, the generated current of AACWSM is rich in 5^{th}, 7^{th}, 11^{th} and 13^{th} harmonics. The generated current and its spectrum are depicted in Fig. 4-7 and Fig. 4-8, respectively. Now it is assumed that it is desired to cancel the harmonics components of parallel nonlinear load. The nonlinear load demands a nonlinear current shown in Fig 4-9 with its frequency spectrum analysis illustrated in Fig. 4-10.

Now, with adding the proper amount of 2^{nd}, 4^{th} and 6^{th} harmonics current into the field excitation, the 5^{th} and 7^{th} harmonics are removed from the utility current. The current of active filter and utility current and their spectrum are plotted in Fig. 4-11 through Fig. 4-14.

As it is clear, the 5^{th} and 7^{th} harmonics current have been removed from utility and the magnitude of 11^{th} and 13^{th} are reduced. In this simulation, AACWSM has produced

165 kVA real power and 60 kVA harmonics power. Gain of total generated harmonics current to the total injected harmonics currents into the field is 18.

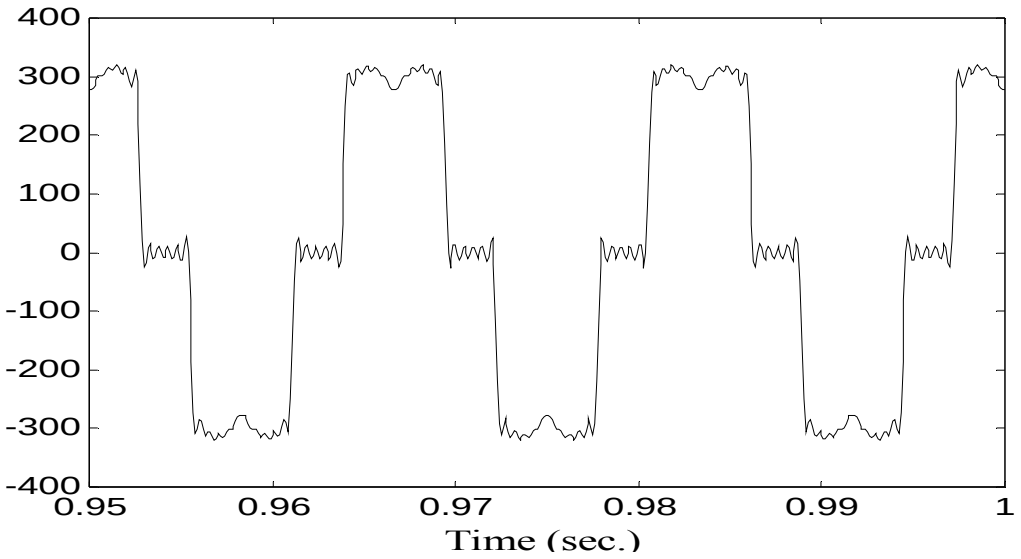

Figure 4-9: Nonlinear load current waveform

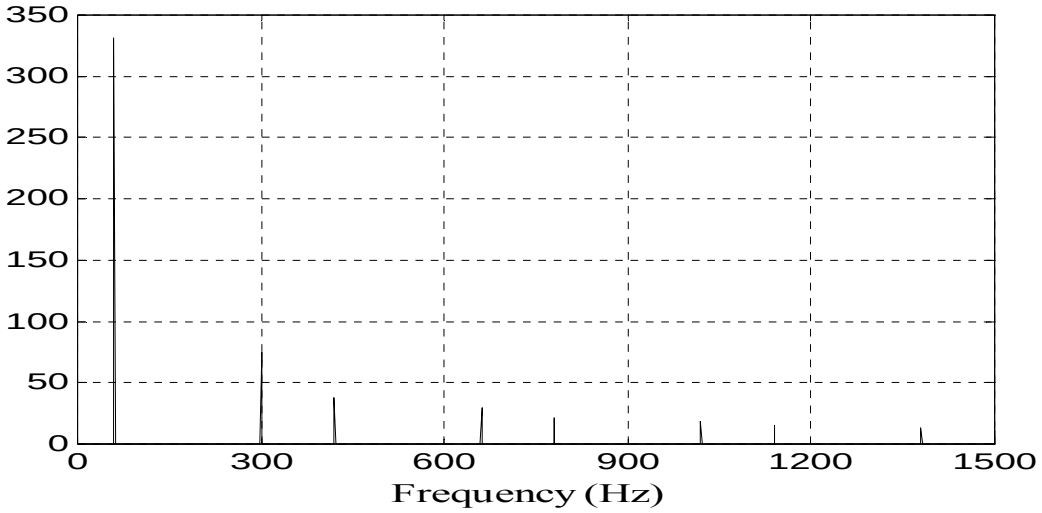

Figure 4-10: Frequency spectrum of nonlinear load

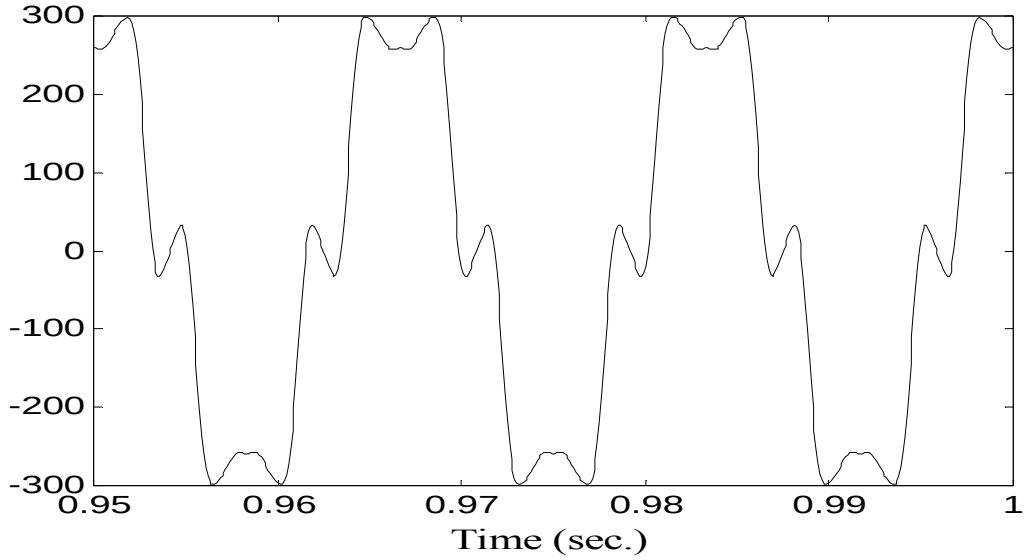

Figure 4-11: Current of AACWSM

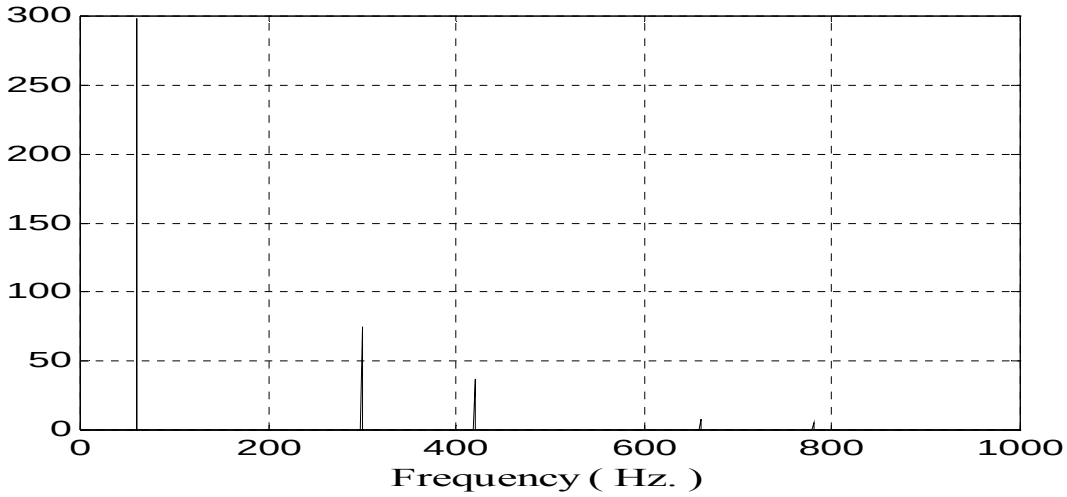

Figure 4-12: Frequency spectrum of AACWSM current

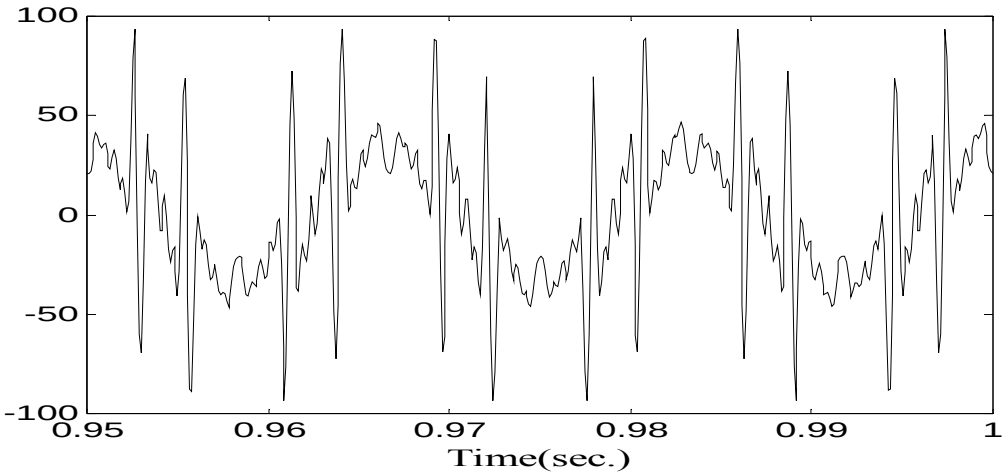

Figure 4-13: Utility line current

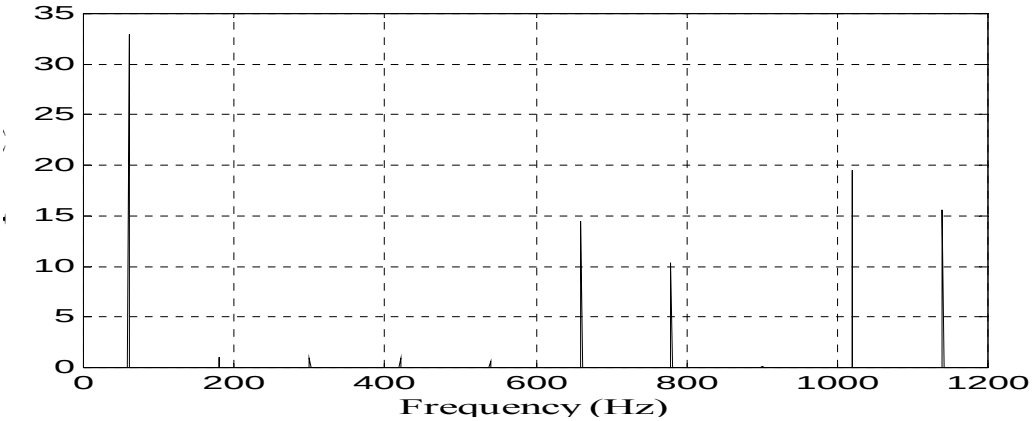

Figure 4-14: Frequency spectrum of utility current

IV.4. CONCLUSIONS

In this chapter, a new electromechanical active harmonic filter has been proposed. By using this method, besides generating active power, the 5^{th} and 7^{th} harmonics, the most troublesome harmonics, can be removed from utility line current. In addition, the magnitudes of the 11^{th} and 13^{th} harmonics are reduced. This approach is based on new Asymmetric Air gap Winding Concentrated Synchronous Machine AACWSM with ac and dc excitation circuit in the field. It was shown that with adding ac signals to the field excitation circuit, the 5^{th} and 7^{th} harmonics would flow in the stator windings such that the phase and amplitude of each one can be controlled independently. The chapter detailed the analysis and simulation of the proposed system. The simulation result also proved the effectiveness of the proposed harmonic compensation method.

CHAPTER V

CONCLUSIONS AND SUGGESTED FUTURE WORK

V.1. CONCLUSIONS

The contemporary era of rapid industrialization and technological development has raised a global energy crisis, which is one of the major concerning issues. The increase rate of depletion of fossil energy resources in one hand and growing energy demand on the other hand has initiated considerable research activity worldwide to explore means for tapping of renewable energy resources. Wind energy due to its freely available, clean and renewable character ranks as the most promising renewable energy resource that could play a key role in solving the worldwide energy crisis.

On the other hand, a recent issue of extreme concern is the electric power quality. Power quality issues cause companies to lose billions of dollars every year to work stoppages, diagnosis, and service damaged equipment. These disruptions can also affect hard-earned reputations. Therefore, clean power is essential to remaining profitable and competitive. The injection of harmonic currents into an electrical distribution system, which is based on a non-mitigating 'conventional design', will normally produce several unacceptable outcomes; such as lower power factor, overheating, high neutral currents and electromagnetic interference (EMI).

In response to these concerns, this dissertation addressed the problem of power quality issue and future energy crisis. The total viable power quality and energy crisis solutions were proposed. In this dissertation, three different methodologies to integrate

the concept of active filtering into the alternators for alternative energy application are proposed. Wind, a green and renewable and nonpolitical energy is considered a viable alternative energy resource.

One of the proposed technologies is an Integrated Doubly-fed Electric Alternator/Active filter (IDEA) for wind energy conversion systems. The IDEA, a viable solution towards energy crisis and power quality issue, is capable of capturing the maximum energy from fluctuating wind, controlling the reactive power and compensating the harmonics currents of the utility. In this dissertation, a field oriented control method was developed to control the rotor-side current regulated voltage source power converter for dynamically excitation of the rotor circuitry of the wound rotor induction generator. The proposed control method controls both fundamental current and harmonics currents. The control strategy is capable to control the generated active and reactive power as well as the amount of harmonic compensation in the grid independently. A rotor position sensoreless method was also developed for rotor-side converter and performance of the system with and without position sensor was compared. The perfect rotor position estimation was observed over a wide variation rang of speed. Vector control method for front-end converter for allowing bi-directional power flow in rotor circuit has also been developed. The laboratory experimental setup for proposed IDEA was fabricated. The stator of the 7.5 kW wound rotor induction machine is connected to the 230V, 60Hz balanced three phase grid and the rotor side is fed via back-to-back IGBT voltage-source inverters with a common dc-bus. The front–end converter (FEC) controls the power flow between the dc bus and the ac side and

allows the system to be operated in sub-synchronous and super synchronous speed. Wind turbine torque-speed characteristics are emulated in the laboratory by a 7.5 kW adjustable speed dc motor drive. A rectifier load is connected to the utility and causes to flow harmonic into the grid. A TMS320F2407 fixed point TI DSP controller platform was designed and employed for implementing the proposed field oriented control method. The processor runs at a clock frequency of 30 MHz and the sampling frequency used is 50 μs. With applying the control method, the proper rotor excitation is provided by the rotor side power converter. Several experimental studies were conducted. The generated harmonics compensate for the harmonic currents needed by the non-linear load. The fundamental current controls the active and reactive powers. With applying this method the harmonics currents of utility were removed. Decoupled control of the active and reactive powers and harmonic compensation are met. The software is assembly coded for fast real-time execution. Laboratory experimental results have proved the effectiveness of the proposed method.

In chapter III, an integrated synchronous machine/active filter was proposed. The proposed electromechanical harmonic filter is essentially a rotating synchronous machine with suitable modification to its field excitation circuit. Field of synchronous machine is excited by dc and ac currents. It was shown that by injecting 2^{nd}, 4^{th} and 6^{th} harmonics currents into the field winding, 5^{th} and 7^{th} harmonic currents were generated in the stator winding. By proper control of the field excitation, the proposed integrated synchronous machine/active filter can compensate for the 5^{th} and 7^{th} harmonic currents in the electric power distribution system. The proposed method is cost effective since it

can be applied to existing standby generators in commercial and industrial plants with minimal modification to the excitation circuit.

To boost the gain of harmonic compensatory, an advanced electric machine was designed and proposed in chapter IV. An Asymmetric Air gap Concentrated Winding Synchronous Machine (AACWSM) with ac and dc excitation field was designed and employed. It was shown that the AACWSM with its unique design, in addition to power generation capability could be used to compensate the most dominant current harmonics of the utility. The back-EMF voltage of this advanced machine behaves as non-sinusoidal voltage source owing to its asymmetric airgap geometry and ac field excitation. With the proper ac field excitation, the proposed electromechanical harmonic filter can compensate for the 5^{th} and 7^{th} harmonic currents in the electric power distribution system. In addition, 11^{th} and 13^{th} harmonics magnitudes are also significantly reduced. This system can be adopted to be used in medium and low voltage in generation or motoring mode of operation. The mathematical model for system was developed and computer simulation was conducted and proved the effectiveness of the proposed technology. It was proved, with using this technology the gain of harmonic compensatory system is gained to 18 compared to integrated synchronous machine/active filter proposed in chapter III of this dissertation with gain of 8.

V.2. SUGGESTED FUTURE WORK

The proposed IDEA is suitable to install in strong and stiff network. To prevent power interruption in weak grids, IDEA can be combined with flywheel system to smooth the output power of wind turbine with fluctuating wind speed and voltage loss in

the grid. The combination of IDEA and power storage equipment will be a great solution to power quality problem in weak grids. A doubly-fed induction can be used for flywheel energy storage system that harmonic compensation feature can be performed in flywheel energy storage system. Converter topologies can also be combined where the system can enjoy with having one front-end converter and two different rotor-side converter for wind turbine and flywheel energy storage system. This configuration will save the number of switches.

Field excitation circuit of integrated synchronous machine/active filter can be adopted with two level resonance circuit. This field excitation circuit will allow for compensation of 11^{th} and 13^{th} harmonics in the grid.

New advanced electrical machines with suitable performance for power quality improvement can also be designed. Configuration with two stator windings may improve the performance of harmonic compensation system.

REFERENCES

[1] IEEE Recommended Practices and Requirements for Harmonic Control in Electrical Power Systems, IEEE Standard 519-1992, Jun. 1992.

[2] Limits for Harmonic Currents Emissions, IEC Standard 61000-3-2, 1995.

[3] H. Fujita and H. Akagi, "A practical approach to harmonic compensation in power systems-series connection of passive and active filter," *IEEE Trans. Industry Applications*, vol.27, pp. 1020 -1025, Nov.-Dec. 1991.

[4] C.A. Quinn and N. Mohan, "Active filtering of harmonic currents in three-phase, four-wire systems with three-phase and single-phase nonlinear loads," in *Proc. 1992 IEEE Applied Power Electronics Conf.*, pp. 829 -836.

[5] J. M. Clemmensen, "Estimating the cost of power quality," *IEEE Spectrum*, vol.30, pp.40-42, Jun. 1993.

[6] N.G. Hingorani and K. E. Stahlkopf, "High power electronics," *Scientific American*, vol.269, pp.78-85, Nov. 1993.

[7] L.H. Hansen, P.H. Madsen, F. Blaabjerg, H.C. Christensen, U. Lindhard and K. Eskildsen, "Generators and power electronics technology for wind turbines," in *Proc. 2001 IEEE Industrial Electronics Society Conf.*, pp. 2000-2005.

[8] T. C. Shuter, H. T. Vollkommer, Jr., and J. L. Kirkpatrick, "Survey of harmonic levels on the American electric power distribution system," *IEEE Trans. Power Delivery*, vol. 4, pp. 2204–2213, Oct. 1989.

[9] A.C. Liew, "Excessive neutral currents in three-phase fluorescent lighting circuits," *IEEE Trans. Industry Applications*, vol. 25, pp. 776–782, Jul.-Aug. 1989.

[10] T. M. Gruzs, "A survey of neutral currents in three-phase computer power systems," *IEEE Trans. Industry Applications*, vol. 26, pp. 719–725, Jul.-Aug. 1990.

[11] J. S. Subjak Jr. and J. S. Mcquilkin, "Harmonics-causes, effects, measurements, analysis: an update," *IEEE Trans. Industry Applications*, vol. 26, pp. 1034–1042, Nov-Dec. 1990.

[12] M. E. Amoli and T. Florence, "Voltage, current harmonic control of a utility system-a summary of 1120 test measurements," *IEEE Trans. Power Delivery*, vol. 5, pp. 1552–1557, Jul. 1990.

[13] P. Packebush, and P. Enjeti, "A survey of neutral current harmonics in campus buildings, suggested remedies," in *Proc. 1994 Power Quality Conf.*, pp.194-205.

[14] E. Emanuel, J. A. Orr, D. Cyganski, and E. M. Gulchenski, "A survey of harmonics voltages, currents at the customer's bus," *IEEE Trans. Power Delivery*, vol. 8, pp. 411–421, Jan. 1993.

[15] H. Akagi, Y. Kanazawa, and A. Nabae, "Instantaneous reactive power compensators comprising switching devices without energy storage components," *IEEE Trans. Industry Applications,* vol.20, pp. 625–630, May-Jun. 1984.

[16] H. Sasaki and T. Machida, "A new method to eliminate ac harmonic currents by magnetic flux compensation-considerations on basic design," *IEEE Trans. Power Apparatus Systems*, vol.90, pp. 2009-2019, Jan. 1971.

[17] Y. Hsu and H. Y. Wu, "A new single-phase active power filter with reduced energy storage capacity," *IEE Proc. Electrical Power Applications*, vol. 143, no. 1, pp. 25-30, Jan. 1996.

[18] A. Taleb, A. J. Kamal, J. Sowaied, and M. R. Khan, "An alternative active power filter," in *Proc. 1996 IEEE Power Electronics, Drives and Energy Systems Conf.,* pp. 410-416.

[19] H. Akagi, "New trends in active filters for improving power quality," in *Proc. 1996 IEEE Power Electronics, Drives and Energy Systems Conf.,* pp. 417-425.

[20] F.Z. Peng, H. Akagi, and A. Nabae, "A novel harmonic power filter," in *Proc. 1988 IEEE Power Electronics Specialists Conf*., pp. 1151-1158.

[21] S. Battacharya, T.M. Frank, D.M. Divan, and B. Banerjee, "Parallel active filter system implementation and design issues for utility interface of adjustable speed drive systems," in *Proc. 1996 IEEE Industry Application Society Conf.*, pp. 1032-1039.

[22] F. Peng, "Application issues of active power filters," *IEEE Industry Applications Magazine*, vol. 4, pp. 21-30, Sept.-Oct. 1998.

[23] S.M.R. Rafiei, R. Ghazi, H.A. Toliyat, and T. Gopalarathnam, "An optimal and flexible control strategy for active filtering and power factor correction under non-sinusoidal line voltage," *IEEE Trans. Power Delivery*, vol. 16, pp. 297-305, Apr. 2001.

[24] F. Takase, M. Tominaga, Y. Ueda, T. Temma, T. Genji, K. Oku, "Harmonic compensation using a synchronous machine with resonant field circuits," *IEEE Trans. Energy Conversion,* vol.12, pp. 143-150, Jun. 1997.

[25] F. Takase, M. Tominaga, Y. Ueda, T. Temma, T. Genji, K. Oku, "Trial construction of a synchronous machine for higher harmonics compensation," in *Proc. 1995 IEEE Power Engineering Society, Summer Meeting Record*, pp.1-6.

[26] Y. Ueda, F. Takase, K. Oku, T. Hira and A. Ashizawa, "Synchronous machine excitation control device for absorbing harmonics superposed onto fundamental current," U.S. Patent 5 886 493, Mar. 23, 1999.

[27] M. Ermiş, H.B. Ertan, M. Demirekler, B.M. Sarıbatır, Y. Uctug, M.E. Sezer and I. Cadirei, "Various induction generator schemes for wind electricity generation," *Journal of Electric Power Systems Research*, vol. 23, pp.71-83, Jan. 1992.

[28] T.S. Jayadev, "Windmills stage a come back," *IEEE Spectrum Magazine*, pp. 45-49, Nov. 1976.

[29] D.S. Zinger, E. Muljadi, "Annualized wind energy improvement using variable speeds," *IEEE Trans Industry Applications*, vol.33, pp.1444-1447, Nov.-Dec. 1997.

[30] R. Hoffmann, P. Mutschler, "The influence of control strategies on the energy capture of wind turbines," in *Proc. 2000 IEEE Industry Applications Conf.*, pp.886-893.

[31] R. Cardenas, "Control of turbines using switched reluctance generators," Ph.D. dissertation, Dept. Elec. Eng., University of Nottingham, UK, 1996.

[32] R. Datta and V.T. Ranganathan, "A method of tracking the peak power points for a variable speed wind energy conversion system," *IEEE Trans. Energy Conversion*, vol.18, pp.163-168, Mar. 2003.

[33] R. Datta, V.T. Ranganathan, "A simple position sensorless algorithm for rotor-side field-oriented control of wound-rotor induction machine," *IEEE Trans. Industrial Electronics*, vol.48, pp.786-793, Aug. 2001.

[34] R. Pena, J.C. Clare and G.M. Asher, "Doubly-fed induction generator using back-to-back PWM converters and its application to variable speed wind energy generation," *IEE Proc. Electric Power Applications*, vol.43, pp.231-241, May 1996.

[35] H. Akagi and H. Sato, "Control and performance of a doubly-fed induction machine intended for a flywheel energy storage system," *IEE Trans. Power Electronics*, vol.17, pp.109-116, Jan.2002.

[36] B. Hopfensperger, D.J. Atkinson and R.A. Lakin, "Stator-flux-oriented control of a doubly-fed induction machine with and without position encoder," *IEE Proc. Electrical Power Applications*, vol.147, pp.241-250, Jul. 2000.

[37] M. A. A. k. Al-Geelani, "Investigation on cycloconverter-fed induction machine system in generator mode," Ph.D. Dissertation, Dept. Elec. Eng., Indian Institute of Technology, Roorkee, India, 2002.

[38] P.M. Hart and W.J. Bonwick, "Harmonic modeling of synchronous machines," *IEE Proc. Electric Power Applications*, vol.135, pp.52 -58, Mar. 1988.

[39] F.X. Wang, and T.A. Lipo, "Analysis and steady state behavior of an optimized converter machine," *IEEE Trans. Power Apparatus and Systems*, vol.102, pp.986-992, Aug. 1983.

[40] T.A. Lipo, and F.X Wang, "Design and performance of a converter optimized ac machine," *IEEE Trans. Industry Application*, vol.20, pp.442-448, Jul.-Aug. 1984.

[41] F.X. Wang and T.A. Lipo, "Waveform optimization design of an ac converter machine," *IEEE Trans. Industry Applications*, vol.25, pp.436-440, May-Jun. 1989.

[42] H.A. Toliyat, and T.A. Lipo, "Analysis of concentrated winding induction machines for adjustable speed drive applications-experimental results," *IEEE Trans. Energy Conversion*, vol. 9, pp. 695-700, Dec. 1994.

[43] N.A. Al-Nuaim, and H.A. Toliyat, "A novel method for modeling dynamic air-gap eccentricity in synchronous machines based on modified winding function theory," *IEEE Trans. Energy Conversion*, vol. 13, pp. 156-162, Jun. 1998.

VITA

Mehdi Towliat Abolhassani

Department of Electrical Engineering
Texas A&M University
College Station, Texas 77843-3128

Mehdi Abolhasani was born in Mashad, Iran in 1973. He received his B.S. and M.S. degree both in electrical engineering from the Tehran University and Iran University of Science and Technology in 1995 and 1999, respectively. He worked in leading companies as a senior electrical engineer in Iran in the area of electric power from 1995 to 2000. He joined the power group at Texas A&M University in January 2000 to pursue a Ph.D degree in electrical engineering. He is currently pursuing an internship in General Motors R&D from June 2003 as project engineer.